Chapter 2
Windings

Contents

V. Ostović, *The Art and Science of Rotating Field Machines Design*,
DOI 10.1007/978-3-319-39081-9_2

Diversity of winding topologies in rotating field machines helps them adapt to arbitrary load characteristic and source properties. Windings of a rotating field machine determine to the largest extent its electromechanical performance. Spatial distribution of conductors along the air gap circumference and connection of coils to particular phases are a clue to the desired machine features. Not less important is the end winding geometry, as a function of the number of winding layers, its design (wave, lap, concentric, tooth wound, etc.), number of poles, etc. Spatial distribution of winding determines its current sheet, MMF, and flux density curves, all of them being periodical functions of the air gap circumferential coordinate. Spatial Fourier analysis is therefore employed as a mathematical tool for predicting the winding performance. Both integer and fractional slot AC, as well as DC field windings are analyzed. Harmonics generated by toothed air gap and their role in electric machines and magnetic gearboxes is illustrated. The mechanism of voltage generation is illustrated on example of rotating field and rotating coil excitation. Spatial spectra of air gap MMF created by regular and discontinuous squirrel cage windings are calculated. Winding failures are analyzed in various types of windings.

2.1 Active Part and End Winding Zone, Air Gap Winding Versus Coils in Slots, Slot Fill Factor

Electric machines are built in such a manner as to have stator and rotor field components in the air gap firmly concatenated with each other. The distance between current-carrying stator and rotor conductors in the end winding region is substantially larger than in its active part. Therefore, the contribution of portions of conductors in the end winding region to the total torque is negligible as compared to the effects in the active part.

On the other hand, it is not unusual that the leakage reactance of the end winding portions of coils, and, even more pronounced, their resistance, is of the same order of magnitude as those of the active part. For this reason the end winding zone is considered a ballast, and numerous tricks of the trade have been tried out in order to diminish its influence on machine performance. However, when modifying the end winding topology in the manner it is done e.g. in tooth-wound machines, one should always try not to deteriorate too much the parameters of windings in the machine's active part and not to worsen its overall characteristics, e.g., by increasing its Carter factor and air gap leakage inductance.

Following the fundamental relation for force acting on a current-carrying conductor in magnetic field $F = B\,\ell\,I$, one would tend to place the machine windings into air gap with flux density B. This well-known equation for force in magnetic field is, however, only a special case of a more general relation, which tells that force is equal to the rate of change of energy stored in magnetic field, $\partial W_{mg}/\partial x$. Therefore, a current-carrying conductor does not have to be directly exposed to magnetic field in order to generate force in it; it is only necessary that the current-carrying conductor is a part of a turn which concatenates external field with flux density B on the place of the conductor. Accordingly, a current-carrying conductor in a slot in which the radial flux density is equal to zero generates the same force as if it were placed in the air gap above the slot, where the radial flux density is equal to B [1].

Placing conductors into slots, instead into air gap, brings electromagnetic and mechanical advantages: Coils in slots require substantially less current in order to generate certain flux level (shorter air gap!), and force does not act directly on conductors, but on teeth. On the other hand, inductances in a machine with a shorter air gap (conductors in slots) are larger than in a machine with a wider gap (conductors in air gap), keeping all other machine parameters unchanged. Besides, transfer of I^2R losses to the cooling air generates less temperature gradient if conductors are directly exposed to the air, than if they are placed in slots.

Conductors in slots are usually insulated against lamination and against each other. Their potential to the ground can reach dozens of kV. Uninsulated conductors (bars) are employed in squirrel cage induction machines and in damper cages of synchronous machines. Insulated conductors are manufactured either as round, or rectangular. Coils with rectangular conductors are more labor-intensive to manufacture than coils with round conductors.

Slot fill factor is an important parameter which determines the machine's rated power. The slot fill factor is equal to the ratio between total conductor area in a slot and slot area. Obviously, the highest slot fill factor (close to one) is achieved by using uninsolated conductors, followed by solid rectangular conductors in rectangular slots with form-wound coils (about 0.7, depending on the rated voltage). Slot fill factor of a coil with random-wound conductors is worse due to two reasons: There is always a space between round conductors in a slot, even when they are ideally aligned parallel to each other. Besides, round conductors are very hard to bring parallel to each other in a slot, as shown in Fig. 2.1a—their position in a slot is more or less chaotic, as shown in Fig. 2.1b. These two reasons limit typical slot fill factor for coils with random-wound conductors to the amounts between 0.4 and 0.5.

Windings of electric machines are usually impregnated with resin, which, among others, improves heat transfer from conductors in slot to air gap and lamination.

The influence of slot fill factor f_{Cu} on the amount of machine's rated power will be illustrated by the following example: a slot with area S_{slot} should generate the MMF of $w \cdot I$ ampere-turns when fed by current I. The I^2R losses in a conductor are equal to

$$P_{cond} = I^2 \rho \frac{l_{ax}}{S_{cond}} \tag{2.1}$$

where S_{cond} denotes the cross-sectional area of a single conductor, and ℓ_{ax} its axial length in the slot. The total I^2R losses generated by w conductors, P_{coil}, are w times larger

$$P_{coil} = w \cdot I^2 \rho \frac{l_{ax}}{S_{cond}} = (w \cdot I)^2 \rho \frac{l_{ax}}{S_{coil}} = (w \cdot I)^2 \rho \frac{l_{ax}}{f_{Cu} \cdot S_{slot}} \tag{2.2}$$

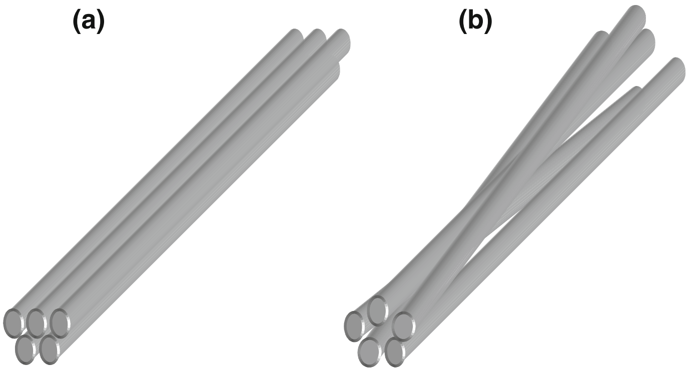

Fig. 2.1 Position of round conductors in a slot: idealized (**a**), and actual (**b**)

where $S_{coil} = w \cdot S_{cond}$. Temperature drop $\Delta\vartheta$ across the insulation layer with thickness d is equal to

$$\Delta\vartheta = \frac{P}{\lambda}\frac{d}{A} \tag{2.3}$$

with P denoting the heat power, λ the thermal conductivity of insulation, and S the area of surface through which the heat spreads. The average temperature drop across insulation can be evaluated by using equivalent slot geometry, as shown in Fig. 2.2.

The equivalent slot as shown in Fig. 2.2c carries a single fictitious conductor, the area of which is equal to the area of actual coil, $S_{coil} = w \cdot h$. The equivalent insulation with thickness d is uniformly distributed around the coil and has the total area S_{ins} of

$$S_{ins} = 2d(h + w) = S_{slot} - S_{coil} = (1 - f_{Cu})S_{slot} \tag{2.4}$$

from which one can write

$$d = S_{slot}\frac{1 - f_{Cu}}{2(h + w)} \tag{2.5}$$

Temperature drop $\Delta\vartheta$ across the insulation layer with thickness d can now be written as

$$\Delta\vartheta = \frac{P_{coil}}{\lambda \cdot l_{ax}} S_{slot}\frac{1 - f_{Cu}}{4(h + w)^2} \tag{2.6}$$

After inserting expression (2.2) for coil losses into Eq. (2.6), one obtains

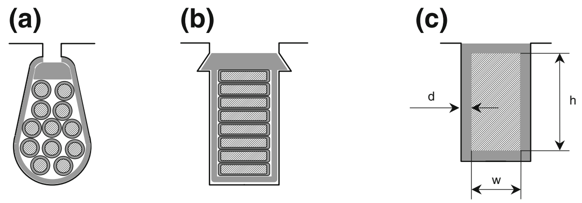

Fig. 2.2 Slot with round (**a**) and rectangular (**b**) conductors and equivalent slot geometry for thermal computations (**c**)

$$\Delta\vartheta = \frac{(w \cdot I)^2}{f_{Cu}}\frac{\rho}{\lambda}\frac{1 - f_{Cu}}{4(h + w)^2} \tag{2.7}$$

For a given temperature drop $\Delta\vartheta$ across the insulation the slot ampere-turns are proportional to

$$w \cdot I \propto \sqrt{\frac{f_{Cu}}{1 - f_{Cu}}} \tag{2.8}$$

which means that slot ampere-turns created by rectangular conductors with $f_{Cu} = 0.7$ are by a factor of

$$\sqrt{\frac{0.7}{1 - 0.7}}\Big/\sqrt{\frac{0.5}{1 - 0.5}} = 1.53 \tag{2.9}$$

larger than slot ampere-turns created by round conductors with $f_{Cu} = 0.5$, considering identical equivalent slot geometry, as shown in Fig. 2.2.

2.2 Single- and Double-Layer Windings, Coil Pitch, Skewing, Feasibility

Polyphase windings for rotating field machines are usually built to satisfy *phase symmetry condition*, which requires identical winding distribution for each phase, and *pole symmetry condition*, which specifies identical winding distribution under each (fundamental) pole. From the point of view of placement in slots, a winding can be carried out as a single layer, double layer, or mixed [2].

Integer slot windings create identical air gap flux density distribution under each pole pair. *Fractional slot windings* produce air gap flux density distributions the fundamental interval of which is larger than one pole pair. An integer slot winding is a special case of fractional slot winding—the coil distribution in an integer slot winding repeats under every pole, whereas the coil pattern in a fractional slot winding spreads over a *fundamental pole*, which comprises an odd number of machine poles.

Fig. 2.3 Coil of a single-layer winding

Integer slot windings can be designed to generate the air gap flux density distribution spectra in which the strongest harmonics are the fundamental and the slot harmonics of the order $N/p \pm 1$. Therefore, integer slot windings can be utilized in both induction and synchronous machines. Fractional slot windings generate spectra in which arbitrary harmonics can dominate. As such, they are suitable for synchronous machines only.

Probably the simplest winding configuration imaginable is the one in which all conductors in a slot belong to a single coil, or a **single-layer winding**, as shown in Fig. 2.3. The total number of coils of a single-layer winding is $N/2$, N denoting the number of slots, since each coil occupies two slots.

Depending on the form of coil ends, single-layer windings are manufactured either as *concentric*, or *distributed*. Both topologies can generate identical MMF distribution as long as the conductor placement in slots is identical.

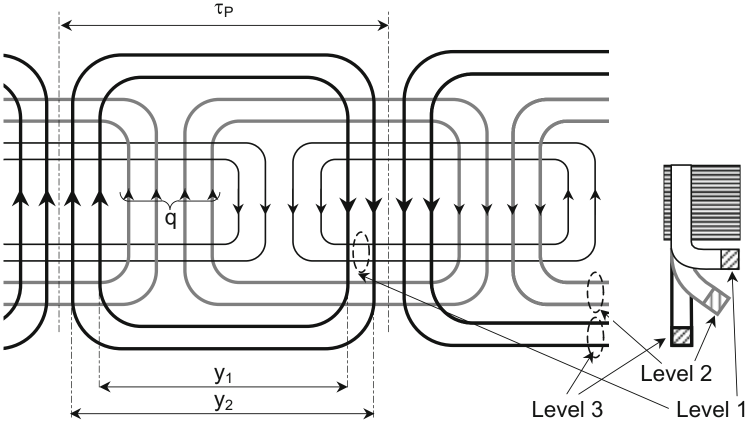

Fig. 2.4 Single-layer concentrated three-phase winding with coil ends manufactured in 3 levels and $q = 4$ slots per pole and phase. Assuming that all coils are wound in the same way, the arrows show direction of slot ampere-turns at time instant when the current in one phase is maximal

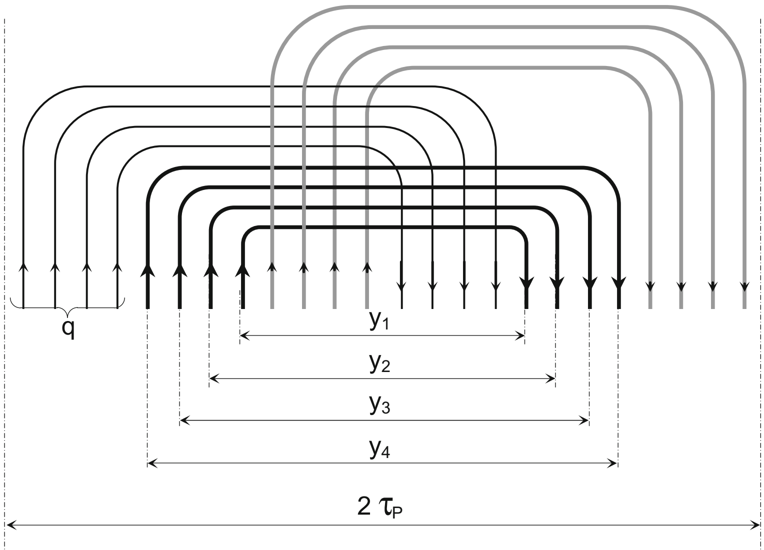

Fig. 2.5 Single-layer concentrated three-phase winding with coil ends manufactured in 3 levels and $q = 4$ slots per pole and phase. Stator with such winding is separable every 2 poles

The most important parameter of a coil is its *pitch*, or the circumferential distance in air gap given in number of teeth between the left-hand side and the right-hand side of a coil. *Winding pitch*, on the other hand, depends on several parameters and can be equal to the coil pitch for some winding topologies. Coils in concentric windings have different pitches and can spread either through three (Figs. 2.4 and 2.5), or two levels (planes) in the end winding zone (Fig. 2.6). The innermost coil of a concentric winding has the shortest pitch (e.g., y_1 as shown in Fig. 2.5), and the outermost coil the largest geometric pitch (y_4 as shown in Fig. 2.5). The winding pitch y of a single-layer concentric winding, defined as the arithmetic mean of all coil pitches, is less or equal to the pole pitch τ_p.

The *zone width q* of a single-layer concentrated winding (Fig. 2.5) is equal to the number of slots under one pole which belong to the same phase, i.e., which generate the same ampere-turns. The zone width is expressed either as a number of slots per pole and phase, $q = N/(2 \cdot p \cdot m)$, or as an electrical angle π/m, m denoting the number of phases.

If the stator outer diameter is too large, its lamination can be segmented in circumferential direction and wound with single-layer windings with 3 coil end levels as shown in Fig. 2.5.

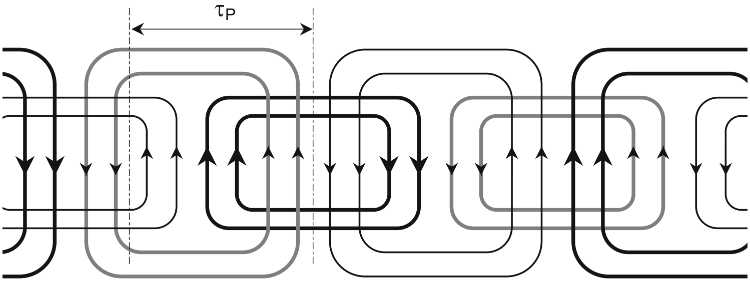

Fig. 2.6 Single-layer concentrated three-phase winding with coil ends manufactured in 2 levels and $q = 2$ slots per pole and phase

Single-layer windings with coil ends manufactured in 2 levels have shorter end windings than those with 3-level coils. Besides, they make use of only two different coil shapes. However, their end coils are concatenated in such a way that they do not allow for segmentation without cutting a coil group belonging to one phase, as shown in Fig. 2.6.

Field windings of synchronous machines are manufactured with concentric coils, as shown in Fig. 2.7. Coil ends are placed next to each other in axial direction and supported against centrifugal forces. The outermost slots are sometimes manufactured with smaller height in order to reduce the level of saturation in poles.

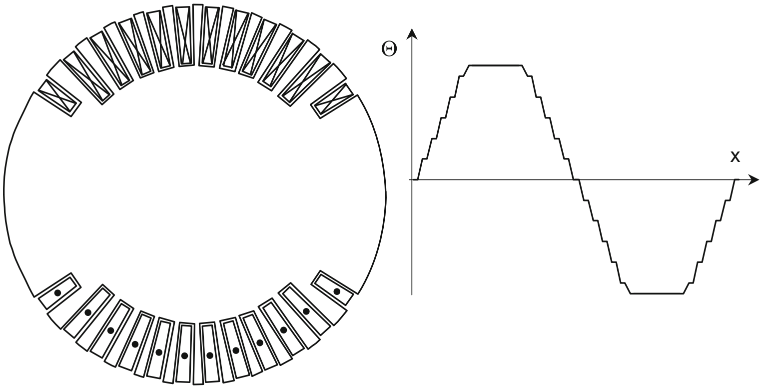

Fig. 2.7 Single-layer winding with concentric coils

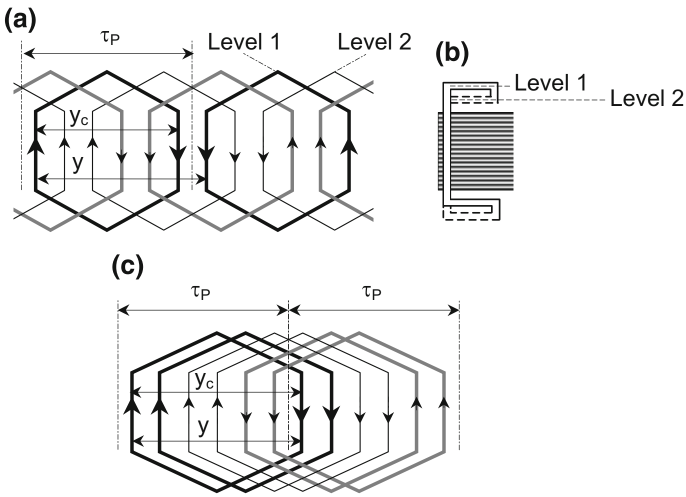

Fig. 2.8 Single-layer distributed three-phase lap windings (**a**), (**c**) and their end winding form (**b**). Winding shown in (**a**) has coil pitch y_c different from, and in (**c**) equal to the winding pitch τ_p. Winding (**c**) allows for segmentation in circumferential direction

Distributed single-layer windings can be manufactured as *wave* or *lap* (Fig. 2.8). Wave windings require less welding, because one phase group (parallel circuit) can be manufactured in a single production stage. All coils of a distributed single-layer lap winding have pitch y_c, which is not necessarily equal to the pole pitch τ_p.

A single-layer distributed winding can be short-pitched (chorded) for the amount of 0, 1, 3, 5, 7, …, etc., slots if the number of slots per pole and phase q is even, as shown in Fig. 2.9. If q is odd, as shown in Fig. 2.10, a single-layer distributed winding can be short-pitched for 0, 2, 4, 6, 8, …, etc., slots. Coil pitch chording for 1 slot has no influence on the winding pitch and, therefore, no influence on the air gap MMF distribution. Chording for more than 1 slot results in phase interleaving (Figs. 2.9 and 2.10). Chorded coils in windings with odd values of q cannot be symmetrically distributed in a two-pole interval. As a result, even harmonics in the air gap MMF distribution are generated, as shown in Fig. 2.10.

Coils of a single-layer distributed winding get themselves in the way because a slot occupied by conductors of one coil cannot be used by conductors of other coils. Such a rigid structure of single-layer windings limits substantially the field of possible applications.

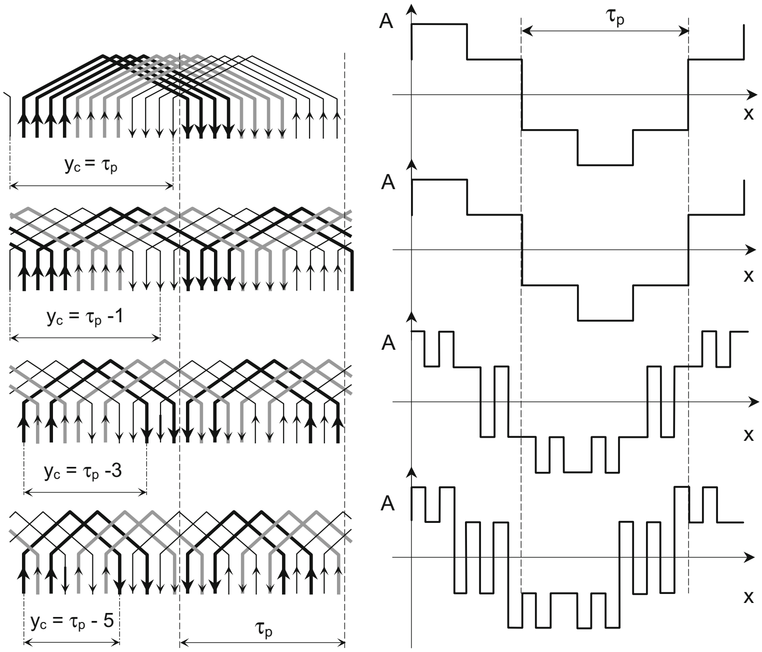

Fig. 2.9 Single-layer distributed three-phase lap windings with $q = 4$ slots per pole and phase and different coil pitch y_c (*left*) and current sheet A at a time instant of maximal current in one phase (*right*). The lower two windings are chorded for more than one slot and, therefore, interleaved

Double-layer windings offer much more freedom in creating air gap MMF distribution than single-layer windings. Each slot of a double-layer winding carries conductors of two coils, which belong either to separate phases (so-called *mixed slots*), or to the same phase (*monoslots*). One side of a coil of symmetrical double-layer winding lies in the bottom layer of one slot, and the other coil side in the top layer of another slot (Fig. 2.11). Thus the number of coils of a double-layer winding equals to the number of slots in which it is placed.

Since the two layers in a slot belong to separate coils, the coil pitch can be selected arbitrarily. Higher harmonics of air gap MMF created by a double-layer winding can be controlled more precisely than for a single-layer winding, which makes the double-layer winding the mostly spread winding type at all.

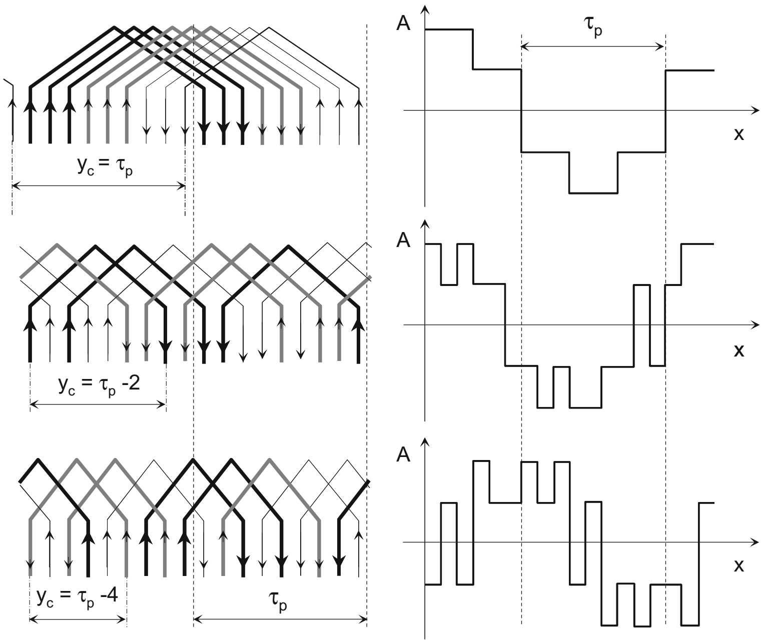

Fig. 2.10 Single-layer distributed three-phase lap windings with $q = 3$ slots per pole and phase and different coil pitch y_c (*left*) and current sheet A at a time instant of maximal current in one phase (*right*). The lower two windings are interleaved and asymmetrically distributed over two poles. As a result, even harmonics of current sheet and air gap MMF are generated

On the other hand, the slot fill factor of a double-layer winding is not as good as in case of a single-layer one, because the two layers have to be insulated against each other. This aspect is especially important in medium voltage machines, which anyway have thick coil insulation.

A comparison of properties of single and double-layer winding is given in Table 2.1.

Fig. 2.11 Coil placement in a double-layer winding

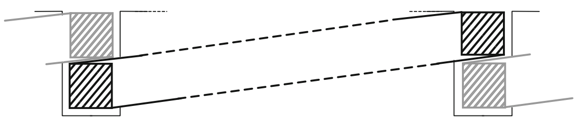

Table 2.1 Comparison of winding-type properties

	Single layer	Double layer
Number of coils	$N/2$ for N slots	N for N slots
Coil pitch	Dependent on type	Arbitrary
Coil form	Dependent on type	Equal for all coils
Slot utilization	High	Moderate
End winding	Dependent on type	Compact
Mechanical strength	Moderate	High
Application	Predominantly small and medium machines	Unlimited

Mixed-layer windings combine single- and double-layer windings, as shown in Fig. 2.12. Coils of a mixed-layer winding are inserted into slots in accordance with their affiliation to a particular phase. In Fig. 2.12 the outermost coils can have twice the number of turns than the other ones if all slots have the same area. Alternatively, the slots for outermost coils can be made smaller than others, and all slots can have the same area. Windings as shown in Fig. 2.12 are suitable for automated production because first all coils of the phase A are inserted, after that all coils of the phase B and at the end all coils of the phase C.

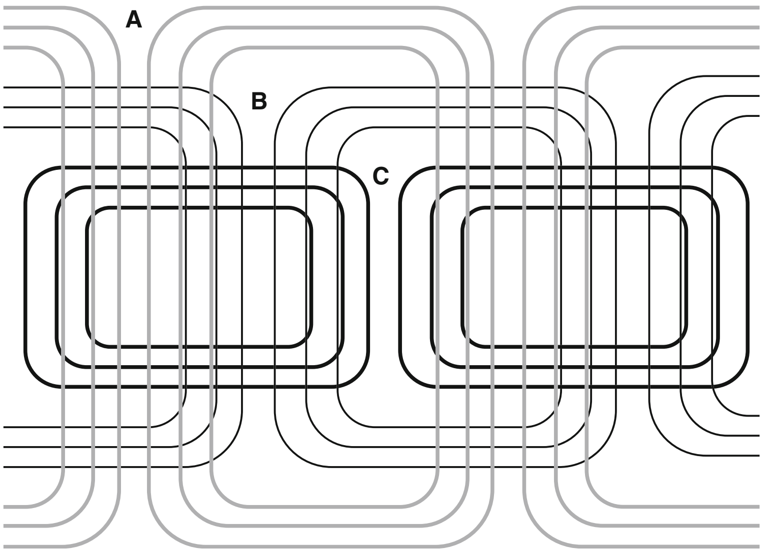

Fig. 2.12 Coil placement in a mixed-layer winding

2.3 Current Sheet and Air Gap MMF

The fundamental idea governing physical and engineering sciences is to build mathematical models of physical phenomena, which reflect all effects of interest for a particular phenomenon, and which are interpreted as physical laws. The simpler the model, the wider the area of its applications. Accordingly, an analytical model gives a significantly deeper insight into a particular phenomenon than its numerical counterpart. Therefore, a numerical model can at best complete machine analytical model, but in no case replace it.

Electric machines are complex 3D structures, the operation of which is based on magnetic circuits with nonlinear magnetic materials, in which electromagnetic quantities permanently change their values and direction in space. A detailed model of an electric machine, which would allow for all physical peculiarities at any time instant and at any point in the machine volume, could only be built as a numerical approximation. As such, it could deliver a quantitative solution to a particular problem at a given accuracy, but it would not allow a qualitative insight into physics of machine operation.

Obviously, the level of complexity has to be reduced if an analytical model of an electric machine should be built which represents the crucial machine properties. Effects neglected in such a model have marginal influence on the accuracy of results.

Analytical model of an electric machine is based on space-time representation of electromagnetic quantities in it, whereas the spatial coordinate is placed in the middle of the air gap and spreads in circumferential direction. Consequently, only the radial component of air gap flux density is considered. It is also assumed that the machine is infinitely long, which legalizes disregarding of axial components of field in its active part.

Winding distribution and affiliation of coils to a particular phase are expressed by means of *current sheet* A, an auxiliary quantity with a meaning of linear current density, defined as

$$A = \frac{i \cdot w}{b} \tag{2.10}$$

with b denoting the width of zone in the air gap in which w conductors, each of which carrying current i, are placed. The sign of current sheet is determined by the orientation of coil and by the current direction.

2.4 Spatial Harmonics in Air Gap MMF, Slot-Opening Factor, Winding Factors

The overwhelming majority of rotating field machines is built as heteropolar, with active part excited by coils the conductors of which are placed between two ferromagnetic structures schematically represented in Fig. 2.13. In general, the current sheet distribution $A(x)$ along the circumference does not necessarily have to be symmetrical with respect to the axis of winding.

In Fig. 2.13, the **x** and • marks within conductors denote products of coil orientation and current sign and, as such, can be interpreted as positive or negative. Orientation of a coil along with sign of current through it determines the sign of current sheet, MMF, and flux density. Therefore, not the current I, but the ampere-turns $I \cdot w$ are the primordial machine spatial quantity, since they carry both the information on the amount and direction of air gap fields.

If the relative permeability μ_r of stator and rotor iron is very large, μ_r >>, the whole MMF drop $\Theta(x)$ created by coil ampere-turns is spent on air gap and can be defined as

$$\Theta(x) = \int A(x)\mathrm{d}x \tag{2.11}$$

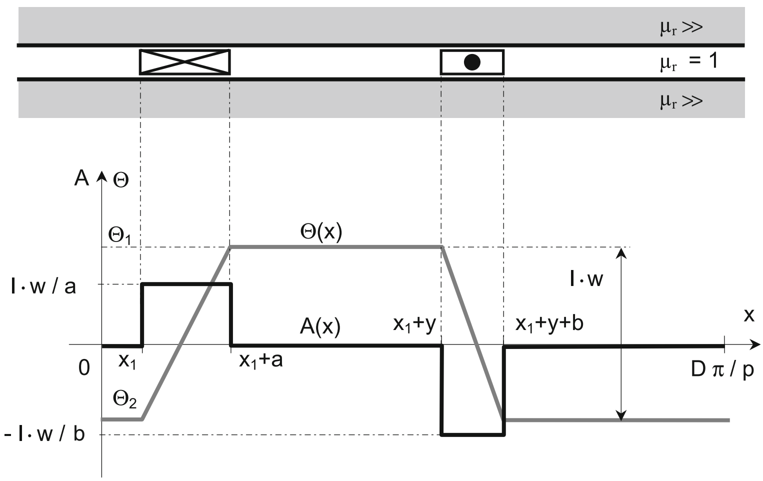

Fig. 2.13 Current sheet distribution $A(x)$ and its integral, the MMF distribution $\Theta(x)$ of an arbitrary coil

with x denoting the air gap circumferential coordinate and $A(x)$ the current sheet created by current I.

Constant MMFs Θ_1 and Θ_2 in Fig. 2.13 are evaluated as

$$\Theta_1 = \frac{2D\pi + p\cdot(a-2y-b)}{2D\pi}\cdot I\cdot w;\quad \Theta_2 = p\cdot\frac{a-2y-b}{2D\pi}\cdot I\cdot w \tag{2.12}$$

Air gap quantities are periodical functions of circumferential coordinate x with period length $2\tau_p$, τ_p being the pole pitch:

$$\tau_p = \frac{D\pi}{2p} \tag{2.13}$$

Spatial distribution $\Theta(x)$ can be expressed in terms of Fourier series as

$$\Theta(x) = \sum_{n=1}^{\infty}\Theta_n \sin n\frac{\pi}{\tau_p}x \tag{2.14}$$

with Θ_n denoting the amplitude of the nth harmonic of the air gap MMF. Fourier coefficients of MMF distribution in Fig. 2.13 are

$$a_0 = 0 \tag{2.15}$$

because there is no homopolar flux (div $\mathbf{B}$ = 0), and

$$a_n = \tau_p\cdot I\cdot w\frac{a\cdot\left[\cos n\frac{\pi}{\tau_p}(x_1+y) - \cos n\frac{\pi}{\tau_p}(x_1+y+b)\right] + b\cdot\left[\cos n\frac{\pi}{\tau_p}(x_1+a) - \cos n\frac{\pi}{\tau_p}x_1\right]}{n^2ab\pi} \tag{2.16}$$

$$b_n = \tau_p\cdot I\cdot w\frac{a\cdot\left[\sin n\frac{\pi}{\tau_p}(x_1+y) - \sin n\frac{\pi}{\tau_p}(x_1+y+b)\right] + b\cdot\left[\sin n\frac{\pi}{\tau_p}(x_1+a) - \sin n\frac{\pi}{\tau_p}x_1\right]}{n^2ab\pi} \tag{2.17}$$

Conventional windings are placed in slots, the width of which in the air gap is called *slot opening d*. Single coil per pole pair placed in slots on one side of air gap as illustrated in Fig. 2.14 generates the MMF distribution which can be expressed in terms of Fourier series with coefficients a_n and b_n:

$$a_n = \frac{2}{\pi}\frac{Iw}{n}\frac{\sin n\frac{d}{\tau_p}\frac{\pi}{2}}{n\frac{d}{\tau_p}\frac{\pi}{2}} \cdot \cos n\frac{\pi}{2} \cdot \sin n\frac{y}{\tau_p}\frac{\pi}{2} \tag{2.18}$$

$$b_n = \frac{2}{\pi}\frac{Iw}{n}\frac{\sin n\frac{d}{\tau_p}\frac{\pi}{2}}{n\frac{d}{\tau_p}\frac{\pi}{2}} \cdot \sin n\frac{\pi}{2} \cdot \sin n\frac{y}{\tau_p}\frac{\pi}{2} \tag{2.19}$$

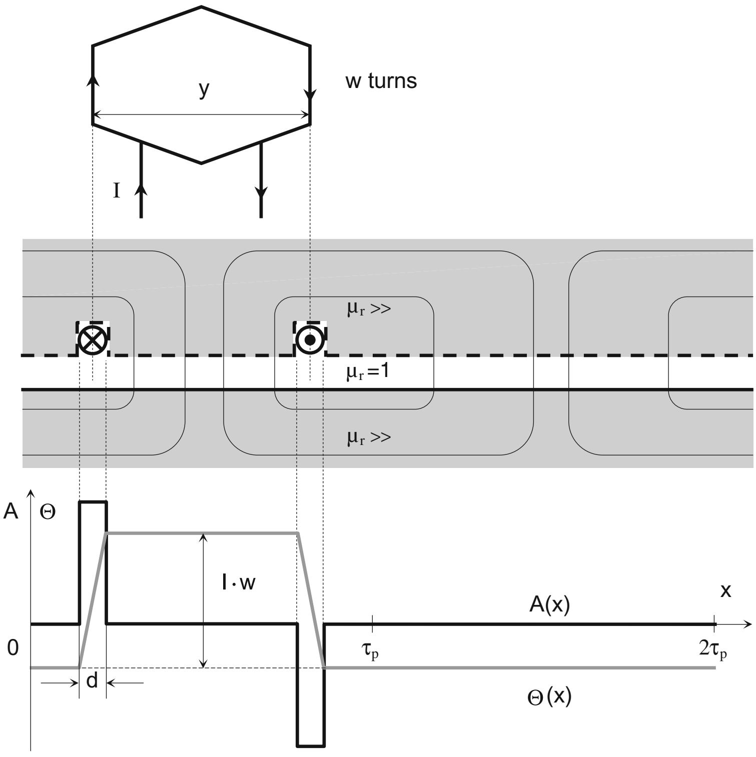

Fig. 2.14 Current sheet distribution $A(x)$ and its integral, the MMF distribution $\Theta(x)$ of single coil per pole pair

Fourier coefficients a_n and b_n are equal to the product of three factors, each of which is smaller or equal to one:

(a) *Slot-opening factor* $f_{o,n}$, defined for the nth harmonic as

$$f_{o,n} = \frac{\sin n\frac{d}{\tau_p}\frac{\pi}{2}}{n\frac{d}{\tau_p}\frac{\pi}{2}} \tag{2.20}$$

The slot-opening factor is a function of the ratio between the slot opening d and pole pitch τ_p. As long as the slot opening d is much smaller than the pole pitch τ_p, the slot-opening factor for the fundamental, $f_{o,1}$, is almost equal to one. Large slot openings, typical for tooth-wound machines, cause low slot-opening factors, thus diminishing resulting MMF and deteriorating machine performance.

(b) A *trigonometric indicator*, defined for cosine terms a_n as $\cos(n \cdot \pi/2)$ and for sine terms b_n as $\sin(n \cdot \pi/2)$. The indicator for cosine terms, $\cos(n \cdot \pi/2)$, is equal to zero for odd harmonics, and indicator for sine terms, $\sin(n \cdot \pi/2)$, is equal to zero for even harmonics. In other words, the phase shift of odd harmonics relative to the origin is equal to zero, and the phase shift of even harmonics relative to the origin is $\pm\pi/2$.

Every odd harmonic from Fourier approximation of MMF distribution has at least one zero crossing point identical with the zero crossing point of the fundamental. Accordingly, every odd harmonic has an extreme at the same point on the circumference where the fundamental is extreme. The character of extreme of adjacent odd harmonics alters permanently between maximum and minimum, as given by the indicator $\sin(n \cdot \pi/2)$. For this reason, the resultant effect of (odd) slot harmonics of MMF on the fundamental of air gap flux density is negligible (see discussion to Fig. 2.37).

(c) *Coil pitch factor* $f_{p,n}$, defined for the nth harmonic as

$$f_{p,n} = \sin n \frac{y}{\tau_{ps}} \frac{\pi}{2} \tag{2.21}$$

where τ_{ps} denotes the pole pitch expressed in number of slots

$$\tau_{ps} = \frac{N}{2p} \tag{2.22}$$

Coil pitch factor quantifies the MMF derogation due to pitching of coils. In extreme case when the product $n \cdot y/\tau_{ps}$ is an even number, the amplitude of the nth harmonic is equal to zero. The influence of coil pitch on the amplitude of the nth harmonic of air gap MMF can be illustrated by the example of the fifth harmonic of MMF created by a coil with pitch of $y/\tau_p = 4/5$, as shown in Fig. 2.15.

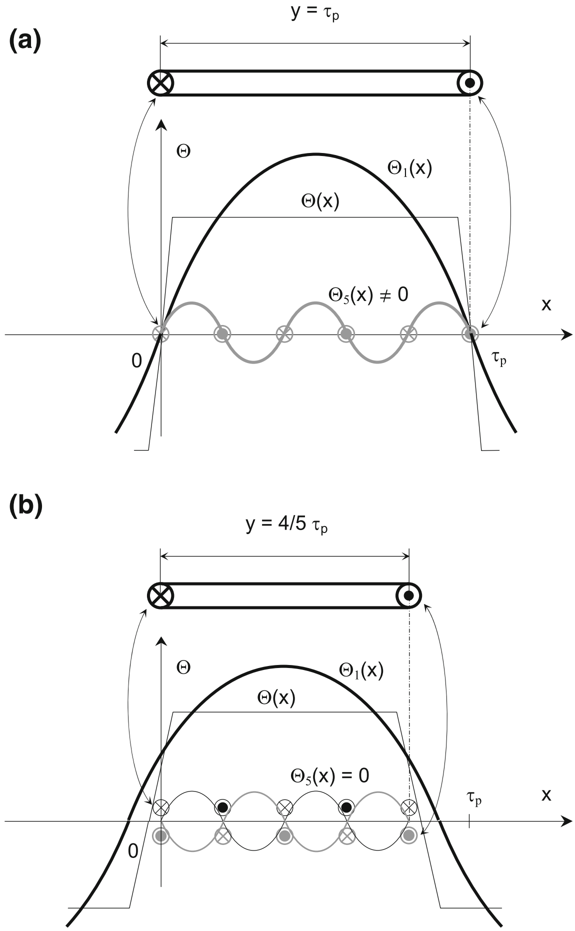

Fig. 2.15 MMF distributions created by a full-pitch coil per pole, $y = \tau_p$ (**a**), and a short-pitch coil per pole, $y = 4/5\ \tau_p$ (**b**). The fifth harmonic in the MMF distribution of the coil below vanishes

The full-pitch coil in Fig. 2.15a creates trapezoidal MMF distribution $\Theta(x)$. One can imagine that the fifth spatial harmonic of the MMF distribution $\Theta(x)$ is created by a fictitious winding, shown gray in Fig. 2.15a, with a coil pitch equal to $\tau_p/5$. At $x = 0$ and $x = \tau_p$, the direction of current and coil orientation of the real and the fictitious winding coincide, which means that the left and the right half of the real coil support each other when creating the fifth harmonic component of the MMF.

The ampere-turns of the left-hand side of the short-pitch coil in Fig. 2.15b with $y = 4/5\ \tau_p$ would create the fifth harmonic of the MMF identical to that drawn with solid black line, originated from fictitious winding with $y = \tau_p/5$. The same fictitious winding would, however, require the ampere-turns on the right-hand side of the coil (at $x = 4/5\ \tau_p$) acting in the *opposite* direction than the real ones created by the coil right portion.

If the ampere-turns of the fictitious winding with $y = \tau_p/5$ should coincide at $x = 4/5\ \tau_p$ with those created by the right-hand side of the real coil, the winding distribution drawn gray in Fig. 2.15b would be valid. This means that the fictitious coil should generate ampere-turns at $x = 0$ *opposite* to the real coil! Obviously, the sum of the black and gray distributions representing fictitious 5th harmonic is equal to zero when $y = 4/5\ \tau_p$.

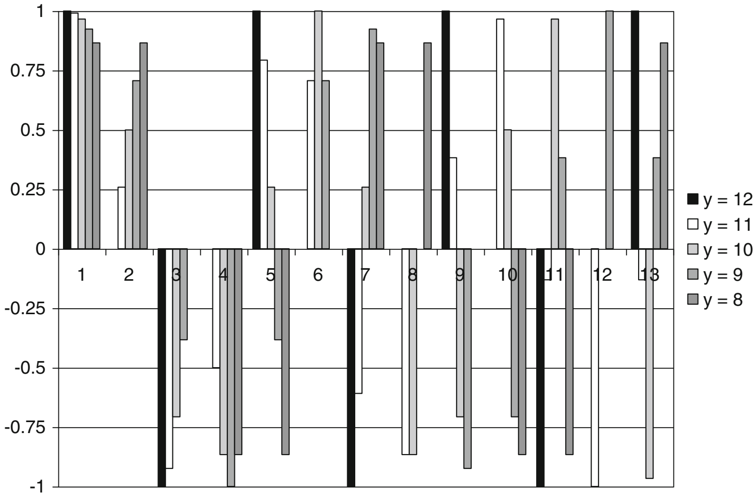

Fig. 2.16 p.u. values of coil pitch factors for higher spatial harmonics in a machine with 12 slots per pole and various values of coil pitch

Pitch factors in p.u. of the fundamental for various spatial harmonics in a machine with 12 slots per pole and various coil pitch values are shown in Fig. 2.16. Coil pitch shortening is a very powerful means for the minimization, or even elimination, of particular harmonics from the MMF distribution. The price paid is a (slight) decrease of the useful fundamental harmonic.

Absolute value of pitch factor for any spatial harmonic n for full-pitch coils ($y = \tau_p$) is equal to 1. By applying the coil shortening, the amplitudes of pitch factors become periodically dependent on harmonic order. One should note that, independently of the coil pitch to pole pitch ratio y/τ_p, spatial harmonics with order $N/p \pm 1$ have always the same pitch factor as the fundamental.

The amplitude c_n of nth harmonic of air gap MMF created by one coil per pole pair can be expressed by means of Eqs. (2.18) and (2.19) as

$$c_n = \sqrt{a_n^2 + b_n^2} = \frac{2}{\pi}\frac{Iw}{n}\frac{\sin n\frac{d}{\tau_p}\frac{\pi}{2}}{n\frac{d}{\tau_p}\frac{\pi}{2}} \cdot \sin n\frac{y}{\tau_p}\frac{\pi}{2} \qquad (2.23)$$

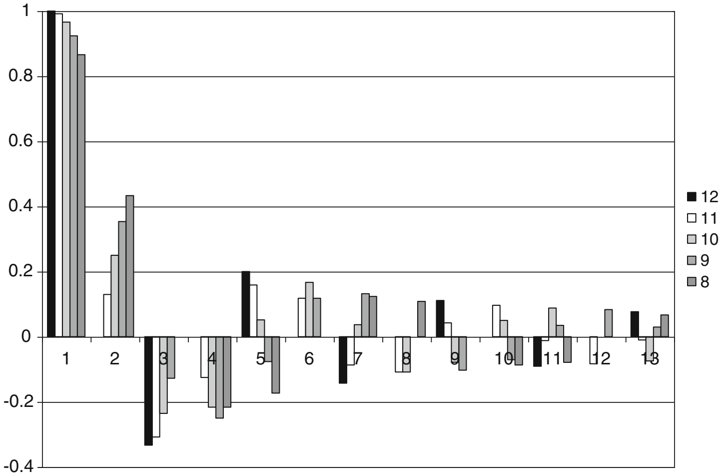

Fig. 2.17 p.u. amplitudes of MMF harmonics created by a single coil per pole pair in a machine with 12 slots per pole. The coil pitch varies between 8 and 12

One coil per pole pair with $y < \tau_p$ *generates both even and odd harmonics of air gap MMF, the amplitudes of which are approximately proportional to the reciprocal of their order*. This property is illustrated in Fig. 2.17, in which p.u. amplitudes of the first 13 harmonics created by a single coil per pole pair for variable values of coil pitch and for $\tau_p = 12$ are shown.

In Fig. 2.17 one can see that only a full-pitch coil per pole pair generates air gap MMF spectrum without even harmonics; as long as the coil is chorded, it acts as a source of both even and odd harmonics. Since a single full-pitch coil per pole pair creates identical MMF spectrum as a full-pitch coil per pole, one can state that even harmonics created by two full-pitch coils per pole pair act against each other.

Case Study 2.1: A 20-pole, 3-phase machine has 30 stator slots. Air gap diameter is 1200 mm and stator slot opening d = 56 mm. Stator winding has y = 1 (tooth-wound). Slot-opening and coil pitch factors of the stator winding along with % amplitudes of harmonics are listed in Table 2.2.

Table 2.2 Parameters of winding in Case Study 2.1

n	1	2	3	4	5	6	7	8
$f_{o,n}$	.99	.94	.87	.78	.67	.55	.42	.29
$f_{p,n}$	.87	.87	0	−.87	−.87	0	.87	.87
%	100	47.8	0	19.8	13.6	0	6.1	3.7

One recognizes in Table 2.2 that the stator winding generates extremely strong 2. and 4. harmonic of the air gap MMF. These harmonics increase substantially the air gap leakage inductance of the selected winding and create additional components of eddy current losses in solid rotor parts, along with pulsating torques on the shaft.

It is easy to demonstrate that not only two fully pitched, but also two identically chorded coils per pole pair generate even harmonics the sum of which is always equal to zero, because

$$\Theta_n \sin\left[n\frac{\pi}{\tau_p}\left(x-\tau_p\right)\right] = \Theta_n \sin\left(n\frac{\pi}{\tau_p}x - n\pi\right) = \Theta_n \sin n\frac{\pi}{\tau_p}x \tag{2.24}$$

for n even, and

$$\Theta_n \sin\left[n\frac{\pi}{\tau_p}\left(x-\tau_p\right)\right] = -\Theta_n \sin n\frac{\pi}{\tau_p}x \tag{2.25}$$

for n odd. Since the ampere-turns of coils under one (N) pole, $(I \cdot w)_N$, have an opposite sign than the ampere-turns under adjacent (S) pole, $(I \cdot w)_S$, odd harmonics created by coils of one pole support odd harmonics created by coils of adjacent pole. Even harmonics created by coils of one pole, on the other hand, act against even harmonics created by coils of adjacent pole.

Vast majority of windings in heteropolar machines is built in such a manner that the winding distribution pattern repeats on pole basis, see Fig. 2.18. As a result, only odd harmonics of air gap MMF can be generated, the amplitudes of which are

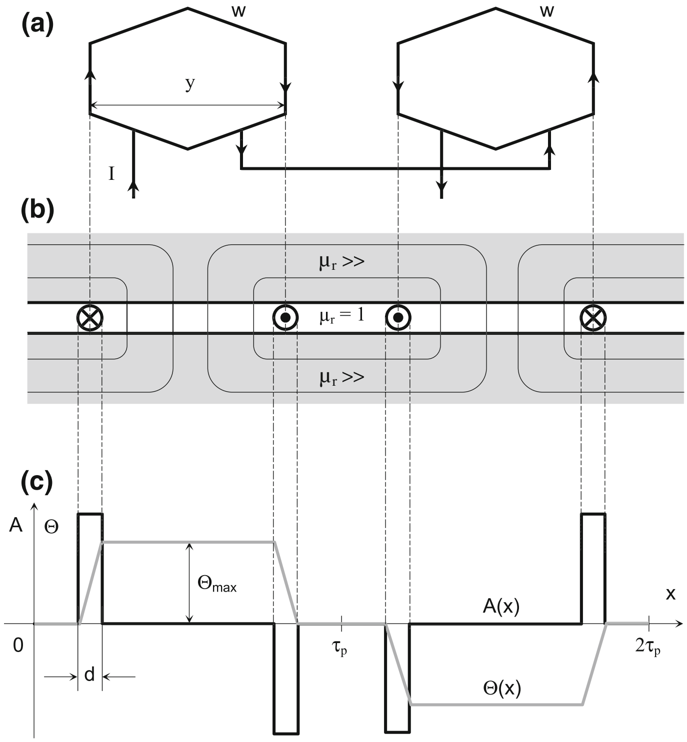

Fig. 2.18 Schematic representation (**a**) of coils in the air gap (**b**), along with the current sheet $A(x)$ and MMF $\Theta(x)$ distributions created by positive current I flowing through the coils (**c**). For distributions $A(x)$ and $\Theta(x)$ it is irrelevant whether the coils are placed in slots, or directly in the air gap

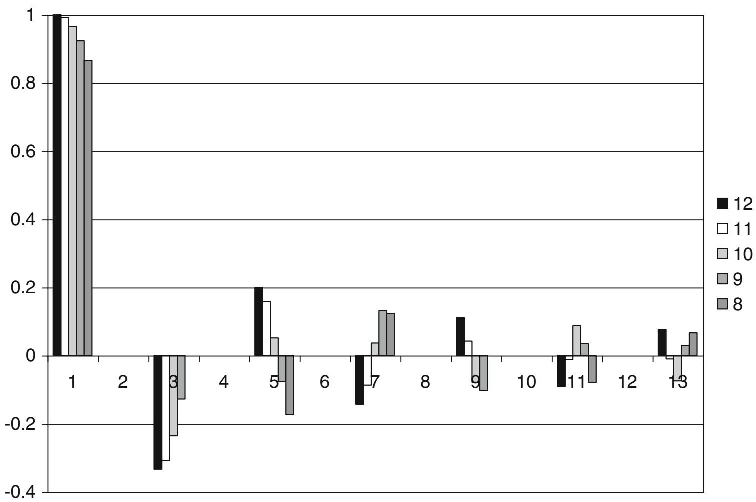

Fig. 2.19 p.u. amplitudes of MMF harmonics created by one coil per pole in a machine with 12 slots per pole. The coil pitch varies between 8 and 12

$$a_n = \frac{4}{\pi}\frac{Iw}{n}\frac{\sin n\frac{d}{\tau_p}\frac{\pi}{2}}{n\frac{d}{\tau_p}\frac{\pi}{2}} \cdot \sin n\frac{\pi}{2} \cdot \ \sin n\pi \cdot \sin n\frac{y}{\tau_p}\frac{\pi}{2} \equiv 0 \tag{2.26}$$

because n is odd, and

$$b_n = \frac{4}{\pi}\frac{Iw}{n}\frac{\sin n\frac{d}{\tau_p}\frac{\pi}{2}}{n\frac{d}{\tau_p}\frac{\pi}{2}} \cdot \sin n\frac{\pi}{2} \cdot \sin n\frac{y}{\tau_p}\frac{\pi}{2} \tag{2.27}$$

MMF spectra of one coil per pole with identical data as in Fig. 2.15 are shown in Fig. 2.19.

Pole symmetry (identical winding distribution under each pole) eliminates even harmonics in air gap MMF spectrum. Even harmonics in air gap MMF spectrum are a sign of pole asymmetry, caused typically by winding short turns. If p [p.u.] turns under one pole are short-circuited, Fourier coefficients of air gap MMF spectrum can be expressed as

$$a_n = \frac{2}{\pi}\frac{Iw}{n}\frac{\sin n\frac{d}{\tau_p}\frac{\pi}{2}}{n\frac{d}{\tau_p}\frac{\pi}{2}} \cdot \ \sin n\frac{y}{\tau_p}\frac{\pi}{2} \cdot \left[\cos n\frac{\pi}{2} - (1-p)\cos 3n\frac{\pi}{2}\right] \tag{2.28}$$

$$b_n = \frac{2}{\pi}\frac{Iw}{n}\frac{\sin n\frac{d}{\tau_p}\frac{\pi}{2}}{n\frac{d}{\tau_p}\frac{\pi}{2}} \cdot \ \sin n\frac{y}{\tau_p}\frac{\pi}{2} \cdot \left[\sin n\frac{\pi}{2} - (1-p)\sin 3n\frac{\pi}{2}\right] \tag{2.29}$$

The amplitude c_n of nth harmonic is equal to

$$c_n = \frac{2}{\pi}\frac{Iw}{n}\frac{\sin n\frac{d}{\tau_p}\frac{\pi}{2}}{n\frac{d}{\tau_p}\frac{\pi}{2}} \cdot \sin n\frac{y}{\tau_p}\frac{\pi}{2} \cdot \sqrt{1 - 2\cdot(1-p)\cdot\cos n\pi + (1-p)^2} \tag{2.30}$$

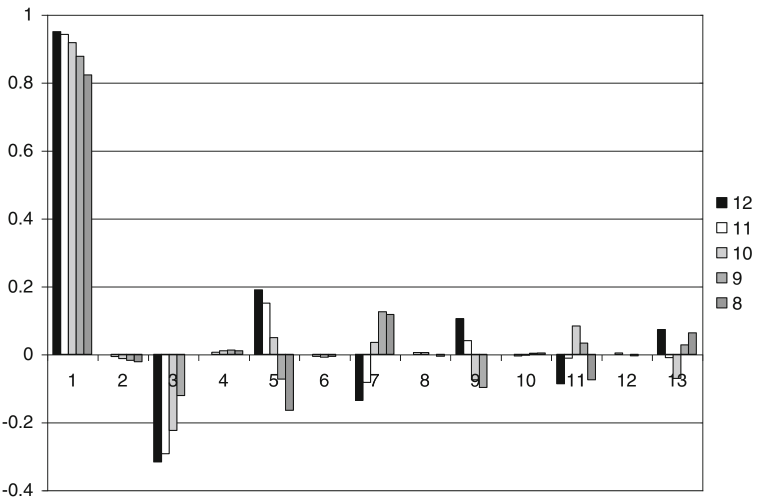

Fig. 2.20 p.u. amplitudes of MMF harmonics created by one coil per pole in a machine with 12 slots per pole for pole asymmetry of p = 0.1 p.u. The coil pitch is varied between 8 and 12

The influence of pole asymmetry on amplitudes of air gap MMF harmonics in a machine with 12 slots per pole is shown in Fig. 2.20. The machine is assumed to have 10 % less turns under one pole (p = 0.1 p.u.) than under another. Besides general decrease of amplitudes of odd harmonics (less ampere-turns!), one recognizes the appearance of even harmonics in Fig. 2.20, the amplitudes of which are dependent on coil pitch y.

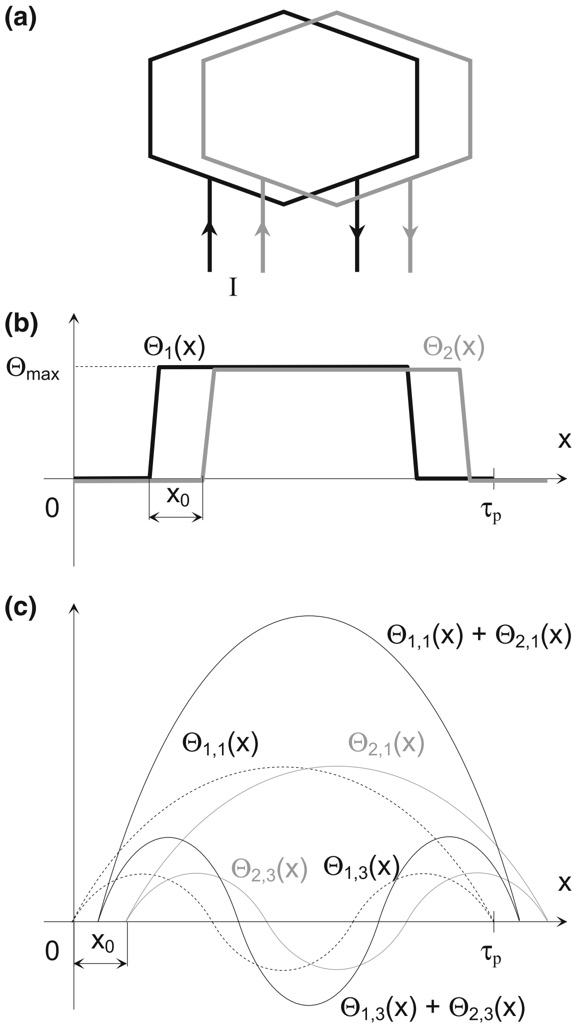

Fig. 2.21 Two coils shifted for x_0 to each other (**a**), their MMF distributions (**b**), and the fundamental and third components of MMF created by each coil (**c**)

Phase windings of electric machines are seldom wound with only one coil per pole. Putting phase coils into adjacent slots under a pole is a further means to suppress higher spatial harmonics. In Fig. 2.21 two coils shifted for the amount of x_0 are shown along with their air gap MMF distributions.

The shift x_0 of the two coils along circumferential coordinate in Fig. 2.21 does not have the same impact on all spatial harmonics of their MMFs, because the higher the order of harmonics n, the bigger the spatial shift $x_{0,n}$

$$x_{0,n} = n \cdot x_0 \tag{2.31}$$

The amplitude $\Theta_{\mathrm{res},1,\max}$ of the fundamental component of the resulting MMF in Fig. 2.21c, $\Theta_{\mathrm{res},1}(x) = \Theta_{1,1}(x) + \Theta_{2,1}(x)$ can be evaluated by using the trigonometric identity

$$\sum_{j=1}^{k} \cos[\alpha + (j-1)\cdot\delta] = \frac{\cos\left(\alpha + \frac{k-1}{2}\delta\right)\cdot \sin\frac{k\cdot\delta}{2}}{\sin\frac{\delta}{2}} \tag{2.32}$$

and setting for $\alpha = 0$, $k = 2$:

$$1 + \cos\delta = \frac{\cos\frac{\delta}{2}\cdot \sin\delta}{\sin\frac{\delta}{2}} = 2\cos^2\frac{\delta}{2} \tag{2.33}$$

which helps one define $\Theta_{\mathrm{res},1,\max}$

$$\Theta_{\mathrm{res},1,\max} = \Theta_{1,\max}\sqrt{(1+\cos\alpha_0)^2 + \sin^2\alpha_0} = \Theta_{1,\max}\sqrt{2\cdot(1+\cos\alpha_0)} \tag{2.34}$$

as

$$\Theta_{\mathrm{res},1,\max} = 2\cdot\Theta_{1,\max}\cos\frac{\alpha_0}{2} \tag{2.35}$$

with $x_0 = R \cdot \alpha_0$, R denoting the air gap radius.

The ratio between the trigonometric and algebraic sum of amplitudes of MMFs created by adjacent coils under one pole is called the *zone factor*, which in case of two coils per zone can be written for the fundamental harmonic as

$$\frac{\Theta_{\mathrm{res},1,\max}}{2\cdot\Theta_{1,\max}} = \cos\frac{\alpha_0}{2}$$

and for a spatial harmonic of the order n

$$\frac{\Theta_{\mathrm{res},n,\max}}{2\cdot\Theta_{n,\max}} = \cos n\frac{\alpha_0}{2}$$

One recalls that the expression for the zone winding factor of the *n*th harmonic, $f_{z,n}$:

$$f_{z,n} = \frac{\sin\frac{nq\alpha_0}{2}}{q\,\sin\frac{n\alpha_0}{2}} \tag{2.36}$$

turns into $\cos(n \cdot \alpha_0/2)$ for $q = 2$.

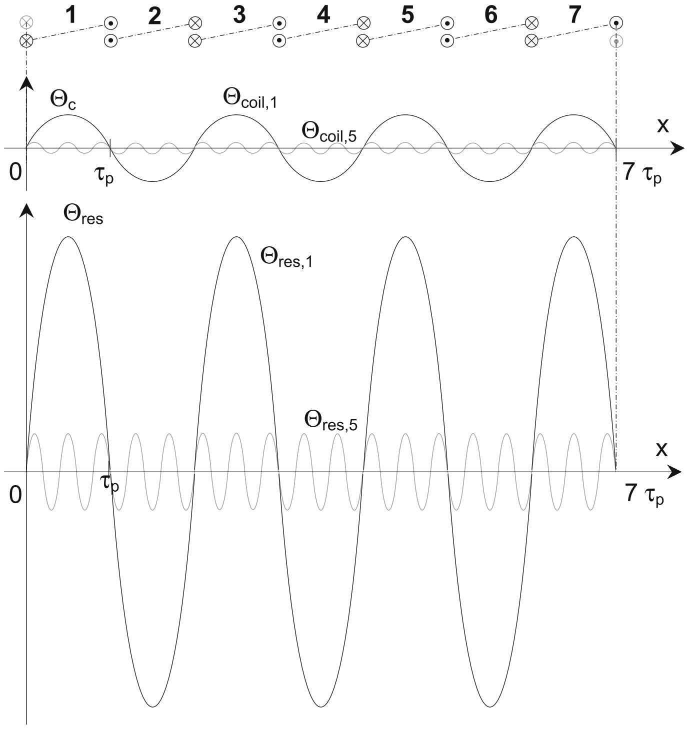

Fig. 2.22 Symmetrical integer slot winding with one coil per pole and phase: coil MMF distribution Θ_c repeats from pole to pole, making the resulting MMF equal to the algebraic sum of coil MMFs, both for the fundamental $\Theta_{coil,1}$ and for the fifth harmonic $\Theta_{coil,5}$

In high-polarity electric machines there is often not enough space for more than one coil per phase under one pole. Both previously discussed countermeasures against high spatial harmonics—chording the coil pitch, or connecting more coils in series under each pole—obviously cannot be applied in this case. Therefore, other means for control of spatial higher harmonics has to be employed: the undesirable harmonics are not compensated within one pole, but within several poles. The winding pattern repeats every *fundamental pole*, the width of which is an odd multiple of the pole pitch τ_p. One refers to *fractional slot winding* in which the number of slots per pole and phase q is not an integer.

In order to illustrate the principle of higher harmonics minimization in a fractional slot winding the air gap MMF distribution in a 84-pole, 3-phase machine with 252 slots and $q = 252/(84 \cdot 3) = 1$ (Fig. 2.22) is compared with air gap MMF distribution in an 84-pole, 3-phase machine with 288 slots, $q = 288/(84 \cdot 3) = 8/7$, as shown in Fig. 2.23. In particular, the influence of winding connection on the resulting fundamental and fifth harmonic is analyzed.

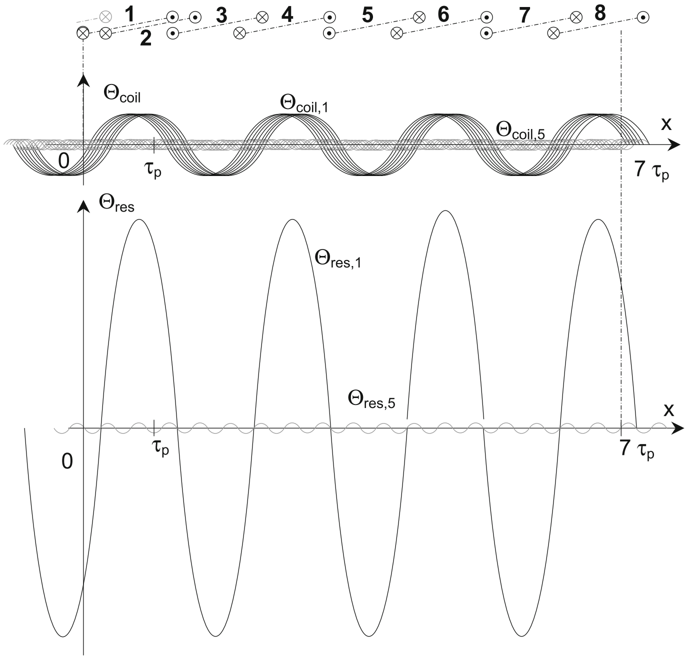

Fig. 2.23 Symmetrical fractional slot winding with $q = 8/7$ coil per pole and phase. The fundamental and 5 harmonic components of all coils are shown

For $q = 1$, as shown in Fig. 2.22, the resulting MMF is equal to the algebraic sum of MMFs created by all coils. In the resulting MMF the ratio between the amplitude of the fifth harmonic and the fundamental term is equal to the ratio between the amplitude of the fifth harmonic and the fundamental term of a coil.

The MMF distribution in a machine with $q = 8/7$, shown in Fig. 2.23, is for the fifth spatial harmonic completely different from that in a machine with $q = 1$. In a machine with fractional slot winding the period length of the winding distribution corresponds to the fundamental pole. A fundamental pole of the winding in Fig. 2.23 with $q = 8/7$ includes seven machine poles. Each phase of the analyzed winding has eight coils per fundamental pole, denoted by numbers 1–8. The coils are connected to each other in such a manner as to maximize the resulting fundamental, and minimize higher harmonics. The sequence of connection of coils in Fig. 2.23 is $1 \rightarrow 4 \rightarrow 6 \rightarrow 8 \rightarrow -3 \rightarrow -5 \rightarrow -7 \rightarrow 2$, with negative signs standing for a reversely connected coils. This sequence of coil connections shifts fundamentals slightly to each other. On the other hand, the fifth harmonic components are significantly shifted to each other. Ultimately, the resulting fundamental component is slightly lower than the algebraic sum of coil MMFs, whereas the resulting fifth harmonic is drastically reduced.

2.5 Air Gap Permeance, Carter Factor, Air Gap Flux Density Distribution

Air gap flux density is the crucial quantity in an electric machine, since it determines both the induced voltage and the torque, the two most important machine attributes. Spatial distribution of air gap flux density, including all higher harmonics, determines time dependencies of induced voltages, torque, and radial forces. Therefore, special attention has to be paid to the proper shaping of the air gap flux density distribution.

Neglecting the MMF drop in iron, one can write for the air gap flux density distribution $B_\delta(x)$:

$$B_\delta(x) = \mu_0 \cdot H_\delta(x) = \mu_0 \frac{\Theta(x)}{\delta(x)} \tag{2.37}$$

i.e., the amount of flux density at a particular point in air gap is proportional to the MMF and inversely proportional to the air gap width at that point.

Windings of electric machines are usually placed in slots separated by teeth, which provide mechanical support. The price for mechanical fixation of windings by putting them into slots is a loss of flux expressed by the Carter factor.

In a machine with **single-slotted air gap** and constant excitation over slots and teeth, the air gap flux density $B(x)$ is minimal along slot centerline (Fig. 2.24). The flux density distribution $B(x)$ can be represented in terms of its average value and fundamental harmonic due to slotting as

$$B_\delta(x) = B_0 + B_s \cos\frac{\pi}{\tau_s} x \tag{2.38}$$

where

$$B_0 = \frac{B_{max} + B_{min}}{2}; \quad B_s = \frac{B_{max} - B_{min}}{2} \tag{2.39}$$

B_s denotes here the amplitude of the fundamental component of air gap flux density due to slotting, and B_0 its average value over one slot pitch τ_s.

The Carter factor k_C is defined as

$$k_C = \frac{\tau_s}{\tau_s - \gamma \cdot \delta} \tag{2.40}$$

and the effective air gap width δ_{eff}:

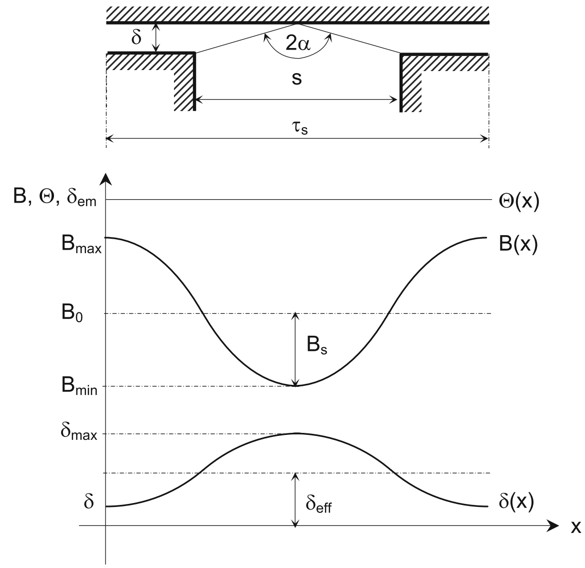

Fig. 2.24 Dominating components of air gap flux density $B(x)$ and electromagnetic air gap width $\delta_{em}(x)$ at constant MMF

$$\delta_{eff} = k_C \cdot \delta \tag{2.41}$$

where

$$\gamma = \frac{4}{\pi}\left[\frac{s}{2\delta}\arctan\frac{s}{2\delta} - \ln\sqrt{1+\left(\frac{s}{2\delta}\right)^2}\right] \tag{2.42}$$

Not the geometrical distance δ between smooth and slotted surface, but the effective air gap width $\delta_{eff} = k_C \cdot \delta$ determines the ampere-turns demand for a given flux density. Carter factor is a function of the ratio between the slot opening s and slot pitch τ_s, and the ratio between the air gap width δ and slot pitch τ_s. By keeping the slot-opening constant for a given slot pitch, the Carter factor decreases as the air gap width increases. On the other hand, by keeping the air gap width for a given slot pitch constant, the Carter factor increases as the slot opening increases.

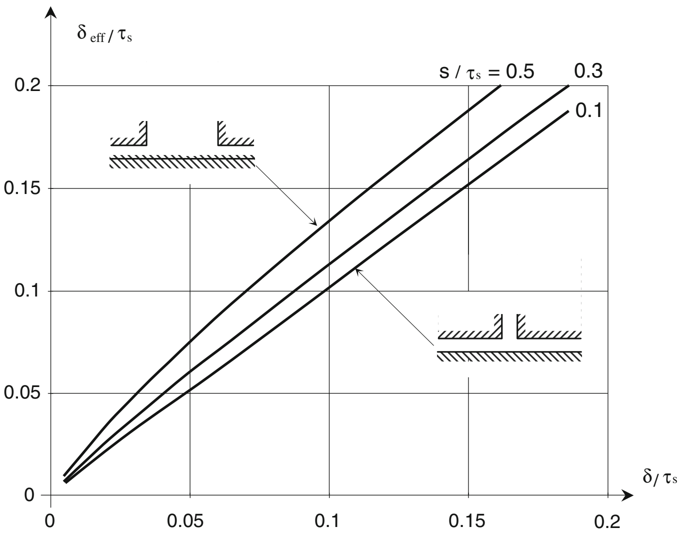

Fig. 2.25 Dependence of normalized effective air gap width δ_{eff}/τ_s on normalized air gap width δ/τ_s with normalized slot opening s/τ_s as a parameter

The analysis of Carter factor can be simplified by normalizing the air gap width and the slot opening to the slot pitch of 1 p.u. Introduce first the normalized air gap width δ_N:

$$\delta_N = \frac{\delta}{\tau_s} \tag{2.43}$$

and the normalized slot width s_N:

$$s_N = \frac{s}{\tau_s} \tag{2.44}$$

The Carter factor can be now written as

$$k_C = \frac{1}{1 - \gamma \cdot \delta_N} \tag{2.45}$$

and the auxiliary function γ

$$\gamma = \frac{4}{\pi}\left[\frac{s_N}{2\delta_N}\arctan\frac{s_N}{2\delta_N} - \ln\sqrt{1 + \left(\frac{s_N}{2\delta_N}\right)^2}\right] \tag{2.46}$$

The dependence of the normalized effective air gap width on normalized air gap width with normalized slot opening as a parameter is shown in Fig. 2.25. One recognizes in this figure that the difference between effective and geometrical air gap width becomes constant for increasing δ/τ_s, which means that the Carter factor in that case slowly decreases.

Introducing the auxiliary quantity u

$$u = \frac{s}{2\delta} + \sqrt{1 + \left(\frac{s}{2\delta}\right)^2} = \frac{s_N}{2\delta_N} + \sqrt{1 + \left(\frac{s_N}{2\delta_N}\right)^2} \tag{2.47}$$

one can define the ratio β (see Fig. 2.24) as

$$\beta = \frac{(1-u)^2}{2 \cdot (1+u^2)} = \sin^2 \frac{\alpha}{2} \tag{2.48}$$

which also can be written as

$$\beta = \frac{B_s}{B_{max}} = \frac{B_{max} - B_{min}}{2B_{max}} \tag{2.49}$$

Now one can write for flux densities B_0 and B_s

$$B_0 = \frac{B_{max} + B_{min}}{2} = (1-\beta)B_{max}; \quad B_s = \frac{B_{max} - B_{min}}{2} = \beta B_{max} \tag{2.50}$$

as well as for their ratio

$$\frac{B_s}{B_0} = \frac{\beta}{1-\beta} \tag{2.51}$$

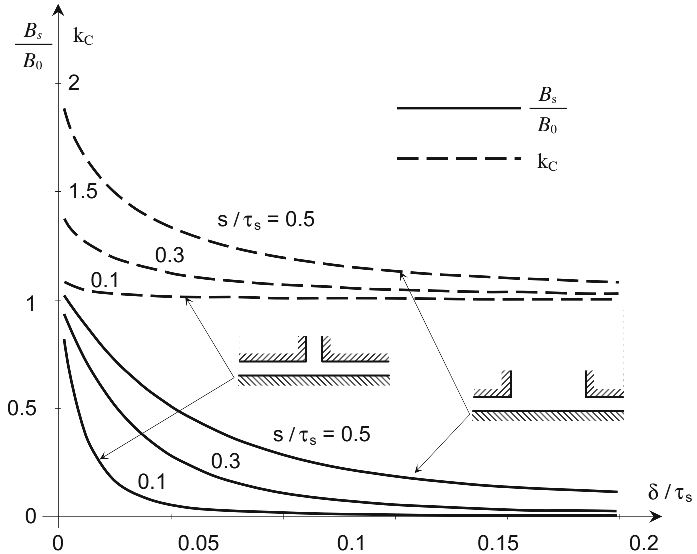

Fig. 2.26 Ratio B_s/B_0 (*solid*) and Carter factor (*dashed*) as functions of normalized air gap width δ/τ_s with normalized slot width s/τ_s as a parameter

The dependence of Carter factor and the ratio between the amplitudes B_0 and B_s on the normalized air gap width for various values of normalized slot-opening width is shown in Fig. 2.26. For small values of normalized air gap width and large values of normalized slot-opening width, the magnitude of the fundamental slot harmonic B_s can be almost as large as the magnitude of the constant term B_0!

Pulsating component of air gap flux density has thermal and mechanical consequences: Eddy current losses in conducting media are proportional to the square of flux density amplitude, as is the radial (attractive) force between stator and rotor. Therefore, special attention has to be paid to the design of air gap geometry and to minimization of slot harmonics in the flux density distribution.

In Fig. 2.24 the electromagnetic air gap width $\delta_{em}(x)$ was introduced, which stands for the length of flux line at a given circumferential coordinate x. The maximum value δ_{max} of the electromagnetic air gap width corresponds to the minimum value B_{min} of air gap flux density $B(x)$:

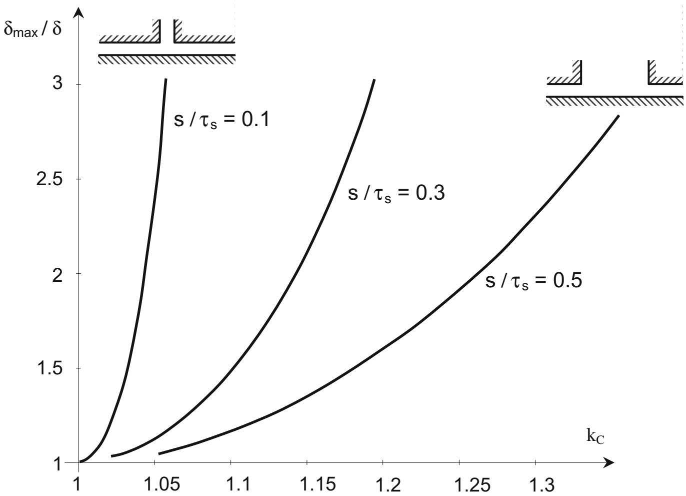

Fig. 2.27 Ratio between maximum electromagnetic air gap width δ_{max} and geometric width δ as a function of the Carter factor k_C for various values of normalized slot width s/τ_s

$$\delta_{max} = \mu_0 \frac{\Theta}{B_{min}} \tag{2.52}$$

By utilizing the parameter β (2.49) one can define the ratio between the maximum and minimum air gap width as

$$\frac{\delta_{max}}{\delta} = \frac{1}{1 - 2\beta} \tag{2.53}$$

The ratio between maximum electromagnetic air gap width δ_{max} and geometric width δ as a function of the Carter factor k_C for various values of normalized slot width s/τ_s is shown in Fig. 2.27.

If the air gap flux density is generated by a $2p$-pole winding placed in N slots, the air gap width $\delta(x)$ can be represented with a constant term and a fundamental harmonic with period length τ_s:

$$\delta(x) = \frac{\delta_{max} + \delta}{2} + \frac{\delta_{max} - \delta}{2} \cos \frac{2\pi}{\tau_s} x = \delta_0 + \delta_1 \cos \frac{N}{p} \frac{\pi}{\tau_p} x \tag{2.54}$$

with τ_s denoting the *slot pitch*

$$\tau_s = \frac{D\pi}{N} = \frac{2p}{N} \tau_p \tag{2.55}$$

and D the average air gap diameter. One should note that the terms δ_0 and δ_1 are both functions of Carter factor and can be of the same order of magnitude.

If the **air gap of an electric machine is doubly slotted** (Fig. 2.28), the resulting Carter factor k_C is equal to the product of the Carter factor for the stator $k_{C,s}$ and for the rotor $k_{C,r}$

$$k_C = k_{C,s} \cdot k_{C,r} \tag{2.56}$$

where both $k_{C,s}$ and $k_{C,r}$ are calculated assuming that the opposite side of air gap has no slots. Here the principle of reciprocity can be applied, since for the computation of Carter factor in electrically excited machines the source of the field is placed outside the air gap. Both stator and rotor windings face the same air gap geometry in Fig. 2.28 and, therefore, the same effective air gap width δ_{eff}.

The air gap width $\delta(x)$ of a doubly slotted machine in Fig. 2.28 can be represented with a constant term, the fundamental harmonic representing the stator slotting, with period length $\tau_{s,s}$, and the fundamental harmonic representing the rotor slotting, with period length $\tau_{s,r}$

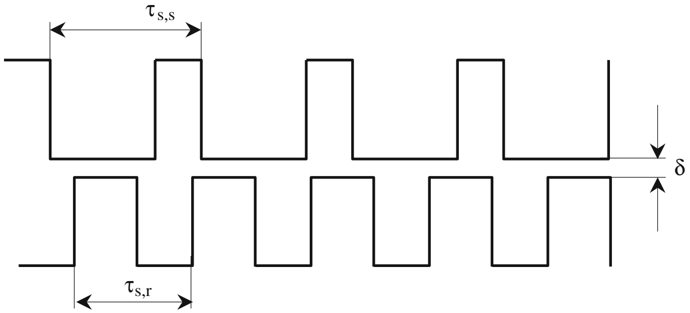

Fig. 2.28 Doubly slotted air gap of an electric machine

$$\delta(x) = \delta_0 + \delta_{1,s} \cos \frac{N_s}{p} \frac{\pi}{\tau_p} x + \delta_{1,r} \cos \frac{N_r}{p} \frac{\pi}{\tau_p} x \tag{2.57}$$

with N_s standing for the number of stator, and N_r for the number of rotor slots.

In order to increase the heat exchange surface and improve the cooling performance, electric machines are often built with radial cooling channels through which the cooling air is blown from inner to outer, or from outer to inner portions of machines. If the lamination contains N_{cc} radial cooling channels, it is built of $N_{cc} + 1$ lamination stacks separated by the cooling channels. Radial cooling channels extend the machine axial length for the amount of $w_{cc} \cdot N_{cc}$ and deteriorate the lamination fill factor. The rate of deterioration can be expressed by using the axial Carter factor $k_{C,ax}$ defined as

$$k_{C,ax} = \frac{l_{ax} - N_{cc} w_{cc}}{l_{ax} - N_{cc} w'_{cc} + 2\delta} \tag{2.58}$$

with

$$w'_{cc} \approx \frac{w_{cc}}{1 + 5 \frac{\delta}{w_{cc}}} \tag{2.59}$$

for the same number of stator and rotor radial cooling channels, and

$$w'_{cc} \approx \frac{w_{cc}}{1 + 2.5 \frac{\delta}{w_{cc}}} \tag{2.60}$$

for different numbers of stator and rotor cooling channels. l_{ax} in Eq. 2.58 denotes the axial length of active part, i.e., the distance between the beginning of the first and the end of the last lamination stack. The resulting Carter factor for a machine with radial cooling channels can be expressed as

$$k_C = k_{C,s} \cdot k_{C,r} \cdot k_{C,ax} \tag{2.61}$$

The principle of reciprocity used for the determination of Carter factor for doubly slotted air gap is disturbed when the excitation on one side of the air gap is relocated from iron structure into the air gap, as is the case in surface-mounted PM machines, as shown in Fig. 2.29.

Permanent magnet in the air gap of the machine in Fig. 2.29a faces teeth and slots on the other side of mechanical air gap δ_m relatively close to its surface. As a consequence, the air gap flux density and the flux density in the magnet below a slot differ significantly from their values below a tooth. Large pulsations of air gap flux density are an indicator of a large Carter factor. When excited by a coil in slots as shown in Fig. 2.29b, the same air gap geometry generates lower amplitudes of flux density pulsations underneath the slots, which is an indicator for a lower Carter factor.

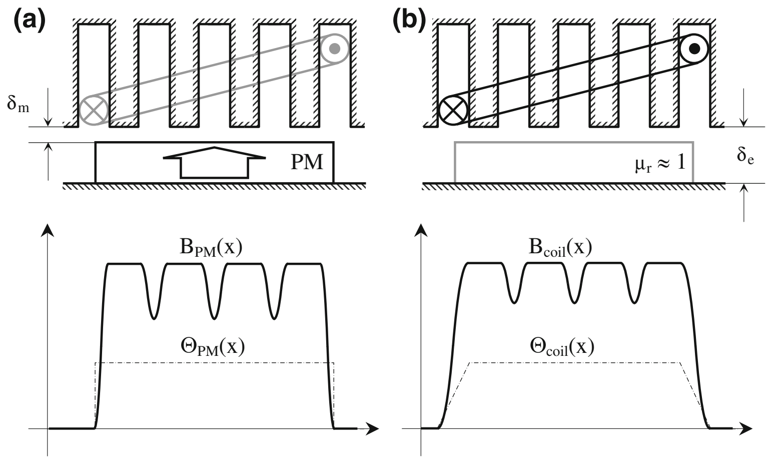

Fig. 2.29 Qualitative air gap flux density distribution in a surface-mounted PM machine created by magnets (**a**) and armature winding (**b**)

2.5.1 Uneven Air Gap and Homopolar Flux

Consider a two-pole machine with a winding only on one side of the air gap, as shown in Fig. 2.30. Winding current i creating spatially alternating flux density in the active part flows through end winding conductors in the given sectional (z, r) plane in the same direction, as shown in Fig. 2.30b, c. Flux lines created by end winding MMF go through bearing shields and shaft (if these are made of magnetic material) into the active part. The total flux through the shaft is equal to zero as long as the magnetic circuit is perfectly symmetrical, as shown in Fig. 2.30b. If there is an asymmetry in the machine's magnetic circuit, such as uneven gap caused e.g. by rotor eccentricity, the total shaft flux Φ_s is not equal to zero any more, as shown in Fig. 2.30c, and the homopolar flux is generated.

Homopolar flux Φ_s can be evaluated by means of the simplified magnetic equivalent circuit of the machine in Fig. 2.31b. One recognizes in this circuit the bridge structure created by gap permeances $G_{\mathrm{sh},\delta,\mathrm{N}}$, $G_{\mathrm{sh},\delta,\mathrm{S}}$, $G_{\delta,\mathrm{N}}$, and $G_{\delta,\mathrm{S}}$. Flux Φ_s is equal to

$$\Phi_s = 2iw \frac{G_{\mathrm{shaft}}\left(G_{\delta,\mathrm{N}}G_{\mathrm{sh},\delta,\mathrm{S}} - G_{\delta,\mathrm{S}}G_{\mathrm{sh},\delta,\mathrm{N}}\right)}{G_{\mathrm{shaft}}\left(G_{\delta,\mathrm{N}} + G_{\delta,\mathrm{S}}\right) + \left(G_{\mathrm{sh},\delta,\mathrm{N}} + G_{\mathrm{sh},\delta,\mathrm{S}}\right)\left(G_{\delta,\mathrm{N}} + G_{\delta,\mathrm{S}} + G_{\mathrm{Shaft}}\right)} \quad (2.62)$$

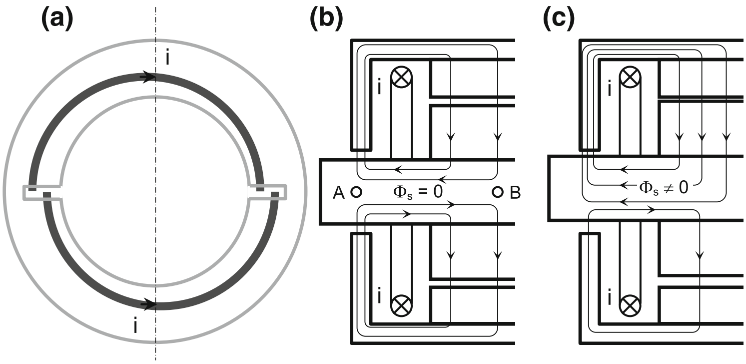

Fig. 2.30 Two-pole machine with stator winding only: **a** schematical representation of the end winding MMF with sectional (z, r) plane denoted by a *dash-dot line*; **b** distribution of fluxes in the (z, r) plane of a machine with perfectly symmetrical magnetic circuit and bearing shields made of magnetic material; **c** distribution of fluxes in the (z, r) plane of a machine with uneven air gap(s) and bearing shields made of magnetic material

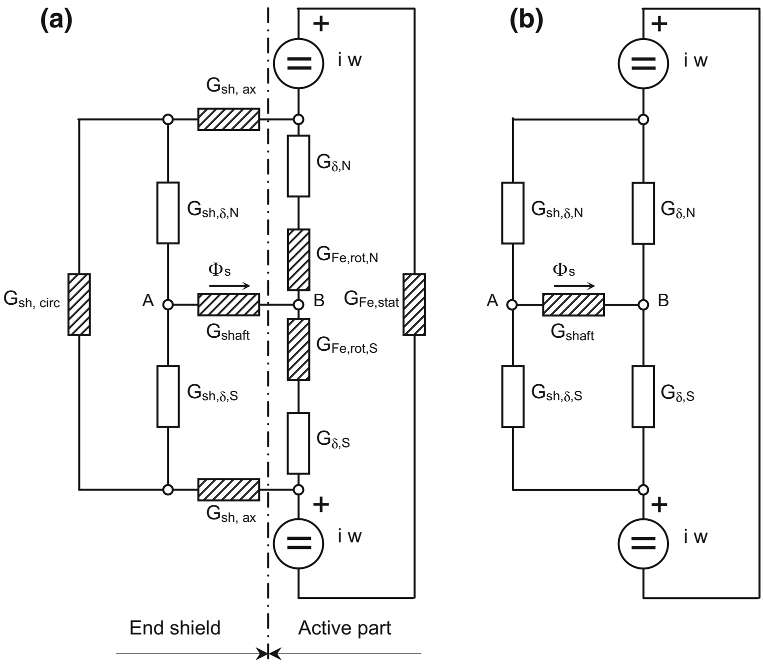

Fig. 2.31 Magnetic equivalent circuit of the portion of the machine in Fig. 2.30b, c: detailed (**a**) and reduced to its most significant components (**b**). Index *sh* relates to the bearing shield, *ax* to axial and *circ* to circumferential direction. Index δ stands for air gap, *rot* for rotor, *stat* for stator, *Fe* for iron, *N* for the N-pole, and *S* for the S-pole. Ampere-turns Iw denote the MMF per pole created by the particular winding

As long as the magnetic circuit in Fig. 2.31 is balanced, the shaft flux is equal to zero. Any unbalance in the bridge of air gap permeances in Fig. 2.31b results in shaft flux. Shaft flux can be constant, or time-dependent. Time dependence of shaft flux is caused either by time-dependent MMFs, or by variation of gap permeances due to rotor motion. Time dependent shaft flux induces shaft voltage, which can cause bearing currents.

2.5.2 Flux Density Distribution in Eccentric Air Gap of a Slotless Machine

The most common reason for nonuniformity of air gap is the rotor eccentricity shown in Fig. 2.32, which can be single or both sided (DE and/or NDE), as well as static or dynamic. The eccentric air gap width varies with periodicity of $2R\pi$, R being the average radius of the gap:

$$\delta = \delta_0 + \varepsilon \cos \frac{x - x_\mathrm{r}}{R} \tag{2.63}$$

The air gap flux density distribution in a $2p$-pole machine with rotor eccentricity can be expressed as

$$\left(\delta_0 + \varepsilon \cos \frac{x - x_\mathrm{r}}{R}\right) \sum_{i=0,1,2,\ldots}^{\infty} B_i \cos i \frac{p}{R}(x - x_i) = \mu_0 \sum_{j=1,3,\ldots}^{\infty} \Theta_j \cos j \frac{p}{R} x \tag{2.64}$$

or

$$\begin{aligned} &\delta_0 \sum_{i=0,1,2,\ldots}^{\infty} B_i \cos i \frac{p}{R}(x - x_i) + \frac{\varepsilon}{2} \sum_{i=0,1,2,\ldots}^{\infty} B_i \cos \frac{(ip+1)x - (ipx_i + x_\mathrm{r})}{R} \\ &+ \frac{\varepsilon}{2} \sum_{i=0,1,2,\ldots}^{\infty} B_i \cos \frac{(ip-1)x - (ipx_i - x_\mathrm{r})}{R} = \mu_0 \sum_{j=1,3,\ldots}^{\infty} \Theta_j \cos j \frac{p}{R} \end{aligned} \tag{2.65}$$

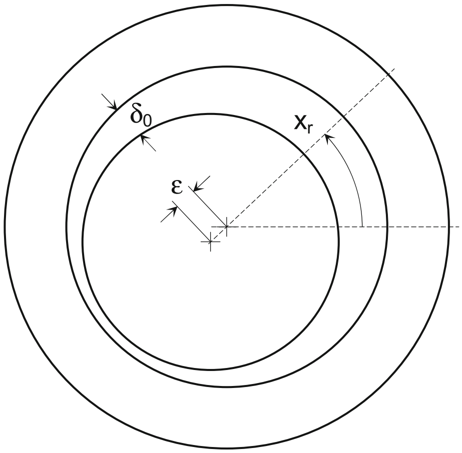

Fig. 2.32 Rotor eccentricity

The solution of Eq. 2.61 depends strongly on the number of pole pairs p, since for $p = 1$ some terms exist which disappear at other pole pairs. Physical reason for different behavior of 2-pole machine is obvious, because the rotor eccentricity repeats with the lowest possible periodicity.

(a) $p = 1$

For a 2-pole machine Eq. 2.61 can be further written as

$$\begin{aligned}
&\delta_0\left(B_0 + B_1\cos\frac{x-x_1}{R} + B_2\cos 2\frac{x-x_2}{R} + B_3\cos 3\frac{x-x_3}{R} + B_4\cos 4\frac{x-x_4}{R} + \cdots\right)\\
&\quad + \varepsilon_+\left(B_0\cos\frac{x-x_\mathrm{r}}{R} + B_1\cos\frac{2x-x_1-x_\mathrm{r}}{R} + B_2\cos\frac{3x-2x_2-x_\mathrm{r}}{R}\right.\\
&\qquad\left. + B_3\cos\frac{4x-3x_3-x_\mathrm{r}}{R} + \cdots\right)\\
&\quad + \varepsilon_-\left(B_0\cos\frac{x+x_\mathrm{r}}{R} + B_1\cos\frac{-x_1+x_\mathrm{r}}{R} + B_2\cos\frac{x-2x_2+x_\mathrm{r}}{R}\right.\\
&\qquad\left. + B_3\cos\frac{2x-3x_3+x_\mathrm{r}}{R} + \cdots\right)\\
&= \mu_0\left(\Theta_1\cos\frac{p}{R}x + \Theta_3\cos 3\frac{p}{R}x + \Theta_5\cos 5\frac{p}{R}x + \cdots\right)
\end{aligned} \tag{2.66}$$

with $\varepsilon_+ = \varepsilon/2$ and $\varepsilon_- = \varepsilon/2$.

The unknowns in Eq. 2.66 are amplitudes B_i of air gap flux density harmonics and their spatial shifts x_i. Since spatial harmonics B_i are orthogonal to each other, one can derive an infinite number of trigonometric identities from Eq. 2.66—one identity for each harmonic:

$$\delta_0 B_0 + \frac{\varepsilon}{2}B_1\cos\frac{x_1-x_\mathrm{r}}{R} = 0 \tag{2.67}$$

$$\varepsilon B_0\cos\frac{x-x_\mathrm{r}}{R} + \delta_0 B_1\cos\frac{x-x_1}{R} + \frac{\varepsilon}{2}B_2\cos\frac{x-2x_2+x_\mathrm{r}}{R} = \mu_0\Theta_1\cos\frac{x}{R} \tag{2.68}$$

$$\frac{\varepsilon}{2}B_1\cos\frac{2x-x_1-x_\mathrm{r}}{R} + \delta_0 B_2\cos 2\frac{x-x_2}{R} + \frac{\varepsilon}{2}B_3\cos\frac{2x-3x_1+x_\mathrm{r}}{R} = 0 \tag{2.69}$$

$$\begin{aligned}&\frac{\varepsilon}{2}B_2\cos\frac{3x-2x_2-x_r}{R}+\delta_0B_3\cos 3\frac{x-x_3}{R}\\&\quad+\frac{\varepsilon}{2}B_4\cos\frac{3x-4x_4+x_r}{R}=\mu_0\Theta_3\cos 3\frac{x}{R}\end{aligned}\tag{2.70}$$

$$\frac{\varepsilon}{2}B_3\cos\frac{4x-3x_3-x_r}{R}+\delta_0B_4\cos 4\frac{x-x_4}{R}+\frac{\varepsilon}{2}B_5\cos\frac{4x-5x_5+x_r}{R}=0\tag{2.71}$$

$$\begin{aligned}&\frac{\varepsilon}{2}B_4\cos\frac{5x-4x_4-x_r}{R}+\delta_0B_5\cos 5\frac{x-x_5}{R}\\&\quad+\frac{\varepsilon}{2}B_6\cos\frac{5x-6x_6+x_r}{R}=\mu_0\Theta_5\cos 5\frac{x}{R}\end{aligned}\tag{2.72}$$

etc. Each air gap flux harmonic can be resolved along axes $x = 0$ and $x = R\pi/2$, which results in cosine

$$\begin{aligned}&\varepsilon B_0\cos\frac{x_r}{R}+\delta_0B_1\cos\frac{x_1}{R}+\frac{\varepsilon}{2}B_2\cos\frac{2x_2-x_r}{R}=\mu_0\Theta_1\\&\frac{\varepsilon}{2}B_1\cos\frac{x_1+x_r}{R}+\delta_0B_2\cos\frac{2x_2}{R}+\frac{\varepsilon}{2}B_3\cos\frac{3x_1-x_r}{R}=0\\&\frac{\varepsilon}{2}B_2\cos\frac{2x_2+x_r}{R}+\delta_0B_3\cos\frac{3x_3}{R}+\frac{\varepsilon}{2}B_4\cos\frac{4x_4-x_r}{R}=\mu_0\Theta_3\\&\frac{\varepsilon}{2}B_3\cos\frac{3x_3+x_r}{R}+\delta_0B_4\cos\frac{4x_4}{R}+\frac{\varepsilon}{2}B_5\cos\frac{5x_5-x_r}{R}=0\\&\frac{\varepsilon}{2}B_4\cos\frac{4x_4+x_r}{R}+\delta_0B_5\cos\frac{5x_5}{R}+\frac{\varepsilon}{2}B_6\cos\frac{6x_6-x_r}{R}=\mu_0\Theta_5\end{aligned}$$

etc., as well as in sine terms

$$\begin{aligned}&\varepsilon B_0\sin\frac{x_r}{R}+\delta_0B_1\sin\frac{x_1}{R}+\frac{\varepsilon}{2}B_2\sin\frac{2x_2-x_r}{R}=0\\&\frac{\varepsilon}{2}B_1\sin\frac{x_1+x_r}{R}+\delta_0B_2\sin\frac{2x_2}{R}+\frac{\varepsilon}{2}B_3\sin\frac{3x_1-x_r}{R}=0\\&\frac{\varepsilon}{2}B_2\sin\frac{2x_2+x_r}{R}+\delta_0B_3\sin\frac{3x_3}{R}+\frac{\varepsilon}{2}B_4\sin\frac{4x_4-x_r}{R}=0\\&\frac{\varepsilon}{2}B_3\sin\frac{3x_3+x_r}{R}+\delta_0B_4\sin\frac{4x_4}{R}+\frac{\varepsilon}{2}B_5\sin\frac{5x_5-x_r}{R}=0\\&\frac{\varepsilon}{2}B_4\sin\frac{4x_4+x_r}{R}+\delta_0B_5\sin\frac{5x_5}{R}+\frac{\varepsilon}{2}B_6\sin\frac{6x_6-x_r}{R}=0\end{aligned}$$

etc. Denoting by $s_r = \sin(x_r/R)$ and $c_r = \cos(x_r/R)$ one can define the matrix $\underline{E}$

$$\underline{E} = \begin{bmatrix} \delta_0 & \frac{\varepsilon}{2}c_r & -\frac{\varepsilon}{2}s_r & 0 & 0 & 0 & 0 & 0 & 0 & \dots \\ \varepsilon c_r & \delta_0 & 0 & \frac{\varepsilon}{2}c_r & -\frac{\varepsilon}{2}s_r & 0 & 0 & 0 & 0 & \dots \\ \varepsilon s_r & 0 & \delta_0 & -\frac{\varepsilon}{2}s_r & \frac{\varepsilon}{2}c_r & 0 & 0 & 0 & 0 & \dots \\ 0 & \frac{\varepsilon}{2}c_r & -\frac{\varepsilon}{2}s_r & \delta_0 & 0 & \frac{\varepsilon}{2}c_r & \frac{\varepsilon}{2}s_r & 0 & 0 & \dots \\ 0 & \frac{\varepsilon}{2}s_r & \frac{\varepsilon}{2}c_r & 0 & \delta_0 & -\frac{\varepsilon}{2}s_r & \frac{\varepsilon}{2}c_r & 0 & 0 & \dots \\ 0 & 0 & 0 & \frac{\varepsilon}{2}c_r & -\frac{\varepsilon}{2}s_r & \delta_0 & 0 & \frac{\varepsilon}{2}c_r & \frac{\varepsilon}{2}s_r & \dots \\ 0 & 0 & 0 & \frac{\varepsilon}{2}s_r & \frac{\varepsilon}{2}c_r & 0 & \delta_0 & -\frac{\varepsilon}{2}s_r & \frac{\varepsilon}{2}c_r & \dots \\ 0 & 0 & 0 & 0 & 0 & \frac{\varepsilon}{2}c_r & -\frac{\varepsilon}{2}s_r & \delta_0 & 0 & \dots \\ 0 & 0 & 0 & 0 & 0 & \frac{\varepsilon}{2}s_r & \frac{\varepsilon}{2}c_r & 0 & \delta_0 & \dots \\ \dots & \dots & \dots & \dots & \dots & \dots & \dots & \dots & \dots & \dots \end{bmatrix} \tag{2.73}$$

and the vector of unknowns $\underline{b}$ as

$$\underline{b} = \begin{bmatrix} B_0 & B_1 \cos\frac{x_1}{R} & B_1 \sin\frac{x_1}{R} & B_2 \cos\frac{2x_2}{R} & B_2 \sin\frac{2x_2}{R} & B_3 \cos\frac{3x_3}{R} & \dots \end{bmatrix}^{\mathrm{T}} \tag{2.74}$$

which along with the vector of applied MMF harmonics $\underline{\theta}$

$$\underline{\theta} = \mu_0 [0 \quad \Theta_1 \quad 0 \quad 0 \quad 0 \quad \Theta_3 \quad 0 \quad 0 \quad 0 \quad \Theta_5 \quad 0 \quad 0 \quad 0 \quad \Theta_7 \quad \dots]^{\mathrm{T}} \tag{2.75}$$

build the system of algebraic equations

$$\underline{E} \cdot \underline{b} = \underline{\theta} \tag{2.76}$$

the solution of which are the magnitudes and phase shifts of air gap flux density harmonics in a machine with eccentric rotor.

In order to illustrate the influence of eccentricity on air gap flux density, a two-pole machine with full-pitch coil and with eccentric rotor was analyzed.

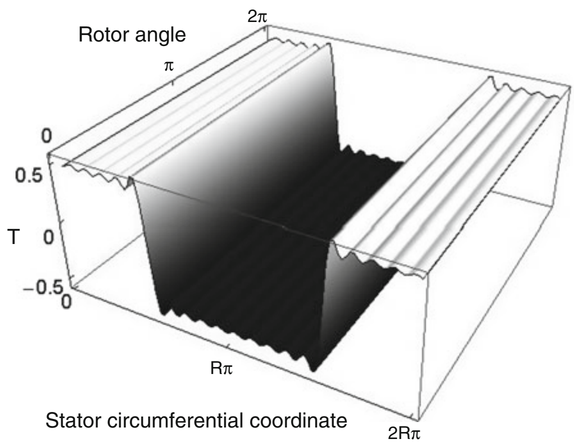

Fig. 2.33 Air gap flux density in a two-pole machine with centric rotor created by the first 19 harmonics of MMF of a full-pitch coil

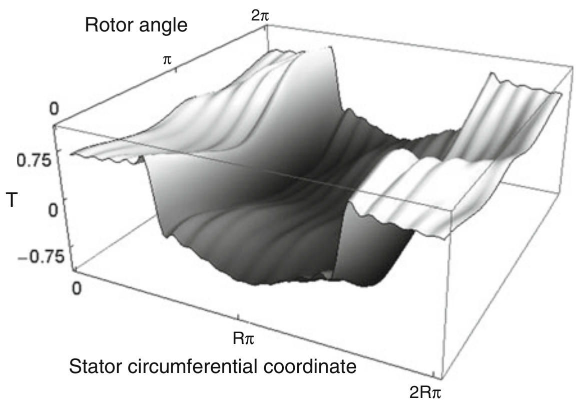

Fig. 2.34 Air gap flux density in a two-pole machine with eccentric rotor created by the first 19 harmonics of MMF of a full-pitch coil

The air gap flux density distribution evaluated for the first 19 harmonics of excitation by a full-pitch coil with an amplitude of the fundamental term of 500 At and for a homogenous air gap width of 1 mm is shown in Fig. 2.33. Apart from small deviations caused by representation of MMF with Fourier series having a finite number of terms, the air gap flux density is constant under one pole, independent of the rotor position. The amplitude of the fundamental term of air gap flux density is equal to $\mu_0\, 500/.001 = 0.628\ T$. The air gap flux density spectrum contains only the terms present in the MMF spectrum, i.e., the 1., 3., 5., etc., harmonics.

If the rotor is eccentric with a maximum eccentricity ε of 0.5 mm, i.e., 50 % of the air gap width, the shape of the air gap flux density distribution becomes dependent on the rotor to stator angle. In addition to terms existing in the MMF distribution, the air gap flux density spectrum contains harmonics generated by variable air gap width due to eccentricity. In particular, the terms with order 0, 2, 4, 6, etc., in the air gap flux density spectrum are generated in addition to odd terms. The air gap flux density distribution under the same conditions as in Fig. 2.33, but with an eccentricity ε of 0.5 mm (or 50 %) is shown in Fig. 2.34.

Amplitudes of harmonics of air gap flux density in Fig. 2.34 as functions of rotor angle are shown in Fig. 2.35. Constant term B_0, as a measure of shaft flux in Fig. 2.32, becomes negative after a rotor shift of $\pi/2$ because the opposite polarity of stator MMF is a source of more flux. Accordingly, the shaft flux in Fig. 2.32 becomes also negative.

One notes in Fig. 2.35 that the amplitudes of all harmonics of air gap flux density in a machine with eccentric rotor pulsate as a function of the rotor angle.

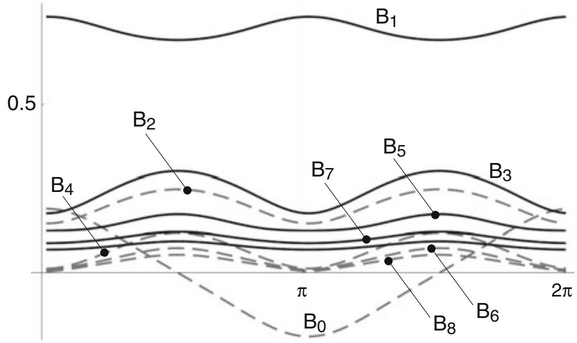

Fig. 2.35 Amplitudes of air gap flux density harmonics as functions of rotor angle in a two-pole machine with eccentric rotor

Consequently, one can write for the amplitude B_0:

$$B_0 = B_{0,\max} \cos \frac{\pi}{\tau_p} x_r \tag{2.77}$$

as well as for the amplitude of the ith harmonic B_i in Eq. 2.60:

$$B_i = B_{i,\mathrm{const}} + B_{i,\max} \cos\left(2\frac{\pi}{\tau_p} x_r \pm \pi\right) \tag{2.78}$$

(b) $p > 1$

For a machine with more than one pole pair, Eq. 2.61 can be written as

$$\begin{aligned}
&\delta_0\Big[B_0 + B_1\Big(\cos p\frac{x}{R}\cos p\frac{x_1}{R} + \sin p\frac{x}{R}\sin p\frac{x_1}{R}\Big) + B_2\Big(\cos 2p\frac{x}{R}\cos 2p\frac{x_1}{R} + \sin 2p\frac{x}{R}\sin 2p\frac{x_1}{R}\Big)\\
&\quad + B_3\Big(\cos 3p\frac{x}{R}\cos 3p\frac{x_1}{R} + \sin 3p\frac{x}{R}\sin 3p\frac{x_1}{R}\Big) + B_4\Big(\cos 4p\frac{x}{R}\cos 4p\frac{x_1}{R} + \sin 4p\frac{x}{R}\sin 4p\frac{x_1}{R}\Big) + \cdots\Big]\\
&\quad + \frac{\varepsilon}{2}\Big[B_0\Big(\cos\frac{x}{R}\cos\frac{x_r}{R} + \sin\frac{x}{R}\sin\frac{x_r}{R}\Big) + B_1\Big(\cos\frac{p+1}{R}x\cos\frac{px_1+x_r}{R} + \sin\frac{p+1}{R}x\sin\frac{px_1+x_r}{R}\Big)\\
&\quad + B_2\Big(\cos\frac{2p+1}{R}x\cos\frac{2px_2+x_r}{R} + \sin\frac{2p+1}{R}x\sin\frac{2px_2+x_r}{R}\Big) + B_3\Big(\cos\frac{3p+1}{R}x\cos\frac{3px_3+x_r}{R} + \sin\frac{3p+1}{R}x\sin\frac{3px_3+x_r}{R}\Big) + \cdots\Big]\\
&\quad + \frac{\varepsilon}{2}\Big[B_0\Big(\cos\frac{x}{R}\cos\frac{x_r}{R} + \sin\frac{x}{R}\sin\frac{x_r}{R}\Big) + B_1\Big(\cos\frac{p-1}{R}x\cos\frac{px_1-x_r}{R} + \sin\frac{p-1}{R}x\sin\frac{px_1-x_r}{R}\Big)\\
&\quad + B_2\Big(\cos\frac{2p-1}{R}x\cos\frac{2px_2-x_r}{R} + \sin\frac{2p-1}{R}x\sin\frac{2px_2-x_r}{R}\Big) + B_3\Big(\cos\frac{3p-1}{R}x\cos\frac{3px_3-x_r}{R} + \sin\frac{3p-1}{R}x\sin\frac{3px_3-x_r}{R}\Big) + \cdots\Big]\\
&= \mu_0\Big(\Theta_1\cos p\frac{x}{R} + \Theta_3\cos 3p\frac{x}{R} + \Theta_5\cos 5p\frac{x}{R} + \cdots\Big)
\end{aligned} \tag{2.79}$$

The orders of harmonics which multiply δ_0 in Eq. 2.79 are 0, p, $2p$, $3p$, …, etc., and of harmonics which multiply $\varepsilon/2$ are 1, $p \pm 1$, $2p \pm 1$, $3p \pm 1$, …, etc. The orders of harmonics of the air gap flux density in a machine with eccentric rotor as functions of the number of machine pole pairs are given in Table 2.3.

Table 2.3 The orders of harmonics multiplying air gap width components δ_0, ε_+, and ε_- after Eq. 2.66 in a machine with eccentric rotor as functions of the number of pole pairs p

δ_0	p	1	2	3	4
	$2p$	2	4	6	8
	$3p$	3	6	9	12
	$4p$	4	8	12	16
ε_+	$p + 1$	2	3	4	5
	$2p + 1$	3	5	7	9
	$3p + 1$	4	7	10	13
	$4p + 1$	5	9	13	17
ε_-	$p - 1$	0	1	2	3
	$2p - 1$	1	3	5	7
	$3p - 1$	2	5	8	11
	$4p - 1$	3	7	11	15

The strongest interaction between harmonics occurs in a two-pole machine with eccentric rotor. The higher the number of poles, the weaker the influence of the rotor eccentricity, e.g., for an 8-pole machine, there exists no single harmonic common for the sets of terms multiplying δ_0, ε_+, and ε_-. In a two-pole machine, on the other hand, every harmonic of the order of 2 and above appears in all three sets of terms multiplying δ_0, ε_+, and ε_-. Only in a two-pole machine the constant term B_0 can appear, see Table 2.3. Therefore, the rotor eccentricity can be a source of significant shaft flux only in a two-pole machine.

2.5.3 *Flux Density Distribution in the Air Gap of a Single-Slotted Machine*

Consider a single-slotted machine the air gap width of which is described by a constant term and an infinite series of harmonics with amplitudes δ_i:

$$\delta(x) = \delta_0 + \sum_{i=1,3,5,\ldots}^{\infty} \delta_i \cos i \frac{N}{p} \frac{\pi}{\tau_p} x \tag{2.80}$$

If the slot geometry is identical for all N slots, the order i of harmonics is an odd number. In most practical cases the influence of slot harmonics with order above 1 is negligible; therefore, the air gap width will be represented with a constant term and the fundamental slot harmonic of the order of N/p:

$$\delta(x) = \delta_0 + \delta_1 \cos \frac{N}{p} \frac{\pi}{\tau_p} x \tag{2.81}$$

For a salient pole machine the number of poles per pole pair $N/p = 2$.

The air gap flux density distribution $B(x)$ created by conventional pole-symmetric winding (only odd harmonics of MMF!), the axis of which is shifted for the amount of x_c relative to the center of the first slot (Fig. 2.36), satisfies equation

$$B(x)\cdot\left(\delta_0+\delta_1\cos\frac{N}{p}\frac{\pi}{\tau_p}x\right)=\mu_0\cdot\sum_{n=1,3,5,\ldots}^{\infty}\Theta_n\cos n\frac{\pi}{\tau_p}(x-x_c) \tag{2.82}$$

Machines with integer numbers of slots per pole have **even number of slots per pole pair N/p**. The air gap flux density distribution $B(x)$ in that case contains only odd terms

$$B(x)=\sum_{n=1,3,5,\ldots}^{\infty}B_n\cos n\frac{\pi}{\tau_p}(x-x_c) \tag{2.83}$$

and satisfies equation

$$\begin{aligned}\delta_0\cdot\sum_{i=1,3,5,\ldots}^{\infty}B_i\cos i\frac{\pi}{\tau_p}(x-x_c)+\delta_1\cdot\sum_{j=1,3,5,\ldots}^{\infty}B_j\cos j\frac{\pi}{\tau_p}(x-x_c)\cdot\cos\frac{N}{p}\frac{\pi}{\tau_p}x\\=\mu_0\cdot\sum_{n=1,3,5,\ldots}^{\infty}\Theta_n\cos n\frac{\pi}{\tau_p}(x-x_c)\end{aligned} \tag{2.84}$$

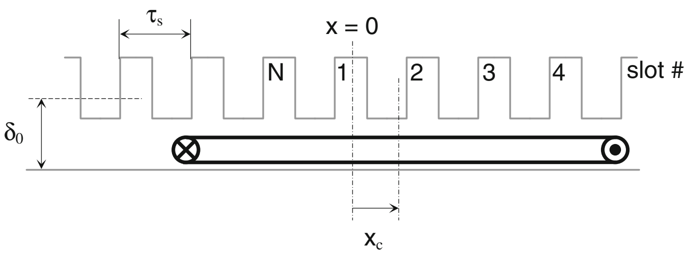

Fig. 2.36 Single-slotted air gap with a coil

The order i of flux density distribution due to constant air gap width δ_0 in Eq. 2.84 must always be equal to the order n of MMF distribution, $i = n$. The order j of flux density distribution due to slotting in Eq. 2.84 must satisfy the condition

$$j=n\pm\frac{N}{p} \tag{2.85}$$

in order to generate flux density components with the same order n as the MMF in Eq. 2.84. Note that for $n < N/p$ the order j can be negative, which means nothing but a 180° phase shift of the particular term. By applying condition in Eq. 2.85, one can write Eq. 2.84 further as

$$\delta_0 \cdot \sum_{i=1,3,5,\ldots}^{\infty} B_i \cos i \frac{\pi}{\tau_p}(x - x_c) + \frac{\delta_1}{2} \sum_{j_+=1,3,5,\ldots}^{\infty} B_{j_+} \cos\left[\left(j_+ + \frac{N}{p}\right) \cdot x - j_+ \cdot x_c\right] \frac{\pi}{\tau_p}$$
$$+ \frac{\delta_1}{2} \sum_{j_-=1,3,5,\ldots}^{\infty} B_{j_-} \cos\left[\left(j_- - \frac{N}{p}\right) \cdot x - j_- \cdot x_c\right] \frac{\pi}{\tau_p}$$
$$= \mu_0 \cdot \sum_{n=1,3,5,\ldots}^{\infty} \Theta_n \cos n \frac{\pi}{\tau_p}(x - x_c) \tag{2.86}$$

The nth (odd) harmonic of applied MMF creates in a single-slotted air gap of an electric machine *three components of flux density with the same order n*:

- B_n (odd), in the amount of $\mu_0\ \Theta_n/\delta_0$,
- $B_{n-N/p}$ (odd), in the amount of $2\ \mu_0\ \Theta_n/\delta_1$, and
- $B_{n+N/p}$ (odd), in the amount of $2\ \mu_0\ \Theta_n/\delta_1$

which satisfy equation

$$\begin{aligned}\mu_0\Theta_n \cos n\frac{\pi}{\tau_p}(x - x_c) = {} & \delta_0 B_n \cos n\frac{\pi}{\tau_p}(x - x_c) \\ & + \frac{\delta_1}{2} B_{n-\frac{N}{p}} \cos\frac{\pi}{\tau_p}\left[nx - \left(n + \frac{N}{p}\right)x_c\right] \\ & + \frac{\delta_1}{2} B_{n+\frac{N}{p}} \cos\frac{\pi}{\tau_p}\left[nx - \left(n - \frac{N}{p}\right)x_c\right]\end{aligned} \tag{2.87}$$

Relationship between the three components of MMF drop and coil MMF harmonic of the order n can be visualized by means of Fig. 2.37. In this figure the nth harmonic of applied air gap MMF and nth, $(n - N/p)$th, and $(n + N/p)$th harmonics of MMF drop are resolved into components along the axis α, coincident with centerline of slot 1, and along the axis β, shifted for $90°_{el}$ to α.

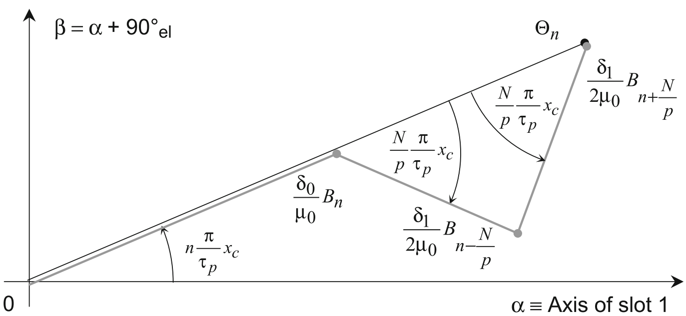

Fig. 2.37 Illustrating relationship between applied MMF and flux density harmonic components in a machine with single-slotted air gap for a given rotor shift x_c

Due to slotting, the nth harmonic of applied MMF created by coil current contributes to the amplitudes of $(n - N/p)$th and $(n + N/p)$th harmonics of air gap flux density along with corresponding fluxes $\Phi_{n-N/p}$ and $\Phi_{n+N/p}$. The fluxes $\Phi_{n-N/p}$ and $\Phi_{N/p+n}$ create MMF drops $\vartheta_{n-N/p}$ and $\vartheta_{n+N/p}$ across the air gap. One distinguishes here between the *applied* MMF Θ_n and its effects, the flux density harmonics B_n, $B_{n-N/p}$, and $B_{n+N/p}$, and the *evoked* MMF harmonics $\vartheta_{n-N/p}$ and $\vartheta_{n+N/p}$, along with all their effects. In order to emphasize this difference, capital letters are used for applied quantities, and small letters for evoked quantities.

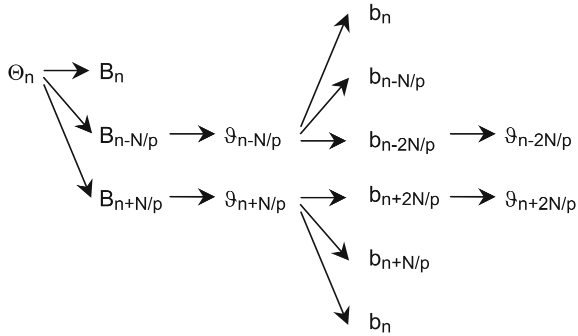

Fig. 2.38 The beginning of the chain of generation of flux density harmonics from a single harmonic of applied MMF in a single-slotted machine

The evoked MMF harmonic $\vartheta_{n-N/p}$ creates flux density harmonics $b_{n-N/p}$, $b_{n-2N/p}$, and b_n, whereas $\vartheta_{n+N/p}$ is a source of $b_{n+N/p}$, $b_{n+2N/p}$, and b_n harmonics, etc. The initial terms of the chain of generation of air gap flux harmonics from a single MMF harmonic in a slotted air gap are shown in Fig. 2.38. Since the number of slots per pole pair N/p is even, an odd harmonic of MMF can create only odd harmonics of air gap flux density.

Table 2.4 Harmonics of flux density *B* created by particular harmonics of MMF Θ in a machine with even number of slots per pole pair $N/p = \nu$

		B														
		1	3	5	…	$\nu - 5$	$\nu - 3$	$\nu - 1$	$\nu + 1$	$\nu + 3$	$\nu + 5$	…	$2\nu - 3$	$2\nu - 1$	$2\nu + 1$	$2\nu + 3$
	1	Xx						Xx	Xx					Xx	Xx	
	3		Xx				Xx			Xx			Xx			Xx
	5			Xx		Xx					Xx					
	…															
	$\nu - 5$			Xx		Xx										
	$\nu - 3$		Xx				Xx						Xx			
	$\nu - 1$	Xx						Xx						Xx		
Θ	$\nu + 1$	Xx							Xx						Xx	
	$\nu + 3$		Xx							Xx						Xx
	$\nu + 5$			Xx							Xx					
	…															
	$2\nu - 3$		Xx				Xx						Xx			
	$2\nu - 1$	Xx						Xx						Xx		
	$2\nu + 1$	Xx							Xx						Xx	
	$2\nu + 3$		Xx							Xx						Xx

All harmonics of flux density contain components both due to applied (denoted by X) and evoked (denoted by x) harmonics of MMF

The nonuniformity of air gap width caused by slotting is a source of higher spatial harmonics in the spectrum of flux density for sinusoidal applied MMF. The mechanism of generation of higher spatial harmonics of air gap flux density due to nonuniform air gap width (cosine terms!) is analogous to the mechanism of creation of higher time harmonics of current in a magnetic circuit with nonlinear B–H curve. Independent of whether a time or spatial problem is analyzed, the nonlinearity is always a source of higher harmonics in the system.

In Table 2.4 the orders of components of air gap flux density distribution in a slotted machine with even number of slots per pole pair are given as functions of orders of applied MMF. The fundamental component of applied MMF creates the fundamental component of air gap flux density, along with harmonics of the order $N/p - 1$ and $N/p + 1$. These two harmonics correspond to evoked harmonics of air gap MMF drops $\vartheta_{n-N/p}$ and $\vartheta_{n+N/p}$ and both of them generate, among other, the fundamental components of flux density due to higher harmonics of MMF.

Using Eq. 2.86 and Table 2.4, one can relate the amplitude of nth harmonic of air gap flux density to corresponding applied and evoked MMFs as

$$
\begin{aligned}
B_n \cos n\frac{\pi}{\tau_\mathrm{p}}(x - x_\mathrm{c}) = \frac{\mu_0}{\delta_0}\Theta_n \cos n\frac{\pi}{\tau_\mathrm{p}}(x - x_\mathrm{c}) \\
+ 2\frac{\mu_0}{\delta_1}\sum_{i=1}^{\infty}\Theta_{i\frac{N}{p}-n}\cos\frac{\pi}{\tau_\mathrm{p}}\left[nx - \left(n + i\frac{N}{p}\right)x_\mathrm{c}\right] \\
+ 2\frac{\mu_0}{\delta_1}\sum_{i=1}^{\infty}\Theta_{i\frac{N}{p}+n}\cos\frac{\pi}{\tau_\mathrm{p}}\left[nx - \left(n - i\frac{N}{p}\right)x_\mathrm{c}\right]
\end{aligned}
\tag{2.88}
$$

Salient pole machine has two poles (teeth) per pole pair, $N/p = 2$ and $\tau_\mathrm{p} = \tau_\mathrm{s}$ (Fig. 2.39). The fundamental harmonic of applied MMF creates with air gap width three components of flux density of the same order 1 (Eq. 2.87):

- B_1 with constant air gap width component in the amount of $\mu_0\,\Theta_1/\delta_0$,
- B_1 with fundamental component of air gap width in the amount of $2\mu_0\Theta_1/\delta_1$, and
- B_3 with fundamental component of air gap width in the amount of $2\mu_0\Theta_1/\delta_1$

which satisfy equation

$$
\Theta_1 = \frac{\delta_0}{\mu_0}B_1 - \frac{\delta_1}{2\mu_0}B_1 - \frac{\delta_1}{2\mu_0}B_3 \tag{2.89}
$$

The fundamental component of air gap flux density B_1 can be found by applying Eq. 2.88, here rewritten for $N/p = 2$:

$$
B_1 = \frac{\mu_0}{\delta_0}\Theta_1 + 2\frac{\mu_0}{\delta_1}\sum_{i=1}^{\infty}(\Theta_{2i-1} - \Theta_{2i+1}) \tag{2.90}
$$

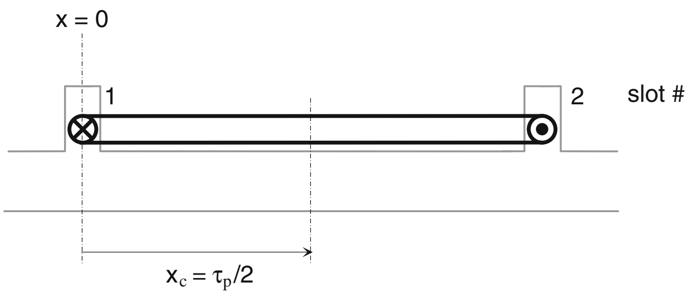

Fig. 2.39 Salient pole machine with a coil

Components of air gap flux density harmonics along perpendicular axes α and β in Fig. 2.37 satisfy simultaneously two algebraic equations (see also Eq. 2.86):

$$\begin{aligned} B_{n,\alpha}\cos n\frac{\pi}{\tau_p}x_c + \frac{\delta_1}{2\delta_0}B_{n-,\alpha}\cos\left(n+i\frac{N}{p}\right)x_c \\ + \frac{\delta_1}{2\delta_0}B_{n+,\alpha}\cos\left(n-i\frac{N}{p}\right)x_c = \frac{\mu_0\cdot\Theta_n}{\delta_0}\cos n\frac{\pi}{\tau_p}x_c \end{aligned} \tag{2.91}$$

and

$$\begin{aligned} B_{n,\beta}\sin n\frac{\pi}{\tau_p}x_c + \frac{\delta_1}{2\delta_0}B_{n-,\beta}\sin\left(n+i\frac{N}{p}\right)x_c \\ + \frac{\delta_1}{2\delta_0}B_{n+,\beta}\sin\left(n-i\frac{N}{p}\right)x_c = \frac{\mu_0\cdot\Theta_n}{\delta_0}\sin n\frac{\pi}{\tau_p}x_c \end{aligned} \tag{2.92}$$

Considering the first r odd harmonics of air gap flux density and MMF, one can write after rearranging of Eqs. 2.91 and 2.92 two matrix equations for the components along the axes α and β as

$$\underline{C}_\delta\cdot\underline{B}_\alpha = \underline{\vartheta}_\alpha \tag{2.93}$$

and

$$\underline{C}_\delta\cdot\underline{B}_\beta = \underline{\vartheta}_\beta \tag{2.94}$$

The vectors ϑ_α and ϑ_β representing the applied MMFs can be written as

$$\underline{\vartheta}_\alpha = \frac{\mu_0}{\delta_0}\cdot\left[\Theta_1\cos\tfrac{\pi}{\tau_p}x_c\ \Theta_3\cos 3\tfrac{\pi}{\tau_p}x_c\ \ \ldots\ \ \Theta_r\cos r\tfrac{\pi}{\tau_p}x_c\right]^T \tag{2.95}$$

$$\underline{\vartheta}_\beta = \frac{\mu_0}{\delta_0}\cdot\left[\Theta_1\sin\tfrac{\pi}{\tau_p}x_c\ \Theta_3\sin 3\tfrac{\pi}{\tau_p}x_c\ \ \ldots\ \ \Theta_r\sin r\tfrac{\pi}{\tau_p}x_c\right]^T \tag{2.96}$$

and the system matrix C_δ

$$\underline{C}_\delta = \begin{array}{c} \text{Column N/p} - 1 \\ \downarrow \\ \begin{bmatrix}
1 & 0 & \cdots & 0 & 0 & \cdots & 0 & r & r & 0 & \cdots & \cdots & 0 & 0 & 0 & 0 & \cdots & 0 & 0 & \cdots & 0 & 0 \\
0 & 1 & \cdots & 0 & 0 & \cdots & r & 0 & 0 & r & \cdots & \cdots & 0 & 0 & 0 & 0 & \cdots & 0 & 0 & \cdots & 0 & 0 \\
\cdots & \cdots & \cdots & \cdots & \cdots & \cdots & \cdots & \cdots & \cdots & \cdots & \cdots & \cdots & \cdots & \cdots & \cdots & \cdots & \cdots & \cdots & \cdots & \cdots & \cdots & \cdots \\
0 & 0 & \cdots & 1 & r & \cdots & 0 & 0 & 0 & 0 & \cdots & \cdots & r & 0 & 0 & 0 & \cdots & 0 & 0 & \cdots & 0 & 0 \\
0 & 0 & \cdots & r & 1 & \cdots & 0 & 0 & 0 & 0 & \cdots & \cdots & 0 & r & 0 & 0 & \cdots & 0 & 0 & \cdots & 0 & 0 \\
\cdots & \cdots & \cdots & \cdots & \cdots & \cdots & \cdots & \cdots & \cdots & \cdots & \cdots & \cdots & \cdots & \cdots & \cdots & \cdots & \cdots & \cdots & \cdots & \cdots & \cdots & \cdots \\
0 & r & \cdots & 0 & 0 & \cdots & 1 & 0 & 0 & 0 & \cdots & \cdots & 0 & 0 & r & 0 & \cdots & 0 & 0 & \cdots & 0 & 0 \\
r & 0 & \cdots & 0 & 0 & \cdots & 0 & 1 & 0 & 0 & \cdots & \cdots & 0 & 0 & 0 & r & \cdots & 0 & 0 & \cdots & 0 & 0 \\
r & 0 & \cdots & 0 & 0 & \cdots & 0 & 0 & 1 & 0 & \cdots & \cdots & 0 & 0 & 0 & 0 & \cdots & r & 0 & \cdots & 0 & 0 \\
0 & r & \cdots & 0 & 0 & \cdots & 0 & 0 & 0 & 1 & \cdots & \cdots & 0 & 0 & 0 & 0 & \cdots & 0 & r & \cdots & 0 & 0 \\
\cdots & \cdots & \cdots & \cdots & \cdots & \cdots & \cdots & \cdots & \cdots & \cdots & \cdots & \cdots & \cdots & \cdots & \cdots & \cdots & \cdots & \cdots & \cdots & \cdots & \cdots & \cdots \\
\cdots & \cdots & \cdots & \cdots & \cdots & \cdots & \cdots & \cdots & \cdots & \cdots & \cdots & \cdots & \cdots & \cdots & \cdots & \cdots & \cdots & \cdots & \cdots & \cdots & \cdots & \cdots \\
0 & 0 & \cdots & r & 0 & \cdots & 0 & 0 & 0 & 0 & \cdots & \cdots & 1 & 0 & 0 & 0 & \cdots & 0 & 0 & \cdots & r & 0 \\
0 & 0 & \cdots & 0 & r & \cdots & 0 & 0 & 0 & 0 & \cdots & \cdots & 0 & 1 & 0 & 0 & \cdots & 0 & 0 & \cdots & 0 & r \\
0 & 0 & \cdots & 0 & 0 & \cdots & r & 0 & 0 & 0 & \cdots & \cdots & 0 & 0 & 1 & 0 & \cdots & 0 & 0 & \cdots & 0 & 0 \\
0 & 0 & \cdots & 0 & 0 & \cdots & 0 & r & 0 & 0 & \cdots & \cdots & 0 & 0 & 0 & 1 & \cdots & 0 & 0 & \cdots & 0 & 0 \\
\cdots & \cdots & \cdots & \cdots & \cdots & \cdots & \cdots & \cdots & \cdots & \cdots & \cdots & \cdots & \cdots & \cdots & \cdots & \cdots & \cdots & \cdots & \cdots & \cdots & \cdots & \cdots \\
0 & 0 & \cdots & 0 & 0 & \cdots & 0 & 0 & r & 0 & \cdots & \cdots & 0 & 0 & 0 & 0 & \cdots & 1 & 0 & \cdots & 0 & 0 \\
0 & 0 & \cdots & 0 & 0 & \cdots & 0 & 0 & 0 & r & \cdots & \cdots & 0 & 0 & 0 & 0 & \cdots & 0 & 1 & \cdots & 0 & 0 \\
\cdots & \cdots & \cdots & \cdots & \cdots & \cdots & \cdots & \cdots & \cdots & \cdots & \cdots & \cdots & \cdots & \cdots & \cdots & \cdots & \cdots & \cdots & \cdots & \cdots & \cdots & \cdots \\
0 & 0 & \cdots & 0 & 0 & \cdots & 0 & 0 & 0 & 0 & \cdots & \cdots & r & 0 & 0 & 0 & \cdots & 0 & 0 & \cdots & 1 & 0 \\
0 & 0 & \cdots & 0 & 0 & \cdots & 0 & 0 & 0 & 0 & \cdots & \cdots & 0 & r & 0 & 0 & \cdots & 0 & 0 & \cdots & 0 & 1
\end{bmatrix} \end{array} \tag{2.97}$$

if the number of slots per pole $N/(2p)$ is even, and

$$\underline{C}_\delta = \begin{array}{c} \text{Column N/p} - 1 \\ \downarrow \\ \begin{bmatrix}
1 & 0 & \cdots & 0 & 0 & 0 & \cdots & 0 & r & r & 0 & \cdots & 0 & 0 & 0 & 0 & \cdots & 0 & 0 & 0 & \cdots & 0 & 0 \\
0 & 1 & \cdots & 0 & 0 & 0 & \cdots & r & 0 & 0 & r & \cdots & 0 & 0 & 0 & 0 & \cdots & 0 & 0 & 0 & \cdots & 0 & 0 \\
\cdots & \cdots & \cdots & \cdots & \cdots & \cdots & \cdots & \cdots & \cdots & \cdots & \cdots & \cdots & \cdots & \cdots & \cdots & \cdots & \cdots & \cdots & \cdots & \cdots & \cdots & \cdots & \cdots \\
0 & 0 & \cdots & 1 & 0 & r & \cdots & 0 & 0 & 0 & 0 & \cdots & r & 0 & 0 & 0 & \cdots & 0 & 0 & 0 & \cdots & 0 & 0 \\
0 & 0 & \cdots & 0 & 1+r & 0 & \cdots & 0 & 0 & 0 & 0 & \cdots & 0 & r & 0 & 0 & \cdots & 0 & 0 & 0 & \cdots & 0 & 0 \\
0 & 0 & \cdots & r & 0 & 1 & \cdots & 0 & 0 & 0 & 0 & \cdots & 0 & 0 & r & 0 & \cdots & 0 & 0 & 0 & \cdots & 0 & 0 \\
\cdots & \cdots & \cdots & \cdots & \cdots & \cdots & \cdots & \cdots & \cdots & \cdots & \cdots & \cdots & \cdots & \cdots & \cdots & \cdots & \cdots & \cdots & \cdots & \cdots & \cdots & \cdots & \cdots \\
0 & r & \cdots & 0 & 0 & 0 & \cdots & 1 & 0 & 0 & 0 & \cdots & 0 & 0 & 0 & 0 & \cdots & 0 & 0 & 0 & \cdots & 0 & 0 \\
r & 0 & \cdots & 0 & 0 & 0 & \cdots & 0 & 1 & 0 & 0 & \cdots & 0 & 0 & 0 & 0 & \cdots & r & 0 & 0 & \cdots & 0 & 0 \\
r & 0 & \cdots & 0 & 0 & 0 & \cdots & 0 & 0 & 1 & 0 & \cdots & 0 & 0 & 0 & 0 & \cdots & 0 & r & 0 & \cdots & 0 & 0 \\
0 & r & \cdots & 0 & 0 & 0 & \cdots & 0 & 0 & 0 & 1 & \cdots & 0 & 0 & 0 & 0 & \cdots & 0 & 0 & r & \cdots & 0 & 0 \\
\cdots & \cdots & \cdots & \cdots & \cdots & \cdots & \cdots & \cdots & \cdots & \cdots & \cdots & \cdots & \cdots & \cdots & \cdots & \cdots & \cdots & \cdots & \cdots & \cdots & \cdots & \cdots & \cdots \\
0 & 0 & \cdots & r & 0 & 0 & \cdots & 0 & 0 & 0 & 0 & \cdots & 1 & 0 & 0 & 0 & \cdots & 0 & 0 & 0 & \cdots & r & 0 \\
0 & 0 & \cdots & 0 & r & 0 & \cdots & 0 & 0 & 0 & 0 & \cdots & 0 & 1 & 0 & 0 & \cdots & 0 & 0 & 0 & \cdots & 0 & r \\
0 & 0 & \cdots & 0 & 0 & r & \cdots & 0 & 0 & 0 & 0 & \cdots & 0 & 0 & 1 & 0 & \cdots & 0 & 0 & 0 & \cdots & 0 & 0 \\
0 & 0 & \cdots & 0 & 0 & 0 & \cdots & 0 & 0 & 0 & 0 & \cdots & 0 & 0 & 0 & 1 & \cdots & 0 & 0 & 0 & \cdots & 0 & 0 \\
\cdots & \cdots & \cdots & \cdots & \cdots & \cdots & \cdots & \cdots & \cdots & \cdots & \cdots & \cdots & \cdots & \cdots & \cdots & \cdots & \cdots & \cdots & \cdots & \cdots & \cdots & \cdots & \cdots \\
0 & 0 & \cdots & 0 & 0 & 0 & \cdots & 0 & r & 0 & 0 & \cdots & 0 & 0 & 0 & 0 & \cdots & 1 & 0 & 0 & \cdots & 0 & 0 \\
0 & 0 & \cdots & 0 & 0 & 0 & \cdots & 0 & 0 & r & 0 & \cdots & 0 & 0 & 0 & 0 & \cdots & 0 & 1 & 0 & \cdots & 0 & 0 \\
0 & 0 & \cdots & 0 & 0 & 0 & \cdots & 0 & 0 & 0 & r & \cdots & 0 & 0 & 0 & 0 & \cdots & 0 & 0 & 1 & \cdots & 0 & 0 \\
\cdots & \cdots & \cdots & \cdots & \cdots & \cdots & \cdots & \cdots & \cdots & \cdots & \cdots & \cdots & \cdots & \cdots & \cdots & \cdots & \cdots & \cdots & \cdots & \cdots & \cdots & \cdots & \cdots \\
0 & 0 & \cdots & 0 & 0 & 0 & \cdots & 0 & 0 & 0 & 0 & \cdots & r & 0 & 0 & 0 & \cdots & 0 & 0 & 0 & \cdots & 1 & 0 \\
0 & 0 & \cdots & 0 & 0 & 0 & \cdots & 0 & 0 & 0 & 0 & \cdots & 0 & r & 0 & 0 & \cdots & 0 & 0 & 0 & \cdots & 0 & 1
\end{bmatrix} \end{array} \tag{2.98}$$

if the number of slots per pole $N/(2p)$ is odd. The coefficient r is defined as

$$r = \frac{\delta_1}{2 \cdot \delta_0} \tag{2.99}$$

and the vectors of α- and β-axes components of resulting flux density as

$$\underline{B}_\alpha = \begin{bmatrix} B_{1,\alpha} & B_{3,\alpha} & \dots & B_{\frac{N}{p}-1,\alpha} & B_{\frac{N}{p}+1,\alpha} & \dots & B_{r-2,\alpha} & B_{r,\alpha} \end{bmatrix}^{\mathrm{T}} \tag{2.100}$$

$$\underline{B}_\beta = \begin{bmatrix} B_{1,\beta} & B_{3,\beta} & \dots & B_{\frac{N}{p}-1,\beta} & B_{\frac{N}{p}+1,\beta} & \dots & B_{r-2,\beta} & B_{r,\beta} \end{bmatrix}^{\mathrm{T}} \tag{2.101}$$

In order to illustrate the mechanism of generation of air gap flux harmonics in single-slotted machines, a machine with 12 slots per pole is excited with sinusoidal air gap MMF containing only the fundamental harmonic in the amount of 1 p.u. and after that with only 5. harmonic in the amount of 0.2 p.u., as shown in Figure 2.40. The excitation with 1 p.u. of fundamental harmonic of MMF creates in this machine the 1., 11., 13., 23., 25, etc., harmonics of air gap flux density. Without contribution of evoked harmonics of MMF, the fundamental harmonic of flux density would be equal to 1 p.u.; in reality, however, it is slightly increased due to action of slot harmonics. The excitation with only fifth harmonic in the amount of 0.2 p.u. results in 5., 7., 17., 19., etc., harmonics of air gap flux density corresponding to the scheme in Table 2.4.

In Fig. 2.41 the air gap flux density distributions in three machines with full-pitch coils and various air gap geometries are shown. The machine denoted by "0" in Fig. 2.41 has no teeth and/or poles (smooth air gap), the machine denoted by "2" has two salient poles on one side of air gap and $r = \delta_1/(2\delta_0) = 0.288$, whereas the machine denoted by "12" has 12 teeth per pole pair on one side of air gap and $r = 0.331$.

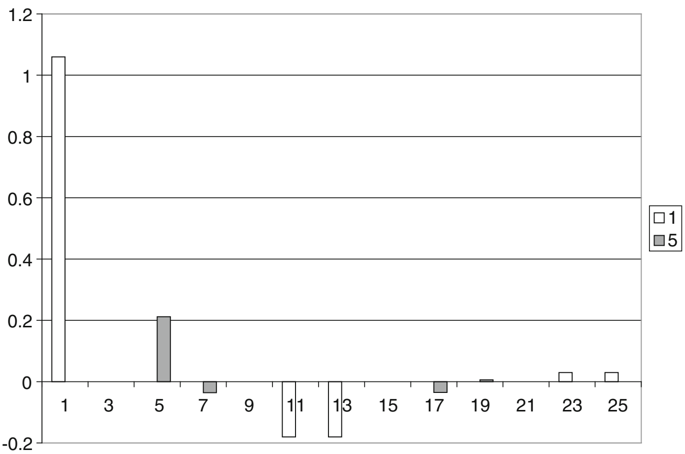

Fig. 2.40 Air gap flux density in p.u. in a machine with 12 slots per pole pair excited by the fundamental (*white bars*) and 5 harmonic (*gray bars*) of MMF

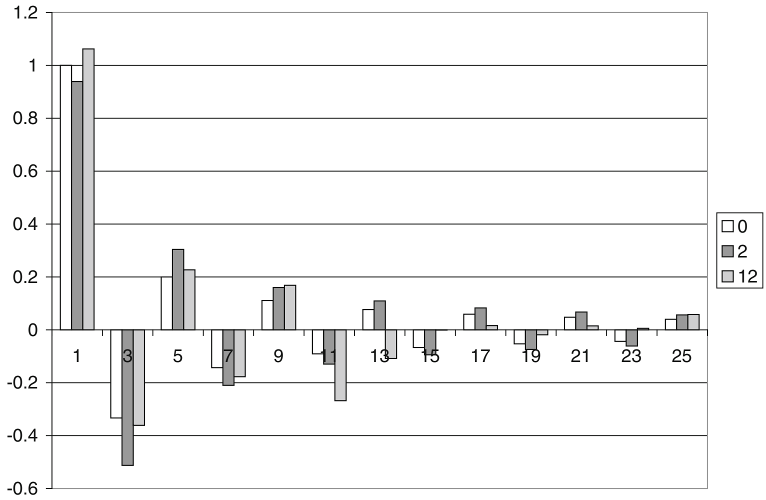

Fig. 2.41 Air gap flux density in p.u. created by current through full-pitch coil in machines with different air gap geometries and even numbers of slots per pole pair

The spectrum of air gap flux density in a machine with smooth air gap in Fig. 2.41 is identical to the spectrum of applied MMF. The amplitude of a particular harmonic of air gap flux density depends solely on the amplitude of air gap MMF with the same order. In a salient pole machine the amplitudes of flux density harmonics are lower due to relatively large interpolar space (Carter factor!). The machine with 12 teeth per pole pair illustrates in the best manner the mechanism of generation of a particular flux density harmonic through evoked harmonics. The fundamental harmonic of air gap flux density is higher than in the machine with smooth air gap, as a consequence of contribution of 11. and 13. air gap MMF harmonics. Besides, the amplitudes of 11. and 13. harmonics of air gap flux density in this machine are significantly larger than the amplitudes of their next neighbors, since very strong fundamental of the MMF contributes to their creation.

One should note that slot harmonics of the order $N/p \pm 1$ are 180° shifted to the fundamental at the axis of slot 1. If the fundamental is oriented in the positive direction of the axis of the first slot, the $(N/p - 1)$th and $(N/p + 1)$th slot harmonics are oriented in its negative direction.

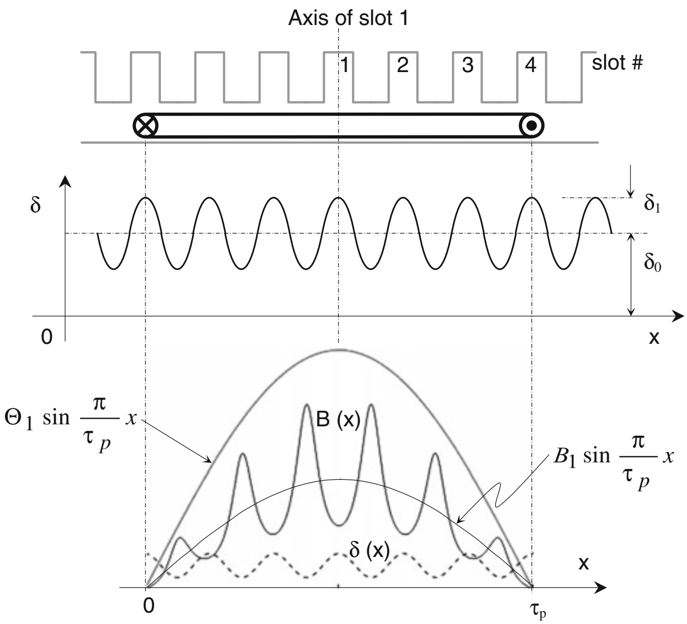

Fig. 2.42 Slotted air gap represented with a constant term and fundamental harmonic of air gap width along with the air gap flux density distribution created by the fundamental harmonic of MMF

Different phase shifts of adjacent slot harmonics are illustrated in Fig. 2.43, in which air gap flux density distribution in a single-slotted machine with 12 teeth per pole pair created by the fundamental component of MMF after Fig. 2.42 is shown.

The air gap flux density distribution in Fig. 2.43 with 12 slots per pole pair has the fundamental harmonic with amplitude B_1 and two slot harmonics with orders $N/p+1=13$ and $N/p-1=11$, as shown in Fig. 2.42

$$B_{\frac{N}{p}\pm 1}(x)=\Theta_1\frac{\mu_0}{2\delta_1}\left[\cos\left(\frac{N}{p}-1\right)\frac{\pi}{\tau_\mathrm{p}}x-\cos\left(\frac{N}{p}+1\right)\frac{\pi}{\tau_\mathrm{p}}x\right]=B_{\frac{N}{p}-1}(x)+B_{\frac{N}{p}+1}(x) \tag{2.102}$$

Slot harmonics with orders $N/p\pm 1$ are at minimum along the axis of slot 1, where the fundamental is maximum, since the air gap width at this position is maximum (slot!).

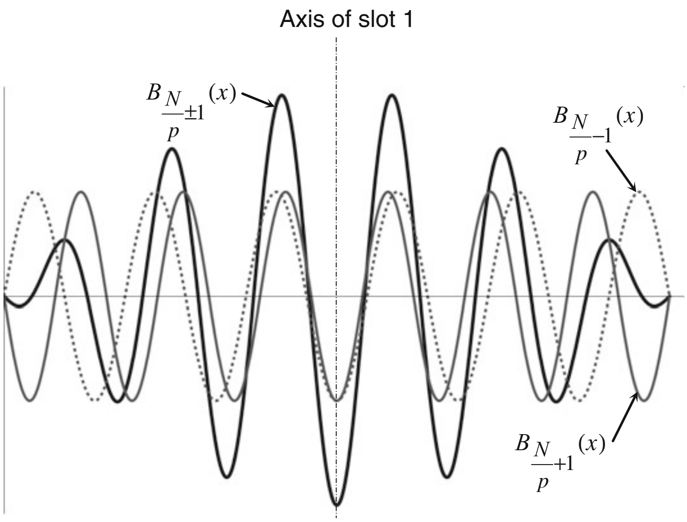

Fig. 2.43 Air gap flux density under one pole in a machine with $N/p = 12$ created by the fundamental component of MMF and fundamental harmonic of air gap width of the order N/p. In addition, two components of air gap flux density with orders $N/p - 1 = 11$ and $N/p + 1 = 13$ are shown

In special case of $N/p = 2$ (salient pole machine), the fundamental component of MMF ($n = 1$) creates

- A portion of the fundamental component ($j = n = 1$) of air gap flux density when acting on constant air gap with width δ_0,
- A portion of the fundamental component ($j = N/p - n = 1$) of air gap flux density when acting on a variable air gap with width δ_1, and
- A portion of the third harmonic component ($j = N/p + n = 3$) of air gap flux density when acting on a variable air gap with width δ_1.

which can be described by equation

$$\begin{aligned}\mu_0\Theta_1 \sin\frac{\pi}{\tau_p}x = \delta_0 B_1 \sin\frac{\pi}{\tau_p}x + \frac{\delta_1}{2}B_1 \sin(1-2)\frac{\pi}{\tau_p}\left(x - x_{0,1}\right)\\ + \frac{\delta_1}{2}B_3 \sin(3-2)\frac{\pi}{\tau_p}\left(x - x_{0,3}\right)\end{aligned} \tag{2.103}$$

as illustrated in Fig. 2.39.

In machines with **odd number of slots per pole pair N/p** the air gap flux density distribution $B(x)$ contains both odd and even harmonics

$$B(x) = \sum_{n=0,1,2,\ldots}^{\infty} B_n \cos n \frac{\pi}{\tau_p}(x - x_c) \tag{2.104}$$

in order to satisfy equation

$$B(x) \cdot \left(\delta_0 + \delta_1 \cos \frac{N}{p} \frac{\pi}{\tau_p} x\right) = \mu_0 \cdot \sum_{n=1,2,3,\ldots}^{\infty} \Theta_n \cos n \frac{\pi}{\tau_p}(x - x_c) \tag{2.105}$$

in which the MMF as well can have both odd and even terms. Note that the air gap flux density spectrum contains a constant term B_0, as a result of interaction between the *N/p*th harmonic of MMF and *N/p*th harmonic of air gap width. Flux lines of air gap flux density B_0 spread in axial direction and modify iron core flux densities in the whole machine in the manner illustrated in Fig. 2.44.

Since iron core losses are proportional to the square of maximum flux density, the shift of operating point of the machine's magnetic circuit due to homopolar flux results in increased iron core losses in the amount of $(B_0/B_m)^2$ [p.u.].

The relationship between MMF and flux density can be further written as

$$\begin{aligned} &\delta_0 \cdot \sum_{i=0,1,2,\ldots}^{\infty} B_i \cos i \frac{\pi}{\tau_p}(x - x_c) + \delta_1 \cdot \sum_{j=0,1,2,\ldots}^{\infty} B_j \cos j \frac{\pi}{\tau_p}(x - x_c) \cdot \cos \frac{N}{p} \frac{\pi}{\tau_p} x \\ &= \mu_0 \cdot \sum_{n=1,2,3,\ldots}^{\infty} \Theta_n \cos n \frac{\pi}{\tau_p}(x - x_c) \end{aligned} \tag{2.106}$$

Since *N/p* is an odd number, odd harmonics of air gap MMF can create only even harmonics of air gap flux density, whereas even harmonics of MMF create odd harmonics of flux density when interacting with the fundamental harmonic of air gap width δ_1. Following the same logic, odd harmonics of air gap MMF can create only odd harmonics of air gap flux density, and even harmonics of air gap MMF can create only even harmonics of air gap flux density when interacting with the constant term of the air gap width δ_0. Therefore,

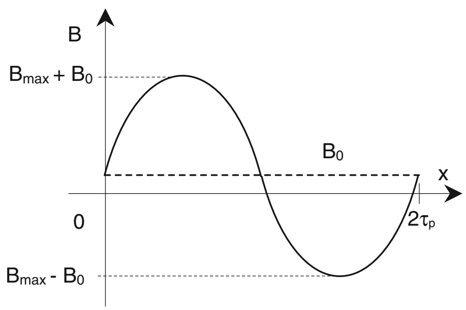

Fig. 2.44 Shift of flux density in iron core due to homopolar flux

$$
\begin{aligned}
&\delta_0 \cdot \sum_{i=0,1,2,\ldots}^{\infty} B_i \cos i \frac{\pi}{\tau_p}(x - x_c) \\
&\quad + \frac{\delta_1}{2} \sum_{j_+=0,1,2,\ldots}^{\infty} B_{j_+} \cos\left[\left(j_+ + \frac{N}{p}\right) \cdot x - j_+ \cdot x_c\right] \frac{\pi}{\tau_p} \\
&\quad + \frac{\delta_1}{2} \sum_{j_-=0,1,2,\ldots}^{\infty} B_{j_-} \cos\left[\left(j_- + \frac{N}{p}\right) \cdot x - j_- \cdot x_c\right] \frac{\pi}{\tau_p} \\
&= \mu_0 \cdot \sum_{n=1,2,3,\ldots}^{\infty} \Theta_n \cos n \frac{\pi}{\tau_p}(x - x_c)
\end{aligned}
\tag{2.107}
$$

If the applied air gap MMF distribution contains only odd terms, its nth harmonic with an amplitude of Θ_n creates in a machine with an odd number of slots per pole pair N/p again *three spatial harmonics of air gap flux density*:

- B_n (odd), in the amount of $\mu_0\ \Theta_n/\delta_0$,
- $B_{N/p-n}$ (even), in the amount of $2\ \mu_0\ \Theta_n/\delta_1$, and
- $B_{N/p+n}$ (even), in the amount of $2\ \mu_0\ \Theta_n/\delta_1$.

with corresponding fluxes Φ_ν, $\Phi_{N/p-n}$, and $\Phi_{N/p+n}$. The chain of generation of higher harmonics of air gap flux density is identical to the one shown in Fig. 2.38.

By using Eq. 2.107 and Table 2.5, one can relate the amplitude of nth harmonic of air gap flux density to corresponding applied and evoked MMFs as

$$
\begin{aligned}
B_n \cos n \frac{\pi}{\tau_p}(x - x_c) = &\frac{\mu_0}{\delta_0} \Theta_n \cos n \frac{\pi}{\tau_p}(x - x_c) \\
&+ 2\frac{\mu_0}{\delta_1} \sum_{i=1}^{\infty} \Theta_{i\frac{N}{p}-n} \cos \frac{\pi}{\tau_p}\left[nx - \left(n + i\frac{N}{p}\right)x_c\right] \\
&+ 2\frac{\mu_0}{\delta_1} \sum_{i=1}^{\infty} \Theta_{i\frac{N}{p}+n} \cos \frac{\pi}{\tau_p}\left[nx - \left(n - i\frac{N}{p}\right)x_c\right]
\end{aligned}
\tag{2.108}
$$

Table 2.5 Harmonics of flux density B created by particular harmonics of MMF Θ in a machine with odd number of slots per pole pair $N/p = \nu$

Θ \ B	0	1	2	3	4	5	…	$\nu-5$	$\nu-4$	$\nu-3$	$\nu-2$	$\nu-1$	ν	$\nu+1$	$\nu+2$	$\nu+3$	$\nu+4$	$\nu+5$
0	x												x					
1		Xx										Xx		Xx				
2			x								x				x			
3				Xx						Xx						Xx		
4					x				x								x	
5						Xx		Xx										Xx
…																		
$\nu-4$					Xx				Xx								Xx	
$\nu-3$				x						x						x		
$\nu-2$			Xx								Xx				Xx			
$\nu-1$		x										x		x				
ν	Xx												Xx					
$\nu+1$		x										x		x				
$\nu+2$			Xx								Xx				Xx			
$\nu+3$				x						x						x		
$\nu+4$					Xx				Xx								Xx	

X denotes harmonics of flux density created by applied, and x by evoked harmonics of MMF for n odd, and

$$B_n \cos n\frac{\pi}{\tau_p}(x - x_c) = \frac{\delta_1}{2\mu_0}\sum_{i=1}^{\infty}\Theta_{i\frac{N}{p}-n}\cos\frac{\pi}{\tau_p}\left[nx - \left(n + i\frac{N}{p}\right)x_c\right] + \frac{\delta_1}{2\mu_0}\sum_{i=1}^{\infty}\Theta_{i\frac{N}{p}+n}\cos\frac{\pi}{\tau_p}\left[nx - \left(n - i\frac{N}{p}\right)x_c\right] \tag{2.109}$$

for n even, except for $n = 0$. The constant term of air gap flux density ($n = 0$) representing homopolar flux is equal to

$$B_0 = \frac{\delta_1}{2\mu_0}\sum_{i=1}^{\infty}\Theta_{i\frac{N}{p}}\cos\frac{\pi}{\tau_p}\left(i\frac{N}{p}x_c\right) \tag{2.110}$$

Components of air gap flux harmonics along perpendicular axes α and β satisfy simultaneously two algebraic equations:

$$B_{n,\alpha}\cos n\frac{\pi}{\tau_p}x_c + \frac{\delta_1}{2\delta_0}B_{n-,\alpha}\cos\left(n + i\frac{N}{p}\right)x_c + \frac{\delta_1}{2\delta_0}B_{n+,\alpha}\cos\left(n - i\frac{N}{p}\right)x_c = \frac{\mu_0 \cdot \Theta_n}{\delta_0}\cos n\frac{\pi}{\tau_p}x_c \tag{2.111}$$

and

$$B_{n,\beta}\sin n\frac{\pi}{\tau_p}x_c + \frac{\delta_1}{2\delta_0}B_{n-,\beta}\sin\left(n + i\frac{N}{p}\right)x_c + \frac{\delta_1}{2\delta_0}B_{n+,\beta}\sin\left(n - i\frac{N}{p}\right)x_c = \frac{\mu_0 \cdot \Theta_n}{\delta_0}\sin n\frac{\pi}{\tau_p}x_c \tag{2.112}$$

for n odd, and

$$B_{n,\alpha}\cos n\frac{\pi}{\tau_p}x_c + \frac{\delta_1}{2\delta_0}B_{n-,\alpha}\cos\left(n + i\frac{N}{p}\right)x_c + \frac{\delta_1}{2\delta_0}B_{n+,\alpha}\cos\left(n - i\frac{N}{p}\right)x_c = 0 \tag{2.113}$$

$$B_{n,\beta}\sin n\frac{\pi}{\tau_p}x_c + \frac{\delta_1}{2\delta_0}B_{n-,\beta}\sin\left(n + i\frac{N}{p}\right)x_c + \frac{\delta_1}{2\delta_0}B_{n+,\beta}\sin\left(n - i\frac{N}{p}\right)x_c = 0 \tag{2.114}$$

for n even (no harmonics of applied MMF).

Denoting by index α the air gap flux components along the axis of the 1. slot, and by β the air gap flux components 90° ahead, one can write a system of linear equations which relate the air gap flux harmonics to the air gap MMF harmonics as

$$\underline{C}_{\delta} \cdot \underline{B}_{\alpha,\beta} = \underline{\theta}_{\alpha,\beta} \tag{2.115}$$

where

$$\underline{C}_{\delta} = \begin{bmatrix}
1 & 0 & 0 & 0 & 0 & \cdots & 0 & 0 & 0 & 0 & r & r & 0 & 0 & 0 & 0 & \cdots & 0 & 0 & \cdots & 0 & 0 \\
0 & 1 & 0 & 0 & 0 & \cdots & 0 & 0 & r & 0 & 0 & 0 & r & 0 & 0 & 0 & \cdots & 0 & 0 & \cdots & 0 & 0 \\
0 & 0 & 1 & 0 & 0 & \cdots & 0 & 0 & 0 & r & 0 & 0 & 0 & r & 0 & 0 & \cdots & 0 & 0 & \cdots & 0 & 0 \\
0 & 0 & 0 & 1 & 0 & \cdots & r & 0 & 0 & 0 & 0 & 0 & 0 & 0 & r & 0 & \cdots & 0 & 0 & \cdots & 0 & 0 \\
0 & 0 & 0 & 0 & 1 & \cdots & 0 & r & 0 & 0 & 0 & 0 & 0 & 0 & 0 & r & \cdots & 0 & 0 & \cdots & 0 & 0 \\
\cdots & \cdots & \cdots & \cdots & \cdots & \cdots & \cdots & \cdots & \cdots & \cdots & \cdots & \cdots & \cdots & \cdots & \cdots & \cdots & \cdots & \cdots & \cdots & \cdots & \cdots & \cdots \\
0 & 0 & 0 & r & 0 & \cdots & 1 & 0 & 0 & 0 & 0 & 0 & 0 & 0 & 0 & 0 & \cdots & 0 & 0 & \cdots & 0 & 0 \\
0 & 0 & 0 & 0 & r & \cdots & 0 & 1 & 0 & 0 & 0 & 0 & 0 & 0 & 0 & 0 & \cdots & 0 & 0 & \cdots & 0 & 0 \\
0 & r & 0 & 0 & 0 & \cdots & 0 & 0 & 1 & 0 & 0 & 0 & 0 & 0 & 0 & 0 & \cdots & 0 & 0 & \cdots & 0 & 0 \\
0 & 0 & r & 0 & 0 & \cdots & 0 & 0 & 0 & 1 & 0 & 0 & 0 & 0 & 0 & 0 & \cdots & 0 & 0 & \cdots & 0 & 0 \\
r & 0 & 0 & 0 & 0 & \cdots & 0 & 0 & 0 & 0 & 0 & 0 & 0 & 0 & 0 & 0 & \cdots & 0 & 0 & \cdots & 0 & 0 \\
r & 0 & 0 & 0 & 0 & \cdots & 0 & 0 & 0 & 0 & 0 & 1 & 0 & 0 & 0 & 0 & \cdots & 0 & 0 & \cdots & 0 & 0 \\
0 & r & 0 & 0 & 0 & \cdots & 0 & 0 & 0 & 0 & 0 & 0 & 1 & 0 & 0 & 0 & \cdots & 0 & 0 & \cdots & 0 & 0 \\
0 & 0 & r & 0 & 0 & \cdots & 0 & 0 & 0 & 0 & 0 & 0 & 0 & 1 & 0 & 0 & \cdots & 0 & 0 & \cdots & 0 & 0 \\
0 & 0 & 0 & r & 0 & \cdots & 0 & 0 & 0 & 0 & 0 & 0 & 0 & 0 & 1 & 0 & \cdots & 0 & 0 & \cdots & 0 & 0 \\
0 & 0 & 0 & 0 & r & \cdots & 0 & 0 & 0 & 0 & 0 & 0 & 0 & 0 & 0 & 1 & \cdots & 0 & 0 & \cdots & 0 & 0 \\
\cdots & \cdots & \cdots & \cdots & \cdots & \cdots & \cdots & \cdots & \cdots & \cdots & \cdots & \cdots & \cdots & \cdots & \cdots & \cdots & \cdots & \cdots & \cdots & \cdots & \cdots & \cdots \\
0 & 0 & 0 & 0 & 0 & \cdots & 0 & 0 & 0 & 0 & 0 & 0 & 0 & 0 & 0 & 0 & \cdots & 1 & 0 & \cdots & r & 0 \\
0 & 0 & 0 & 0 & 0 & \cdots & 0 & 0 & 0 & 0 & 0 & 0 & 0 & 0 & 0 & 0 & \cdots & 0 & 1 & \cdots & 0 & r \\
\cdots & \cdots & \cdots & \cdots & \cdots & \cdots & \cdots & \cdots & \cdots & \cdots & \cdots & \cdots & \cdots & \cdots & \cdots & \cdots & \cdots & \cdots & \cdots & \cdots & \cdots & \cdots \\
0 & 0 & 0 & 0 & 0 & \cdots & 0 & 0 & 0 & 0 & 0 & 0 & 0 & 0 & 0 & 0 & \cdots & r & 0 & \cdots & 1 & 0 \\
0 & 0 & 0 & 0 & 0 & \cdots & 0 & 0 & 0 & 0 & 0 & 0 & 0 & 0 & 0 & 0 & \cdots & 0 & r & \cdots & 0 & 1
\end{bmatrix} \tag{2.116}$$

and

$$\underline{B}_{\alpha,\beta} = \begin{bmatrix} B_0 & B_{1,\alpha} & B_{1,\beta} & B_{2,\alpha} & B_{2,\beta} & \ldots & B_{n-1,\alpha} & B_{n-1,\beta} & B_{n,\alpha} & B_{n,\beta} \end{bmatrix}^T \tag{2.117}$$

Here again the coefficient r was used

$$r = \frac{\delta_1}{2 \cdot \delta_0} \tag{2.118}$$

The vector of applied MMFs has only odd terms

$$\underline{\Theta}_{\alpha,\beta} = \frac{\mu_0}{\delta_0}\begin{bmatrix} 0 \\ \Theta_1 \cos\frac{\pi}{\tau_p}x_c \\ \Theta_1 \sin\frac{\pi}{\tau_p}x_c \\ 0 \\ 0 \\ \Theta_3 \cos 3\frac{\pi}{\tau_p}x_c \\ \Theta_3 \sin 3\frac{\pi}{\tau_p}x_c \\ \cdots \\ \cdots \\ \Theta_{n-2} \cos(n-2)\frac{\pi}{\tau_p}x_c \\ \Theta_{n-2} \sin(n-2)\frac{\pi}{\tau_p}x_c \\ 0 \\ 0 \\ \Theta_n \cos n\frac{\pi}{\tau_p}x_c \\ \Theta_n \sin n\frac{\pi}{\tau_p}x_c \end{bmatrix} \tag{2.119}$$

The previous considerations can be illustrated by means of Fig. 2.45, in which the air gap flux density spectrum in a tooth-wound machine with $N/p = 3$ and in a machine with $N/p = 11$ are shown for a coil shift of $x_{coil} = 0$. The spectrum of applied MMF in the machine with $N/p = 3$ contains both odd and even harmonics, and in the machine with $N/p = 11$ only odd harmonics were present. In both cases, however, even harmonics of air gap flux density, including the homopolar flux, are generated. The amplitudes of air gap flux density harmonics in Fig. 2.45 are shown along with their phase shifts.

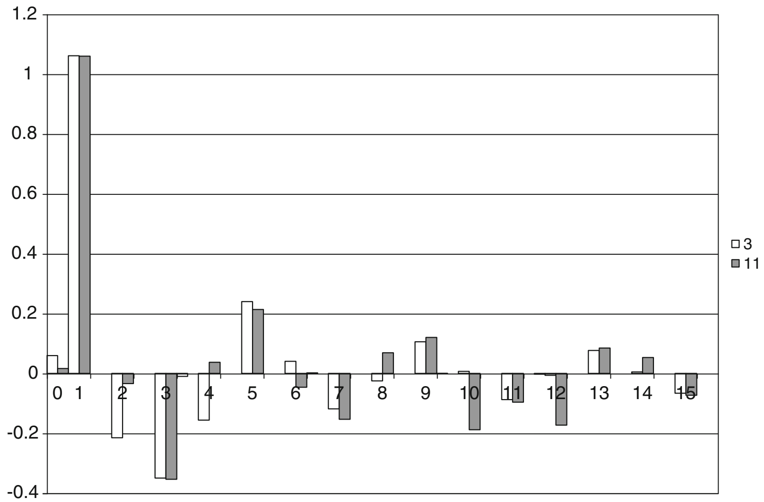

Fig. 2.45 Air gap flux density harmonics in p.u. created by current-carrying coil in machines with 3 and 11 slots per pole pair

Slot harmonics with order $N/p \pm 1$ are in both machines even and have relatively large amplitudes. Besides, a homopolar flux is generated, which is proportional to B_0.

The two components of air gap flux density with period lengths of $\tau_p/(N/p \pm 1)$ are sources of higher harmonics in the induced voltage, pulsating torque on the shaft, and vibrations due to pulsating radial forces. For these reasons, the amplitudes of the two components of flux density must be reduced.

Pitch factor for slot harmonics of order $N/p \pm 1$ is equal to (see Eq. 2.21):

$$f_{\mathrm{p},\frac{N}{p}\pm 1} = \sin\left(\frac{N}{p} \pm 1\right)\frac{y}{\tau_{\mathrm{ps}}}\frac{\pi}{2} = \sin\left(\frac{N}{p}\frac{y}{\frac{N}{2p}}\frac{\pi}{2} \pm \frac{y}{\tau_{\mathrm{ps}}}\frac{\pi}{2}\right) = \sin\left(y\pi \pm \frac{y}{\tau_{\mathrm{ps}}}\frac{\pi}{2}\right)$$
$$= \pm\sin\frac{y}{\tau_{\mathrm{ps}}}\frac{\pi}{2} \tag{2.120}$$

which is the pitch factor for the fundamental. Since the coil pitch is selected in such a manner as not to decrease too much the fundamental, the pitch factor for air gap slot harmonics with orders $N/p \pm 1$ is high. Pitching the coils cannot fight slot harmonics.

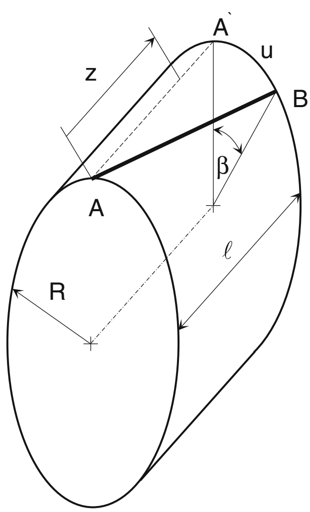

Fig. 2.46 Axial skewing of a conductor for an angle β

One recalls that higher harmonics of the MMF can be reduced on the coil, pole, and/or fundamental pole basis. In all three cases, the coil parameters in *circumferential* direction are modified. In heteropolar machines, the coil geometry offers a possibility of impacting the air gap quantities by *skewing* the coils in *axial* direction, as shown in Fig. 2.46.

Effects of skewing in Fig. 2.46 can be illustrated in the circumferential–axial (x, z) plane in the manner shown in Fig. 2.47. The black drawn coil has a pitch y and is skewed for the amount of u

$$u = \beta \cdot R \tag{2.121}$$

The fundamental component of air gap flux density can be written as

$$B_1(x) = B_{\max} \sin \frac{\pi}{\tau_p} x \tag{2.122}$$

The amount of flux concatenated by the skewed coil in Fig. 2.47 is equal to

$$\Phi_1 = \int_0^l \int_{x_0 + \frac{u}{l}z}^{x_0 + \frac{u}{l}z + y} B_{\max} \sin \frac{\pi}{\tau_p} x \mathrm{d}x \mathrm{d}z = \frac{l \tau_p^2}{u \pi^2} \cdot \left[-\sin \frac{\pi}{\tau_p} x_0 + \sin \frac{\pi}{\tau_p}(u + x_0) + \sin \frac{\pi}{\tau_p}(y + x_0) - \sin \frac{\pi}{\tau_p}(u + y + x_0) \right] \tag{2.123}$$

or, after some trigonometric simplifications

$$\Phi_1 = \frac{2}{\pi} l \tau_p B_{\max} \cdot \frac{\sin \frac{\beta_{el}}{2}}{\frac{\beta_{el}}{2}} \cdot \sin\left(\frac{y}{\tau_p} \frac{\pi}{2}\right) \cdot \sin\left(\frac{2x_0 + u + y}{2} \frac{\pi}{\tau_p}\right) \tag{2.124}$$

As expected, the flux concatenated between the fundamental component of air gap flux density and a coil is a function of coil shift x_0. The concatenated flux is reduced by two factors: the pitch factor, and the skewing factor $f_{sk,1}$

$$f_{sk,1} = \frac{\sin \frac{\beta_{el}}{2}}{\frac{\beta_{el}}{2}} \tag{2.125}$$

where

$$\beta_{el} = p \cdot \beta = p \cdot \frac{u}{R} \tag{2.126}$$

The skewing factor is a measure for loss of flux due to skewing and is always less than one. For an arbitrary nth harmonic, the concatenated flux is equal to

$$\Phi_n = \frac{2}{\pi} l \tau_p B_{\max} \cdot \frac{\sin n \frac{\beta_{el}}{2}}{n \frac{\beta_{el}}{2}} \cdot \sin\left(n \frac{y}{\tau_p} \frac{\pi}{2}\right) \cdot \sin\left(\frac{2nx_0 + u + y}{2} \frac{\pi}{\tau_p}\right) \tag{2.127}$$

and the skewing factor $f_{sk,n}$:

$$f_{\mathrm{sk},n} = \frac{\sin n \frac{\beta_{\mathrm{el}}}{2}}{n \frac{\beta_{\mathrm{el}}}{2}} \tag{2.128}$$

If the machine is skewed for one slot pitch

$$u = \frac{2R\pi}{N}; \quad \beta_{\mathrm{el}} = p \cdot \frac{u}{R} = p \frac{2\pi}{N} \tag{2.129}$$

Fig. 2.47 Representation of a skewed coil in the (x, z) plane

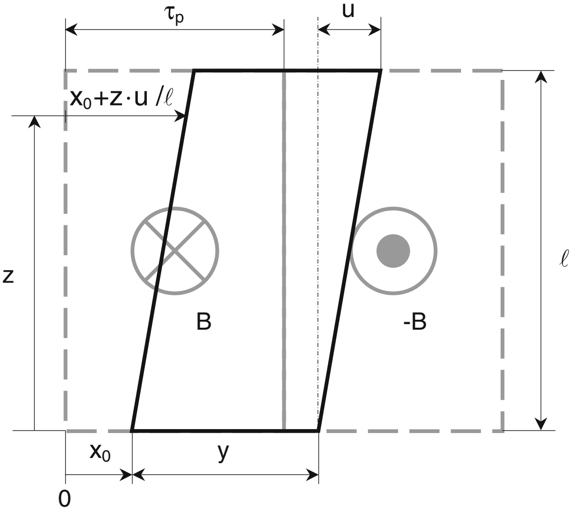

the skewing factor becomes

$$f_{\mathrm{sk},n} = \frac{\sin np \frac{\pi}{N}}{np \frac{\pi}{N}} \tag{2.130}$$

The skewing factor for slot harmonics of the order $n = N/p \pm 1$ can now be expressed as

$$f_{\mathrm{sk},\frac{N}{p}\pm 1} = \frac{\sin\left(\frac{N}{p} \pm 1\right) p \frac{\pi}{N}}{\left(\frac{N}{p} \pm 1\right) p \frac{\pi}{N}} = \pm \frac{\sin p \frac{\pi}{N}}{p \frac{\pi}{N}} \frac{1}{\frac{N}{p} \pm 1} = \pm f_{\mathrm{sk},1} \cdot \frac{1}{\frac{N}{p} \pm 1} \tag{2.131}$$

By skewing the slots for one slot pitch, the amplitude of the nth harmonic of concatenated flux decreases to $1/(N/p \pm 1)$ of the amplitude of the fundamental. Slot skewing is the only efficient means to decrease the amplitudes of slot harmonics in the air gap flux density distribution.

2.5.4 Magnetic Gears

Relationships between the orders of harmonic in a single-slotted air gap, summarized in Tables 2.4 and 2.5, can be illustrated by the example of magnetic gears, as shown in Fig. 2.48. The magnetic gear in this figure has three concentric shells, each of which can freely rotate. The outer and inner shells carry excitation, usually permanent magnets, and the intermediate shell is used to modulate the permeance between the two.

Denoting by n the number of pole pairs of the inner shell, by k the order of lowest harmonic of the air gap permeance created by the intermediate shell, and by ℓ the number of pole pairs of the outer shell, one can express the condition for interaction between harmonics given in Tables 2.4 and 2.5 as

$$k = n \pm l \tag{2.132}$$

If the sign of ℓ in Eq. 2.132 is positive, the inner and outer field must rotate in opposite directions in order to build a torque with the given number of poles of the intermediate shell. If the sign is negative, both inner and outer shells rotate in the same direction.

Gear ratio i, i.e., the ratio between speeds of outer and inner shells is obviously equal to

$$i = \frac{n}{l} \tag{2.133}$$

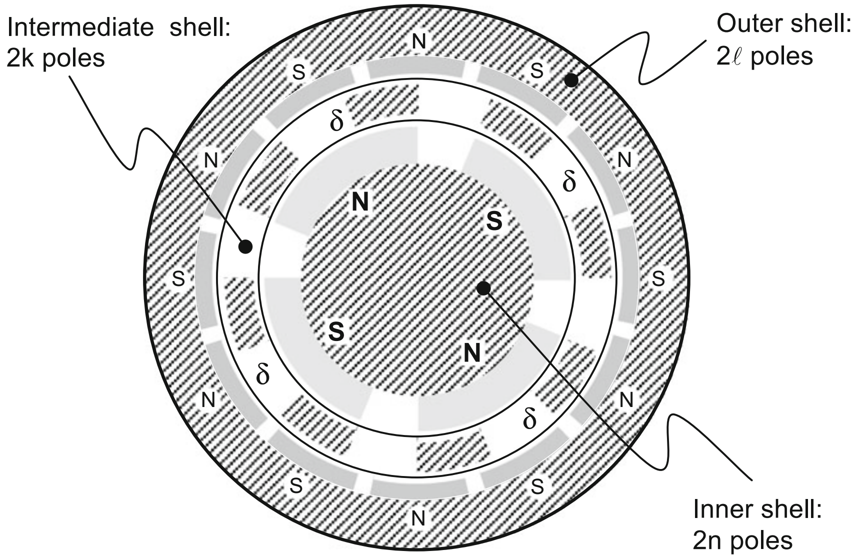

Fig. 2.48 Magnetic gear. *Shaded area* iron; *gray area* magnets; *white area* non-magnetic

2.5.5 Flux Density Distribution in the Air Gap of a Double-Slotted Machine

Consider a double-slotted machine, the air gap width of which is described as

$$\delta(x) = \delta_0 + \sum_{i=1,3,5,\ldots}^{\infty} \delta_{s,i} \cos i \frac{N_s}{p} \frac{\pi}{\tau_p} x + \sum_{j=1,3,5,\ldots}^{\infty} \delta_{r,j} \cos j \frac{N_r}{p} \frac{\pi}{\tau_p} (x - x_0) \qquad (2.134)$$

where index "s" is related to stator, and "r" to rotor quantities, and x_0 is the rotor shift. A double-slotted machine with excitation on both sides of the air gap is shown in Fig. 2.49.

Due to their minor influence on machine performance, higher harmonics of stator and rotor air gap widths can be neglected. With this assumption, one can write for air gap quantities

$$\begin{aligned} &B(x, x_0) \cdot \left[\delta_0 + \delta_{s,1} \cos \frac{N_s}{p} \frac{\pi}{\tau_p} x + \delta_{r,1} \cos \frac{N_r}{p} \frac{\pi}{\tau_p} (x - x_0)\right] \\ &= \mu_0 \cdot \left[\sum_{n=1,3,5,\ldots}^{\infty} \Theta_{s,n} \cos n \frac{\pi}{\tau_p} x + \sum_{k=1,3,5,\ldots}^{\infty} \Theta_{r,k} \cos k \frac{\pi}{\tau_p} (x - x_0)\right] \end{aligned} \qquad (2.135)$$

where

$$B(x, x_0) = \sum_{i=0,1,2,\ldots}^{\infty} B_i \cos i \frac{\pi}{\tau_p} (x - x_i) \qquad (2.136)$$

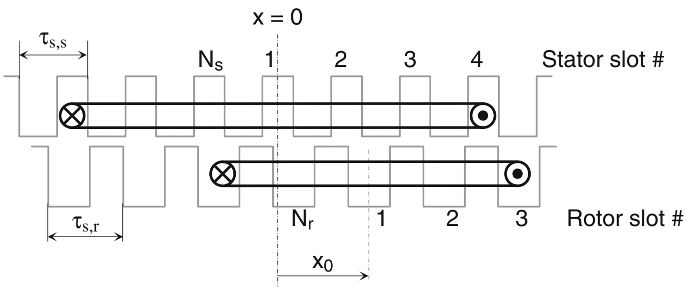

Fig. 2.49 Double-slotted air gap with stator and rotor excitation

The nth harmonic of total (stator plus rotor) applied MMF can be written as

$$\Theta_n = \Theta_{n,\max} \cos n \frac{\pi}{\tau_p} (x - \xi_n) \tag{2.137}$$

where

$$\Theta_{n,\max} = \sqrt{\Theta_{s,n}^2 + \Theta_{r,n}^2 + 2\Theta_{s,n}\Theta_{r,n} \cos n \frac{\pi}{\tau_p} x_0} \tag{2.138}$$

and

$$\xi_n = \frac{\tau_p}{\pi} \arctan \varepsilon_n; \quad \varepsilon_n = \frac{\Theta_{r,n} \sin n \frac{\pi}{\tau_p} x_0}{\Theta_{s,n} + \Theta_{r,n} \cos n \frac{\pi}{\tau_p} x_0} \tag{2.139}$$

The shift ξ_n denotes the position of maximum of total MMF. Constant term in the flux density spectrum B_0 is generated when either N_s/p or N_r/p is odd. Accordingly

$$\begin{aligned}
&\delta_0 \sum_{i=0,1,2,\ldots}^{\infty} B_i \cos i \frac{\pi}{\tau_p} (x - \xi_i) \\
&\quad + \delta_{s,1} \sum_{j=0,1,2,\ldots}^{\infty} B_j \cos j \frac{\pi}{\tau_p} \left(x - \xi_j\right) \cdot \cos \frac{N_s}{p} \frac{\pi}{\tau_p} x \\
&\quad + \delta_{r,1} \sum_{k=0,1,2,\ldots}^{\infty} B_k \cos k \frac{\pi}{\tau_p} (x - \xi_k) \cdot \cos \frac{N_r}{p} \frac{\pi}{\tau_p} (x - x_0) \\
&= \mu_0 \sum_{n=1,3,5,\ldots}^{\infty} \Theta_{n,\max} \cos n \frac{\pi}{\tau_p} (x - \xi_n)
\end{aligned} \tag{2.140}$$

or

$$\begin{aligned}
&\delta_0 \sum_{i=0,1,2,\ldots}^{\infty} B_i \cos i \frac{\pi}{\tau_p} (x - \xi_i) + \frac{\delta_{s,1}}{2} \sum_{j=0,1,2,\ldots}^{\infty} B_j \cos \frac{\pi}{\tau_p} \left[\left(\frac{N_s}{p} + j \right) \cdot x - j \cdot \xi_j \right] \\
&+ \frac{\delta_{s,1}}{2} \sum_{j=0,1,2,\ldots}^{\infty} B_j \cos \frac{\pi}{\tau_p} \left[\left(\frac{N_s}{p} - j \right) \cdot x + j \cdot \xi_j \right] + \frac{\delta_{r,1}}{2} \sum_{k=0,1,2,\ldots}^{\infty} B_k \cos \frac{\pi}{\tau_p} \left[\left(\frac{N_r}{p} + k \right) \cdot x - k \cdot \left(\xi_k + \frac{N_r}{p} x_0 \right) \right] \\
&+ \frac{\delta_{r,1}}{2} \sum_{k=0,1,2,\ldots}^{\infty} B_k \cos \frac{\pi}{\tau_p} \left[\left(\frac{N_r}{p} - k \right) \cdot x + k \cdot \left(\xi_k - \frac{N_r}{p} x_0 \right) \right] = \mu_0 \sum_{n=1,3,5,\ldots}^{\infty} \Theta_{n,\max} \cos n \frac{\pi}{\tau_p} (x - \xi_n)
\end{aligned} \tag{2.141}$$

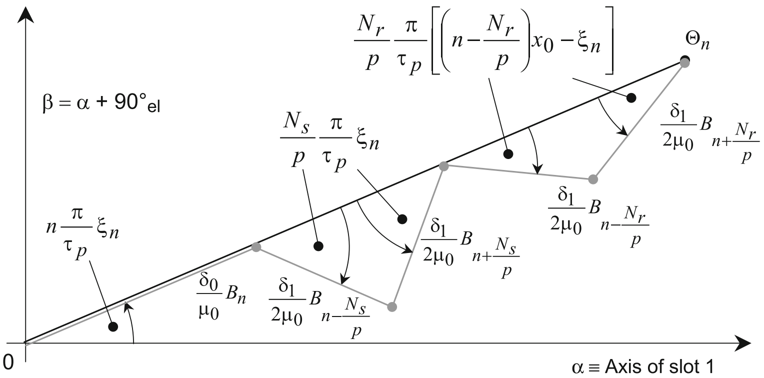

Fig. 2.50 Illustrating the relationship between MMF and flux density harmonic components in a machine with double-slotted air gap

Assume for the purpose of simplicity that both N_s/p and N_r/p are even. The nth (odd) harmonic of applied MMF creates *five components of flux density with the same order n* (Fig. 2.50):

- B_n (odd), in the amount of $\mu_0\ \Theta_n/\delta_0$,
- $B_{n-N_s/p}$ (odd), in the amount of $2\ \mu_0\ \Theta_n/\delta_1$,
- $B_{n+N_s/p}$ (odd), in the amount of $2\ \mu_0\ \Theta_n/\delta_1$,
- $B_{n-N_r/p}$ (odd), in the amount of $2\ \mu_0\ \Theta_n/\delta_1$, and
- $B_{n+N_r/p}$ (odd), in the amount of $2\ \mu_0\ \Theta_n/\delta_1$.

which satisfy equation

$$\begin{aligned}\mu_0\Theta_{n,\max}\cos n\frac{\pi}{\tau_p}(x-\xi_n) &= \delta_0 B_n\cos n\frac{\pi}{\tau_p}(x-\xi_n)+\frac{\delta_{s,1}}{2}B_{n-\frac{N_s}{p}}\cos\frac{\pi}{\tau_p}\left[nx-\left(n+\frac{N_s}{p}\right)\xi_n\right]\\&+\frac{\delta_{s,1}}{2}B_{n+\frac{N_s}{p}}\cos\frac{\pi}{\tau_p}\left[nx-\left(n-\frac{N_s}{p}\right)\xi_n\right]+\frac{\delta_{r,1}}{2}B_{n-\frac{N_r}{p}}\cos\frac{\pi}{\tau_p}\left[nx-\left(n-\frac{N_r}{p}\right)\left(\xi_n+\frac{N_r}{p}x_0\right)\right]\\&+\frac{\delta_{r,1}}{2}B_{n+\frac{N_r}{p}}\cos\frac{\pi}{\tau_p}\left[nx-\left(n-\frac{N_r}{p}\right)\left(\xi_n-\frac{N_r}{p}x_0\right)\right]\end{aligned} \tag{2.142}$$

The nth harmonic of total (stator plus rotor) applied MMF contributes to the nth, $N_s/p - n$, $N_s/p + n$, $N_r/p - n$, and $N_r/p + n$ harmonics of the air gap flux density, since these harmonics, when modulated with corresponding slot harmonics, have the same order equal to n.

Table 2.6 Initial harmonics of flux density *B* created by particular harmonics of MMF Θ in a double-slotted machine with even number of slots per pole pair ν on one side of the air gap and μ. on the other

		B																
		1	3	5	…	ν − 5	ν − 3	ν − 1	ν + 1	ν + 3	ν + 5	…	μ − 5	μ − 3	μ − 1	μ + 1	μ + 3	μ + 5
Θ	1	**Xx**						Xx	Xx						*Xx*	*Xx*		
	3		**Xx**				Xx			Xx				*Xx*			*Xx*	
	5			**Xx**		Xx					Xx		*Xx*					*Xx*
	…																	
	ν − 5			Xx		**Xx**					*Xx*							
	ν − 3		Xx				**Xx**			*Xx*								
	ν − 1	Xx						**Xx**	*Xx*									
	ν + 1	Xx						*Xx*	**Xx**									
	ν + 3		Xx				*Xx*			**Xx**								
	ν + 5			Xx		*Xx*					**Xx**							
	…																	
	μ − 5			*Xx*									**Xx**					
	μ − 3		*Xx*											**Xx**				
	μ − 1	*Xx*													**Xx**			
	μ + 1	*Xx*														**Xx**		
	μ + 3		*Xx*														**Xx**	
	μ + 5			*Xx*														**Xx**

X denotes harmonics of flux density created by applied, and x by evoked harmonics of MMF

Initial terms of the chain of generation of flux density from a single harmonic of total applied MMF is shown in Fig. 2.51.

By using the scheme in Fig. 2.51, one can generate Table 2.6 in which the relationship between applied and evoked MMF harmonics on one side and air gap flux density harmonics on the other is given. Here symbol ν is used to denote the number of slots per pole pair on one side of the air gap, and μ on the other. Normal font letters denote harmonics due to ν, and italic styled those due to μ. Harmonics denoted by bold letters contain components due to both ν and μ.

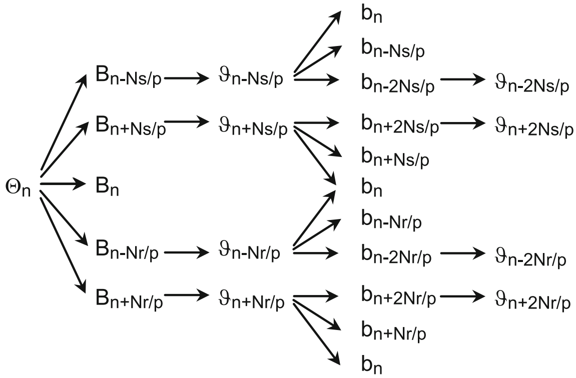

Fig. 2.51 The beginning of the chain of generation of flux density harmonics from a single harmonic of total applied MMF in a double-slotted machine

Using Eq. 2.142 and Table 2.6, one can relate the amplitude of *n*th harmonic of air gap flux density to corresponding applied and evoked MMFs as

$$\begin{aligned}
B_n \cos n\frac{\pi}{\tau_p}(x-\xi_n) &= \frac{\mu_0}{\delta_0}\Theta_{n,\max}\cos n\frac{\pi}{\tau_p}(x-\xi_n) \\
&+ 2\frac{\mu_0}{\delta_{s,1}}\sum_{i=1}^{\infty}\Theta_{i\frac{N_s}{p}-n}\cos\frac{\pi}{\tau_p}\left[nx-\left(n+i\frac{N_s}{p}\right)\xi_n\right] \\
&+ 2\frac{\mu_0}{\delta_{s,1}}\sum_{i=1}^{\infty}\Theta_{i\frac{N_s}{p}+n}\cos\frac{\pi}{\tau_p}\left[nx-\left(n-i\frac{N_s}{p}\right)\xi_n\right] \\
&+ 2\frac{\mu_0}{\delta_{r,1}}\sum_{i=1}^{\infty}\Theta_{i\frac{N_r}{p}-n}\cos\frac{\pi}{\tau_p}\left[nx-\left(n+i\frac{N_r}{p}\right)\left(\xi_n+\frac{N_r}{p}x_0\right)\right] \\
&+ 2\frac{\mu_0}{\delta_{r,1}}\sum_{i=1}^{\infty}\Theta_{i\frac{N_r}{p}+n}\cos\frac{\pi}{\tau_p}\left[nx-\left(n-i\frac{N_r}{p}\right)\left(\xi_n-\frac{N_r}{p}x_0\right)\right]
\end{aligned} \tag{2.143}$$

Components of air gap flux created by applied MMF harmonics along perpendicular axes α and β in Fig. 2.50 satisfy for $i = 1$ simultaneously two algebraic equations

$$
\begin{aligned}
&B_{n,\alpha}\cos n\frac{\pi}{\tau_\mathrm{p}}\xi_n+\frac{\delta_1}{2\delta_0}B_{n-,\alpha}\cos\left(n+\frac{N_\mathrm{s}}{p}\right)\xi_n+\frac{\delta_1}{2\delta_0}B_{n+,\alpha}\cos\left(n-\frac{N_\mathrm{s}}{p}\right)\xi_n\\
&\quad+\frac{\delta_1}{2\delta_0}B_{n-,\alpha}\cos\left(n+\frac{N}{p}\right)\left(\xi_n+\frac{N_\mathrm{r}}{p}x_0\right)\\
&\quad+\frac{\delta_1}{2\delta_0}B_{n+,\alpha}\cos\left(n-\frac{N}{p}\right)\left(\xi_n-\frac{N_\mathrm{r}}{p}x_0\right)=\frac{\mu_0\cdot\Theta_n}{\delta_0}\cos n\frac{\pi}{\tau_\mathrm{p}}\xi_n
\end{aligned}
\tag{2.144}
$$

and

$$
\begin{aligned}
&B_{n,\alpha}\sin sn\frac{\pi}{\tau_\mathrm{p}}\xi_n+\frac{\delta_1}{2\delta_0}B_{n-,\alpha}\sin\left(n+\frac{N_\mathrm{s}}{p}\right)\xi_n+\frac{\delta_1}{2\delta_0}B_{n+,\alpha}\sin\left(n-\frac{N_\mathrm{s}}{p}\right)\xi_n\\
&\quad+\frac{\delta_1}{2\delta_0}B_{n-,\alpha}\sin\left(n+\frac{N}{p}\right)\left(\xi_n+\frac{N_\mathrm{r}}{p}x_0\right)\\
&\quad+\frac{\delta_1}{2\delta_0}B_{n+,\alpha}\sin\left(n-\frac{N}{p}\right)\left(\xi_n-\frac{N_\mathrm{r}}{p}x_0\right)=\frac{\mu_0\cdot\Theta_n}{\delta_0}\sin n\frac{\pi}{\tau_\mathrm{p}}\xi_n
\end{aligned}
\tag{2.145}
$$

By applying the principle of orthogonality of trigonometric functions through the separation of sine and cosine terms, one can derive from Eq. 2.143 a system of $2n + 1$ algebraic equations (one for the constant term plus two for each harmonic) for air gap quantities in a doubly slotted machine:

$$\left(\underline{C}_{\mathrm{s},\delta}+\underline{C}_{\mathrm{r},\delta}\right)\cdot\underline{B}_{\alpha,\beta}=\underline{\vartheta}_{\alpha,\beta} \tag{2.146}$$

where the solution vector of air gap flux density harmonics $B_{\alpha,\beta}$ is defined as

$$\underline{B}_{\alpha,\beta}=\left[B_0\quad B_{1,\alpha}\quad B_{1,\beta}\quad B_{2,\alpha}\quad B_{2,\beta}\quad \ldots\quad B_{n-1,\alpha}\quad B_{n-1,\beta}\quad B_{n,\alpha}\quad B_{n,\beta}\right] \tag{2.147}$$

By making use of substitutions

$$r_\mathrm{s}=\frac{\delta_{\mathrm{s},1}}{2\cdot\delta_0};\quad r_\mathrm{r}=\frac{\delta_{\mathrm{r},1}}{2\cdot\delta_0} \tag{2.148}$$

one can define the system matrices $C_{\mathrm{s},\delta}$ (Eq. 2.149) and $C_{\mathrm{r},\delta}$ (Eq. 2.150) as

$$
\underline{C}_{\mathrm{s},\delta} = \begin{bmatrix}
1 & 0 & 0 & 0 & 0 & \cdots & 0 & 0 & 0 & 0 & r_\mathrm{s} & r_\mathrm{s} & 0 & 0 & 0 & 0 & \cdots & 0 & 0 & \cdots & 0 & 0 \\
0 & 1 & 0 & 0 & 0 & \cdots & 0 & 0 & r_\mathrm{s} & 0 & 0 & 0 & r_\mathrm{s} & 0 & 0 & 0 & \cdots & 0 & 0 & \cdots & 0 & 0 \\
0 & 0 & 1 & 0 & 0 & \cdots & 0 & 0 & 0 & r_\mathrm{s} & 0 & 0 & 0 & r_\mathrm{s} & 0 & 0 & \ldots & 0 & 0 & \cdots & 0 & 0 \\
0 & 0 & 0 & 1 & 0 & \cdots & r_\mathrm{s} & 0 & 0 & 0 & 0 & 0 & 0 & 0 & r_\mathrm{s} & 0 & \cdots & 0 & 0 & \cdots & 0 & 0 \\
0 & 0 & 0 & 0 & 1 & \cdots & 0 & r_\mathrm{s} & 0 & 0 & 0 & 0 & 0 & 0 & 0 & r_\mathrm{s} & \cdots & 0 & 0 & \cdots & 0 & 0 \\
\ldots & \ldots & \ldots & \ldots & \ldots & \ldots & \ldots & \ldots & \ldots & \ldots & \ldots & \ldots & \ldots & \ldots & \ldots & \ldots & \ldots & \ldots & \ldots & \ldots & \ldots & \ldots \\
0 & 0 & 0 & r_\mathrm{s} & 0 & \cdots & 1 & 0 & 0 & 0 & 0 & 0 & 0 & 0 & 0 & 0 & \cdots & 0 & 0 & \cdots & 0 & 0 \\
0 & 0 & 0 & 0 & r_\mathrm{s} & \cdots & 0 & 1 & 0 & 0 & 0 & 0 & 0 & 0 & 0 & 0 & \cdots & 0 & 0 & \cdots & 0 & 0 \\
0 & r_\mathrm{s} & 0 & 0 & 0 & \cdots & 0 & 0 & 1 & 0 & 0 & 0 & 0 & 0 & 0 & 0 & \cdots & 0 & 0 & \cdots & 0 & 0 \\
0 & 0 & r_\mathrm{s} & 0 & 0 & \cdots & 0 & 0 & 0 & 1 & 0 & 0 & 0 & 0 & 0 & 0 & \cdots & 0 & 0 & \cdots & 0 & 0 \\
r_\mathrm{s} & 0 & 0 & 0 & 0 & \cdots & 0 & 0 & 0 & 0 & 0 & 0 & 0 & 0 & 0 & 0 & \cdots & 0 & 0 & \cdots & 0 & 0 \\
r_\mathrm{s} & 0 & 0 & 0 & 0 & \cdots & 0 & 0 & 0 & 0 & 0 & 1 & 0 & 0 & 0 & 0 & \cdots & 0 & 0 & \cdots & 0 & 0 \\
0 & r_\mathrm{s} & 0 & 0 & 0 & \cdots & 0 & 0 & 0 & 0 & 0 & 0 & 1 & 0 & 0 & 0 & \cdots & 0 & 0 & \cdots & 0 & 0 \\
0 & 0 & r_\mathrm{s} & 0 & 0 & \cdots & 0 & 0 & 0 & 0 & 0 & 0 & 0 & 1 & 0 & 0 & \cdots & 0 & 0 & \cdots & 0 & 0 \\
0 & 0 & 0 & r_\mathrm{s} & 0 & \cdots & 0 & 0 & 0 & 0 & 0 & 0 & 0 & 0 & 1 & 0 & \cdots & 0 & 0 & \cdots & 0 & 0 \\
0 & 0 & 0 & 0 & r_\mathrm{s} & \cdots & 0 & 0 & 0 & 0 & 0 & 0 & 0 & 0 & 0 & 1 & \cdots & 0 & 0 & \cdots & 0 & 0 \\
\ldots & \ldots & \ldots & \ldots & \ldots & \ldots & \ldots & \ldots & \ldots & \ldots & \ldots & \ldots & \ldots & \ldots & \ldots & \ldots & \ldots & \ldots & \ldots & \ldots & \ldots & \ldots \\
0 & 0 & 0 & 0 & 0 & \cdots & 0 & 0 & 0 & 0 & 0 & 0 & 0 & 0 & 0 & 0 & \cdots & 1 & 0 & \cdots & r_\mathrm{s} & 0 \\
0 & 0 & 0 & 0 & 0 & \cdots & 0 & 0 & 0 & 0 & 0 & 0 & 0 & 0 & 0 & 0 & \cdots & 0 & 1 & \cdots & 0 & r_\mathrm{s} \\
\ldots & \ldots & \ldots & \ldots & \ldots & \ldots & \ldots & \ldots & \ldots & \ldots & \ldots & \ldots & \ldots & \ldots & \ldots & \ldots & \ldots & \ldots & \ldots & \ldots & \ldots & \ldots \\
0 & 0 & 0 & 0 & 0 & \cdots & 0 & 0 & 0 & 0 & 0 & 0 & 0 & 0 & 0 & 0 & \cdots & r_\mathrm{s} & 0 & \cdots & 1 & 0 \\
0 & 0 & 0 & 0 & 0 & \cdots & 0 & 0 & 0 & 0 & 0 & 0 & 0 & 0 & 0 & 0 & \cdots & 0 & r_\mathrm{s} & \cdots & 0 & 1
\end{bmatrix}
\tag{2.149}
$$

$$
\underline{C}_{\mathrm{r},\delta} = \begin{bmatrix}
1 & 0 & 0 & 0 & 0 & \cdots & 0 & 0 & 0 & 0 & r_\mathrm{r} & r_\mathrm{r} & 0 & 0 & 0 & 0 & \cdots & 0 & 0 & \cdots & 0 & 0 \\
0 & 1 & 0 & 0 & 0 & \cdots & 0 & 0 & r_\mathrm{r} & 0 & 0 & 0 & r_\mathrm{r} & 0 & 0 & 0 & \cdots & 0 & 0 & \cdots & 0 & 0 \\
0 & 0 & 1 & 0 & 0 & \cdots & 0 & 0 & 0 & r_\mathrm{r} & 0 & 0 & 0 & r_\mathrm{r} & 0 & 0 & \ldots & 0 & 0 & \cdots & 0 & 0 \\
0 & 0 & 0 & 1 & 0 & \cdots & r_\mathrm{r} & 0 & 0 & 0 & 0 & 0 & 0 & 0 & r_\mathrm{r} & 0 & \cdots & 0 & 0 & \cdots & 0 & 0 \\
0 & 0 & 0 & 0 & 1 & \cdots & 0 & r_\mathrm{r} & 0 & 0 & 0 & 0 & 0 & 0 & 0 & r_\mathrm{r} & \cdots & 0 & 0 & \cdots & 0 & 0 \\
\ldots & \ldots & \ldots & \ldots & \ldots & \ldots & \ldots & \ldots & \ldots & \ldots & \ldots & \ldots & \ldots & \ldots & \ldots & \ldots & \ldots & \ldots & \ldots & \ldots & \ldots & \ldots \\
0 & 0 & 0 & r_\mathrm{r} & 0 & \cdots & 1 & 0 & 0 & 0 & 0 & 0 & 0 & 0 & 0 & 0 & \cdots & 0 & 0 & \cdots & 0 & 0 \\
0 & 0 & 0 & 0 & r_\mathrm{r} & \cdots & 0 & 1 & 0 & 0 & 0 & 0 & 0 & 0 & 0 & 0 & \cdots & 0 & 0 & \cdots & 0 & 0 \\
0 & r_\mathrm{r} & 0 & 0 & 0 & \cdots & 0 & 0 & 1 & 0 & 0 & 0 & 0 & 0 & 0 & 0 & \cdots & 0 & 0 & \cdots & 0 & 0 \\
0 & 0 & r_\mathrm{r} & 0 & 0 & \cdots & 0 & 0 & 0 & 1 & 0 & 0 & 0 & 0 & 0 & 0 & \cdots & 0 & 0 & \cdots & 0 & 0 \\
r_\mathrm{r} & 0 & 0 & 0 & 0 & \cdots & 0 & 0 & 0 & 0 & 0 & 0 & 0 & 0 & 0 & 0 & \cdots & 0 & 0 & \cdots & 0 & 0 \\
r_\mathrm{r} & 0 & 0 & 0 & 0 & \cdots & 0 & 0 & 0 & 0 & 0 & 1 & 0 & 0 & 0 & 0 & \cdots & 0 & 0 & \cdots & 0 & 0 \\
0 & r_\mathrm{r} & 0 & 0 & 0 & \cdots & 0 & 0 & 0 & 0 & 0 & 0 & 1 & 0 & 0 & 0 & \cdots & 0 & 0 & \cdots & 0 & 0 \\
0 & 0 & r_\mathrm{r} & 0 & 0 & \cdots & 0 & 0 & 0 & 0 & 0 & 0 & 0 & 1 & 0 & 0 & \cdots & 0 & 0 & \cdots & 0 & 0 \\
0 & 0 & 0 & r_\mathrm{r} & 0 & \cdots & 0 & 0 & 0 & 0 & 0 & 0 & 0 & 0 & 1 & 0 & \cdots & 0 & 0 & \cdots & 0 & 0 \\
0 & 0 & 0 & 0 & r_\mathrm{r} & \cdots & 0 & 0 & 0 & 0 & 0 & 0 & 0 & 0 & 0 & 1 & \cdots & 0 & 0 & \cdots & 0 & 0 \\
\ldots & \ldots & \ldots & \ldots & \ldots & \ldots & \ldots & \ldots & \ldots & \ldots & \ldots & \ldots & \ldots & \ldots & \ldots & \ldots & \ldots & \ldots & \ldots & \ldots & \ldots & \ldots \\
0 & 0 & 0 & 0 & 0 & \cdots & 0 & 0 & 0 & 0 & 0 & 0 & 0 & 0 & 0 & 0 & \cdots & 1 & 0 & \cdots & r_\mathrm{r} & 0 \\
0 & 0 & 0 & 0 & 0 & \cdots & 0 & 0 & 0 & 0 & 0 & 0 & 0 & 0 & 0 & 0 & \cdots & 0 & 1 & \cdots & 0 & r_\mathrm{r} \\
\ldots & \ldots & \ldots & \ldots & \ldots & \ldots & \ldots & \ldots & \ldots & \ldots & \ldots & \ldots & \ldots & \ldots & \ldots & \ldots & \ldots & \ldots & \ldots & \ldots & \ldots & \ldots \\
0 & 0 & 0 & 0 & 0 & \cdots & 0 & 0 & 0 & 0 & 0 & 0 & 0 & 0 & 0 & 0 & \cdots & r_\mathrm{r} & 0 & \cdots & 1 & 0 \\
0 & 0 & 0 & 0 & 0 & \cdots & 0 & 0 & 0 & 0 & 0 & 0 & 0 & 0 & 0 & 0 & \cdots & 0 & r_\mathrm{r} & \cdots & 0 & 1
\end{bmatrix}
\tag{2.150}
$$

The vector $\vartheta_{\alpha,\beta}$ representing applied MMFs is equal to

$$\underline{\vartheta}_{\alpha,\beta} = \frac{\mu_0}{\delta_0}\begin{bmatrix} 0 \\ \Theta_{s,1} + \Theta_{r,1}\cos\frac{\pi}{\tau_p}x_0 \\ \Theta_{r,1}\sin\frac{\pi}{\tau_p}x_0 \\ \Theta_{s,2} + \Theta_{r,2}\cos 2\frac{\pi}{\tau_p}x_0 \\ \Theta_{s,2} + \Theta_{r,2}\sin 2\frac{\pi}{\tau_p}x_0 \\ \Theta_{s,3} + \Theta_{r,3}\cos 3\frac{\pi}{\tau_p}x_0 \\ \Theta_{r,3}\sin 3\frac{\pi}{\tau_p}x_0 \\ \cdots \\ \cdots \\ \Theta_{s,n-2} + \Theta_{r,n-2}\cos(n-2)\frac{\pi}{\tau_p}x_0 \\ \Theta_{r,n-2}\sin(n-2)\frac{\pi}{\tau_p}x_0 \\ \Theta_{s,n-1} + \Theta_{r,n-1}\cos(n-1)\frac{\pi}{\tau_p}x_0 \\ \Theta_{r,n-1}\sin(n-1)\frac{\pi}{\tau_p}x_0 \\ \Theta_{s,n} + \Theta_{r,n}\cos n\frac{\pi}{\tau_p}x_0 \\ \Theta_{r,n}\sin n\frac{\pi}{\tau_p}x_0 \end{bmatrix} \tag{2.151}$$

In Fig. 2.52 the results of analysis of air gap flux density in a machine with 18 stator slots per pole pair, $r_s = \delta_{s,1}/(2\delta_0) = r_r = \delta_{r,1}/(2\delta_0) = 0.33$, and

(a) 2 rotor poles;
(b) 14 rotor slots per pole pair; and
(c) 20 rotor slots per pole pair

are shown.

The machine with 2 rotor (salient) poles has a spectrum similar to that of a machine with smooth stator and salient poles, as shown in Fig. 2.33—both fundamental and 3. harmonic of the air gap flux density are lower than in case of completely smooth air gap, as a consequence of 180° phase shift of rotor slot harmonics. In addition, stator slot harmonics (17. and 19.) are stronger than their next neighbors.

In the machine with 14 rotor slots per pole pair, both stator (17. and 19.) and rotor (13. and 15.) slot harmonics are strong as compared to their next neighbors.

The air gap flux density in the machine with 20 rotor slots has a very strong peak at the common slot harmonic of the order 19 (=20 − 1 = 18 + 1). This high peak is typical for all machines with slot combinations $N_s - N_r = \pm 2p$.

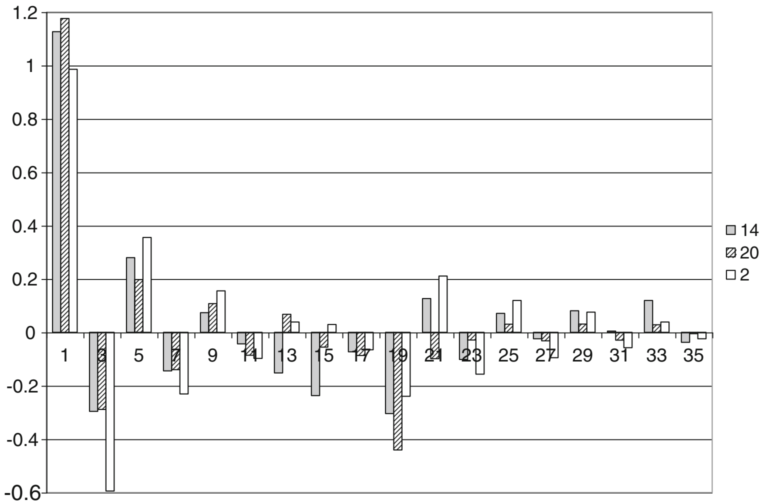

Fig. 2.52 Air gap flux density harmonics in p.u. created by currents through a stator and a rotor full-pitch coil in machines with doubly slotted air gap, 18 stator slots per pole pair and 2, 14, and 20 rotor slots per pole pair

The spectrum of air gap flux density harmonics in a machine with equal number of stator and rotor slots is shown in Fig. 2.53, along with the spectrum of air gap flux density harmonics in a machine with the same number of stator teeth and smooth rotor.

Various factors affecting the amplitude of the nth harmonic of MMF can be expressed in terms of the winding factor for the nth harmonic $f_{w,n}$, defined as

$$f_{w,n} = f_{o,n} \cdot f_{p,n} \cdot f_{z,n} \cdot f_{sk,n} \tag{2.152}$$

By dividing the winding factor for the nth harmonic through the Carter factor, one obtains the *excitation efficacy* factor $f_{ee,n}$ for the nth harmonic

$$f_{ee,n} = \frac{f_{w,n}}{k_C} \tag{2.153}$$

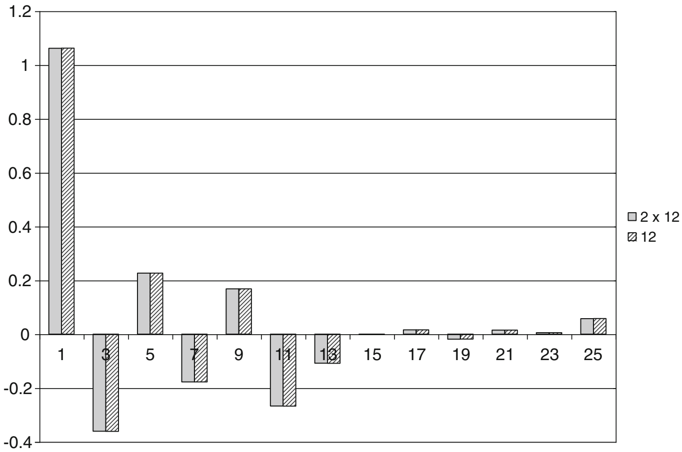

Fig. 2.53 Air gap flux density harmonics in p.u. created by currents through a stator and a rotor full-pitch coil in a machine with doubly slotted air gap, 12 stator slots per pole pair and 12 rotor slots per pole pair (denoted by "2 × 12"). The spectrum of air gap flux density in a machine with 12 stator teeth and smooth rotor (denoted by "12") is shown as reference. The two spectra differ only slightly from each other

Physical meaning of the excitation efficacy factor becomes obvious when one analyzes the relationship between the nth harmonic of flux density and MMF which created it:

$$B_n = \mu_0 \frac{\Theta_n}{k_\mathrm{C} \cdot \delta} = I \cdot w \cdot \frac{\sin \frac{n\pi}{2}}{n} \cdot \frac{\mu_0}{\delta} \cdot \frac{4}{\pi} \cdot \frac{f_{\mathrm{w},n}}{k_\mathrm{C}} = I \cdot w \cdot \frac{\sin \frac{n\pi}{2}}{n} \cdot \frac{\mu_0}{\delta} \cdot \frac{4}{\pi} \cdot f_{\mathrm{ee},n} \qquad (2.154)$$

The excitation efficacy factor determines how much flux density the ampere-turns $I \cdot w$ can generate in an air gap with a width δ.

2.5.6 Flux Density Distribution in Eccentric Air Gap of a Single-Slotted Machine

Air gap width in a single-slotted machine with eccentric rotor can be described by equation

$$\delta = \delta_0 + \delta_1 \cos \frac{N}{p} \frac{\pi}{\tau_\mathrm{p}} (x - x_\mathrm{r}) + \varepsilon \cos \frac{\pi}{\tau_\mathrm{p}} (x - x_\mathrm{r}) \qquad (2.155)$$

Air gap flux density created by odd harmonics of MMF contains harmonics of the order 0, 1, 2, 3,…, etc., as discussed in previous sections. In special case of salient pole machine with $p = 1$, the air gap flux density can be expressed as

$$\delta = \delta_0 + \delta_1 \cos 2\frac{\pi}{\tau_p}(x - x_r) + \varepsilon \cos\frac{\pi}{\tau_p}(x - x_r) \qquad (2.156)$$

The fundamental spatial component of MMF Θ_1 creates homopolar flux density B_0, the amplitude of which varies with period length of 2 τ_p, along with the fundamental B_1 second B_2, and third harmonic B_3 of air gap flux density. The amplitudes of all harmonics with order equal to or larger than 1 pulsate with period length of τ_p.

2.5.7 The Influence of Saturation

In the previous sections it was assumed that the MMF drop across iron core is negligible and only those additional harmonics of air gap flux density were calculated, which originated in non-even air gap width. In reality, however, the MMF drop across iron core cannot be neglected (Fig. 2.54).

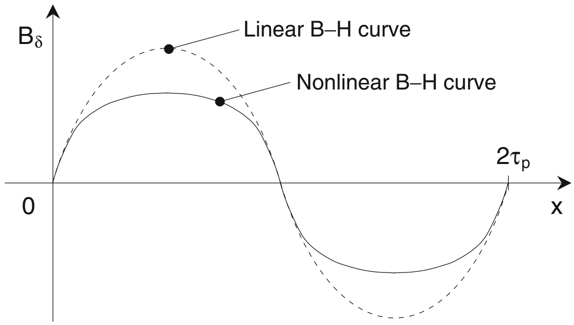

Fig. 2.54 Flattening of the air gap flux density distribution created by the fundamental harmonic of MMF and saturation in iron in a machine with constant air gap

Although there exists no analytical expression for B–H curve of iron core and, therefore, the decrease of flux density for a given MMF can only be described qualitatively, the orders of harmonics of air gap flux density due to saturation along with their influence on machine performance can be precisely quantified.

Flattening of air gap flux density distribution due to saturation in iron is a source of additional odd harmonics in its spectrum. Harmonics due to saturation act in rotating field in a different manner than harmonics created by discrete winding distribution.

Case Study 2.2: The influence of machine topology on ampere-turns demand for a given air gap flux density and on the amplitude of its pulsating component will be illustrated on five representative machine types:

- Large cylindrical rotor synchronous machine;
- Medium-size squirrel cage induction machine;
- Large low-speed surface-mounted permanent magnet machine with distributed stator windings;
- Large low-speed surface-mounted permanent magnet machine with tooth-wound stator;
- Large high-speed tooth-wound machine with embedded magnets in flux concentration geometry with data as described in Case Study 2.1.

The machines were analyzed from the point of view of excitation demand and the amplitude of the pulsating component of air gap flux density. The results of analysis are presented in Table 2.7.

The large wound rotor synchronous machine has a wide air gap and, therefore, a Carter factor close to one. The pulsating component of the air gap flux density due to stator slots is very low (4.1 % of the average). The excitation efficacy factor for the fundamental harmonic of flux density is rather high (0.893), which means that almost 90 % of a single coil ampere-turns produce the fundamental component of the air gap flux density. The value of excitation efficacy factor of 0.893 is taken as 100 % in this comparison.

The medium-size squirrel cage induction machine has high excitation efficacy, along with considerable amplitude of pulsating component of flux density due to slotting. The relatively high amplitude of B_s after Eq. 2.39 generates surface losses in the rotor, which, however, are not critical because the rotor magnetic circuit is laminated. Local effect of pulsating air gap flux density—attractive force between stator and rotor iron surfaces proportional to the square of flux density—can be large enough to generate vibrations and audible noise in this machine.

Permanent magnet machines in Table 2.7 have poorer excitation efficacy basically due to two reasons: a larger Carter factor, and, in case of tooth-wound machines, a poorer winding factor caused by large slot openings. The poorest excitation efficacy factor characterizes the tooth-wound surface-mounted PM machine, in which slightly more than 50 % of available ampere-turns can be utilized for generation of the fundamental component of air gap flux density. In other words, in order to produce the same magnitude of air gap flux density, the field winding of a wound rotor synchronous machine has to generate only 60.5 % (=0.54/0.893) of ampere-turns created by permanent magnets in a tooth-wound PM machine with equally wide air gap. This is another reason for supremacy of wound rotor over permanent magnet machines.

Table 2.7 Comparison of crucial parameters of AC machines

	Cylindrical rotor synchronous	Squirrel cage induction	PM surface mounted	PM surface mounted	PM flux concentration
Stator winding	Distributed	Distributed	Distributed	Tooth wound	Tooth wound
Air gap radius	440	155	2400	1500	600
Poles	2	4	84	70	20
Stator slots	42	48	288	72	30
Pole pitch	1382.3	243.5	179.5	134.6	188.5
Slot width	26.6	3.5	23	70	56
Stator slot height	200	40.5	117	150	156
Axial length	3420	380	770	480	700
Coil pitch	17	10	3	1	1
Slot-opening factor $f_{o,1}$	1.00	1.00	0.993	0.892	0.964
Pitch factor $f_{p,1}$	0.956	0.966	0.981	0.999	0.866
Air gap width	35	0.9	6	5	7.5
Carter factor k_C	1.07	1.082	1.236	1.65	1.364
B_s/B_0 (%)	4.1	37.2	36.7	75.2	58.9
Excitation efficacy $f_{ee,1}$	**0.893** (100 %)	**0.893** (100 %)	**0.788** (88.3 %)	**0.54** (60.5 %)	**0.612** (68.5 %)

2.6 Time-Dependent Excitation, Rotating Field Generation, MMF Wave Speed, Positive and Negative Sequence Components

Rotating field in the air gap of electric machine is generated either mechanically, by rotation of current-carrying coil(s), or electrically, by supplying stationary or rotating winding(s) by alternating or constant current(s) respectively, see Table 2.8.

Only those stator and a rotor harmonics of the air gap MMF which rotate at the same speed can generate a torque with an average value different from zero and produce mechanical work. Assuming that stator winding generates a rotating field which revolves at synchronous speed n_s, mechanical work will be produced if:

– A DC-excited rotor rotates at synchronous speed, whereas the DC excitation is generated either by a constant current flowing through a coil, or by permanent magnets; and
– AC-fed windings generate rotating field with speed of rotation relative to the stator rotating field equal to zero.

Table 2.8 Modes of rotating field generation and results of their interaction

			Stator		
			At standstill		Rotating
			Polyphase excited	DC fed	DC fed
Rotor	At standstill	Polyphase excited	Rotary phase shifting transformer	–	–
	Rotating	DC fed	Synchronous machine	–	Clutch
		AC excited	Induction machine	Brake	–

One should keep in mind that spatially distributed electromagnetic quantities in a machine—its current sheet, MMF and flux density distributions—are *periodical*, as is the current, flux, induced voltage, etc.

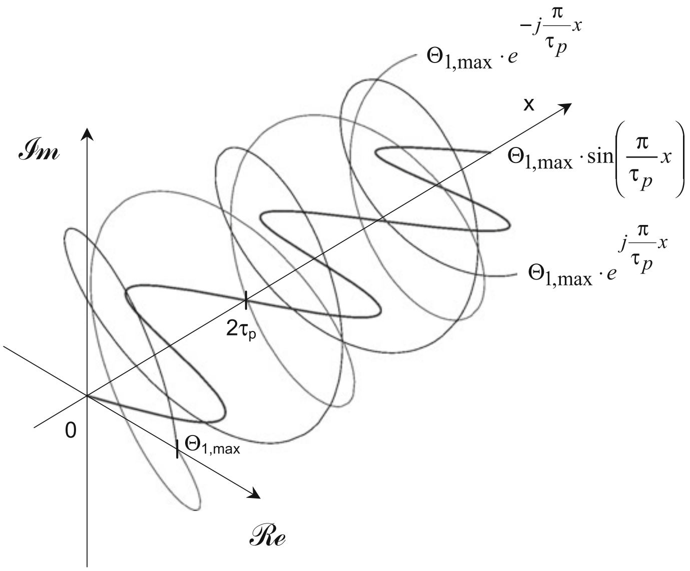

Fig. 2.55 The fundamental component of stationary air gap MMF $\Theta_1(x) = \Theta_{1,max}$ sin $(\pi/\tau_p \cdot x)$ represented in the complex circumferential space by means of complex conjugates $\Theta_{1,max}e^{j\frac{\pi}{\tau_p}x}$ and $\Theta_{1,max}e^{-j\frac{\pi}{\tau_p}x}$

Although the current and the MMF have the same dimension [A], these two quantities have different physical meanings and properties. Current I is a scalar, which alone cannot create physical effects in the air gap, because it does not carry information on position of conductor in the air gap. Only if the current flows through a spatially distributed winding, it can influence the electromagnetic condition of the air gap.

Whereas the alternating current can be represented in the complex plane in the manner shown in Appendix, one more dimension—the circumferential coordinate—is necessary in order to represent the air gap MMF correctly. This can be done in *the complex circumferential space*, as shown in Fig. 2.55. The complex circumferential space emerges from the complex plane, through the origin of which the machine circumferential coordinate goes perpendicularly into the plane.

The value of the fundamental component of MMF at a given circumferential coordinate x in Fig. 2.55 is proportional to the sine of angle $\pi/\tau_p \cdot x$. By applying Euler's equation, a sine function of a real argument is represented in the complex plane as a sum of complex conjugates, whereas the real argument can be time, space, or both of them

$$\Theta_1(x,t) = \Theta_{1,\max} \sin\left(\frac{\pi}{\tau_p}x - \omega t\right) = \Theta_{1,\max} \frac{e^{j\left(\frac{\pi}{\tau_p}x-\omega t\right)} - e^{-j\left(\frac{\pi}{\tau_p}x-\omega t\right)}}{2j} \tag{2.157}$$

The two functions $\Theta_{1,\max}e^{j\left(\frac{\pi}{\tau_p}x-\omega t\right)}$ and $\Theta_{1,\max}e^{-j\left(\frac{\pi}{\tau_p}x-\omega t\right)}$ in the complex circumferential space (Re, Im, x) are spirals with radius $\Theta_{1,\max}$ and axis coincident with the x-axis. Their projections to the complex plane (Re, In) are located on a circle with radius $\Theta_{1,\max}$ and angles $\pm$ arc sin $(\pi/\tau_p \cdot x - \omega \cdot t)$, as shown in Fig. 2.55.

At a given time instant the coil current is constant and the MMF distribution along the x-axis is stationary. As the circumferential coordinate x increases, the positions of the corresponding points in the complex real space begin to slide along the two MMF spirals. The difference of the associated complex conjugates divided by $2j$ lies on the real axis of the complex plane and gives the amount of corresponding MMF.

The spirals $\Theta_{1,\max}e^{j\left(\frac{\pi}{\tau_p}x-\omega t\right)}$ and $\Theta_{1,\max}e^{-j\left(\frac{\pi}{\tau_p}x-\omega t\right)}$ in the complex circumferential space determine the character of the air gap MMF in the following manner:

– Stationary air gap MMF created by a constant current through coil(s): one set of stationary spirals as in Fig. 2.55, the radius $\Theta_{1,\max}$ of which is determined by the amount of coil current;
– Rotating air gap MMF created by a system of coils: one set of spirals with constant radius $\Theta_{1,\max}$ as in Fig. 2.55, rotating in the positive direction;
– Pulsating air gap MMF created by a single coil: two sets of spirals with constant radius $\Theta_{1,\max}$ as in Fig. 2.55, rotating in opposite directions.

2.6.1 MMF Waves Generated by Rotating DC-Fed Coil(s) on One Side of Air Gap

A DC-fed coil shifted for x_0 from zero point of the circumferential coordinate generates the air gap MMF distribution

$$\Theta(x, x_0) = \sum_{n=1,2,3,\ldots}^{\infty} \Theta_n \sin n \frac{\pi}{\tau_p}(x - x_0) \tag{2.158}$$

If the coil rotates at velocity $v = x_0/t$, its air gap MMF distribution rotates too:

$$\Theta(x, t) = \sum_{n=1,2,3,\ldots}^{\infty} \Theta_n \sin n \frac{\pi}{\tau_p}(x - v \cdot t) \tag{2.159}$$

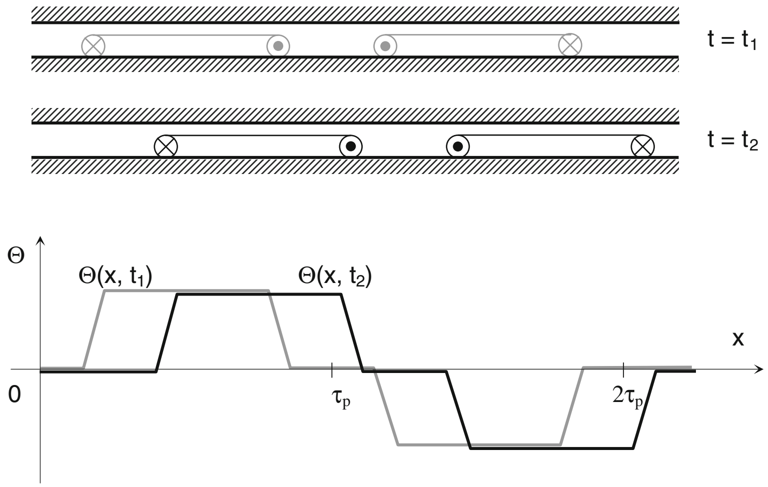

Fig. 2.56 Air gap MMF created by rotating coils fed from a DC source

The velocity of the nth harmonic of MMF is evaluated by setting the corresponding argument of sine function to a constant, the physical meaning of which is a (constant) distance between the observer and the zero crossing point of the MMF:

$$n \frac{\pi}{\tau_p}(x - v \cdot t) = \text{const} \tag{2.160}$$

the time derivative of which gives the relative velocity v_r between the observer and zero crossing point of the air gap MMF. By setting the relative velocity v_r equal to zero (the observer does not move relative to MMF), one obtains for the velocity v_n of the nth harmonic of the MMF

$$v_n = \frac{dx}{dt} = v \tag{2.161}$$

i.e., the nth harmonic of the MMF wave generated by rotating DC coil rotates at a circumferential velocity equal to the coil velocity. Since all higher harmonics travel at the same velocity as the fundamental wave of air gap MMF, they do not move relative to each other and the air gap MMF distribution retains its shape all the time, as shown in Fig. 2.56.

From the point of view of air gap MMF generation, permanent magnets have identical properties as DC-fed coils.

2.6.2 MMF Waves Generated by Symmetrically Wound Stationary Coils Carrying Symmetrical Alternating Currents on One Side of Air Gap

Consider now a single full-pitch coil per pole fed from an AC source

$$i(t) = \sum_{k=1}^{\infty} I_k \cos k(\omega t - \varphi_k) \tag{2.162}$$

If the coil axis is shifted for x_0, its MMF is equal to

$$\Theta(x, x_0, t) = \frac{4}{\pi} w \sum_{n=1,2,3,\ldots}^{\infty} \sum_{k=1}^{\infty} I_k \cos k(\omega t - \varphi_k) \frac{\sin \frac{n\pi}{2}}{n} f_{o,n} \sin n \frac{\pi}{\tau_p}(x - x_0) \tag{2.163}$$

The MMF distribution created by an alternating current does not qualitatively change its form; quantitatively, the MMF changes proportionaly to the coil current. The kth time harmonic of current creates a spatial MMF distribution component $\Theta_k(x, x_0, t)$

$$\Theta_k(x, x_0, t) = \frac{4}{\pi} w \sum_{n=1,3,5,\ldots}^{\infty} I_k \cos k(\omega t - \varphi_k) \cdot \frac{\sin \frac{n\pi}{2}}{n} f_{\mathrm{w},n} \sin n \frac{\pi}{\tau_\mathrm{p}} (x - x_0) \quad (2.164)$$

The nth spatial harmonic of MMF distribution $\Theta_{k,n}(x, x_0, t)$

$$\Theta_{k,n}(x, x_0, t) = I_k \cdot \frac{4}{\pi} w \cdot \frac{\sin \frac{n\pi}{2}}{n} \cdot f_{\mathrm{w},n} \cdot \sin n \frac{\pi}{\tau_\mathrm{p}} (x - x_0) \cdot \cos k(\omega t - \varphi_k) \quad (2.165)$$

is a standing wave

$$\Theta_{k,n}(x, x_0, t) = \Theta_{k,n,\max} \cdot \sin n \frac{\pi}{\tau_\mathrm{p}} (x - x_0) \cdot \cos k(\omega t - \varphi_k) \quad (2.166)$$

which can be represented as a sum of two waves with equal amplitudes traveling in opposite directions

$$\Theta_{k,n}(x, x_0, t) = \frac{\Theta_{k,n,\max}}{2} \cdot \left\{ \sin\left[k(\omega t - \varphi_k) - n \frac{\pi}{\tau_\mathrm{p}} (x - x_0) \right] + \sin\left[k(\omega t - \varphi_k) + n \frac{\pi}{\tau_\mathrm{p}} (x - x_0) \right] \right\} \quad (2.167)$$

The component of wave in Eq. 2.167 traveling in the positive direction is called the *positive sequence*, and that traveling in negative direction, the *negative sequence*. The traveling speed of the two waves is obtained by setting their arguments to a constant, and differentiating thus obtained equation with respect to time

$$\frac{\mathrm{d}}{\mathrm{d}t} \left\{ k(\omega t - \varphi_k) \pm n \frac{\pi}{\tau_\mathrm{p}} (x - x_0) = \mathrm{const} \right\} \Rightarrow n \frac{\pi}{\tau_\mathrm{p}} \frac{\mathrm{d}x}{\mathrm{d}t} = \pm k\omega \quad (2.168)$$

As a result, the circumferential velocity $v_{k,n}$ and *mechanical angular speed* $\Omega_{k,n}$ of the kth time and nth spatial harmonic are obtained

$$v_{k,n} = \pm \frac{k}{n} \cdot \frac{\tau_\mathrm{p}}{\pi} \cdot \omega; \quad \Omega_{k,n} = \pm \frac{k}{n} \cdot \frac{\omega}{p} \quad (2.169)$$

The positive sign in the velocity equations is related to the positive sequence component of MMF, and the negative sign to the negative sequence component of MMF. The higher the order n of a spatial harmonic, the lower its speed of propagation through the air gap. This principle is a consequence of the condition that after one period T of current, i.e., at time instant $t + T$, the spatial distribution of

MMF has to have the same shape as at time instant t. This condition is fulfilled only if each spatial harmonic covers a distance of $2\tau_p/n$ within time T, n being the harmonic order.

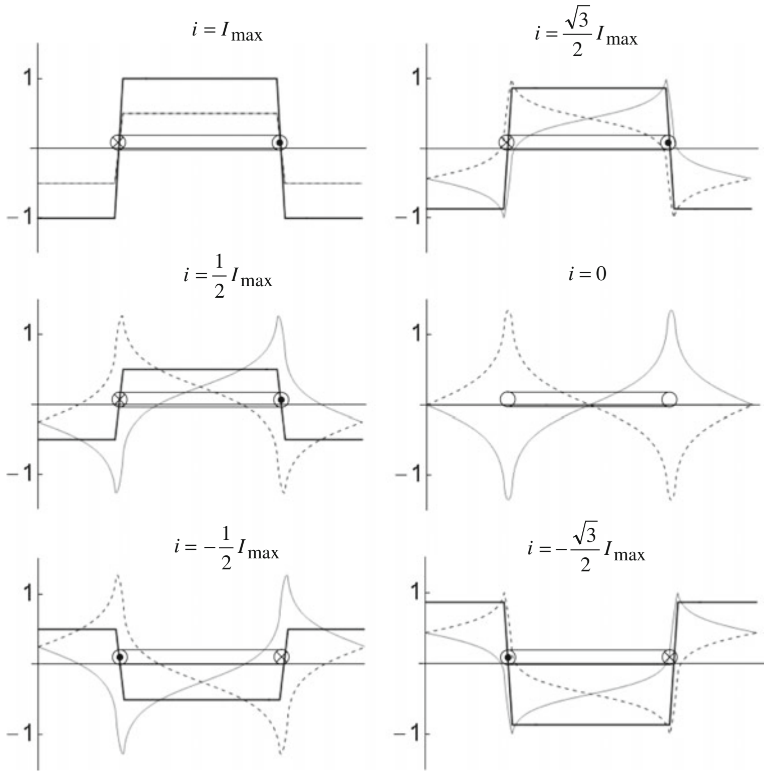

Fig. 2.57 Air gap MMF created by one stationary full-pitch coil per pole fed from an AC source. The total (pulsating) MMF is represented with a *solid black curve*, the total positive sequence component with a *solid gray*, and the total negative sequence component with *dashed gray curve*. Time step between figures is 30°

The nth spatial harmonic of MMF, created by the kth time harmonic of current, travels k times faster and n times slower than the fundamental. This means that spatial harmonics created by alternating current travel relative to each other, as opposed to spatial harmonics created by DC-carrying coil rotating at angular speed Ω, which all travel at the same, mechanical speed of rotation.

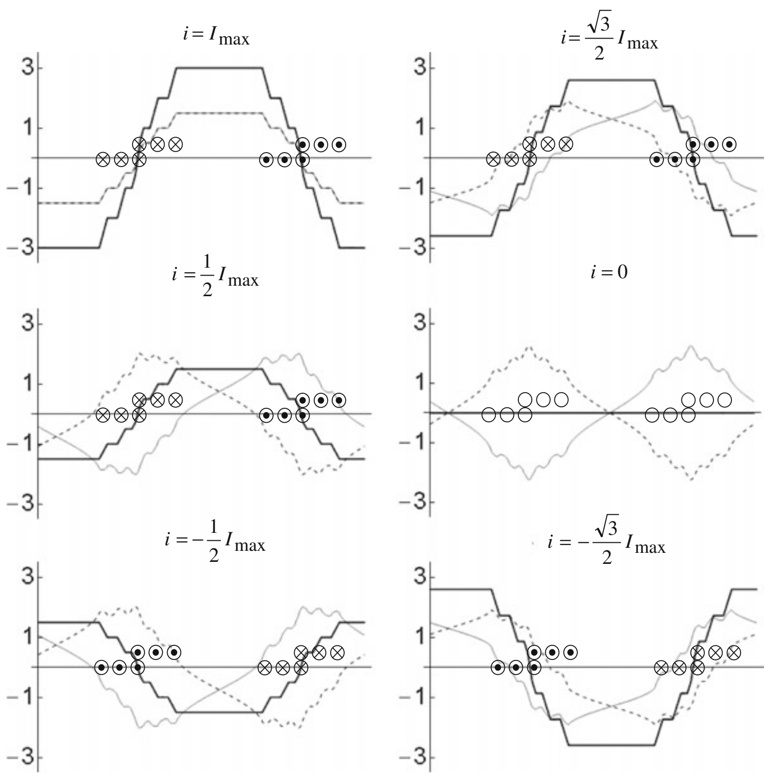

Fig. 2.58 Air gap MMF created by three stationary coils per pole with $y/\tau_p = 7/9$, carrying the same alternating current. The maximum value of resulting MMF is 3 p.u. The total (pulsating) MMF is represented with a *solid black curve*, the total positive sequence component with a *solid gray*, and the total negative sequence component with *dashed gray curve*. Time step between figures is 30°

Since the spatial harmonics created by alternating current move relative to each other, their sum—the total MMF—changes permanently its shape in time. This is illustrated in Fig. 2.57, in which the total MMF created by a full-pitch coil, along with its positive and negative sequence components within one half period of the coil current are shown.

In Fig. 2.57, the peaks of positive and negative sequence MMFs, which are fixed to the left-hand side and right-hand side of each conductor, can be recognized. At these points the MMF distribution changes abruptly its slope, i.e., its first derivative is discontinuous. Since Fourier series representation is defined only for continuously derivable functions, it cannot deliver proper results at points of discontinuity (Gibb's phenomenon).

Air gap MMF distribution created by three coils with shorted pitch 7/9 is shown in Fig. 2.58. The total MMF pulsates, as is the case with the MMF created by a single coil. In the higher harmonics spectrum of the total MMF some terms from the spectrum of a single coil are either missing, or suppressed. Therefore, both the positive and negative sequence components in Fig. 2.58 have waveforms much closer to sine function than in case of a single coil in Fig. 2.57.

Consider now a set of *2m identically wound groups of q coils* placed in adjacent slots in interval $(0,2\tau_p)$ along the circumferential coordinate x. In case of pole symmetry, oppositely wound coils are shifted for τ_p and carry the same currents as their counterparts. Therefore, only m sources (phases) with a phase shift of $2\pi/m$ are needed. The fundamental spatial harmonic (n = 1) of MMF created by the fundamental harmonic of current (k = 1) in the jth coil group (j = 1, 2, …, 2m) is equal to

$$\begin{aligned}&\Theta_{1,1,j}\left(x, x_{0,j}, t\right)\\&\quad=\frac{\Theta_{1,1,\max}}{2}\cdot\left\{\sin\left[\left(\omega t-\varphi_{1,j}\right)-\frac{\pi}{\tau_p}\left(x-x_{0,j}\right)\right]+\sin\left[\left(\omega t-\varphi_{1,j}\right)+\frac{\pi}{\tau_p}\left(x-x_{0,j}\right)\right]\right\}\end{aligned} \tag{2.170}$$

with $x_{0,j}$ standing for the coil group axis shift along the circumferential coordinate x, $\Theta_{1,1,\max}$ for the amplitude of the fundamental time and spatial component of the MMF created by *one coil group per pole pair*, and $\varphi_{1,j}$ for the phase shift of the fundamental current harmonic in the jth coil group. Denoting by $\gamma_{1,j,+}$ the argument of the positive, and by $\gamma_{1,j,-}$ of the negative sequence MMF

$$\gamma_{1,j,+}=\left(\omega t-\varphi_{1,j}\right)-\frac{\pi}{\tau_p}\left(x-x_{0,j}\right);\quad \gamma_{1,j,-}=\left(\omega t-\varphi_{1,j}\right)+\frac{\pi}{\tau_p}\left(x-x_{0,j}\right) \tag{2.171}$$

one can further write

$$\Theta_{1,1,j}\left(x, x_{0,j}, t\right)=\frac{\Theta_{1,1,\max}}{2}\cdot\sin\gamma_{1,j,+}+\frac{\Theta_{1,1,\max}}{2}\cdot\sin\gamma_{1,j,-}=\Theta_{1,1,j,+}+\Theta_{1,1,j,-} \tag{2.172}$$

The total positive sequence MMF is maximum if arguments $\gamma_{1,j,+}$ are equal for j = 1, 2, …, 2m. If the condition of equal arguments is applied to arbitrary coil groups i and j, the equation is obtained

$$\gamma_{1,i,+}=\gamma_{1,j,+}\Rightarrow\left(\omega t-\varphi_{1,i}\right)-\frac{\pi}{\tau_p}\left(x-x_{0,i}\right)=\left(\omega t-\varphi_{1,j}\right)-\frac{\pi}{\tau_p}\left(x-x_{0,j}\right) \tag{2.173}$$

the solution of which is a phase angle of the current in *j*th coil group for which the positive sequence MMFs of the *i*th and *j*th coil group, $\Theta_{1,1,i,+}$ and $\Theta_{1,1,j,+}$, are in phase

$$\varphi_{1,j} = \varphi_{1,i} + \frac{\pi}{\tau_p}\left(x_{0,j} - x_{0,i}\right) \tag{2.174}$$

Positive sequence MMFs $\Theta_{1,1,i,+}$ and $\Theta_{1,1,j,+}$ created by two coil groups the axes of which are shifted along the circumferential coordinate x for $x_{0,j} - x_{0,i}$ are *in phase* if and only if *the coil group currents are out of phase*! Phase shift between coil group currents $\varphi_{1,j} - \varphi_{1,i}$ has to be equal to the electrical angle $(x_{0,j} - x_{0,i})\pi/\tau_p$ between the coil group axes. Arguments $\gamma_{1,i,+}$ and $\gamma_{1,j,+}$ of the positive sequence components $\Theta_{1,1,i,+}$ and $\Theta_{1,1,j,+}$ in the *i*th and *j*th coil group are in that case equal

$$\begin{aligned}\gamma_{1,j,+} &= \left[\omega t - \varphi_{1,i} - \frac{\pi}{\tau_p}\left(x_{0,j} - x_{0,i}\right)\right] - \frac{\pi}{\tau_p}\left(x - x_{0,j}\right) = \left(\omega t - \varphi_{1,i}\right) - \frac{\pi}{\tau_p}\left(x - x_{0,i}\right)\\ &= \gamma_{1,i,+}\end{aligned} \tag{2.175}$$

The angle between the negative sequence components $\Theta_{1,1,i,-}$ and $\Theta_{1,1,j,-}$ created by the coil group j and i can be written as

$$\begin{aligned}\gamma_{1,j,-} - \gamma_{1,i,-} &= \left(\omega t - \varphi_{1,j}\right) + \frac{\pi}{\tau_p}\left(x - x_{0,j}\right) - \left(\omega t - \varphi_{1,i}\right) - \frac{\pi}{\tau_p}\left(x - x_{0,i}\right)\\ &= 2\frac{\pi}{\tau_p}\left(x_{0,i} - x_{0,j}\right)\end{aligned} \tag{2.176}$$

Previous considerations are illustrated in Fig. 2.59, in which the MMF components created by two out of phase currents flowing through two coil groups at a given time instant t are shown. Phase shift between the currents is equal to the electrical spatial angle between the axes of two coil groups. Δ_i in Fig. 2.59 denotes the distance which the positive sequence MMF of the *i*th coil group has passed at a given time instant. At the same time, the negative sequence MMF of the *i*th coil group has passed the distance $-\Delta_i$. Similar considerations are valid for the *j*th coil group and the distance Δ_j.

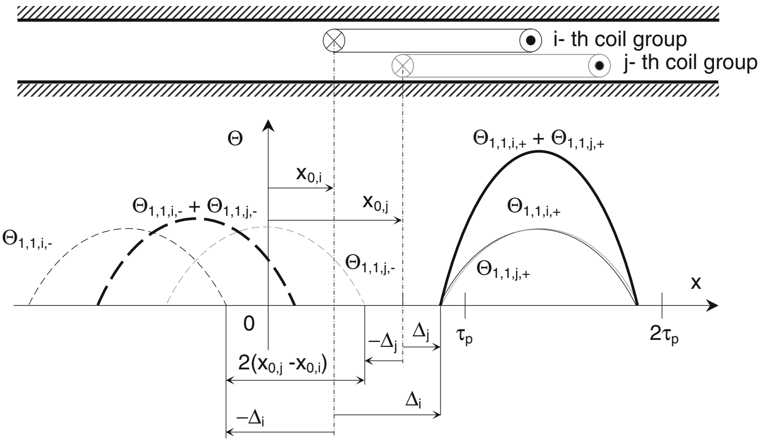

Fig. 2.59 Fundamental components of air gap MMF created by two stationary coil groups per pole fed by currents shifted for an angle equal to the electrical angle between the coil group axes. The two positive sequence components add algebraically, because the angle between them is permanently equal to zero. Phase shift between negative sequence components is equal to the twice the electrical angle between the coil axes. For the purpose of simplicity, only the positive half waves of the MMF components are shown

Whereas for a given phase shift between the coil group currents at each time instant the positive sequence components of the MMF created by the *i*th and *j*th coil group, $\Theta_{1,1,i,+}$ and $\Theta_{1,1,j,+}$, overlap along the circumferential coordinate, the negative sequence components $\Theta_{1,1,i,-}$ and $\Theta_{1,1,j,-}$ remain shifted for the amount of $2(x_{0,j} - x_{0,i})$, as shown in Fig. 2.59. If the phase shift between currents in two coil groups is equal to the electrical angle between the coil group axes, the resulting positive sequence of MMF is twice as big as its single component, and the resulting negative sequence of MMF is smaller than the algebraic sum of components $\Theta_{1,1,i,-}$ and $\Theta_{1,1,j,-}$

If the arbitrary distribution of $2m$ identical coil groups along the two poles $2\,\tau_p$ is now modified in terms of fixing the shift between adjacent coil groups to τ_p/m

$$x_{0,i+1} = x_{0,i} + \frac{\tau_p}{m} = x_{0,1} + i\frac{\tau_p}{m} \tag{2.177}$$

and the phase shift between currents in adjacent coils accordingly to π/m

$$\varphi_{1,i+1} = \varphi_{1,i} + \frac{\pi}{\tau_p}\left(x_{0,i+1} - x_{0,i}\right) = \varphi_{1,i} + \frac{\pi}{m} = \varphi_{1,1} + i\frac{\pi}{m} \tag{2.178}$$

the argument of the positive sequence MMF created by the *i*th coil group is

$$\gamma_{1,i,+} = \left(\omega t - \varphi_{1,i}\right) - \frac{\pi}{\tau_p}\left(x - x_{0,i}\right) = \left(\omega t - \varphi_{1,1}\right) - \frac{\pi}{\tau_p}\left(x - x_{0,1}\right) \qquad (2.179)$$

i.e., the same as for the first coil group. In other words, all positive sequence components are aligned along the same (radial) axis at each time instant.

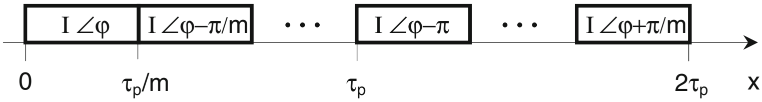

Fig. 2.60 Schematic representation of a symmetrical winding carrying symmetrical currents. As a result, the total negative sequence MMF created by fundamental components of MMF is equal to zero

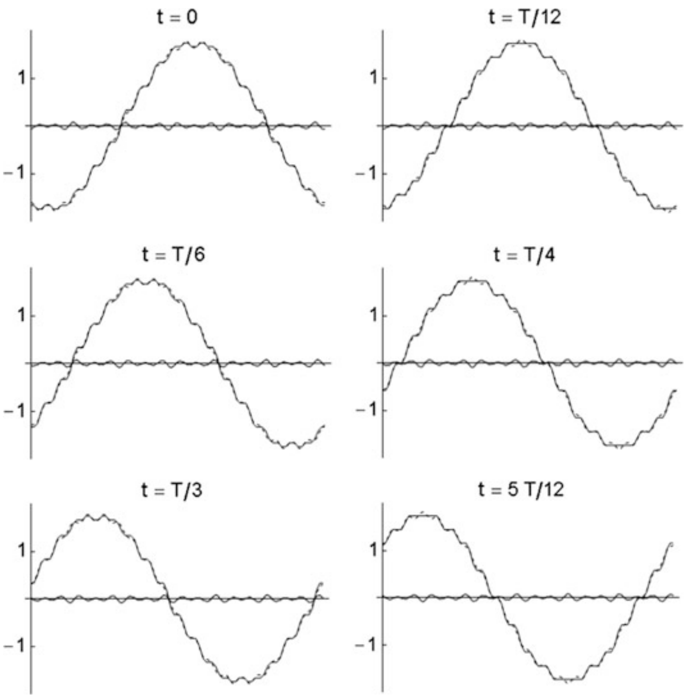

Fig. 2.61 Air gap MMF created by three groups of three stationary coils per pole with $y/\tau_p = 7/9$, carrying AC 60° out of phase in each coil group. The scale on the y-axis is in p.u.; 0.5 p.u. corresponds to the amplitude of positive sequence MMF created by a single coil group. The total MMF is represented with a *solid black curve*, the dominating resulting positive sequence component with a *dashed gray*, and the minor negative sequence component with *solid gray curve*

The total positive sequence component is equal to

$$\begin{aligned}\Theta_{1,1,+}(x,t) &= \sum_{j=1}^{2m} \frac{\Theta_{1,1,\max}}{2} \cdot \sin\left[\omega t - \varphi_{1,1} - \frac{\pi}{\tau_p}\left(x - x_{0,1}\right)\right] \\ &= m \cdot \Theta_{1,1,\max} \cdot \sin\left[\omega t - \varphi_{1,1} - \frac{\pi}{\tau_p}\left(x - x_{0,1}\right)\right]\end{aligned} \tag{2.180}$$

with $\Theta_{1,1,\max}$ denoting the amplitude of the fundamental time and spatial component of the MMF created by one out of *2m* coil groups per pole pair.

Similarly, one can express the argument of the negative sequence MMF created by the *i*th coil group as

$$\gamma_{1,i,-} = \left(\omega t - \varphi_{1,i}\right) + \frac{\pi}{\tau_p}\left(x - x_{0,i}\right) = \left(\omega t - \varphi_{1,1}\right) + \frac{\pi}{\tau_p}\left(x - x_{0,1}\right) - (i-1)\frac{2\pi}{m} \tag{2.181}$$

Consequently, if the MMF amplitudes of all *2m* coils are equal, the sum of negative sequence components of MMF over two poles is equal to zero

$$\Theta_{1,1,-}(x,t) = \sum_{j=1}^{2m} \frac{\Theta_{1,1,\max}}{2} \cdot \sin\left[\omega t - \varphi_{1,1} + \frac{\pi}{\tau_p}\left(x - x_{0,1}\right) - (j-1)\frac{2\pi}{m}\right] = 0 \tag{2.182}$$

Negative sequence components of MMFs created by *2m* coils are out of phase, with an angle of π/m between components created in adjacent coil groups. Symmetrical winding with *2m* coil groups per pole pair (Fig. 2.60) fed from a symmetrical *m*-phase source creates *rotating field* characterized by constant amplitude and constant speed of rotation. Each coil group (*zone*) of the symmetrical winding in Fig. 2.60 occupies $1/m$ of the pole pitch τ_p.

The description "*m-phase machine*" is always related to the number of supply phases; windings of conventional machines have *m* coil groups per pole. Coil groups shifted for τ_p to each other can be connected in series or parallel (the latter usually only in large turbogenerators) to the same supply phase. Electromagnetically, however, they count as separate machine phases.

Rotating field contains only one (positive or negative sequence) component of the MMF. Since the amplitude of each component of coil MMF is equal to 50 % of the total MMF, the resulting amplitude of rotating field created by *2m* coil groups per pole pair is equal to *m* times the MMF amplitude of a single coil group.

In Fig. 2.61 the air gap MMF created by fundamental components of currents flowing through 3 groups of three coils per pole at several time instants is shown. The phase shift of currents flowing through adjacent groups of coils under each pole is 60°. Fundamental components of air gap MMF distribution created by the coils create rotating field characterized by no negative sequence term. Higher harmonics of air gap MMF, however, do generate their own traveling fields with the fundamental component of the coils current. In Fig. 2.61 one recognizes different speeds of traveling waves of higher harmonics, resulting in permanently changing shape of the resulting MMF.

2.6.3 The Influence of the Number of Phases

As discussed in the previous section, a symmetrical winding consisting of *2m* coil groups per pole pair (Fig. 2.60) fed from an m-phase symmetrical source of currents with fundamental angular frequency ω generates not only the fundamental rotating field, but also a spectrum of higher harmonic fields described by equation

$$\Theta(x,t) = \sum_{j=1}^{2m}\sum_{k=1}^{\infty}\sum_{n=1}^{\infty}\Theta_{k,n,\max}\cdot\sin n\frac{\pi}{\tau_p}\left(x - x_0 - \frac{j-1}{m}\tau_p\right)\cdot\cos k\left(\omega t - \varphi_0 - \frac{j-1}{m}\pi\right) \tag{2.183}$$

the positive sequence component of which can be written as

$$\Theta_+(x,t) = \sum_{j=1}^{2m}\sum_{k=1}^{\infty}\sum_{n=1}^{\infty}\frac{\Theta_{k,n,\max}}{2}\cdot\sin\left[k(\omega t - \varphi_0) - n\frac{\pi}{\tau_p}(x - x_0) - (j-1)\frac{k-n}{m}\pi\right] \tag{2.184}$$

and the negative sequence component as

$$\Theta_-(x,t) = \sum_{j=1}^{2m}\sum_{k=1}^{\infty}\sum_{n=1}^{\infty}\frac{\Theta_{k,n,\max}}{2}\cdot\sin\left[k(\omega t - \varphi_0) + n\frac{\pi}{\tau_p}(x - x_0) - (j-1)\frac{k+n}{m}\pi\right] \tag{2.185}$$

Positive sequence components of MMF created by adjacent phases are shifted to each other for an angle of

$$\gamma_+ = \frac{k-n}{m}\pi \tag{2.186}$$

and negative sequence components for

$$\gamma_- = \frac{k+n}{m}\pi \tag{2.187}$$

If the angle γ_+ or γ_- is an integer multiple of 2π, the particular components (positive or negative) of MMF in all m phases are in phase, and the resulting sequence is $m/2$ times larger than in a single phase consisting of two coil groups over two poles. In other words, the kth time and nth spatial harmonic in an m-phase machine will generate a positive sequence MMF if

$$\frac{k-n}{m} = \text{even} \tag{2.188}$$

and a negative sequence harmonic for

$$\frac{k+n}{m} = \text{even} \tag{2.189}$$

One should note that conditions expressed in Eqs. 2.188 and 2.189 are more precise than those found in majority of textbooks on electric machines, namely that $(k \pm n)/m$ = integer. One recalls that this condition is valid for an assumption of m coil groups across two poles, which further implies the phase shift of $2\pi/m$ between currents. This result seduces, because it works perfectly for a 3-phase machine; however, in a two-phase machine, $m = 2$, it defines a phase angle of $2\pi/m = \pi$ between two currents, which is far from reality. Furthermore, fundamental space and time harmonics in a two-phase machine generate both positive and negative sequence components of MMF according to equation $(k \pm n)/m = (1 \pm 1)/2 = 0$ or 1, i.e., a pulsating MMF! In reality, however, there exists only a positive sequence MMF in a 2-phase machine. Equations 2.188 and 2.189 deliver an even number (here 0) only for a difference of harmonic orders, $(1 - 1)/2$, i.e., only for the positive sequence MMF!

If the angle γ_+ in Eq. 2.186 or γ_- in Eq. 2.187 is not an even multiple of π, the particular components (positive or negative) of MMF in all m phases build a symmetrical MMF star, which adds up to zero.

In Table 2.9 angular velocities of MMF waves created by the fundamental time and nth spatial harmonic as multiples of ω/p are given for various numbers of phases m. The width of the zone which belongs to a coil group under one pole is equal to 180° el./m, where m denotes the number of supply phases. This principle is illustrated in Fig. 2.62, in which axes of phase windings in symmetrically wound machines with m = 2–6 are shown.

One should note that in a symmetrically connected polyphase machine either pulsating, or rotating field is generated, but never elliptical. Another property of symmetrically connected coil groups in a polyphase machine is that they do not let pass air gap MMF harmonics the order n of which is an integer multiple of the number of phases. For example, in a symmetrically wound three-phase machine, the 3., 9., 15., etc., harmonic can exist in MMF of each phase, but not in the resulting air gap MMF.

When analyzing results in Table 2.9, one comes to a conclusion that in a symmetrical m-phase winding fed from a symmetrical system of sinusoidal currents

(k = 1) the order n_ℓ of the lowest higher spatial harmonic which can create rotating air gap MMF is equal to $2m - 1$. By applying Eqs. 2.188 and 2.189, one can find the order n_ℓ of the lowest higher spatial harmonic in the air gap MMF wave created by the kth current harmonic in an m-phase machine: By inserting 2 for the lowest even number in Eqs. 2.188 and 2.189, one becomes $n_\ell = 2m - k$. The spatial harmonic of the order n_ℓ creates a negative sequence MMF.

Consider now a symmetrical winding with $q = 1$ and full-pitch coils. The winding has as many slots per pole as the number of phases, $N/(2p) = m$, and the lowest higher harmonic of rotating MMF created by the fundamental of current has the order $n_\ell = N/p - 1$, which is the order of slot harmonic, see Table 2.9. Despite the fact that the absolute value of the pitch factor for each spatial harmonic of full-pitch coils is equal to one, higher harmonics (with exception of slot harmonics) do not exist in the resulting rotating field! Obviously the winding with one slot per pole and phase, as is the case with squirrel cage, creates rotating air gap MMF the spectrum of which contains the lowest content of higher harmonics among all conventional winding types.

Table 2.9 Angular velocities of MMF waves (as multiples of ω/p) created by the fundamental harmonic of current (k = 1) and spatial harmonics $1 \le n \le 29$ as a function of the number of supply phases m

	Number of supply phases m/Zone width (° el.)								
n	m = 1 180°	m = 2 90°	m = 3 60°	m = 4 45°	m = 5 36°	m = 6 30°	m = 7 25.7°	m = 8 22.5°	m = 9 20°
1	±1	1	1	1	1	1	1	1	1
3	±1/3	−1/3	–	–	–	–	–	–	–
5	±1/5	1/5	−1/5	–	–	–	–	–	–
7	±1/7	−1/7	1/7	−1/7	–	–	–	–	–
9	±1/9	1/9	–	1/9	−1/9	–	–	–	–
11	±1/11	−1/11	−1/11	–	1/11	−1/11	–	–	–
13	±1/13	1/13	1/13	–	–	1/13	−1/13	–	–
15	±1/15	−1/15	–	−1/15	–	–	1/15	−1/15	–
17	±1/17	1/17	−1/17	1/17	–	–	–	1/17	−1/17
19	±1/19	−1/19	1/19	–	−1/19	–	–	–	1/19
21	±1/21	1/21	–	–	1/21	–	–	–	–
23	±1/23	−1/23	−1/23	−1/23	–	−1/23	–	–	–
25	±1/25	1/25	1/25	1/24	–	1/25	–	–	–
27	±1/27	−1/27	–	–	–	–	−1/27	–	–
29	±1/29	1/29	−1/29	–	−1/29	–	1/29	–	–

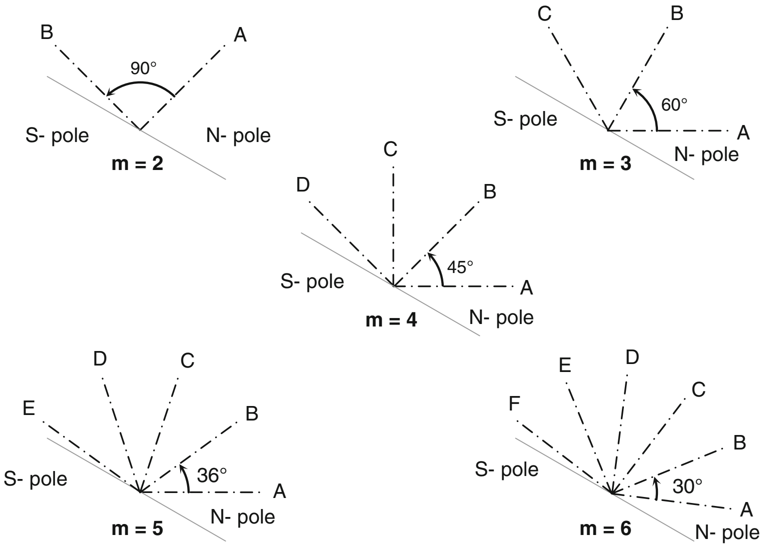

Fig. 2.62 Axes of windings in a symmetrically wound machine under one pole for different numbers of supply phases

2.6.4 MMF Waves Generated by Asymmetrically Wound Stationary Coils Carrying Asymmetrical Alternating Currents on One Side of Air Gap

If an m-phase winding is asymmetrical, or carries phase and/or amplitude asymmetrical currents, both positive and negative sequence components of air gap MMF can be generated for a given combination of spatial and time harmonics. Denoting by $\Theta_{\max,i}$ the amplitude of the MMF created by ith phase, by φ_i the phase shift of the current in the ith phase and by γ_i the electrical angle of axis of the ith phase winding, one can express the MMF created by the kth time and nth spatial harmonic in the ith phase as

$$\Theta_{i,k,n} = \Theta_{\max,i} \sin\left[n\left(\frac{\pi}{\tau_\mathrm{p}}x - \gamma_i\right)\right] \cos[k(\omega t - \varphi_i)] \tag{2.190}$$

The amplitude $\Theta_{+,k,n}$ of the positive sequence component of the resulting MMF created by the kth time and nth spatial harmonic is equal to the geometric sum of positive sequence components created by all m phases

$$\Theta_{+,k,n} = \frac{1}{2}\sqrt{\left[\sum_{i=1}^{m} \Theta_{i,k,n} \cos(\varphi_i - \gamma_i)\right]^2 + \left[\sum_{i=1}^{m} \Theta_{i,k,n} \sin(\varphi_i - \gamma_i)\right]^2} \tag{2.191}$$

whereas the amplitude of the negative sequence component can be expressed as

$$\Theta_{-,k,n} = \frac{1}{2}\sqrt{\left[\sum_{i=1}^{m} \Theta_{i,k,n} \cos(\varphi_i + \gamma_i)\right]^2 + \left[\sum_{i=1}^{m} \Theta_{i,k,n} \sin(\varphi_i + \gamma_i)\right]^2} \qquad (2.192)$$

If the amplitude of negative sequence component of MMF is different from zero and smaller than the amplitude of the positive sequence component, the air gap field is elliptical. An overview of air gap MMF forms is shown in Table 2.10, and their basic shapes are shown in Fig. 2.63. Here it is assumed that the air gap MMF is created by the fundamental time and fundamental spatial harmonics, i.e., $k = 1$ and $n = 1$.

Fundamental component of elliptical field can be represented as a sum of the fundamental positive sequence component with amplitude Θ_+, and the fundamental negative sequence component with amplitude Θ_-

Table 2.10 Forms of air gap field created by m identical coils carrying currents with equal rms values. $\Theta_{1,1}$ denotes the amplitude of the MMF created by coils in one zone

Type of MMF	Amplitude of the positive sequence component Θ_+	Amplitude of the negative sequence component Θ_-
Pulsating	$m \cdot \Theta_{1,1}$	$m \cdot \Theta_{1,1}$
Elliptical	$< m \cdot \Theta_{1,1}$	$< m \cdot \Theta_{1,1}$
Rotating	$m \cdot \Theta_{1,1}$	0

$$\Theta(x,t) = \Theta_+ \cdot \sin\left(\omega t - \frac{\pi}{\tau_p}x\right) + \Theta_- \cdot \sin\left(\omega t + \frac{\pi}{\tau_p}x\right) = \Theta_e \cdot \sin(\omega t + \gamma) \qquad (2.193)$$

where

$$\Theta_e = \sqrt{\Theta_+^2 + \Theta_-^2 + 2 \cdot \Theta_+ \cdot \Theta_- \cdot \cos\frac{2\pi}{\tau_p}x} \qquad (2.194)$$

and

$$\gamma = \arctan\frac{\Theta_- - \Theta_+}{\Theta_- + \Theta_+}\tan\frac{\pi}{\tau_p}x \qquad (2.195)$$

The trajectory of Θ_e is an ellipse in the polar coordinate system ($\Theta_{e,}$ γ). The angular speed Ω of Θ_e can be written as

$$\Omega = \frac{d\gamma}{dt} = \frac{\frac{\Theta_- - \Theta_+}{\Theta_- + \Theta_+} \cdot \frac{\pi}{\tau_p}}{\cos^2 \frac{\pi}{\tau_p} x + \left(\frac{\Theta_- - \Theta_+}{\Theta_- + \Theta_+}\right)^2 \sin^2 \frac{\pi}{\tau_p} x} \cdot \frac{dx}{dt} \tag{2.196}$$

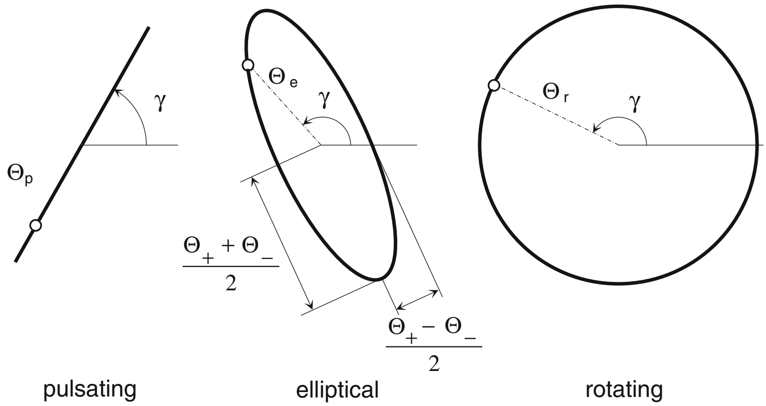

Fig. 2.63 Pulsating, elliptical, and rotating air gap MMF

Fig. 2.64 The p.u. amplitude of resulting MMF as a function of circumferential coordinate x with ratio Θ_-/Θ_+ as a parameter

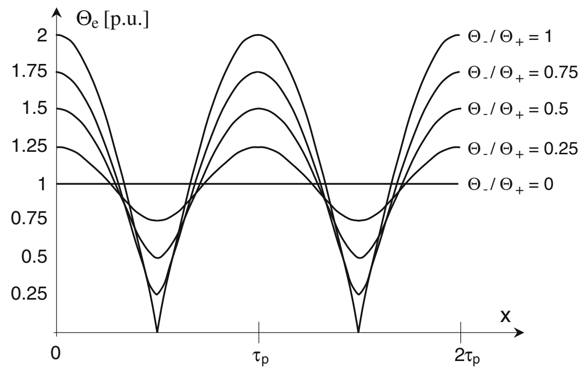

Since

$$\frac{dx}{dt} = v_{1,1} = \pm \frac{\tau_p}{\pi} \cdot \omega \tag{2.197}$$

one can express the angular speed Ω of the resulting MMF as

$$\Omega = \frac{\mathrm{d}\gamma}{\mathrm{d}t} = \pm \frac{\frac{\Theta_- - \Theta_+}{\Theta_- + \Theta_+}}{\cos^2 \frac{\pi}{\tau_p} x + \left(\frac{\Theta_- - \Theta_+}{\Theta_- + \Theta_+} \right)^2 \sin^2 \frac{\pi}{\tau_p} x} \cdot \omega \tag{2.198}$$

The variation of amplitude of elliptical MMF as a function of the grade of asymmetry and the circumferential coordinate is shown in Fig. 2.64. The largest variation of amplitude of elliptic MMF occurs for $\Theta_+ = \Theta_-$ (pulsating field), where it changes between 0 and 2. In rotating field the deviation of amplitude of resulting MMF from its average value of 1 is equal to zero.

The angular speed Ω of the resulting MMF as a function of circumferential coordinate x and the grade of asymmetry Θ_+/Θ_- as a parameter is shown in Fig. 2.65. Only in case of rotating field ($\Theta_- = 0$), the resulting MMF rotates at a constant speed; elliptic field *permanently accelerates and decelerates*. The larger the negative sequence component, the bigger the difference between maximum and minimum speed of rotation. Elliptic field rotates at highest speed at those points of circumference where the positive and negative sequence components are shifted for 180°, thus acting against each other (ellipse minor axis), and at slowest speed when they act in the same direction (ellipse major axis).

Virtual work performed by magnetic energy in the air gap can be expressed in terms of differential area swept by the magnitude Θ_e in Fig. 2.63:

$$\mathrm{d}A = \frac{1}{2} \cdot \Theta_e \cdot (\Theta_e \mathrm{d}\gamma) \tag{2.199}$$

and the corresponding areal velocity, which analogously has a dimension of power

$$\frac{\mathrm{d}A}{\mathrm{d}t} = \frac{1}{2} \cdot \Theta_e^2 \cdot \frac{\mathrm{d}\gamma}{\mathrm{d}t} \tag{2.200}$$

After substitution of expressions for Θ_e and $\mathrm{d}\gamma/\mathrm{d}t$ one can write

Fig. 2.65 p.u. angular speed of resulting MMF as a function of circumferential coordinate x with ratio Θ_-/Θ_+ as parameter

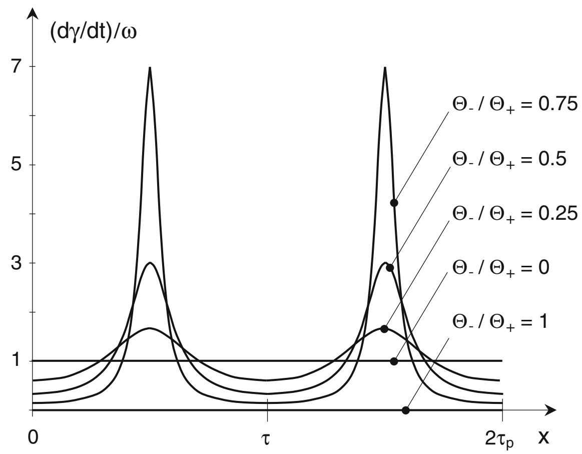

Fig. 2.66 Areal velocity of resulting MMF (power!) as a function of ratio Θ_{-}/Θ_{+}

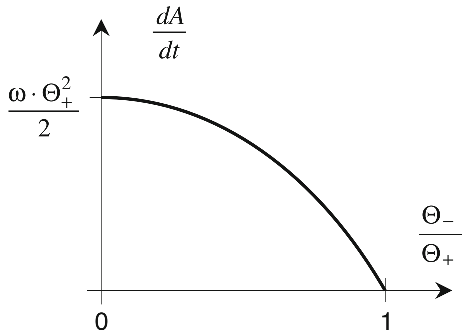

$$\frac{\mathrm{d}A}{\mathrm{d}t} = \pm \frac{\omega \cdot \Theta_{+}^{2}}{2} \cdot \frac{1 + r^{2} + 2r\cos 2\frac{\pi}{\tau_{\mathrm{p}}}x}{\cos^{2}\frac{\pi}{\tau_{\mathrm{p}}}x + \left(\frac{r-1}{r+1}\right)^{2}\sin^{2}\frac{\pi}{\tau_{\mathrm{p}}}x} \cdot \frac{r-1}{r+1} \tag{2.201}$$

with r standing for the ratio between amplitude of negative and positive sequence component of MMF

$$r = \frac{\Theta_{-}}{\Theta_{+}} \tag{2.202}$$

Applying trigonometric identities, Eq. (2.201) for areal velocity can be simplified to

$$\frac{\mathrm{d}A}{\mathrm{d}t} = \pm \frac{\omega \cdot \Theta_{+}^{2}}{2} \cdot \left(r^{2} - 1\right) = \pm \frac{\omega}{2} \cdot \left(\Theta_{+}^{2} - \Theta_{-}^{2}\right) \tag{2.203}$$

which is constant. *The magnitude of air gap MMF sweeps equal areas during equal intervals of time*, which is analogous to **the second Kepler's law** of planetary motion!

Physical interpretation of the identical mathematical property is of course different in a rotating field machine than in celestial mechanics. In an electric machine the constant area swept by the air gap MMF means nothing but that the torque, as a partial derivative of magnetic energy accumulated in the air gap with respect to angle, is time invariant.

The dependence of areal velocity on the ratio Θ_{-}/Θ_{+} is shown in Fig. 2.66.

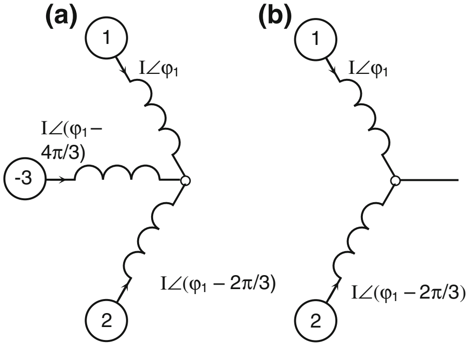

Fig. 2.67 Three-phase winding connection with one phase reversed (**a**), and with one phase disconnected (**b**)

The power generated by pulsating field, i.e. for equal amplitudes of positive and negative sequence MMF, is equal to zero.

Elliptical MMF is created in a three-phase machine when terminals of one supply phase are reversed, or if a phase is disconnected. Denoting by $\Theta_{1,1,\max}$ the amplitude of the fundamental component of MMF created by one coil per pole pair, the positive sequence MMF in a machine with reversed phase terminals as in Fig. 2.67a is equal to

$$\begin{aligned}\Theta_{1,1,,+}(x,t) &= \frac{\Theta_{1,1,\max}}{2}\cdot\sin\left[\omega t-\varphi_{1,1}-\frac{\pi}{\tau_p}(x-x_{0,1})\right]+\frac{\Theta_{1,1,\max}}{2}\cdot\sin\left[\omega t-\varphi_{1,1}-\frac{\pi}{\tau_p}(x-x_{0,1})-\pi\right]+\\&+\sum_{j=3}^{4}\frac{\Theta_{1,1,\max}}{2}\cdot\sin\left[\omega t-\varphi_{1,1}-\frac{\pi}{\tau_p}(x-x_{0,1})\right]+\frac{\Theta_{1,1,\max}}{2}\cdot\sin\left[\omega t-\varphi_{1,1}-\frac{\pi}{\tau_p}(x-x_{0,1})-\pi\right]\\&+\frac{\Theta_{1,1,\max}}{2}\cdot\sin\left[\omega t-\varphi_{1,1}-\frac{\pi}{\tau_p}(x-x_{0,1})\right]=\Theta_{1,1,\max}\cdot\sin\left[\omega t-\varphi_{1,1}-\frac{\pi}{\tau_p}(x-x_{0,1})\right]\end{aligned}\tag{2.204}$$

and the negative sequence

$$\begin{aligned}\Theta_{1,1,,-}(x,t) &= \frac{\Theta_{1,1,\max}}{2}\cdot\sin\left[\omega t-\varphi_{1,1}+\frac{\pi}{\tau_p}(x-x_{0,1})\right]+\frac{\Theta_{1,1,\max}}{2}\cdot\sin\left[\omega t-\varphi_{1,1}+\frac{\pi}{\tau_p}(x-x_{0,1})-\frac{5\pi}{3}\right]\\&+\sum_{j=3}^{4}\frac{\Theta_{1,1,\max}}{2}\cdot\sin\left[\omega t-\varphi_{1,1}+\frac{\pi}{\tau_p}(x-x_{0,1})-(j-1)\frac{2\pi}{3}\right]+\frac{\Theta_{1,1,\max}}{2}\cdot\sin\left[\omega t-\varphi_{1,1}+\frac{\pi}{\tau_p}(x-x_{0,1})-\frac{5\pi}{3}\right]\\&+\frac{\Theta_{1,1,\max}}{2}\cdot\sin\left[\omega t-\varphi_{1,1}+\frac{\pi}{\tau_p}(x-x_{0,1})-\frac{10\pi}{3}\right]=2\cdot\Theta_{1,1,\max}\cdot\sin\left[\omega t-\varphi_{1,1}+\frac{\pi}{\tau_p}(x-x_{0,1})-\frac{5\pi}{3}\right]\end{aligned}\tag{2.205}$$

The amplitude of the negative sequence component in a three-phase machine with terminals of one phase reversed is twice as large as the amplitude of the positive sequence component of the air gap MMF! Consequently, the resulting elliptic MMF rotates in negative direction.

The positive sequence MMF in a machine with one phase disconnected as shown in Fig. 2.67b is equal to

$$\begin{aligned}\Theta_{1,1,,+}(x,t) &= \sum_{j=1}^{4} \frac{\Theta_{1,1,\max}}{2} \cdot \sin\left[\omega t - \varphi_{1,1} - \frac{\pi}{\tau_\mathrm{p}}\left(x - x_{0,1}\right)\right] \\ &= 2 \cdot \Theta_{1,1,\max} \cdot \sin\left[\omega t - \varphi_{1,1} - \frac{\pi}{\tau_\mathrm{p}}\left(x - x_{0,1}\right)\right]\end{aligned} \tag{2.206}$$

and the negative sequence

$$\Theta_{1,1,,-}(x,t) = \Theta_{1,1,\max} \cdot \sin\left[\omega t - \varphi_{1,1} + \frac{\pi}{\tau_\mathrm{p}}\left(x - x_{0,1}\right) - \frac{4\pi}{3}\right] \tag{2.207}$$

The amplitude of the positive sequence component in a three phase machine with one phase disconnected is twice as large as the amplitude of the negative sequence component of the air gap MMF. The resulting elliptic MMF rotates in positive direction.

2.6.5 MMF Waves Generated by Rotating Coil(s) Carrying Constant Frequency Current(s)

Consider now a rotor coil fed from current source $i_\mathrm{r}(t)$

$$i_\mathrm{r}(t) = \sum_{k=1}^{\infty} I_{k,\mathrm{r}} \cos k_\mathrm{r}\left(\omega_\mathrm{r} t - \varphi_{k,\mathrm{r}}\right) \tag{2.208}$$

shifted for an amount of $x_{0,\mathrm{r}}$ along the circumferential coordinate x_r and rotating at angular speed Ω. The k_rth time and n_rth spatial harmonic of air gap MMF wave created by the rotating coil is equal to

$$\begin{aligned}\Theta_{k_\mathrm{r},n_\mathrm{r}}\left(x_\mathrm{r}, x_{0,\mathrm{r}}, t\right) &= \frac{\Theta_{k_\mathrm{r},n_\mathrm{r},\max}}{2} \cdot \sin\left[k_\mathrm{r}\left(\omega_\mathrm{r} t - \varphi_{k,\mathrm{r}}\right) - n_\mathrm{r}\frac{\pi}{\tau_\mathrm{p}}\left(x_\mathrm{r} - x_{0,\mathrm{r}}\right)\right] \\ &+ \frac{\Theta_{k_\mathrm{r},n_\mathrm{r},\max}}{2} \cdot \sin\left[k_\mathrm{r}\left(\omega_\mathrm{r} t - \varphi_{k,\mathrm{r}}\right) + n_\mathrm{r}\frac{\pi}{\tau_\mathrm{p}}\left(x_\mathrm{r} - x_{0,\mathrm{r}}\right)\right]\end{aligned} \tag{2.209}$$

Rotor circumferential coordinate x_r can be expressed in terms of stator circumferential coordinate x as

$$x_\mathrm{r} = x + x_0 + \Omega \cdot t \cdot R = x + x_0 + \Omega \cdot t \cdot \frac{p\tau_\mathrm{p}}{\pi} \tag{2.210}$$

with x_0 denoting the initial rotor shift and R the air gap mean radius. The k_rth time and n_rth spatial harmonic of the air gap MMF wave can now be expressed in the stationary system as

$$\begin{aligned}\Theta_{k_\mathrm{r},n_\mathrm{r}}(x, x_0, t) &= \frac{\Theta_{k_\mathrm{r},n_\mathrm{r},\max}}{2} \cdot \sin\left[k_\mathrm{r}\left(\omega_\mathrm{r} t - \varphi_{k,\mathrm{r}}\right) - n_\mathrm{r}\frac{\pi}{\tau_\mathrm{p}}\left(x + x_0 + \Omega \cdot t \cdot \frac{p\tau_\mathrm{p}}{\pi} - x_{0,\mathrm{r}}\right)\right] \\ &+ \frac{\Theta_{k_\mathrm{r},n_\mathrm{r},\max}}{2} \cdot \sin\left[k_\mathrm{r}\left(\omega_\mathrm{r} t - \varphi_{k,\mathrm{r}}\right) + n_\mathrm{r}\frac{\pi}{\tau_\mathrm{p}}\left(x + x_0 + \Omega \cdot t \cdot \frac{p\tau_\mathrm{p}}{\pi} - x_{0,\mathrm{r}}\right)\right]\end{aligned} \tag{2.211}$$

and

$$\begin{aligned}\Theta_{k_\mathrm{r},n_\mathrm{r}}(x, x_0, t) &= \frac{\Theta_{k_\mathrm{r},n_\mathrm{r},\max}}{2} \cdot \sin\left[(k_\mathrm{r}\omega_\mathrm{r} - n_\mathrm{r} p\Omega) \cdot t - n_\mathrm{r}\frac{\pi}{\tau_\mathrm{p}} x - k_\mathrm{r}\varphi_{k,\mathrm{r}} - n_\mathrm{r}\frac{\pi}{\tau_\mathrm{p}}\left(x_0 - x_{0,\mathrm{r}}\right)\right] \\ &+ \frac{\Theta_{k_\mathrm{r},n_\mathrm{r},\max}}{2} \cdot \sin\left[(k_\mathrm{r}\omega_\mathrm{r} - n_\mathrm{r} p\Omega) \cdot t + n_\mathrm{r}\frac{\pi}{\tau_\mathrm{p}} x - k_\mathrm{r}\varphi_{k,\mathrm{r}} + n_\mathrm{r}\frac{\pi}{\tau_\mathrm{p}}\left(x_0 - x_{0,\mathrm{r}}\right)\right]\end{aligned} \tag{2.212}$$

The angular speed of rotation ω of the k_rth time and n_rth spatial harmonic of the air gap MMF wave relative to the stator can be found by setting the argument of sine function equal to a constant and then differentiating it w.r.t. time

$$\begin{aligned}&\frac{\mathrm{d}}{\mathrm{d}t}\left\{(k_\mathrm{r}\omega_\mathrm{r} - n_\mathrm{r} p\Omega) \cdot t \mp n_\mathrm{r}\frac{\pi}{\tau_\mathrm{p}} x - k_\mathrm{r}\varphi_{k,\mathrm{r}} \mp n_\mathrm{r}\frac{\pi}{\tau_\mathrm{p}}\left(x_0 - x_{0,\mathrm{r}}\right) = \mathrm{const}\right\} \\ &\Rightarrow n_\mathrm{r}\frac{\pi}{\tau_\mathrm{p}}\frac{\mathrm{d}x}{\mathrm{d}t} = \pm(k_\mathrm{r}\omega_\mathrm{r} - n_\mathrm{r} p\Omega)\end{aligned} \tag{2.213}$$

from which the angular speed ω can be expressed as

$$\omega = \Omega \pm \frac{k_\mathrm{r}}{n_\mathrm{r}} \cdot \frac{\omega_\mathrm{r}}{p} \tag{2.214}$$

The air gap MMF component created by k_rth time harmonic of rotor current and n_rth spatial harmonic of rotor air gap MMF travels relative to stator at rotor mechanical speed augmented or diminished by the component speed relative to the rotor. Positive sequence component of the rotor MMF created by fundamental time and spatial harmonic is at standstill relative to the stator if the rotor mechanical speed is equal to the negative synchronous speed.

Stationary coil(s) generate the fundamental component of air gap MMF wave rotating at the same angular speed ω as in Eq. 2.214 if fed by current(s) with angular frequency ω_s

$$\omega_s = p \cdot \Omega \pm \frac{k_r}{n_r} \cdot \omega \tag{2.215}$$

Accordingly, rotor DC creates air gap MMF fundamental component ($n_r = 1$) which rotates at angular speed Ω and which is observed on the stator side as if it were generated by an AC with angular frequency $\omega_s = p\,\Omega$.

2.6.6 *MMF Waves Generated by Rotating Coil(s) Carrying Variable Frequency Currents on One Side of Air Gap*

Assume that a coil (group) rotates at mechanical angular speed Ω and that it is fed from an AC source

$$i_r(t) = \sum_{k_r=1}^{\infty} I_{k_r} \cos k_r \left(s\omega t - \varphi_{k_r}\right) \tag{2.216}$$

with s denoting the slip

$$s = \frac{\omega - p \cdot \Omega}{\omega} \tag{2.217}$$

Each coil (group) per pole creates an MMF

$$\Theta\left(x_r, x_{0,r}, t\right) = \frac{4}{\pi} w \sum_{n_r=1,3,5,\ldots}^{\infty} \sum_{k_r=1}^{\infty} I_{k_r} \cos k_r \left(s\omega t - \varphi_{k_r}\right) \cdot f_{w,n} \sin n_r \frac{\pi}{\tau_p}\left(x_r - x_{0,r}\right) \tag{2.218}$$

with x_0 denoting the shift of the coil (group) axis to the circumferential coordinate $x = 0$ and $f_{w,n}$ the winding factor for the nth spatial harmonic. The coil (group) MMF created by the kth time and nth spatial harmonic can be represented in terms of positive and negative sequence components, as given in Eq. 2.163, the speed of which *relative to the coil (group)* is

$$v_{k_r,n_r} = \pm \frac{k_r}{n_r} \cdot \frac{\tau_p}{\pi} \cdot s\omega; \quad \omega_{k_r,n_r} = \pm \frac{k_r}{n_r} \cdot \frac{s\omega}{p} \tag{2.219}$$

Since the coil (group) rotates at angular speed Ω, the angular speed of the positive and negative sequence components *relative to stator* $\omega_{k,n,\mathrm{st}}$ is equal to

$$\omega_{k,n,\mathrm{st}} = \Omega + \omega_{k_r,n_r} = \Omega \pm \frac{k_r}{n_r} \cdot \frac{s\omega}{p} = \Omega \pm \frac{k_r}{n_r} \cdot \frac{\omega - p \cdot \Omega}{p} \tag{2.220}$$

For the fundamental time (k = 1) and spatial (n = 1) harmonic one can further write

$$\omega_{1,1,\mathrm{st}} = \Omega + \omega_{1,1} = \Omega \pm \frac{s\omega}{p} = \Omega \pm \frac{\omega - p \cdot \Omega}{p} \tag{2.221}$$

The angular speed of the positive sequence is

$$\omega_{1,1,\mathrm{st},+} = \Omega + \frac{\omega - p \cdot \Omega}{p} = \frac{\omega}{p} \tag{2.222}$$

i.e., it is constant and equal to the synchronous speed of the fundamental wave of stator MMF. The angular speed of the negative sequence component of the rotor MMF is

$$\omega_{1,1,\mathrm{st},-} = \Omega - \frac{\omega - p \cdot \Omega}{p} = 2\Omega - \frac{\omega}{p} \tag{2.223}$$

For mechanical angular speed values Ω below one half of the synchronous speed $\omega/(2p)$ the negative sequence component of the rotor MMF rotates opposite to the direction of rotation of the rotor; above one half of the synchronous speed the negative sequence MMF rotates in the direction of rotation of the rotor. The negative sequence component of the rotor MMF created by rotating coil(s) is at standstill when the rotor mechanical speed is equal to one half the synchronous speed. This property of rotor pulsating field is called **Görges phenomenon**.

The slip of the negative sequence component of the rotor MMF is equal to

$$s_- = \frac{\omega - p \cdot \omega_{1,1,\mathrm{st},-}}{\omega} = \frac{\omega - 2p\Omega + \omega}{\omega} = 2s \tag{2.224}$$

2.6.7 Resulting MMF Waves Generated by Coils on Both Sides of Air Gap

Consider the fundamental component of air gap MMF wave created by a symmetrical stator winding carrying symmetrical currents, $\Theta_s(x, t)$, and the fundamental component of the air gap MMF created by rotor winding, $\Theta_r(x, t)$. The rotor MMF is created either by a symmetrical rotor winding carrying symmetrical currents with appropriate frequency, or by a DC-fed coil rotating at synchronous speed. The resulting air gap MMF $\Theta_\delta(x, t)$ can be written as

$$\Theta_\delta(x,t) = \Theta_s(x,t) + \Theta_r(x,t) \tag{2.225}$$

or

$$\Theta_\delta \sin\left(\omega t - \frac{\pi}{\tau_p}x + \gamma\right) = \Theta_s \sin\left(\omega t - \frac{\pi}{\tau_p}x + \Psi_s\right) + \Theta_r \sin\left(\omega t - \frac{\pi}{\tau_p}x + \Psi_r\right) \tag{2.226}$$

where

$$\Theta_\delta^2 = \Theta_s^2 + \Theta_r^2 + 2 \cdot \Theta_s \cdot \Theta_r \cdot \cos(\Psi_s - \Psi_r) \tag{2.227}$$

and

$$\gamma = \arctan\frac{\Theta_s \cdot \sin\Psi_s + \Theta_r \cdot \sin\Psi_r}{\Theta_s \cdot \cos\Psi_s + \Theta_r \cdot \cos\Psi_r} \tag{2.228}$$

The three MMF components $\Theta_s(x, t)$, $\Theta_r(x, t)$, and $\Theta_\delta(x, t)$ can be represented in the complex plane in the manner shown in Fig. 2.68.

By positioning the resulting air gap MMF Θ_δ to the negative real axis ($\gamma = \pi$), one can further write

$$\Theta_s = -\Theta_r \frac{\sin\Psi_r}{\sin\Psi_s} \tag{2.229}$$

Keeping resulting MMF constant, Θ_δ = const., one can determine the amplitude of the rotor MMF Θ_r necessary to generate given stator MMF Θ_s at a given angle Ψ_s. In order to do this, substitute first the equation for stator MMF into the relationship between the three MMF amplitudes

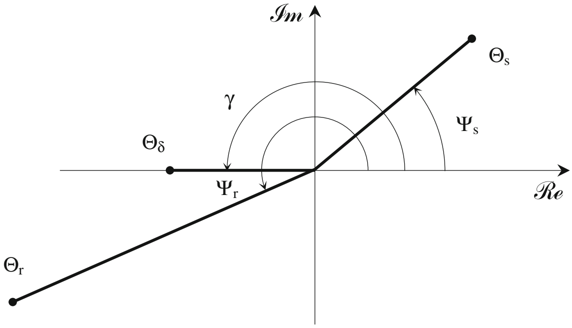

Fig. 2.68 Stator, rotor, and resulting air gap MMF

$$\Theta_\delta^2 = \left(\Theta_r \frac{\sin \Psi_r}{\sin \Psi_s}\right)^2 + \Theta_r^2 - 2 \cdot \frac{\sin \Psi_r}{\sin \Psi_s} \cdot \Theta_r^2 \cdot \cos(\Psi_s - \Psi_r) \tag{2.230}$$

which can be rewritten as

$$\left(\frac{\Theta_\delta}{\Theta_r}\right)^2 - 1 = \left(\frac{\sin \Psi_r}{\sin \Psi_s}\right)^2 - 2 \cdot \frac{\sin \Psi_r}{\sin \Psi_s} \cdot \cos(\Psi_s - \Psi_r) \tag{2.231}$$

and solved in form of

$$\Theta_s \left(\frac{\Theta_r}{\Theta_\delta}\right)_{\Psi_s = \text{const}} \tag{2.232}$$

which is nothing but the equation of V-curves of a synchronous machine, as shown in Fig. 2.69! One should keep in mind that setting Θ_δ = const. determines the amount of air gap flux. If in addition the angle γ of the resulting MMF is kept constant, the stator-induced voltage remains unchanged, no matter how big the stator MMF and where it is relative to the resulting MMF.

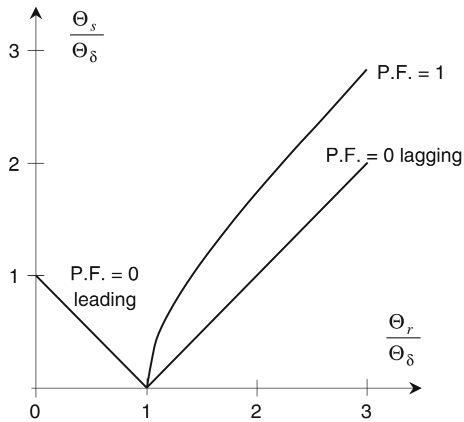

Fig. 2.69 V-curves of a synchronous machine as a solution of Eq. 2.231 for a given set of machine parameters

Neglecting voltage drops across the stator resistance and Potier reactance, the fixing of the amplitude and angle of Θ_δ means nothing but connecting the stator winding of a synchronous machine to an infinite bus.

2.6.8 Air Gap Flux Density Waves in a Single-Slotted Machine with Linear Magnetization Curve

If the B–H curve of stator and rotor irons is linear with $\mu_r >> 1$, the coil ampere-turns are equal to the MMF drop in the air gap, and the air gap flux density is proportional to the inverse of the air gap width δ. As shown previously, the amplitudes of slot harmonics with order $n = N/p \pm 1$ are neither influenced by the coil pitch, nor by the number of in series connected adjacent coils. A question can be posed whether the number of winding phases can modify the amplitude of slot harmonics in a similar manner as it eliminates the harmonics the order of which is equal to integer multiples of the number of phases. The machine is assumed to have unskewed slots.

Traveling waves created by slot harmonics of the order $n = N/p \pm 1$ and by the fundamental time component of current ($k = 1$) are always present in the spectrum of the resulting air gap MMF, because these fulfill the condition

$$\frac{1 \pm n}{m} = \text{even} \tag{2.233}$$

One can express the order n of slot harmonics by means of the *zone width* $q = N/(2 \cdot p \cdot m)$ as

$$n = \frac{N}{p} \pm 1 = 2mq \pm 1 \tag{2.234}$$

Now one can apply the condition for existence of a particular component of resulting MMF (Eqs. 2.188 and 2.189) as

$$\frac{1 \pm n}{m} = \frac{1 \pm (2mq \pm 1)}{m} = \text{even} \tag{2.235}$$

By taking altering signs inside and outside the brackets, one obtains that the condition above is fulfilled as long as $2q$ is an even number, which is always true in integer slot windings. Therefore, slot harmonics are as well present in the spectrum of resulting air gap MMF created by integer slot windings.

In fractional slot windings $2q$ is never an even number and slot harmonics of the order $n = N/p \pm 1$ do not exist in air gap distributions. Nevertheless, slot harmonics of the order $n = N/p_F \pm 1$, with p_F denoting the number of fundamental poles, are present in the air gap flux density spectrum. However, since the fundamental harmonic component of air gap MMF with period length $D \cdot \pi/p_F$ in a fractional slot machine has intentionally low amplitude, the discussed slot harmonics are of minor importance.

As shown in the previous sections, the spectrum of air gap flux density spatial components created by a coil in a machine with slotted air gap is different from the spectrum of coil MMF. If the coil is fed from an AC source, the slot harmonics $N/p - n$ and $N/p + n$ of air gap flux density $B_{n,\mathrm{slot}}$ created by the nth harmonic of the applied MMF and the fundamental harmonic of air gap width due to slotting, $i = 1$, can be written as

$$\begin{aligned} B_{n,\mathrm{slot}} &= 2\frac{\mu_0}{\delta_1}\frac{4}{\pi} \cdot w \cdot f_{\mathrm{w},\frac{N}{p}-n} \sum_{k=1}^{\infty} I_k \cos(k\omega t - \varphi_k) \cos\frac{\pi}{\tau_\mathrm{p}}\left[nx - \left(n + \frac{N}{p}\right)x_\mathrm{c}\right] \\ &\quad + 2\frac{\mu_0}{\delta_1}\frac{4}{\pi} \cdot w \cdot f_{\mathrm{w},\frac{N}{p}+n} \sum_{k=1}^{\infty} I_k \cos(k\omega t - \varphi_k) \cos\frac{\pi}{\tau_\mathrm{p}}\left[nx - \left(n - \frac{N}{p}\right)x_\mathrm{c}\right] \end{aligned} \tag{2.236}$$

The kth harmonic of coil current in Eq. 2.236 creates the rotating wave of air gap flux density due to slotting $B_{n-,k,\mathrm{slot}}$ equal to

$$\begin{aligned} B_{n-,k,\mathrm{slot}} &= \frac{\mu_0}{\delta_1}\frac{4}{\pi} I_k \cdot w \cdot f_{w,\frac{N}{p}-n} \\ &\cdot \left\{\cos\left\{k\omega t - \varphi_k + \frac{\pi}{\tau_\mathrm{p}}\left[nx - \left(n + \frac{N}{p}\right)x_\mathrm{c}\right]\right\} + \cos\left\{k\omega t - \varphi_k - \frac{\pi}{\tau_\mathrm{p}}\left[nx - \left(n + \frac{N}{p}\right)x_\mathrm{c}\right]\right\}\right\} \end{aligned} \tag{2.237}$$

as well as $B_{n+,k,\mathrm{slot}}$, defined as

$$\begin{aligned} B_{n+,k,\mathrm{slot}} &= \frac{\mu_0}{\delta_1}\frac{4}{\pi} I_k \cdot w \cdot f_{w,\frac{N}{p}+n} \\ &\cdot \left\{\cos\left\{k\omega t - \varphi_k + \frac{\pi}{\tau_\mathrm{p}}\left[nx - \left(n - \frac{N}{p}\right)x_\mathrm{c}\right]\right\} + \cos\left\{k\omega t - \varphi_k - \frac{\pi}{\tau_\mathrm{p}}\left[nx - \left(n - \frac{N}{p}\right)x_\mathrm{c}\right]\right\}\right\} \end{aligned} \tag{2.238}$$

As long as the coil does not move relative to the teeth, x_c = const., the speed of both components $B_{n-,k,\mathrm{slot}}$ and $B_{n+,k,\mathrm{slot}}$ is equal to the speed of the nth spatial and kth time harmonic of MMF which created them, namely $\pm k/n \cdot \omega/p$.

If the coil rotates at a constant mechanical angular velocity Ω relative to slots, the coil shift coordinate x_c can be represented as

$$x_\mathrm{c} = R \cdot \Omega \cdot t \tag{2.239}$$

with R denoting the air gap radius. The angular speeds of rotation $\omega_{n-,k,\pm}$ of positive and negative sequence waves of air gap flux density due to slotting $B_{n-,k,\mathrm{slot}}$ become in that case

$$\omega_{n-,k,\pm} = \pm\left(n - \frac{N}{p}\right) \cdot \Omega + \frac{k}{n}\frac{\omega}{p} \tag{2.240}$$

with positive sign in front of parentheses standing for the positive, and negative sign for the negative sequence component of $B_{n-,k,\text{slot}}$.

Analogously, the angular speeds of rotation $\omega_{n+,k,\pm}$ of positive and negative sequence waves of air gap flux density due to slotting $B_{n+,k,\text{slot}}$ can be expressed as

$$\omega_{n+,k,\pm} = \pm\left(n + \frac{N}{p}\right) \cdot \Omega + \frac{k}{n}\frac{\omega}{p} \tag{2.241}$$

The angular speeds of the four components of air gap flux density due to slotting can be expressed as

$$\omega_{n\pm,k,\pm} = \pm\left(n \pm \frac{N}{p}\right) \cdot \Omega + \frac{k}{n}\frac{\omega}{p} \tag{2.242}$$

where every combination of signs stands for a particular higher harmonic and symmetrical component, respectively.

Coil mechanical angular velocities Ω_0 at which the positive or negative sequence wave of air gap flux density due to slotting $B_{n-,k,\text{slot}}$ and $B_{n+,k,\text{slot}}$ is at standstill relative to the teeth, i.e., $\omega_{n\pm,k,\pm} = 0$, can now be expressed as

$$\Omega_0 = \pm k \frac{\omega}{pn \pm N} \tag{2.243}$$

The positive sign in front of the expression on the right-hand side of Eq. 2.243 stands for positive sequence components, and the negative sign for negative sequence components of $B_{n-,k,\text{slot}}$ or $B_{n+,k,\text{slot}}$. The positive sign in front of the number of slots N in Eq. 2.243 is related to a slot harmonic with an order above N/p, and the negative to a slot harmonic with an order below N/p.

2.6.9 Air Gap Flux Density Waves in a Double-Slotted Machine with Linear Magnetization Curve

If the stator and rotor coils in Fig. 2.49 are fed from AC sources with angular frequencies ω_s and ω_r respectively, slot harmonics $N_s/p - n$, $N_s/p + n$, $N_r/p - n$ and $N_r/p + n$ of air gap flux density $B_{n,\text{slot}}$ created by the nth harmonic of applied MMFs and fundamental harmonics of air gap width due to slotting, $i = 1$, can be written as

$$B_{\frac{N_s}{p}-n} = 2\frac{\mu_0}{\delta_1}\frac{4}{\pi}\cdot w_s \cdot f_{w,s,\frac{N_s}{p}-n}\sum_{k=1}^{\infty} I_k \cos(k\omega_s t - \varphi_k)\cos\frac{\pi}{\tau_p}\left[nx - \left(n + \frac{N_s}{p}\right)\xi_n\right] \tag{2.244}$$

$$B_{\frac{N_s}{p}+n} = 2\frac{\mu_0}{\delta_1}\frac{4}{\pi}\cdot w_s \cdot f_{w,s,\frac{N_s}{p}+n}\sum_{k=1}^{\infty} I_k \cos(k\omega_s t - \varphi_k)\cos\frac{\pi}{\tau_p}\left[nx - \left(n - \frac{N_s}{p}\right)\xi_n\right] \tag{2.245}$$

$$\begin{aligned} B_{\frac{N_r}{p}-n} = {} & 2\frac{\mu_0}{\delta_1}\frac{4}{\pi}\cdot w_r \\ & \cdot f_{w,r,\frac{N_r}{p}-n}\sum_{j=1}^{\infty} I_j \cos\left(j\omega_r t - \varphi_j\right)\cos\frac{\pi}{\tau_p}\left[nx - \left(n + \frac{N_r}{p}\right)\left(\xi_n + \frac{N_r}{p}x_0\right)\right] \end{aligned} \tag{2.246}$$

$$\begin{aligned} B_{\frac{N_r}{p}+n} = {} & 2\frac{\mu_0}{\delta_1}\frac{4}{\pi}\cdot w_r \\ & \cdot f_{w,r,\frac{N_r}{p}+n}\sum_{j=1}^{\infty} I_j \cos\left(j\omega_r t - \varphi_j\right)\cos\frac{\pi}{\tau_p}\left[nx - \left(n - \frac{N_r}{p}\right)\left(\xi_n - \frac{N_r}{p}x_0\right)\right] \end{aligned} \tag{2.247}$$

$$B_{n,\mathrm{slot}} = B_{\frac{N_s}{p}-n} + B_{\frac{N_s}{p}+n} + B_{\frac{N_r}{p}-n} + B_{\frac{N_r}{p}+n} \tag{2.248}$$

Each of the pulsating harmonics in Eqs. 2.244–2.248 consists of a positive and a negative sequence component, the speeds of rotation of which can be found in the manner shown previously in this chapter. When determining the rotational speed of rotor harmonics one has to consider the rotor mechanical speed of rotation Ω defined in the previous section.

Denoting by $\dot{\xi}_n$ the derivative of the position coordinate of the maximum of resulting MMF

$$\dot{\xi}_n = n\Theta_{r,n}\frac{\Theta_{r,n} + \Theta_{s,n}\cos n\frac{\pi}{\tau_p}x_0}{\Theta_{r,n}^2 + \Theta_{s,n}^2 + 2\Theta_{r,n}\Theta_{s,n}\cos n\frac{\pi}{\tau_p}x_0}\frac{\mathrm{d}x_0}{\mathrm{d}t} \tag{2.249}$$

one can express the angular speeds of harmonics of air gap flux density created by harmonics of stator and rotor currents with equal orders, j = k, and the fundamental harmonics due to slotting (i = 1) in the manner shown in Table 2.11.

Table 2.11 Angular speeds of air gap flux density harmonics created by *n*th harmonics of stator and rotor MMF and fundamental harmonics of stator and rotor slottings in a double-slotted machine

	Pos. seq.	Neg. seq.
$B_{\frac{N_s}{p}-n}$	$\frac{k}{n}\frac{\omega_s}{p}+\frac{1}{np}\left(n+\frac{N_s}{p}\right)\frac{\pi}{\tau_p}\dot{\xi}_n$	$\frac{k}{n}\frac{\omega_s}{p}-\frac{1}{np}\left(n+\frac{N_s}{p}\right)\frac{\pi}{\tau_p}\dot{\xi}_n$
$B_{\frac{N_s}{p}+n}$	$\frac{k}{n}\frac{\omega_s}{p}+\frac{1}{np}\left(n-\frac{N_s}{p}\right)\frac{\pi}{\tau_p}\dot{\xi}_n$	$\frac{k}{n}\frac{\omega_s}{p}-\frac{1}{np}\left(n-\frac{N_s}{p}\right)\frac{\pi}{\tau_p}\dot{\xi}_n$
$B_{\frac{N_r}{p}-n}$	$\frac{k}{n}\frac{\omega_r}{p}+\frac{1}{np}\left(n+\frac{N_r}{p}\right)\left(\frac{\pi}{\tau_p}\dot{\xi}_n+\Omega\right)$	$\frac{k}{n}\frac{\omega_r}{p}-\frac{1}{np}\left(n+\frac{N_r}{p}\right)\left(\frac{\pi}{\tau_p}\dot{\xi}_n+\Omega\right)$
$B_{\frac{N_r}{p}+n}$	$\frac{k}{n}\frac{\omega_r}{p}+\frac{1}{np}\left(n-\frac{N_r}{p}\right)\left(\frac{\pi}{\tau_p}\dot{\xi}_n+\Omega\right)$	$\frac{k}{n}\frac{\omega_r}{p}-\frac{1}{np}\left(n-\frac{N_r}{p}\right)\left(\frac{\pi}{\tau_p}\dot{\xi}_n+\Omega\right)$

One should note that for a given number of stator and rotor phases and slots per pole pair some harmonics of air gap flux density discussed here may have amplitudes equal to zero.

2.6.10 Air Gap Flux Density Waves in a Slotless Machine with Nonlinear Magnetization Curve

In order to increase the flux level, electric machines are built in such a manner that the operating point in the iron portion of their magnetic circuit is located more or less in saturated region.

A steep increase of MMF drop across iron core as a consequence of increasing flux density results in a slower increase of MMF drop across the air gap. The machine's magnetic circuit acts as if the air gap reluctance has increased, i.e., as if the air gap width became larger.

A comparison of influence of air gap geometry and iron B–H curve on equivalent air gap width is shown in Fig. 2.70.

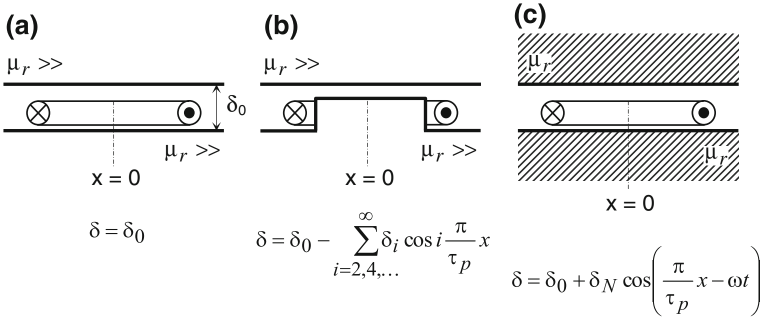

Fig. 2.70 Representation of air gap structure by means of air gap width: **a** linear iron curve, constant air gap width; **b** linear iron magnetization curve, salient poles—periodical decrease of air gap width under the poles; **c** nonlinear iron magnetization curve—periodical increase of air gap width

Whereas air gap becomes electromagnetically shorter as a consequence of saliency, saturation in iron makes it electromagnetically larger. A narrower air gap is attached to a salient pole. A wider air gap representing saturation in iron, on the other hand, travels around the periphery with angular speed of the fundamental of MMF which produced it and can be represented as

$$\delta = \delta_0 + \delta_N \cos 2\left(\frac{\pi}{\tau_p}x - \omega t\right) \tag{2.250}$$

because it is assumed that only the fundamental component of applied MMF determines the level of saturation in iron.

Ampère's circuital law applied to the machine's magnetic circuit in which the increased MMF drop in iron is represented with a wider air gap can be written as

$$\left[\delta_0 + \delta_N \cos 2\left(\frac{\pi}{\tau_p}x - \omega t\right)\right] \sum_{i=1,3,5,\ldots}^{\infty} B_i \cos i\left(\frac{\pi}{\tau_p}x - \omega t\right) = \mu_0 \Theta_1 \cos\left(\frac{\pi}{\tau_p}x - \omega t\right) \tag{2.251}$$

from which one becomes relations between amplitudes of air gap flux density harmonics as

$$\left(\delta_0 + \frac{\delta_N}{2}\right)B_1 + \frac{\delta_N}{2}B_3 = \mu_0\Theta_1 \tag{2.252}$$

$$\frac{\delta_N}{2}B_1 + \left(\delta_0 + \frac{\delta_N}{2}\right)B_3 + \frac{\delta_N}{2}B_5 = 0 \tag{2.253}$$

$$\frac{\delta_N}{2}B_3 + \left(\delta_0 + \frac{\delta_N}{2}\right)B_5 + \frac{\delta_N}{2}B_7 = 0 \tag{2.254}$$

etc. Saturation in iron generates higher harmonics of air gap flux density which travel at the speed of the fundamental. If the MMF distribution contains higher spatial harmonics, their speed decreases with order of harmonic. This means that saturation in iron is a source of higher harmonics of air gap flux density which have the same spatial order as higher harmonics of air gap flux density created by higher harmonics of MMF, but a different time order. As a consequence, there exist two components of nth order of flux density harmonic which travel relative to each other at angular speeds given for a three-phase machine in Table 2.12.

Table 2.12 Angular speeds of air gap flux density harmonics due to MMF and due to saturation. For the sake of comparison, the speed differences for harmonics of the same order and different sources are shown

Order	Angular speed of MMF harmonic	Angular speed of harmonic due to saturation	Speed difference
1	ω_s	ω_s	0
3	–	ω_s	ω_s
5	$-\omega_s/5$	ω_s	$6/5\ \omega_s$
7	$\omega_s/7$	ω_s	$6/7\ \omega_s$
9	–	ω_s	ω_s

2.7 Induced Voltage

2.7.1 Rotating Air Gap Flux Density

Assume a coil with w turns and pitch y traveling in air gap at speed v_c, as shown in Fig. 2.71. The air gap is excited with a flux density wave $B(x, t)$ created by nth spatial harmonic of a symmetrical $2p$-pole winding fed by symmetrical currents with angular frequency $k\omega$. The air gap flux density wave $B(x, t)$ can be represented as

$$B(x,t) = B_{\max}\cos\left[k\omega t - \varphi_k \pm n\frac{\pi}{\tau_p}(x - x_n)\right] \tag{2.255}$$

with φ_k standing for kth time and x_n for nth spatial harmonic phase shift, respectively.

The air gap flux density wave $B(x, t)$ travels at speed $\pm k/n \cdot \tau_p/\pi \cdot \omega$ relative to the stator, with positive sign denoting the same direction of rotation as the coil, and negative sign the opposite direction of rotation to the coil velocity v_c. At time instant t the position x_c of the coil can be expressed as

Fig. 2.71 Coil in air gap and a wave of air gap flux density

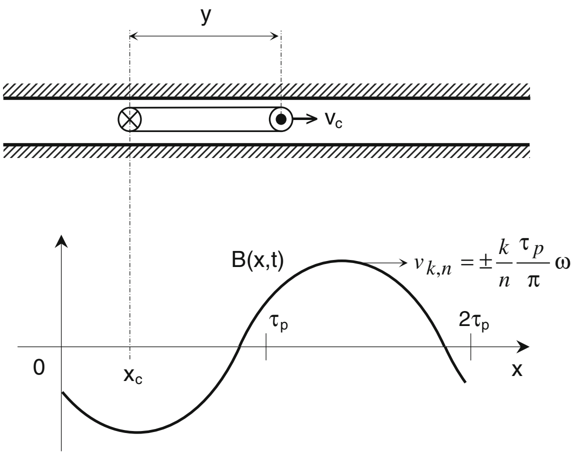

$$x_c = v_c t + x_0 \tag{2.256}$$

where x_0 denotes the coil position at $t = 0$. At time instant t each turn of the coil concatenates the flux $\Phi(t)$ in the amount of

$$\Phi(t) = l_{ax} \int_{x_c}^{x_c + y} B(x,t)\mathrm{d}x = l_{ax} B_{max} \int_{v_c t + x_0}^{v_c t + x_0 + y} \cos\left[k\omega t - \varphi_k \pm n \frac{\pi}{\tau_p}(x - x_n)\right]\mathrm{d}x \tag{2.257}$$

or

$$\begin{aligned}\Phi(t) = -\frac{l_{ax}\tau_p B_{max}}{n\pi}\Bigg\{&\sin\left[k\omega t - \varphi_k \pm n\frac{\pi}{\tau_p}(v_c t + x_0 + y - x_n)\right]\\ &+ \sin\left[k\omega t - \varphi_k \pm n\frac{\pi}{\tau_p}(v_c t + x_0 - x_n)\right]\Bigg\}\end{aligned} \tag{2.258}$$

By applying addition theorem for trigonometric functions, one obtains

$$\begin{aligned}\Phi(t) = -\frac{l_{ax}\tau_p B_{max}}{n\pi}\Bigg\{&\sin\left[\left(k\omega \pm n\frac{\pi}{\tau_p}v_c\right)t - \varphi_k \pm n\frac{\pi}{\tau_p}(x_0 - x_n)\right]\left(\cos n\frac{\pi}{\tau_p}y - 1\right)\\ &- \cos\left[\left(k\omega \pm n\frac{\pi}{\tau_p}v_c\right)t - \varphi_k \pm n\frac{\pi}{\tau_p}(x_0 - x_n)\right]\sin\left(n\frac{\pi}{\tau_p}y\right)\Bigg\}\end{aligned} \tag{2.259}$$

or

$$\Phi(t) = -\frac{2 l_{ax}\tau_p B_{max}}{n\pi}\sin\left(n\frac{y}{\tau_p}\frac{\pi}{s}\right)\sin\left[\left(k\omega \pm n\frac{\pi}{\tau_p}v_c\right)t - \varphi_k - \varphi_{y,n} \pm n\frac{\pi}{\tau_p}(x_0 - x_n)\right] \tag{2.260}$$

where

$$\varphi_{y,n} = \arctan\frac{\cos n\frac{\pi}{\tau_p}y - 1}{\sin n\frac{\pi}{\tau_p}y} \tag{2.261}$$

Define now the maximum flux Φ_{max} concatenated by each turn of a coil with pitch y and created by sinusoidal flux density B_{max} as

$$\Phi_{max} = \frac{2}{\pi} l_{ax}\tau_p B_{max}\sin\left(n\frac{y}{\tau_p}\frac{\pi}{2}\right) \tag{2.262}$$

(recall that the factor 2/π is a consequence of the sinusoidal shape of B, the average of which over half a period is 2/π B_{max}).

Now one can write for the concatenated flux $\Phi(t)$:

$$\Phi(t) = -\frac{\Phi_{\mathrm{max}}}{n}\sin\left[\left(k\omega \pm n\frac{\pi}{\tau_{\mathrm{p}}}v_{\mathrm{c}}\right)t - \varphi_k - \varphi_{y,n} \pm n\frac{\pi}{\tau_{\mathrm{p}}}(x_0 - x_n)\right] \tag{2.263}$$

and for the flux linkage $\Psi(t)$

$$\Psi(t) = w\Phi(t) = -\frac{w\Phi_{\mathrm{max}}}{n}\sin\left[\left(k\omega \pm n\frac{\pi}{\tau_{\mathrm{p}}}v_{\mathrm{c}}\right)t - \varphi_k - \varphi_{y,n} \pm n\frac{\pi}{\tau_{\mathrm{p}}}(x_0 - x_n)\right] \tag{2.264}$$

The induced voltage $u_i(t)$ is equal to

$$u_i(t) = \left(k\omega - n\frac{\pi}{\tau_{\mathrm{p}}}v_{\mathrm{c}}\right)\frac{w\Phi_{\mathrm{max}}}{n}\cos\left[\left(k\omega \pm n\frac{\pi}{\tau_{\mathrm{p}}}v_{\mathrm{c}}\right)t - \varphi_k - \varphi_{y,n} \pm n\frac{\pi}{\tau_{\mathrm{p}}}(x_0 - x_n)\right] \tag{2.265}$$

and its amplitude U_{max}:

$$U_{\mathrm{max}} = \left(k\omega \pm n\frac{\pi}{\tau_{\mathrm{p}}}v_{\mathrm{c}}\right)\frac{w\Phi_{\mathrm{max}}}{n} = \left(k\omega \pm n\frac{\pi}{\tau_{\mathrm{p}}}v_{\mathrm{c}}\right)\frac{w}{n}\frac{2}{\pi}l_{\mathrm{ax}}\tau_{\mathrm{p}}B_{\mathrm{max}}\sin\left(n\frac{y}{\tau_{\mathrm{p}}}\frac{\pi}{s}\right) \tag{2.266}$$

The induced voltage in Eq. 2.266 has two components, U_{wave} and U_{coil}, the amplitudes of which can be written as

$$U_{\mathrm{max,wave}} = \frac{k}{n}\omega w\Phi_{\mathrm{max}} = \frac{k}{n}\omega\frac{\tau_{\mathrm{p}}}{\pi}2wl_{\mathrm{ax}}B_{\mathrm{max}}\sin\left(n\frac{y}{\tau_{\mathrm{p}}}\frac{\pi}{s}\right) \tag{2.267}$$

or, by utilizing expression 132 for circumferential velocity $v_{k,n}$:

$$U_{\mathrm{max,wave}} = 2wB_{\mathrm{max}}v_{k,n}l_{\mathrm{ax}}\sin\left(n\frac{y}{\tau_{\mathrm{p}}}\frac{\pi}{s}\right) \tag{2.268}$$

and

$$U_{\mathrm{max,coil}} = n\frac{\pi}{\tau_{\mathrm{p}}}v_{\mathrm{c}}\frac{w\Phi_{\mathrm{max}}}{n} = 2wB_{\mathrm{max}}v_{\mathrm{c}}l_{\mathrm{ax}}\sin\left(n\frac{y}{\tau_{\mathrm{p}}}\frac{\pi}{s}\right) \tag{2.269}$$

The induced voltage in one conductor of a full-pitch coil is accordingly

$$U_{\text{max,turn}} = B_{\text{max}} l_{\text{ax}} \left(v_{k,n} \pm v_{\text{c}} \right) \tag{2.270}$$

which is nothing but $B \cdot \ell \cdot v$ equation, with v denoting the relative speed between the flux density wave and the coil!

Angular frequency of induced voltage ω_i is equal to

$$\omega_i = k\omega \pm n \frac{\pi}{\tau_{\text{p}}} v_{\text{c}} = k\omega \pm np\Omega \tag{2.271}$$

i.e., to a linear combination of the angular frequency $k\omega$ of the current which generated the flux density wave and an n times increased coil electrical angular speed $p\Omega$. Since the nth spatial harmonic of the air gap flux density travels n times slower than the fundamental, the apparent coil speed $np\Omega$ is n times higher than its actual electrical speed $p\Omega$.

If the coil angular speed Ω is expressed in terms of slip s and fundamental angular frequency ω of currents which generate the rotating wave of flux density $B(x, t)$, one can write for the angular frequency of induced voltage

$$\omega_i = k\omega \pm n(1 - s)\omega = \omega[k \pm n(1 - s)] \tag{2.272}$$

Angular frequencies of coil voltage induced by the fundamental time harmonic ($k = 1$) and various spatial harmonics n of air gap flux density wave $B(x, t)$ traveling in the same ($\omega_{i,+}$) and opposite ($\omega_{i,-}$) direction of the coil velocity v_{c} are given in Table 2.13. In addition, the values of slip are given in this table for which the frequencies $\omega_{i,+}$ and $\omega_{i,-}$ are equal to zero, i.e., at which the particular air gap flux density harmonic travels at the same speed as the coil. In the last two columns of Table 2.13 mechanical angular velocities are given at which a particular air gap flux density harmonic travels at the same speed as the coil (synchronism).

The nth spatial harmonic of air gap flux density travels at a speed n times smaller than the fundamental, but it has to pass an n times shorter way in order to complete a distance of two machine poles divided by its order. Therefore, the nth spatial harmonic needs the same time interval in order to complete one revolution as the fundamental, i.e., the frequency of voltage that it induces in a stationary coil is equal to the frequency of the fundamental.

As long as the coil speed is lower than the speed of flux density wave, the amplitude of induced voltage is positive. If the coil travels at a speed above the flux density wave speed, the amplitude of induced voltage formally changes its sign, which is identical to a phase angle skip of 180°. If the coil carries current with the same frequency as the induced voltage, the product of current and induced voltage—i.e., the power—changes its sign.

If the coil is at standstill ($v_{\text{c}} = 0$), its position remains constant, $x_{\text{c}} = x_0$, Eq. 2.256. In that case, both the amplitude and the frequency of induced voltage are a function only of the order k of time harmonic, but *not of the order n of spatial harmonic* of the air gap flux density wave:

$$u_i(t) = k\omega \frac{w\Phi_{\max}}{n} \cos\left[k\omega t - \varphi_k - \varphi_{y,n} \pm n\frac{\pi}{\tau_p}(x_0 - x_n)\right] \tag{2.273}$$

One recognizes in Eq. 2.273 that only the phase shift of induced voltage in a stationary coil is a function of coil position x_0.

Table 2.13 Frequencies of voltages induced by the fundamental time and nth spatial harmonic of air gap flux density in a coil rotating at mechanical angular speed Ω

n	$\omega_{i,+}$	$\omega_{i,-}$	s for $\omega_{i,+} = 0$	s for $\omega_{i,-} = 0$	Ω for $\omega_{i,+} = 0$	Ω for $\omega_{i,-} = 0$
1	$\boldsymbol{s \cdot \omega}$	$(2 - s) \cdot \omega$	**0**	2	$\boldsymbol{\omega/p}$	$-\omega/p$
3	$(-2 + 3s) \cdot \omega$	$(4 - 3s) \cdot \omega$	2/3	4/3	$\omega/(3p)$	$-\omega/(3p)$
5	$(-4 + 5s) \cdot \omega$	$\boldsymbol{(6 - 5s) \cdot \omega}$	4/5	**6/5**	$\omega/(5p)$	$\boldsymbol{-\omega/(5p)}$
7	$\boldsymbol{(-6 + 7s) \cdot \omega}$	$(8 - 7s) \cdot \omega$	**6/7**	8/7	$\boldsymbol{\omega/(7p)}$	$-\omega/(7p)$
9	$(-8 + 9s) \cdot \omega$	(10-9 s)·ω	8/9	10/9	ω/(9p)	$-\omega/(9p)$
11	(−10 + 11–) · ω	$\boldsymbol{(12 - 11s) \cdot \omega}$	10/11	**12/11**	$\omega/(11p)$	$\boldsymbol{-\omega/(11p)}$
13	$\boldsymbol{(-12 + 13s) \cdot \omega}$	$(14 - 13s)\cdot\omega$	**12/13**	14/13	$\boldsymbol{\omega/(13p)}$	$-\omega/(13p)$
15	$(-14 + 15s) \cdot \omega$	$(16 - 15s) \cdot \omega$	14/15	16/15	$\omega/(15p)$	$-\omega/(15p)$
17	$(-16 + 17s) \cdot \omega$	$\boldsymbol{(18 - 17s)\cdot\omega}$	16/17	**18/17**	ω/(17–)	$\boldsymbol{-\omega/(17p)}$
19	$\boldsymbol{(-18 + 19s) \cdot \omega}$	$(20 - 19s) \cdot \omega$	**18/19**	20/19	$\boldsymbol{\omega/(19p)}$	$-\omega/(19p)$

In addition, slip values at which a particular harmonic travels at the same angular velocity Ω as the coil, and mechanical synchronous speeds of selected harmonics are given. Bold printed are the values related to a symmetrical 3-phase flux density distribution

2.7.2 *Elliptic Air Gap Flux Density*

Assume now that the air gap is excited with elliptic flux density consisting of a positive sequence component $B_+(x, t)$:

$$B_+(x,t) = B_{\max,+} \cos\left[k\omega t - \varphi_k - n\frac{\pi}{\tau_p}(x - x_n)\right] \tag{2.274}$$

and a negative sequence component $B_-(x, t)$:

$$B_-(x,t) = B_{\max,-} \cos\left[k\omega t - \varphi_k + n\frac{\pi}{\tau_p}(x - x_n)\right] \tag{2.275}$$

each of which induces its own voltage in a coil with coil pitch y, Eq. 2.205:

$$u_+(t) = \left(k\omega - n\frac{\pi}{\tau_p}v_c\right)\frac{w\Phi_{\max,+}}{n}\cos\left[\left(k\omega - n\frac{\pi}{\tau_p}v_c\right)t - \varphi_k - \varphi_{y,n} - n\frac{\pi}{\tau_p}(x_0 - x_n)\right] \tag{2.276}$$

$$u_-(t) = \left(k\omega - n\frac{\pi}{\tau_p}v_c\right)\frac{w\Phi_{max,-}}{n}\cos\left[\left(k\omega + n\frac{\pi}{\tau_p}v_c\right)t - \varphi_k - \varphi_{y,n} + n\frac{\pi}{\tau_p}(x_0 - x_n)\right] \tag{2.277}$$

or, in a more compact form:

$$u_+(t) = U_{max,+}\cos(\omega_+ t - \varphi_+) \tag{2.278}$$

and

$$u_-(t) = U_{max,-}\cos(\omega_- t - \varphi_-) \tag{2.279}$$

where

$$U_{max,+} = \left(k\omega - n\frac{\pi}{\tau_p}v_c\right)\frac{w}{n}\frac{2}{\pi}l_{ax}\tau_p B_{max,+}\sin\left(n\frac{y}{\tau_p}\frac{\pi}{2}\right) \tag{2.280}$$

and

$$U_{max,-} = \left(k\omega + n\frac{\pi}{\tau_p}v_c\right)\frac{w}{n}\frac{2}{\pi}l_{ax}\tau_p B_{max,-}\sin\left(n\frac{y}{\tau_p}\frac{\pi}{2}\right) \tag{2.281}$$

The total induced voltage in the coil can now be written as

$$u_{coil}(t) = U_{max,+}\cos(\omega_+ t - \varphi_+) + U_{max,-}\cos(\omega_- t - \varphi_-) \tag{2.282}$$

or

$$\begin{aligned} u_{coil}(t) = U_{max,+}&\left[\cos(\omega_+ t - \varphi_+) + \cos(\omega_- t - \varphi_-)\right] \\ &+ (U_{max,-} - U_{max,+})\cos(\omega_- t - \varphi_-) \end{aligned} \tag{2.283}$$

Introducing substitutions

$$\alpha - \beta = \omega_+ t - \varphi_+; \quad \alpha + \beta = \omega_- t - \varphi_- \tag{2.284}$$

or

$$\alpha = \frac{1}{2}\left[(\omega_+ + \omega_-)\cdot t - \varphi_+ - \varphi_-\right] = k\omega t - \varphi_k - n\frac{\pi}{\tau_p}x_0 \tag{2.285}$$

$$\beta = \frac{1}{2}\left[(-\omega_+ + \omega_-)\cdot t + \varphi_+ - \varphi_-\right] = n\frac{\pi}{\tau_p}(v_c t - x_n) \tag{2.286}$$

one can express the component of induced voltage with amplitude $U_{max,+}$, Eq. 2.221, as

$$\begin{aligned}&U_{\max,+}\left[\cos\left(\omega_+t-\varphi_+\right)+\cos(\omega_-t-\varphi_-)\right]\\&\quad=2U_{\max,+}\cos\left(k\omega t-\varphi_k-n\frac{\pi}{\tau_{\mathrm{p}}}x_0\right)\cos\left[n\frac{\pi}{\tau_{\mathrm{p}}}\left(v_{\mathrm{c}}t-x_n\right)\right]\end{aligned}\tag{2.287}$$

and the total induced voltage, Eq. 2.282:

$$\begin{aligned}u_{\mathrm{coil}}(t)&=2U_{\max,+}\cos\left(k\omega t-\varphi_k-n\frac{\pi}{\tau_{\mathrm{p}}}x_0\right)\cos\left[n\frac{\pi}{\tau_{\mathrm{p}}}\left(v_{\mathrm{c}}t-x_n\right)\right]\\&\quad+\left(U_{\max,-}-U_{\max,+}\right)\cos\left[\left(k\omega+n\frac{\pi}{\tau_{\mathrm{p}}}v_{\mathrm{c}}\right)t-\varphi_k-\varphi_{y,n}-n\frac{\pi}{\tau_{\mathrm{p}}}\left(x_0-x_n\right)\right]\end{aligned}\tag{2.288}$$

In case of pulsating field, $B_{\max,+} = B_{\max,-} = B_{\max}$, one can write

$$U_{\max,-}-U_{\max,+}=2n\frac{\pi}{\tau_{\mathrm{p}}}v_{\mathrm{c}}\frac{w}{n}\frac{2}{\pi}l_{\mathrm{ax}}\tau_{\mathrm{p}}B_{\max,-}\sin\left(n\frac{y}{\tau_{\mathrm{p}}}\frac{\pi}{2}\right)\tag{2.289}$$

Combining Eqs. 2.288 and 2.289 one can express the voltage in a stationary coil induced by pulsating field as

$$u_{\mathrm{coil}}(t)=2U_{\max,+}\cos\left(n\frac{\pi}{\tau_{\mathrm{p}}}x_n\right)\cdot\cos\left(k\omega t-\varphi_k-\varphi_{y,n}-n\frac{\pi}{\tau_{\mathrm{p}}}x_0\right)\tag{2.290}$$

The amplitude of voltage in a stationary coil induced by pulsating field is dependent on the spatial shift x_n of the harmonic which induced it, i.e., on the position of source of pulsating field $B_+(x, t) + B_-(x, t)$.

2.7.3 DC Flux Density Traveling at Angular Speed Ω

Field coils of conventional synchronous machines travel at synchronous speed and generate air gap MMF as described in previous equations. Assuming constant air gap width, the air gap flux density of a field coil can be expressed as

$$B(x,t)=\sum_{n=1,2,3,\ldots}^{\infty}B_{\max,n}\sin n\frac{\pi}{\tau_{\mathrm{p}}}(x-v\cdot t)\tag{2.291}$$

with v denoting the circumferential velocity of the field coil. The flux which nth harmonic of air gap flux density in Eq. 2.291 concatenates with an armature coil with pitch y is equal to (see Eq. 2.257)

$$\Phi(t) = l_{\text{ax}} \int\limits_{x_c}^{x_c + y} B(x,t)\text{d}x = l_{\text{ax}} B_{\max,n} \int\limits_{v_c t + x_0}^{v_c t + x_0 + y} \sin n \frac{\pi}{\tau_p} (x - v \cdot t)\text{d}x \tag{2.292}$$

or

$$\Phi(t) = 2\frac{\tau_p}{n\pi} \sin\left(n\frac{y}{\tau_p}\frac{\pi}{2}\right) l_{\text{ax}} B_{\max,n} \cos n \frac{\pi}{\tau_p}\left[(v - v_c)\cdot t - x_0 - \varphi_{y,n}\right] \tag{2.293}$$

with $\varphi_{y,n}$ already introduced in Eq. 2.202. Voltage induced in a coil with w turns is equal to

$$u_i(t) = 2w(v - v_c) \sin\left(n\frac{y}{\tau_p}\frac{\pi}{2}\right) l_{\text{ax}} B_{\max,n} \sin n \frac{\pi}{\tau_p}\left[(v - v_c)\cdot t - x_0 - \varphi_{y,n}\right] \tag{2.294}$$

The amplitude of the induced voltage in a stationary full-pitch coil with one turn (two conductors!) is equal to

$$u_{i,1}(t) = 2v l_{\text{ax}} B_{\max,n} \tag{2.295}$$

i.e., the amplitude of induced voltage in a single conductor is again $B \cdot \ell \cdot v$, as is the case with voltage induced by traveling wave of flux density, Eq. 2.269.

2.8 Fractional Slot Windings: Fundamental and Principal Poles; Single-Tooth Winding

Vast majority of rotating field electric machines is built with an integer number of slots per pole and phase q in such a manner as to create an MMF distribution the largest harmonic of which repeats at a rate of twice as large as the greatest pole pitch. As long as there is enough space along the air gap circumference, several coils carrying the same phase current can be placed next to each other into adjacent slots under one pole, resulting in appropriately large values of q. Due to manufacturing limitations, however, the slot width cannot be decreased arbitrarily in order to put high number of teeth under a pole of a high-polarity machine. An increase of number of poles, keeping all other parameters unchanged, means a decrease of q and less possibility to control the amplitudes of higher spatial harmonics by means of the zone factor. Higher harmonics of an integer slot winding with $q = 1$ can be controlled only by varying the coil pitch. In case of a three-phase winding with $q = 1$, the only reasonable chording is 2/3, which significantly deteriorates the fundamental harmonic.

Connection scheme in an integer slot winding is extremely simple and repeats each pole: the total of q adjacent coils is grouped together m times under each pole.

This means that higher spatial harmonics of MMF created by such windings are suppressed on a single-pole base, which is an inefficient approach in case of low number of phases and $q = 1$. Obviously, another method has to be applied in high-polarity machines with low numbers of phases.

It sounds reasonable to enlarge the interval along which higher harmonics are fought into r adjacent poles, instead of only one, as is the case with integer slot windings. In that case, one refers to a **fractional slot winding**. Basic difference between fractional and integer slot winding is that in an integer slot winding the poles with the largest possible pole pitch are at the same time those with the largest flux per pole, whereas in a fractional slot winding this is not the case. Accordingly, one distinguishes among *fundamental poles* and *principal poles* of a fractional slot winding. Fundamental poles are those having the largest possible pole pitch; principal poles are those having the largest flux per pole.

Denoting by p_{f} the number of fundamental pole pairs, and by p_{p} the number of principal pole pairs of a fractional pitch winding, one can write

$$\tau_{\mathrm{p,f}} = \frac{N}{2p_{\mathrm{f}}} \tag{2.296}$$

and

$$\tau_{\mathrm{p,p}} = \frac{N}{2p_{\mathrm{p}}} \tag{2.297}$$

where

$$\tau_{\mathrm{p,f}} = r \cdot \tau_{\mathrm{p,p}} \tag{2.298}$$

with $\tau_{\mathrm{p,f}}$ denoting the fundamental pole pitch, and $\tau_{\mathrm{p,p}}$ the principal pole pitch, both in number of slots, and r the (odd) number of principal poles over which given harmonic(s) are suppressed. The order n_{f} of a higher spatial harmonic over the period length of $2\tau_{\mathrm{p,f}}$ is r times larger than the order n_{p} of a higher spatial harmonic over the period length of $2\tau_{\mathrm{p,p}}$

$$n_{\mathrm{f}} = r \cdot n_{\mathrm{p}} \tag{2.299}$$

The fundamental harmonic on the principal pole basis, i.e., in interval of $2p_{\mathrm{p}}$ poles, is the rth harmonic on the fundamental pole basis, or in interval of $2p_{\mathrm{f}}$ poles.

The number of slots per phase and principal pole q_{p} of a fractional slot winding is not an integer

$$q_{\mathrm{p}} = \frac{N}{2p_{\mathrm{p}}m} = \frac{q_{\mathrm{f}}}{r} \tag{2.300}$$

as opposed to the number of slots per phase and fundamental pole q_{f}, which is always an integer

$$q_{\mathrm{f}} = \frac{N}{2p_{\mathrm{f}}m} = r \cdot q_{\mathrm{p}} \tag{2.301}$$

The mixed fraction q_{p} is equal to the ratio between the number of slots per phase and fundamental pole and the number of principal poles per fundamental pole r.

An integer slot winding is characterized by

$$p_{\mathrm{f}} = p_{\mathrm{p}} = p \tag{2.302}$$

i.e., there are as many fundamental as principal poles, $r = 1$. Whereas the fundamental and the $(N/p - 1)$st harmonics of an integer slot winding with $2p$ poles have the largest zone factor in the spectrum bandwidth of N/p spatial harmonics, the rth and $(N/p_{\mathrm{f}} - r)$th harmonics have the largest zone factor in a fractional pitch winding with $2p_{\mathrm{f}}$ fundamental poles, as shown in Fig. 2.72. Integer slot winding is, accordingly, a special case of fractional slot winding with $r = 1$ in which the fundamental component of MMF dominates as a consequence of specific winding topology—the placement of phase coils next to each other under each pole. Such connection of coils is characterized by a minimum angle between MMFs of adjacent coils and, consequently, maximum total MMF and zone factor.

Coil pitch of an integer slot winding is usually equal to, or shorter than the pole pitch, whereas the coil pitch of a fractional slot winding is approximately equal to the principal pole pitch, $y \approx \tau_{\mathrm{p,p}}$.

The pitch factor $f_{\mathrm{p,r}}$ for the rth harmonic created by a coil of a fractional slot winding with fundamental pole pitch of $\tau_{\mathrm{p,f}}$ can be expressed as

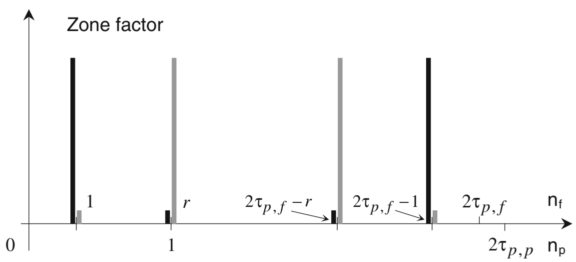

Fig. 2.72 Zone factor for selected spatial harmonics n of an integer slot winding with $p = p_{\mathrm{f}}$ (*black lines*) and a fractional slot winding (*gray lines*)

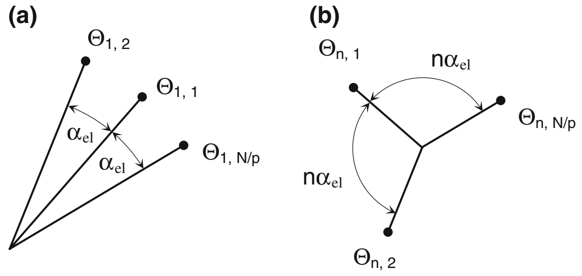

Fig. 2.73 Spatial representation of fundamental (**a**) and nth harmonics (**b**) of air gap MMF created by coils of an integer slot winding

$$f_{\mathrm{p,r}} = \sin r \frac{y}{\tau_{\mathrm{p,f}}} \frac{\pi}{2} \approx \sin r \frac{\tau_{\mathrm{p,p}}}{\tau_{\mathrm{p,f}}} \frac{\pi}{2} = 1 \tag{2.303}$$

with y denoting the coil pitch expressed in number of slots.

Sometimes the harmonic with period length of $2\tau_{\mathrm{p,p}}$ is described as fundamental, and one uses the construction "subharmonic" in order to describe all periodic quantities with periods longer than $2\tau_{\mathrm{p,p}}$. As opposed to higher harmonics, or simply harmonics, a "subharmonic" cannot be defined in terms of Fourier analysis and, therefore, it is not a valid quantity which could describe either spatial, or time periodic functions.

For the sake of clarity, further analysis will be performed for symmetrical fractional slot windings, i.e., for those with identical winding topologies in all m phases and with equal shift of $\tau_{\mathrm{p,f}}/m$ between adjacent phases at each fundamental pole. The number of slots per fundamental pole $N/(2p_{\mathrm{f}})$ of a symmetrical fractional slot winding is an integer multiple of the number of phases.

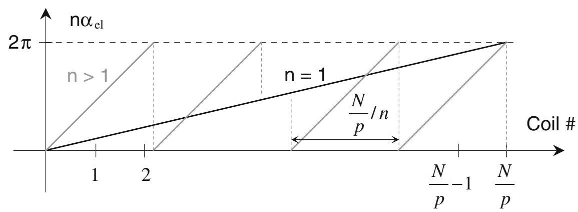

Fig. 2.74 Electrical angle between fundamental (*black line*) and nth harmonic components (*gray lines*) of MMF created by adjacent coils of a double-layer winding. Periodical character of angle causes the saw-tooth form for $n > 1$

If the resulting rth harmonic of q coils under one fundamental pole ought to be maximized, the angles between rth harmonic components of the coils must be minimal. This is obvious in a $2p$-pole integer slot winding ($r = 1$) placed in N slots, where the angle α_{el} between fundamental components of MMF of adjacent coils,

$\Theta_{1,N/p}$, $\Theta_{1,1}$, $\Theta_{1,2}$, etc. is equal to $\alpha_{el} = p \cdot \alpha_g = p \cdot 2\pi/N$, as shown in Fig. 2.73a. The total of N/p coils per pole pair builds the star of fundamental components of MMF with an angle α_{el} between adjacent legs. The angle between nth harmonics of MMF of adjacent coils, $\Theta_{n,N/p}$, $\Theta_{n,1}$, $\Theta_{n,2}$ etc., is $n \cdot \alpha_{el}$, as shown in Fig. 2.73b. This means that N/p coils per pole pair build n stars of nth harmonic components of MMF with an angle of $n \cdot \alpha_{el}$ between adjacent arms.

Since the angle is a periodic quantity with a period length of 2π, as shown in Fig. 2.74, the n stars of nth harmonic components of MMF overlap n times and end up in a single MMF star. The adjacent arms in the single MMF star of nth harmonic MMFs do not belong to adjacent coils, as is the case with the star of fundamental components of MMF. This key property of electrical angle of nth harmonic makes it possible to determine the sequence of coils under a fundamental pole of a fractional slot winding in such a manner as to maximize the rth spatial harmonic of MMF, as shown in Fig. 2.75.

Considering $N/(2p_f)$ slots per fundamental pole of a fractional slot winding, one groups q_f coils, the rth harmonics of which are placed next to each other in the MMF star in Fig. 2.75a, and connects them in series. The zone factor $f_{z,r}$ for q_f adjacent coils is equal to

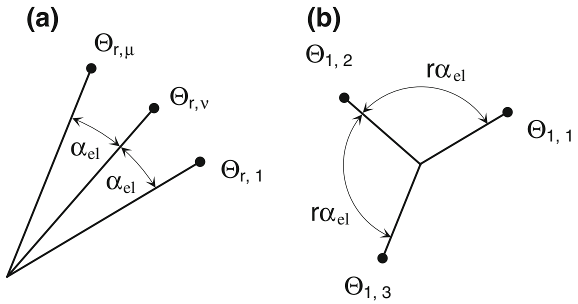

Fig. 2.75 Spatial representation of rth (**a**) and fundamental harmonics (**b**) of air gap MMF created by coils of a fractional slot winding

$$f_{z,r} = \frac{\sin q_f \frac{\alpha_{el}}{2}}{q_f \sin \frac{\alpha_{el}}{2}} \tag{2.304}$$

where $\alpha_{el} = p_f \cdot \alpha_g, = p_f \cdot 2\pi/N$. Therefore,

$$f_{z,r} = \frac{2p_f m}{N} \frac{\sin \frac{1}{m}\frac{\pi}{2}}{\sin p_f \frac{\pi}{N}} \tag{2.305}$$

If coils of a fractional slot winding have $y = 1$, one refers to **single-tooth winding**. In order to maximize the coil pitch factor, one selects the number of principal poles r close or equal to the fundamental pole pitch $\tau_{p,f}$, since in that case (Eq. 2.303)

$$f_{\mathrm{p,r}} = \sin r \frac{y}{\tau_{\mathrm{p,f}}} \frac{\pi}{2} \approx 1 \tag{2.306}$$

A single-tooth winding has short end windings. This advantage is compensated by unfavorably high zone factors for higher harmonics. Besides, in large machines large slot openings are necessary for manufacturing purposes (inserting the coils radially from the air gap), which decrease the slot-opening factor and increase the Carter factor, making ultimately the electromagnetic air gap width significantly larger than the geometric.

Since the order of the air gap MMF harmonics of a single-tooth-wound machine with the largest zone factor is close to $\tau_{\mathrm{p,f}}$, one can represent the zone factor for selected harmonics as shown in Fig. 2.76. Analogously to the zone factor distribution for selected harmonics, represented in Fig. 2.72, the zone factors for an integer slot winding are shown in Fig. 2.76 for the purpose of comparison.

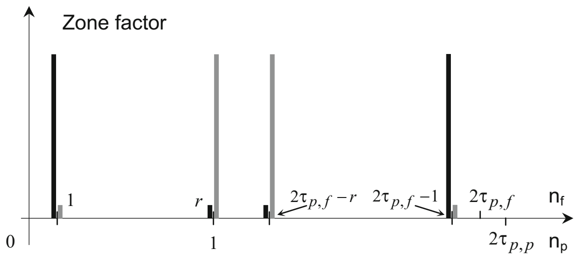

Fig. 2.76 Zone factors for selected spatial harmonics n of an integer slot winding with $p = p_f$ (*black lines*) and a single-tooth winding (*gray lines*)

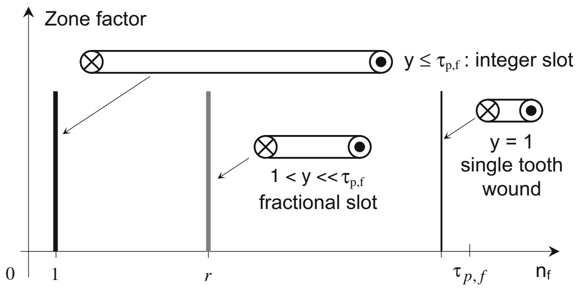

Fig. 2.77 Comparison of positions of dominating terms in air gap MMF spectra for various winding types. The pitch $\tau_{\mathrm{p,f}}$ is expressed in the number of slots, and n_{f} is the order of harmonic on the fundamental pole base

In extreme case $r = \tau_{\mathrm{p,f}} \pm 1$, and the harmonics with largest zone factor are positioned next to each other in Fig. 2.76.

One should note that groups of q_{f} adjacent coils of a single-tooth winding with number of slots close to the number of poles, i.e., with $r \approx \tau_{\mathrm{p,f}}$ belong to the same phase.

In Fig. 2.77, the strongest harmonics of air gap MMF spectra for various winding types are compared with each other.

Case Study 2.3: Stator winding of a three-phase, 84-pole electric machine is placed in 288 slots and has a coil pitch of $y = 3$. The number of slots per principal pole and phase q_{p} is equal to (Eq. 2.300)

$$q_{\mathrm{p}} = \frac{N}{2p_{\mathrm{p}}m} = \frac{8}{7}$$

By selecting the 7. spatial harmonic of the fundamental pole pitch to be the first harmonic of the principal pole pitch, $r = 7$, one obtains for $p_{\mathrm{f}} = p_{\mathrm{p}}/7 = 6$ and $\tau_{\mathrm{p,f}} = N/(2p_{\mathrm{f}}) = 24$. There are 24 slots per fundamental pole in which a symmetrical three-phase, double-layer winding ought to be placed. The number of slots per fundamental pole and phase q_{f} is equal to 8, the numerator of q_{p}. The electrical angle α_{el} between slots is equal to $\alpha_{\mathrm{el}} = p_{\mathrm{f}} \cdot 2\pi/N = \pi/24$ (7.5°), and the electrical angle between 7. harmonics of MMF created by coils in adjacent slots is $7\alpha_{\mathrm{el}} = 52.5°$. Electrical angles of 7. harmonics of all coils, along with affiliation of a coil to a particular phase, are given in Table 2.8.

The normalized interval (0,360°) in Table 2.8 is divided into $2m = 6$ subintervals, each of which is 60°wide. In order to generate the phase sequence for a symmetrical 3-phase machine in form of A → −C → B → −A → C → −B, the coil connections have to be arranged as shown in column 4 of Table 2.14.

Table 2.14 Electrical angles of 7. harmonic components in an 84-pole, three-phase machine with 288 slots, along with phase affiliation of coils

Coil Nr. i	Electrical angle of the 7. harmonic $\alpha_{\mathrm{el},i}$	Electrical angle normalized to interval (0,360°)	Phase
1	0	0	+A
2	52.5°	52.5°	+A
3	105°	105°	−C
4	157.5°	157.5°	+B
5	210°	210°	−A
6	262.5°	262.5°	+C
7	315°	315°	−B
8	367.5°	7.5°	+A
9	420°	60°	−C
10	472.5°	112.5°	−C
11	525°	165°	+B
12	577.5°	217.5°	−A
13	630°	270°	+C
14	682.5°	322.5°	−B
15	735°	15°	+A
16	787.5°	67.5°	−C
17	840°	120°	+B
18	892.5°	172.5°	+B
19	945°	225°	−A
20	997.5°	277.5°	+C
21	1050°	330°	−B
22	1102.5°	22.5°	+A
23	1155°	75°	−C
24	1207.5°	127.5°	+B

In particular, coils with an electrical angle of the 7. harmonic between 0° (included) and 60° (not included) are positively oriented and belong to the phase A. Coils with an electrical angle of the 7. harmonic between 180° (included) and 240° (not included) are negatively oriented and also belong to the phase A.

The pitch factor for $r = 7$ equals to (Eq. 2.303)

$$f_{p,7} = \sin 7 \frac{3}{24} \frac{\pi}{2} = 0.981$$

whereas the zone factors for the first 49 harmonics on interval $(0, 2\tau_{p,f})$ are

$$f_{z,n} = \frac{1}{q_f} \sqrt{\left(\sum_i s_i \sin n\alpha_{el,i}\right)^2 + \left(\sum_i s_i \cos n\alpha_{el,i}\right)^2} \tag{2.307}$$

with s_i denoting the sign of a given component:

$$s_i = \frac{\sin n\alpha_{el,i}}{\left|\sin n\alpha_{el,i}\right|} \tag{2.308}$$

and $\alpha_{el,i}$ the angles of coils affiliated to the same phase. For the phase A one can write accordingly (Table 2.15).

Table 2.15 Angles and signs of components in Eq. 2.307

i	1	2	5	8	12	15	19	22
$\alpha_{el,i}$	0	52.5°	210°	367.5°	577.5°	735°	945°	1102.5°
s_i	+1	+1	−1	+1	−1	+1	−1	+1

Zone factors for the first 49 harmonics are shown in Fig. 2.78. One recognizes the dominant 7. and 48 − 7 = 41. harmonics, along with second strongest 21. and 27. harmonics on the fundamental pole basis.

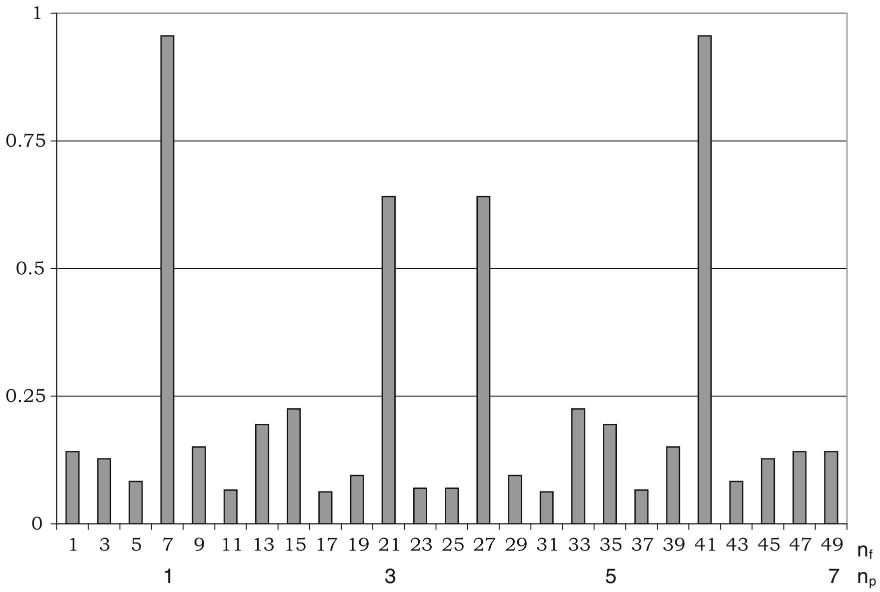

Fig. 2.78 Zone factors of the fractional pitch winding in Case Study 2.3 as a function of harmonic orders on the fundamental (n_f) and principal (n_p) pole basis

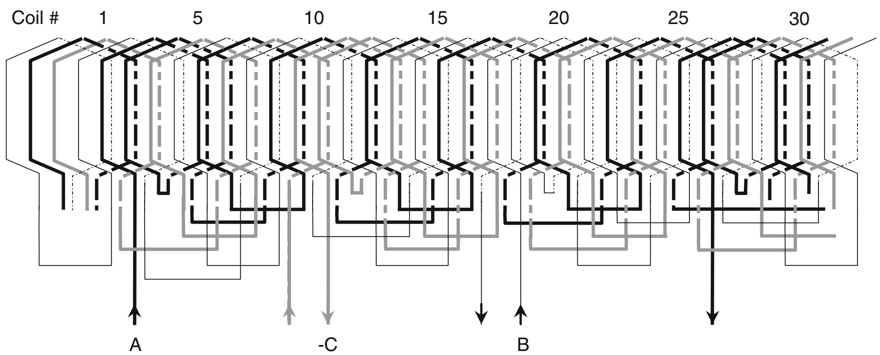

Fig. 2.79 Winding scheme for the machine in Case Study 2.3

Winding scheme for the first 30 slots of a three-phase, 84-pole generator with 288 slots and a coil pitch of $y = 3$ is given in Fig. 2.79. The winding is fully symmetrical and can be manufactured with a maximum of 288/24 = 12 parallel circuits.

Case Study 2.4: Stator winding of a three-phase, 70-pole generator is placed on 72 teeth and has a coil pitch of $y = 1$ (single-tooth winding). The number of slots per principal pole and phase q_p is equal to (Eq. 2.300)

$$q_{\mathrm{p}} = \frac{N}{2p_{\mathrm{p}}m} = \frac{12}{35}$$

and the number of slots per fundamental pole and phase q_{f} (Eq. 2.238) to

$$q_{\mathrm{f}} = \frac{N}{2p_{\mathrm{f}}m} = 12$$

By selecting the 35. spatial harmonic of the fundamental pole pitch to be the first harmonic of the principal pole pitch, $r = 35$, one obtains for the number of fundamental pole pairs $p_{\mathrm{f}} = p_{\mathrm{p}}/35 = 1$ and $\tau_{\mathrm{p,f}} = N/(2p_{\mathrm{f}}) = 36$. There are 36 teeth per fundamental pole carrying a symmetrical three-phase, double-layer winding. The two layers are placed in slots next to each other, instead of above each other, as is the case in conventional double-layer winding. The electrical angle α_{el} between slots is equal to $\alpha_{\mathrm{el}} = p_{\mathrm{f}} \cdot 2\pi/N = \pi/36$ (5°), and the electrical angle between 35. harmonics of MMF created by coils in adjacent slots is $35\alpha_{\mathrm{el}} = 175°$. Electrical angles of 35. harmonics of all coils, along with affiliation of a coil to a particular phase, are given in Table 2.16.

Table 2.16 Electrical angles of 35. harmonic components in an 70-pole, three-phase single-tooth-wound machine with 72 slots, along with phase affiliation of coils

Coil Nr. i	Electrical angle of the 35. harmonic $\alpha_{\mathrm{el},i}$	Electrical angle normalized to interval (0,360°)	Phase
1	0	0	+A
2	175°	175°	+B
3	350°	350°	−B
4	525°	165°	+B
5	700°	340°	−B
6	875°	155°	+B
7	1050°	330°	−B
8	1225°	145°	+B
9	1400°	320°	−B
10	1575°	135°	+B
11	1750°	310°	−B
12	1925°	125°	+B
13	2100°	300°	−B
14	2275°	115°	−C
15	2450°	290°	+C
16	2625°	105°	−C
17	2800°	280°	+C
18	2975°	95°	−C
19	3150°	270°	+C

(continued)

Table 2.16 (continued)

Coil Nr. i	Electrical angle of the 35. harmonic $\alpha_{el,i}$	Electrical angle normalized to interval (0,360°)	Phase
20	3325°	85°	+C
21	3500°	260°	+C
22	3675°	75°	−C
23	3850°	250°	+C
24	4025°	65°	−C
25	4200°	240°	+C
26	4375°	55°	+A
27	4550°	230°	−A
28	4725°	45°	+A
29	4900°	220°	−A
30	5075°	35°	+A
31	5250°	210°	−A
32	5425°	25°	+A
33	5600°	200°	−A
34	5775°	15°	+A
35	5950°	190°	−A
36	6125°	5°	+A

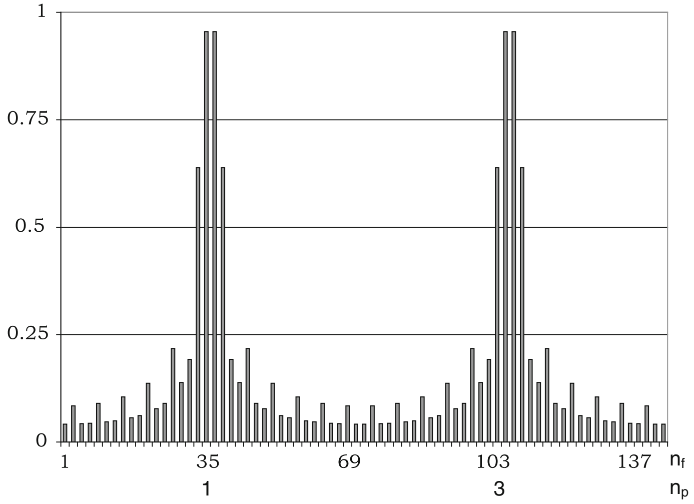

Fig. 2.80 Zone factors of the single-tooth winding in Case Study 2.4 as a function of harmonic orders on the fundamental (n_f) and principal (n_p) pole basis

In Fig. 2.80 the spectrum of air gap MMF harmonics of the tooth-wound machine in Case Study 2.4 is shown up to the range of twice the number of teeth (140 in this case). The third spatial harmonic of air gap MMF on the principal pole basis coincides with the $35 \cdot 3 = 105$. harmonic on the fundamental pole basis, the fifth harmonic on the principal pole basis with the $35 \cdot 5 = 175$. harmonic on the fundamental pole basis, etc.

Case Study 2.5: Stator winding of a three-phase, 20-pole machine is placed on $N = 30$ teeth and has a coil pitch of $y = 1$ (single-tooth winding), see also Case Study 2.1. The number of slots per principal pole and phase q_p is equal to (Eq. 2.300)

$$q_\mathrm{p} = \frac{N}{2p_\mathrm{p}m} = \frac{1}{2}$$

as is the number of slots per fundamental pole and phase q_f (Eq. 2.301), because $p_\mathrm{p} = p_\mathrm{f} = 10$. Geometric angle between stator slots is equal to $360°/N = 12°$, and electric angle $\alpha_\mathrm{el} = p \cdot 360°/N = 120°$.

Despite a non-integer number of slots per pole and phase, the stator winding in this case study is not a fractional slot one, because the number of fundamental poles is equal to the number of principal poles. Besides, the number of slots per pole and phase q is defined under an assumption of identical winding distribution at each pole, which is not valid in the case of a machine with one coil per pole pair.

2.9 Squirrel Cage Winding

Squirrel cage winding is unique among AC winding types because it has no electric terminals, no predefined number of phases m and no predefined number of poles $2p$. The only way a squirrel cage winding can communicate with other windings in a machine is through magnetic coupling with them, as shown in Fig. 2.81.

The number of phases of a squirrel cage winding depends on the number of rotor slots N and the number of pole pairs of stator winding. The number of phases m can be expressed as

$$m = \min\left\{N, \frac{N}{2}, \frac{N}{p}, \frac{N}{2p}\right\} \tag{2.309}$$

Since a squirrel cage winding does not have a predefined number of poles, it responds with its own MMF distribution to every spatial harmonic of stator created air gap flux density excitation of the order $n \cdot p$.

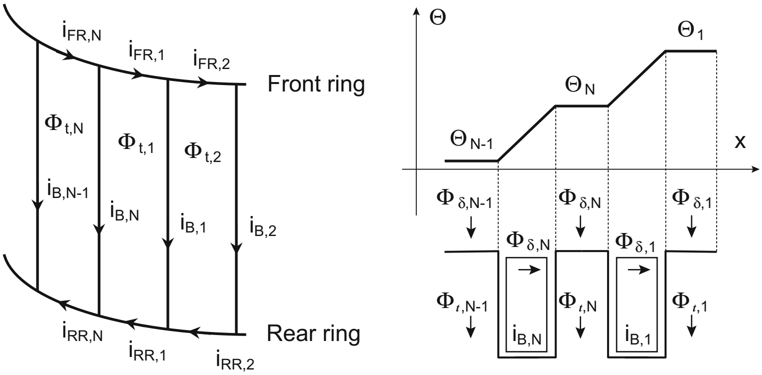

Fig. 2.81 Squirrel cage winding and the air gap MMF distribution created by bar currents

One recalls that the end winding form of a wound coil does not play any role when determining its air gap MMF distribution. Analogously, the fact that bars of a squirrel cage are short-circuited by means of rings on their ends is irrelevant for the analysis of air gap MMF created by such winding. Assume for the purpose of clarity that the number of rotor slots N is divisible by the number of poles $2p$, i.e., $m = N/2p$. In that case, the phase shift of currents in bars n, $n + N/2p$, $n + N/p$, $n + 3N/2p$, …, etc., alters for 180°, which is identical to the current distribution in slots of full-pitch coils of an m-phase machine. In other words, two bars of a squirrel cage winding placed in slots n and $n + N/2p$ create identical MMF distribution as a regular full-pitch coil. As shown in previous sections, a full-pitch coil creates a rectangularly distributed MMF characterized by unity pitch factor of all harmonics. A complete cage, however, generates only those harmonics of rotating MMF which satisfy conditions expressed in Eqs. 2.188 and 2.189. In conventional squirrel cage induction machine the number of rotor phases is large due to a large number of rotor slots. When symmetrically excited, e.g., with sinusoidal air gap flux density, a symmetrical squirrel cage winding generates an air gap MMF with fundamental component and slot harmonics only.

Taking for the number of rotor phases $m = N/2p$, one can express the total positive sequence air gap MMF Θ_+ created by the fundamental time component of squirrel cage currents as

$$\begin{aligned}\Theta_+ &= \sum_{i=0}^{\infty} \Theta_{2im+1} \cos\left[(2im+1)\frac{\pi}{\tau_p}x - \omega t\right] \\ &= \sum_{i=0}^{\infty} \Theta_{iN/p+1} \cos\left[\left(i\frac{N}{p}+1\right)\frac{\pi}{\tau_p}x - \omega t\right]\end{aligned} \tag{2.310}$$

as well as the negative sequence Θ_-

$$\begin{aligned}\Theta_{-} &= \sum_{i=1}^{\infty} \Theta_{2im-1} \cos\left[(2im-1)\frac{\pi}{\tau_{\mathrm{p}}}x + \omega t\right] \\ &= \sum_{i=1}^{\infty} \Theta_{iN/p-1} \cos\left[\left(i\frac{N}{p}-1\right)\frac{\pi}{\tau_{\mathrm{p}}}x + \omega t\right]\end{aligned} \tag{2.311}$$

The lowest order of higher harmonics of rotating MMF is $N/p - 1$. Therefore, the rotating MMF created by a squirrel cage winding is almost sinusoidal. Squirrel cage winding is a perfect example of how lower harmonics in the air gap MMF distribution can be suppressed by increasing the number of phases.

Assume now that stator winding generates an air gap flux density distribution B_{δ} which tries to penetrate into the squirrel cage. The corresponding fluxes $\Phi_{\delta,1} - \Phi_{\delta,N}$ are related to leakage fluxes $\Phi_{\sigma,1} - \Phi_{\sigma,\mathrm{N}}$ and tooth fluxes $\Phi_{\mathrm{t},1} - \Phi_{\mathrm{t},N}$ as

$$\Phi_{\delta,n} = \Phi_{\mathrm{t},n} + \Phi_{\sigma,n} - \Phi_{\sigma,n-1} \tag{2.312}$$

where $1 \leq n \leq N$. Denoting by $G_{\mathrm{s},n}$ the permeance of the nth slot for tangential flux

$$G_{\mathrm{s},n} = \frac{1}{3}\mu_0 \frac{l_{\mathrm{ax}} h_n}{b_n} \tag{2.313}$$

and by $k_{\mathrm{L},n}$ the skin effect factor for inductance, one can further write

$$\Phi_{\delta,n} = \Phi_{\mathrm{t},n} + \frac{1}{3}\mu_0 k_{\mathrm{L},n} \frac{l_{\mathrm{ax}} h_n}{b_n} i_{\mathrm{B},n} - \frac{1}{3}\mu_0 k_{\mathrm{L},n-1} \frac{l_{\mathrm{ax}} h_n}{b_n} i_{\mathrm{B},n-1} \tag{2.314}$$

and

$$\Phi_{\delta,n} = \Phi_{\mathrm{t},n} + k_{\mathrm{L},n} G_{\mathrm{s},n} i_{\mathrm{B},n} - k_{\mathrm{L},n-1} G_{\mathrm{s},n-1} i_{\mathrm{B},n-1} \tag{2.315}$$

Voltage differential equation written for the nth loop of the squirrel cage winding in Fig. 2.66, $1 \leq n \leq N$, yields

$$u_n = \frac{\mathrm{d}\Phi_{\mathrm{t},n}}{\mathrm{d}t} + R_{\mathrm{FR},n} \cdot i_{\mathrm{FR},n} + R_{\mathrm{B},n} \cdot i_{\mathrm{B},n} + R_{\mathrm{RR},n} \cdot i_{\mathrm{RR},n} - R_{\mathrm{B},n-1} \cdot i_{\mathrm{B},n-1} = 0 \tag{2.316}$$

with $R_{\mathrm{FR},n}$ denoting the resistance of the nth front ring segment, $R_{\mathrm{RR},n}$ the resistance of the nth rear ring segment, $R_{\mathrm{B},n}$ the AC resistance of the nth bar, and $\Phi_{\mathrm{t},n}$ the flux of the nth tooth. Considering heteropolar machine structure, one can write continuity equations

$$\sum_{j=1}^{N} \Phi_{\mathrm{t},j} = 0 \tag{2.317}$$

and

$$\sum_{j=1}^{N} i_{\mathrm{B},j} = 0 \tag{2.318}$$

as well as voltage equations for the front and rear end ring:

$$\sum_{j=1}^{N} R_{\mathrm{FR},j} \cdot i_{\mathrm{FR},j} = 0 \tag{2.319}$$

and

$$\sum_{j=1}^{N} R_{\mathrm{RR},j} \cdot i_{\mathrm{RR},j} = 0 \tag{2.320}$$

because the flux linked by front and end ring is equal to zero. Equations of the I Kirchhoff's law for bar, front and rear end ring currents can be written as

$$i_{\mathrm{B},n} = i_{\mathrm{FR},n} - i_{\mathrm{FR},n+1} \tag{2.321}$$

and

$$i_{\mathrm{B},n} = i_{\mathrm{RR},n} - i_{\mathrm{RR},n+1} \tag{2.322}$$

By combining Eqs. 2.319 and 2.321 one obtains matrix equation

$$\begin{bmatrix} 1 & -1 & 0 & \dots & 0 & 0 \\ 0 & 1 & -1 & \dots & 0 & 0 \\ 0 & 0 & 1 & \dots & 0 & 0 \\ \dots & \dots & \dots & \dots & \dots & \dots \\ 0 & 0 & 0 & \dots & 1 & -1 \\ R_{\mathrm{FR},1} & R_{\mathrm{FR},2} & R_{\mathrm{FR},3} & \dots & R_{\mathrm{FR},N-1} & R_{\mathrm{FR},N} \end{bmatrix} \cdot \begin{bmatrix} i_{\mathrm{FR},1} \\ i_{\mathrm{FR},2} \\ i_{\mathrm{FR},3} \\ \dots \\ i_{\mathrm{FR},N-1} \\ i_{\mathrm{FR},N} \end{bmatrix} = \underline{I}' \cdot \begin{bmatrix} i_{\mathrm{B},1} \\ i_{\mathrm{B},2} \\ i_{\mathrm{B},3} \\ \dots \\ i_{\mathrm{B},N-1} \\ i_{B,N} \end{bmatrix} \tag{2.323}$$

with $\underline{I}'$ denoting the modified identity matrix:

$$\underline{I}' = \begin{bmatrix} 1 & 0 & 0 & \dots & 0 & 0 \\ 0 & 1 & 0 & \dots & 0 & 0 \\ 0 & 0 & 1 & \dots & 0 & 0 \\ \dots & \dots & \dots & \dots & \dots & \dots \\ 0 & 0 & 0 & \dots & 1 & 0 \\ 0 & 0 & 0 & \dots & 0 & 0 \end{bmatrix} \tag{2.324}$$

Introducing vectors $\underline{i}_{\mathrm{B}}$, $\underline{i}_{\mathrm{FR}}$ and $\underline{i}_{\mathrm{RR}}$, defined as

$$\underline{i}_{\mathrm{B}} = \begin{bmatrix} i_{\mathrm{B},1} & i_{\mathrm{B},2} & \ldots & i_{\mathrm{B},N} \end{bmatrix}^{\mathrm{T}} \tag{2.325}$$

$$\underline{i}_{\mathrm{FR}} = \begin{bmatrix} i_{\mathrm{FR},1} & i_{\mathrm{FR},2} & \ldots & i_{\mathrm{FR},N} \end{bmatrix}^{\mathrm{T}} \tag{2.326}$$

$$\underline{i}_{\mathrm{RR}} = \begin{bmatrix} i_{\mathrm{RR},1} & i_{\mathrm{RR},2} & \ldots & i_{\mathrm{RR},N} \end{bmatrix}^{\mathrm{T}} \tag{2.327}$$

as well as matrix $\underline{C}_{\mathrm{F}}$:

$$\underline{C}_{\mathrm{F}} = \begin{bmatrix} 1 & -1 & 0 & \ldots & 0 & 0 \\ 0 & 1 & -1 & \ldots & 0 & 0 \\ 0 & 0 & 1 & \ldots & 0 & 0 \\ \ldots & \ldots & \ldots & \ldots & \ldots & \ldots \\ 0 & 0 & 0 & \ldots & 1 & -1 \\ R_{\mathrm{FR},1} & R_{\mathrm{FR},2} & R_{\mathrm{FR},3} & \ldots & R_{\mathrm{FR},N-1} & R_{\mathrm{FR},N} \end{bmatrix} \tag{2.328}$$

one can rewrite Eq. 2.323 as

$$\underline{C}_{\mathrm{F}} \cdot \underline{i}_{\mathrm{FR}} = \underline{I}' \cdot \underline{i}_{\mathrm{B}} \tag{2.329}$$

Similarly one can write

$$\underline{C}_{\mathrm{R}} \cdot \underline{i}_{\mathrm{RR}} = \underline{I}' \cdot \underline{i}_{\mathrm{B}} \tag{2.330}$$

where $\underline{C}_{\mathrm{R}}$ is defined as

$$\underline{C}_{\mathrm{R}} = \begin{bmatrix} 1 & -1 & 0 & \ldots & 0 & 0 \\ 0 & 1 & -1 & \ldots & 0 & 0 \\ 0 & 0 & 1 & \ldots & 0 & 0 \\ \ldots & \ldots & \ldots & \ldots & \ldots & \ldots \\ 0 & 0 & 0 & \ldots & 1 & -1 \\ R_{\mathrm{RR},1} & R_{\mathrm{RR},2} & R_{\mathrm{RR},3} & \ldots & R_{\mathrm{RR},N-1} & R_{\mathrm{RR},N} \end{bmatrix} \tag{2.331}$$

Due to linear dependence between tooth fluxes (Eq. 2.317), only $N - 1$ linearly independent voltage equations 2.316 can be written, the solution of which are bar currents. The Nth equation for bar currents follows from 2.318. Consequently, one can write the system of equations for bar currents and tooth fluxes as

$$\underline{I}' \cdot \frac{\mathrm{d}}{\mathrm{dt}} \underline{\Phi}_{\mathrm{t}} = -\underline{I}' \cdot \underline{R}_{\mathrm{FR}} \cdot \underline{i}_{\mathrm{FR}} - \underline{I}' \cdot \underline{R}_{\mathrm{RR}} \cdot \underline{i}_{\mathrm{RR}} + \underline{R}_{\mathrm{B}} \cdot \underline{i}_{\mathrm{B}} \tag{2.332}$$

where

$$\underline{R}_{\mathrm{B}} = \begin{bmatrix} -R_{\mathrm{B},1} & 0 & 0 & \dots & 0 & 0 & R_{\mathrm{B},N} \\ R_{\mathrm{B},1} & -R_{\mathrm{B},2} & 0 & \dots & 0 & 0 & 0 \\ 0 & R_{\mathrm{B},2} & -R_{\mathrm{B},3} & \dots & 0 & 0 & 0 \\ \dots & \dots & \dots & \dots & \dots & \dots & \dots \\ 0 & 0 & 0 & \dots & -R_{\mathrm{B},N-2} & 0 & 0 \\ 0 & 0 & 0 & \dots & R_{\mathrm{B},N-2} & -R_{\mathrm{B},N-1} & 0 \\ 1 & 1 & 1 & \dots & 1 & 1 & 1 \end{bmatrix} \tag{2.333}$$

$$\underline{R}_{\mathrm{FR}} = \operatorname{diag}\left\{R_{\mathrm{FR},1}, R_{\mathrm{FR},2}, \ldots, R_{\mathrm{FR},N}\right\} \tag{2.334}$$

$$\underline{R}_{\mathrm{BR}} = \operatorname{diag}\left\{R_{\mathrm{BR},1}, R_{\mathrm{BR},2}, \ldots, R_{\mathrm{BR},N}\right\} \tag{2.335}$$

and

$$\underline{\Phi}_{\mathrm{t}} = \begin{bmatrix} \Phi_{\mathrm{t},1} & \Phi_{\mathrm{t},2} & \dots & \Phi_{\mathrm{t},N} \end{bmatrix}^{\mathrm{T}} \tag{2.336}$$

Inserting Eqs. 2.326 and 2.327 in Eq. 2.332, one becomes

$$\underline{I}' \cdot \frac{\mathrm{d}}{\mathrm{dt}}\underline{\Phi}_{\mathrm{t}} = \left(-\underline{I}' \cdot \underline{R}_{\mathrm{FR}} \cdot \underline{C}_{\mathrm{F}}^{-1} \cdot \underline{I}' - \underline{I}' \cdot \underline{R}_{\mathrm{RR}} \cdot \underline{C}_{\mathrm{R}}^{-1} \cdot \underline{I}' + \underline{R}_{\mathrm{B}}\right) \cdot \underline{i}_{\mathrm{B}} \tag{2.337}$$

Introducing matrix $\underline{R}_{\mathrm{CAGE}}$, defined as

$$\underline{R}_{\mathrm{CAGE}} = \underline{R}_{\mathrm{B}} - \underline{I}' \cdot \underline{R}_{\mathrm{FR}} \cdot \underline{C}_{\mathrm{F}}^{-1} \cdot \underline{I}' - \underline{I}' \cdot \underline{R}_{\mathrm{RR}} \cdot \underline{C}_{R}^{-1} \cdot \underline{I}' \tag{2.338}$$

one can finally write for bar currents and tooth fluxes:

$$\underline{i}_{\mathrm{B}} = \underline{R}_{\mathrm{CAGE}}^{-1} \cdot \underline{I}' \cdot \frac{\mathrm{d}}{\mathrm{dt}}\underline{\Phi}_{\mathrm{t}} \tag{2.339}$$

Introducing matrix $\underline{G}_{\mathrm{mg}}$ defined as

$$\underline{G}_{\mathrm{mg}} = \begin{bmatrix} k_{\mathrm{L},1}G_{\mathrm{S},1} & 0 & \dots & 0 & 0 & 0 & \dots & -k_{\mathrm{L},N}G_{\mathrm{S},N} \\ -k_{\mathrm{L},1}G_{\mathrm{S},1} & k_{\mathrm{L},2}G_{\mathrm{S},2} & \dots & 0 & 0 & 0 & \dots & 0 \\ \dots & \dots & \dots & \dots & \dots & \dots & \dots & \dots \\ 0 & 0 & \dots & k_{\mathrm{L},n-1}G_{\mathrm{S},n-1} & 0 & 0 & \dots & 0 \\ 0 & 0 & \dots & -k_{\mathrm{L},n-1}G_{\mathrm{S},n-1} & k_{\mathrm{L},n}G_{\mathrm{S},n} & 0 & \dots & 0 \\ 0 & 0 & \dots & 0 & -k_{\mathrm{L},n}G_{\mathrm{S},n} & k_{\mathrm{L},n+1}G_{\mathrm{S},n+1} & \dots & 0 \\ \dots & \dots & \dots & \dots & \dots & \dots & \dots & \dots \\ 0 & 0 & \dots & 0 & 0 & 0 & \dots & k_{\mathrm{L},N}G_{\mathrm{S},N} \end{bmatrix} \tag{2.340}$$

and substituting time derivatives of tooth fluxes $\Phi_{\mathrm{t},1} - \Phi_{\mathrm{t},N}$ from Eq. 2.316 in Eq. 2.247, one obtains the matrix system of differential equations

$$\underline{G}_{\mathrm{mg}} \cdot \frac{\mathrm{d}}{\mathrm{d}t}\underline{i}_{\mathrm{B}} + \underline{R}_{\mathrm{CAGE}} \cdot \underline{i}_{\mathrm{B}} = \frac{\mathrm{d}}{\mathrm{d}t}\underline{\Phi}_{\delta} \tag{2.341}$$

Assuming constant parameters and sinusoidal excitation, one can rewrite Eq. 2.339 in terms of real and imaginary components of solution as

$$\omega\underline{G}_{\mathrm{mg}} \cdot \underline{I}_{\mathrm{B,Im}} - \underline{R}_{\mathrm{CAGE}} \cdot \underline{I}_{\mathrm{B,Re}} = \omega\underline{\Phi}_{\delta,\mathrm{Re}} \tag{2.342}$$

and

$$\omega\underline{G}_{\mathrm{mg}} \cdot \underline{I}_{\mathrm{B,Re}} + \underline{R}_{\mathrm{CAGE}} \cdot \underline{I}_{\mathrm{B,Im}} = \omega\underline{\Phi}_{\delta,\mathrm{Im}} \tag{2.343}$$

where

$$\underline{I}_{\mathrm{B,Re}} = \begin{bmatrix} I_{\mathrm{B},1}\cos\varphi_1 \\ I_{\mathrm{B},2}\cos\varphi_2 \\ \cdots \\ I_{\mathrm{B},N}\cos\varphi_N \end{bmatrix}; \ \underline{I}_{\mathrm{B,Im}} = \begin{bmatrix} I_{\mathrm{B},1}\sin\varphi_1 \\ I_{\mathrm{B},2}\sin\varphi_2 \\ \cdots \\ I_{\mathrm{B},N}\sin\varphi_N \end{bmatrix} \tag{2.344}$$

and

$$\underline{\Phi}_{\delta,\mathrm{Re}} = \begin{bmatrix} \Phi_{\delta,1}\sin\gamma_1 \\ \Phi_{\delta,2}\sin\gamma_2 \\ \cdots \\ \Phi_{\delta,N}\sin\gamma_N \end{bmatrix}; \quad \underline{\Phi}_{\delta,\mathrm{Im}} = \begin{bmatrix} \Phi_{\delta,1}\cos\gamma_1 \\ \Phi_{\delta,2}\cos\gamma_2 \\ \cdots \\ \Phi_{\delta,N}\cos\gamma_N \end{bmatrix} \tag{2.345}$$

The solution of the system of Eqs. 2.338 and 2.339 yields

$$\underline{I}_{\mathrm{B,Im}} = \left(\omega^2\underline{G}_{\mathrm{mg}} \cdot \underline{R}_{\mathrm{CAGE}}^{-1} \cdot \underline{G}_{\mathrm{mg}} + \underline{R}_{\mathrm{CAGE}}\right)^{-1}\omega\left(\underline{\Phi}_{\delta,\mathrm{Im}} + \omega\underline{G}_{\mathrm{mg}} \cdot \underline{R}_{\mathrm{CAGE}}^{-1} \cdot \underline{\Phi}_{\delta,\mathrm{Re}}\right) \tag{2.346}$$

and

$$\underline{I}_{\mathrm{B,Re}} = \underline{R}_{\mathrm{CAGE}}^{-1}\omega\left(\underline{G}_{\mathrm{mg}} \cdot \underline{I}_{\mathrm{B,Im}} - \underline{\Phi}_{\delta,\mathrm{Re}}\right) \tag{2.347}$$

For air gap MMFs in Fig. 2.81, one can write

$$\Theta_{n+1} = \Theta_n + i_{\mathrm{B},n+1} \tag{2.348}$$

where $1 \leq n \leq N - 1$. The continuity equation for air gap MMFs can be written as

$$\sum_{j=1}^{N}\Theta_j = 0 \tag{2.349}$$

Combining $N - 1$ Eq. 2.348 with Eq. 2.329, one obtains

$$\begin{bmatrix} 1 & 0 & 0 & \dots & 0 & -1 \\ -1 & 1 & 0 & \dots & 0 & 0 \\ 0 & -1 & 1 & \dots & 0 & 0 \\ \dots & \dots & \dots & \dots & \dots & \dots \\ 0 & 0 & 0 & \dots & 1 & 0 \\ 1 & 1 & 1 & \dots & 1 & 1 \end{bmatrix} \cdot \begin{bmatrix} \Theta_1 \\ \Theta_2 \\ \Theta_3 \\ \dots \\ \Theta_{N-1} \\ \Theta_N \end{bmatrix} = \underline{I}' \cdot \underline{i}_{\mathrm{B}} \tag{2.350}$$

or

$$\underline{C}_{\Theta} \cdot \underline{\Theta} = \underline{I}' \cdot \underline{i}_{\mathrm{B}}$$

the solution of which is

$$\underline{\Theta} = \underline{C}_{\Theta}^{-1} \cdot \underline{I}' \cdot \underline{i}_{\mathrm{B}} \tag{2.351}$$

By comparing previous equations, one concludes that the air gap MMF distribution $\underline{\Theta}$ created by a squirrel cage with identical ring segment resistances is identical to the front ($\underline{i}_{\mathrm{FR}}$) or rear ($\underline{i}_{\mathrm{RR}}$) ring segment current distribution.

Case Study 2.6: The rotor of a 4-pole, 100-kW, 400-V, 50-Hz squirrel cage induction machine has a total of 40 slots. Copper bars are 5.5 mm wide and 50 mm high, and ring dimensions are 50 × 10 mm. At standstill, the sinusoidally distributed tooth flux density has an amplitude of 0.35 T, which corresponds to some 50 % of its no-load value.

Rotor bar current density distribution in sound cage created by the flux density distribution in Fig. 2.82 is shown in Fig. 2.83, and the front ring segment current density distribution in Fig. 2.84. Ring segment currents are 90° shifted in space relative to bar currents. Bar current density at standstill equals to 32 A/mm^2, and at rated point 5.1 A/mm^2.

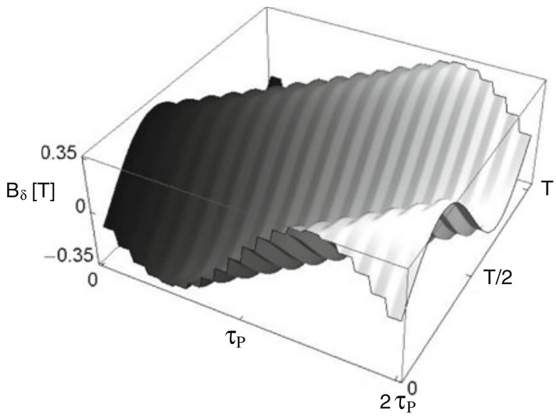

Fig. 2.82 The impressed tooth flux density distribution at short circuit

Fig. 2.83 Rotor bar current density distribution at short circuit in sound cage generated by impressed air gap fluxes in Fig. 2.82

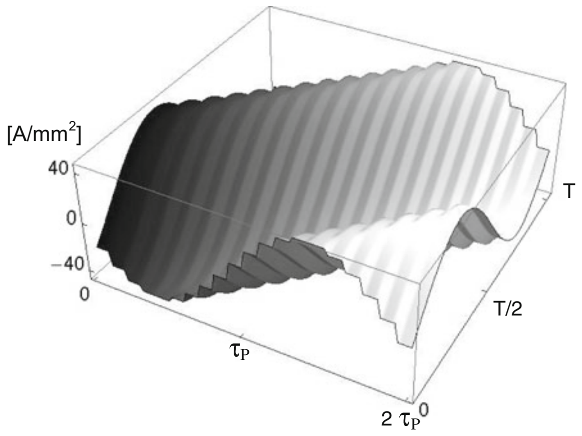

The air gap MMF created by the rotor bar currents in Fig. 2.83 is shown in Fig. 2.85. The amplitude of air gap MMF in Fig. 2.85 is as large as the amplitude of ring current, as shown in Fig. 2.84 and equals to 40 kA.

The spectrum (in % value of the fundamental) of air gap MMF in Fig. 2.85 is shown in Fig. 2.86. The spectrum contains only the fundamental and the slot harmonics, because a symmetrical squirrel cage winding filters all harmonics besides fundamental below the order of the number of slots per pole pair decreased by 1, see Eqs. 2.188 and 2.189, and Table 2.9. Both fundamental and slot harmonics contain only positive sequence components.

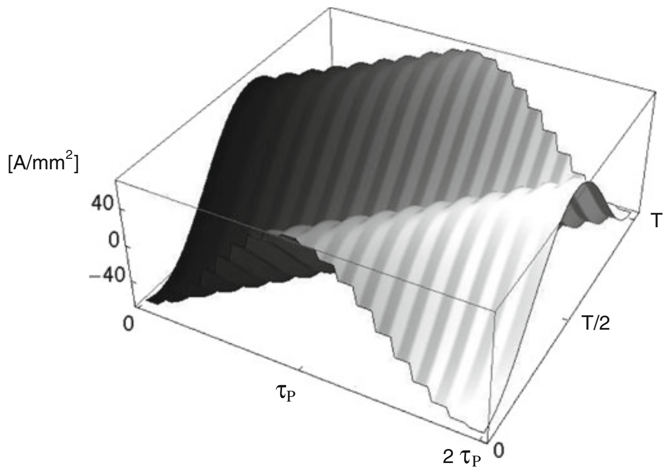

Fig. 2.84 Rotor front end ring segment current density distribution at short circuit in sound cage generated by impressed air gap fluxes in Fig. 2.67

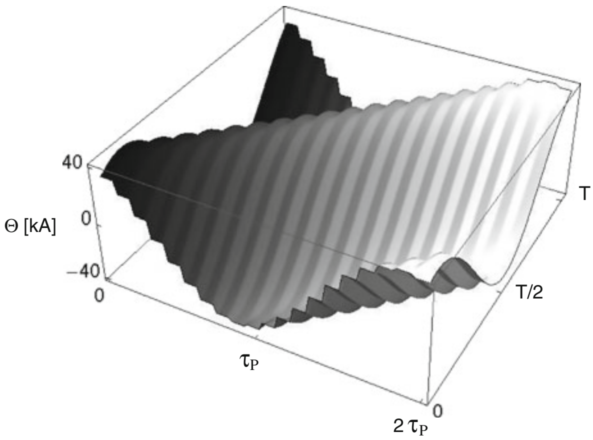

Fig. 2.85 Air gap MMF distribution created by bar currents in sound cage excited by impressed air gap fluxes in Fig. 2.82

Assume now that bars Nr. 11 and 12 are broken, i.e., without contact to the front and rear cage. The two bar currents are equal to zero, as shown in Fig. 2.87, and the front, along with rear end ring current densities in corresponding segments have equal amounts, as shown in Fig. 2.88.

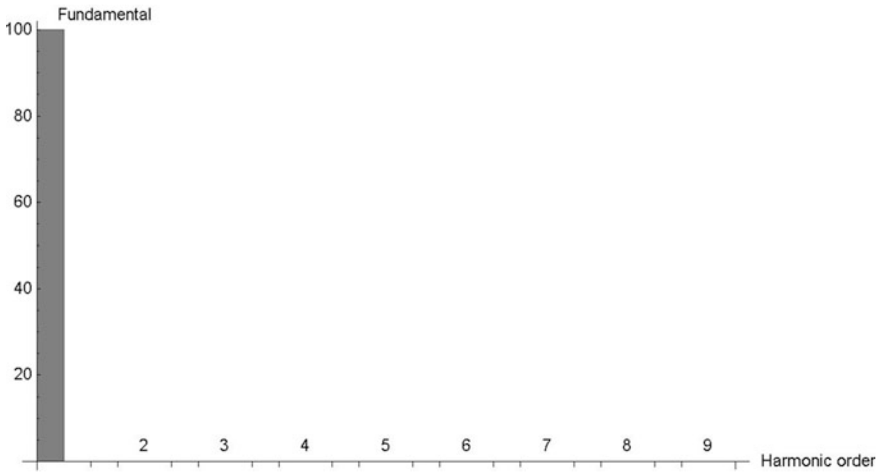

Fig. 2.86 Spectrum of air gap MMF distribution in Fig. 2.85 (in % value of the fundamental) created by bar currents in sound cage excited by impressed air gap fluxes in Fig. 2.82

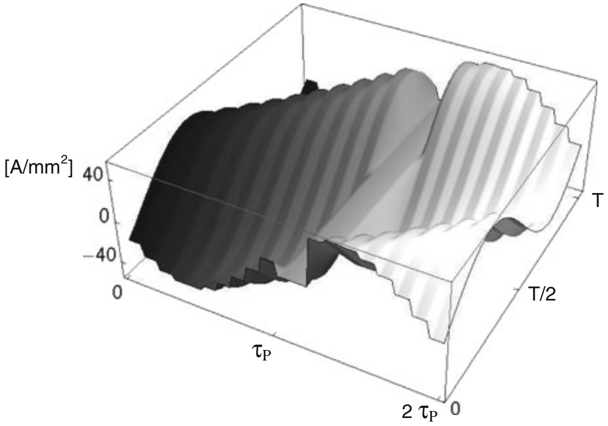

Fig. 2.87 Rotor bar current density distribution in a broken cage generated by impressed air gap flux densities in Fig. 2.82. Bars Nr. 11 and 12 are broken

The air gap MMF distribution created by currents in a broken squirrel cage is shown in Fig. 2.89. MMF of teeth surrounded by slots with broken bars is constant because there is no contribution from those slots to the MMF.

The amplitudes of bar currents are shown in Fig. 2.90. One recognizes typical increase of current amplitudes on both sides of broken bars and decrease of current amplitudes in farther bars.

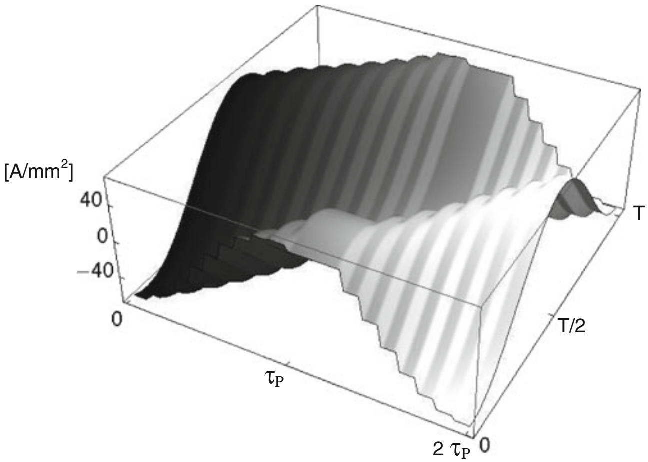

Fig. 2.88 Rotor front ring current density distribution in a broken cage generated by impressed air gap flux densities in Fig. 2.82. Since the bars Nr. 11 and 12 are broken, current densities in ring segments connected to these bars are equal to each other

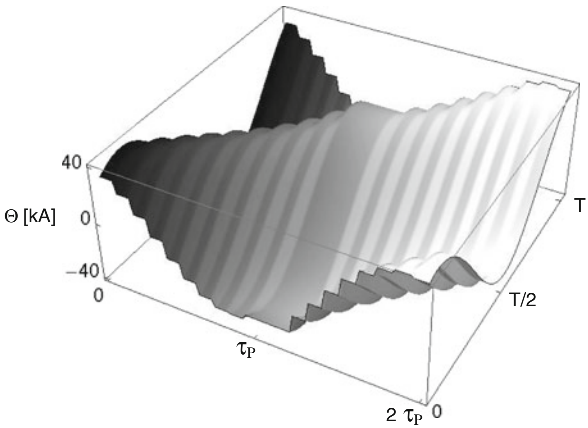

Fig. 2.89 Air gap MMF distribution created by the bar currents in a broken cage excited by impressed air gap fluxes in Fig. 2.67. Bars Nr. 11 and 12 are broken

The amplitudes of tooth MMFs are shown in Fig. 2.91. One recognizes a significant loss of MMF due to broken bars, as well as unequal amplitudes of tooth MMFs.

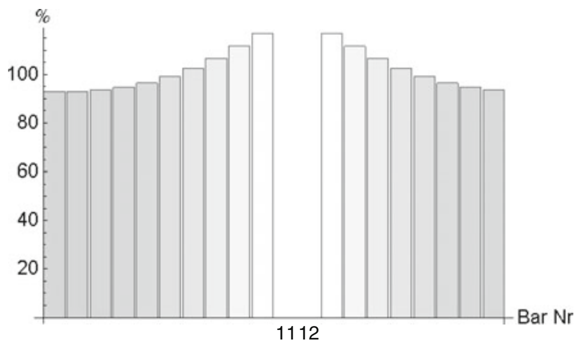

Fig. 2.90 Bar current amplitudes in a broken cage as percentage values of currents in sound cage. The cage is excited by impressed air gap flux densities shown in Fig. 2.67. Bars Nr. 11 and 12 are broken

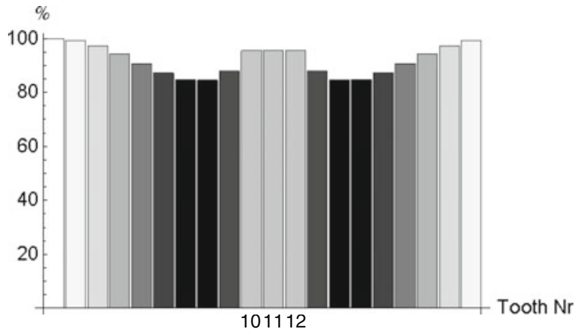

Fig. 2.91 Air gap MMF amplitudes, as percentage values of MMFs of sound cage, created by bar currents in a broken cage excited by impressed air gap flux densities in Fig. 2.82. Bars Nr. 11 and 12 are broken

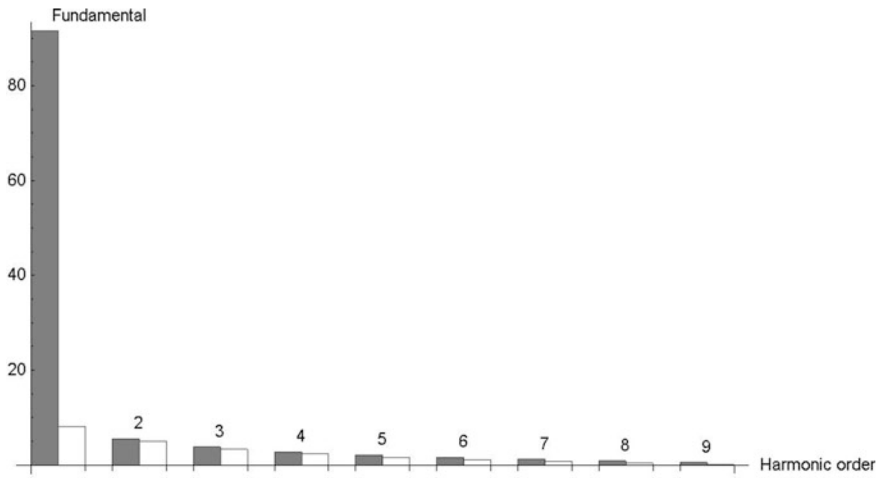

Fig. 2.92 Spectrum of the air gap MMF distribution (in % value of the fundamental of a sound cage) created by bar currents in broken cage excited by impressed air gap flux densities in Fig. 2.82. For each harmonic the maximum (*gray*) and minimum (*white*) values are given

The spectrum (in % value of the fundamental created by sound cage) of air gap MMF in Fig. 2.89 is shown in Fig. 2.92. The spectrum contains all harmonics from the interval between the fundamental and the slot harmonic, as a consequence of cage asymmetry introduced by broken bars.

The positive sequence component of the fundamental component of air gap MMF in Fig. 2.89 amounts 92.3 % of the positive sequence in a sound machine, whereas the negative sequence MMF in case of 2 broken bars increases to 2.6 % of the positive sequence in a sound machine

Case Study 2.7: The rotor of a 3.75 MVA, 50 Hz, cos φ = 0.8 lagging, salient pole synchronous machine has a damper cage with 6 slots per pole shifted 10° el. to one another. In the interpolar space, there are no bars; the front and rear end rings are continuous. The DC bar resistance equals to 82.5 μΩ and the DC ring segment resistance 5.31 μΩ. After sudden loading, the rotor oscillates for a while with a frequency of 1 Hz. During the transient, the air gap flux density is sinusoidally distributed along the periphery and has a constant amplitude of 0.75 T.

Bar currents distribution in case of *continuous ring* is shown in Fig. 2.93. One recognizes an increase of bar current amplitudes closer to pole boundaries, which compensates for a portion of missing bar currents in the interpolar space. The corresponding front end ring currents distribution is shown in Fig. 2.94, and the air gap MMF distribution in Fig. 2.95.

The amplitudes of bar currents for a given excitation are shown in Fig. 2.96. One recognizes typical increase of currents in bars closer to edges of poles.

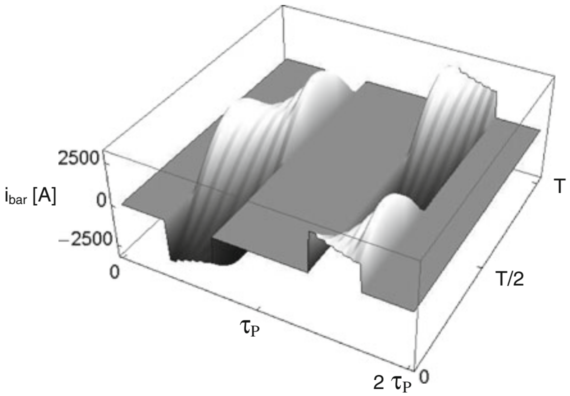

Fig. 2.93 Bar currents in a damper cage with continuous end rings, generated during load change by a 0.75 *T* air gap flux density at 1 Hz

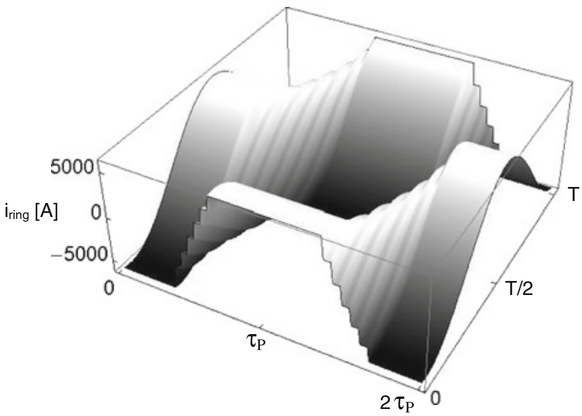

Fig. 2.94 Ring currents in a damper cage with continuous end rings, generated during load change

One of the consequences of missing bar currents in the interpolar space is constant amplitudes of tooth MMFs, as shown in Figs. 2.95 and 2.97. Denoting by 100 % the amplitudes of MMF in the interpolar space, one can represent the percentage amplitudes of spatial harmonics of air gap in the manner shown in Fig. 2.96. The amplitude of the positive sequence component of air gap in Fig. 2.97 equals to 92 %, and of the negative sequence component to 7.2 % of maximum MMF.

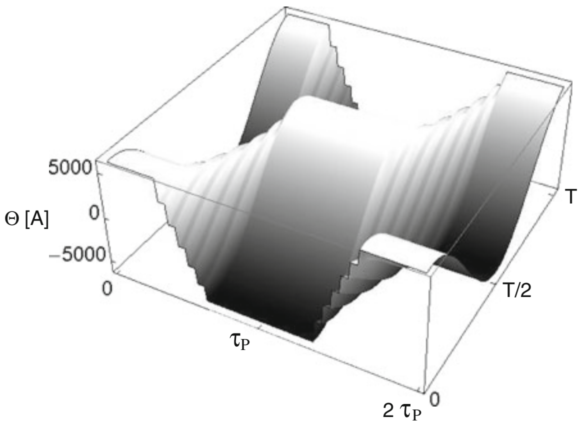

Fig. 2.95 Air gap MMF distribution created by a damper cage with continuous end rings generated during load change

Fig. 2.96 Bar current amplitudes in a damper cage with continuous end rings generated during load change

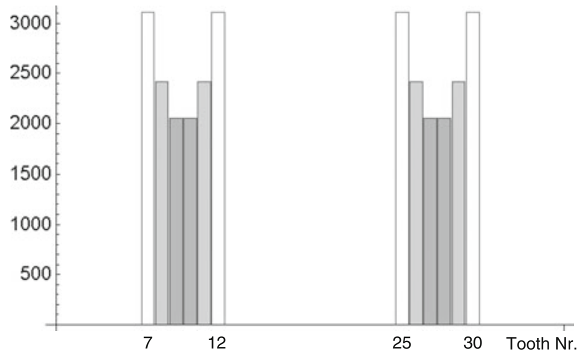

As opposed to asymmetrically broken bars in an induction machine from Case Study 2.6, which generated both odd and even spatial harmonics of MMF, the symmetrically missing bars of damper cage in this example lead to creation of odd harmonics only, as shown in Fig. 2.98.

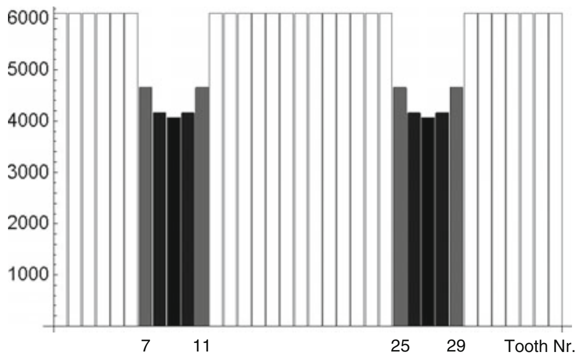

Fig. 2.97 Air gap MMF amplitudes created by currents in a damper cage with continuous end rings generated during load change

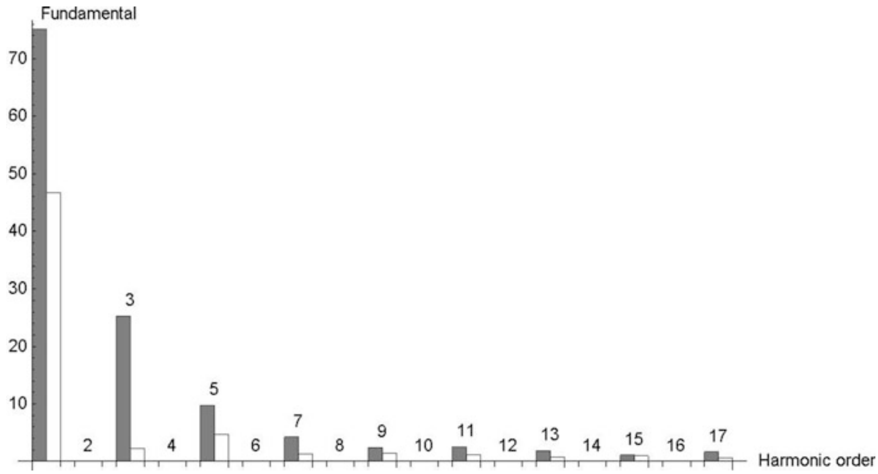

Fig. 2.98 Spectrum of the air gap MMF distribution (in % value of the largest fundamental in Fig. 2.82) created by currents in a damper cage with continuous end rings during load change. For each harmonic, the maximum (*gray*) and minimum (*white*) values are given

A continuous damper cage with bars in the interpole space creates tooth MMFs with equal amplitudes. Since in interpolar space of the analyzed machine there are no bars, the amplitude of the fundamental spatial harmonic of air gap MMF (Fig. 2.99) is obviously smaller than the amplitude of tooth harmonics in interpolar space in Fig. 2.97.

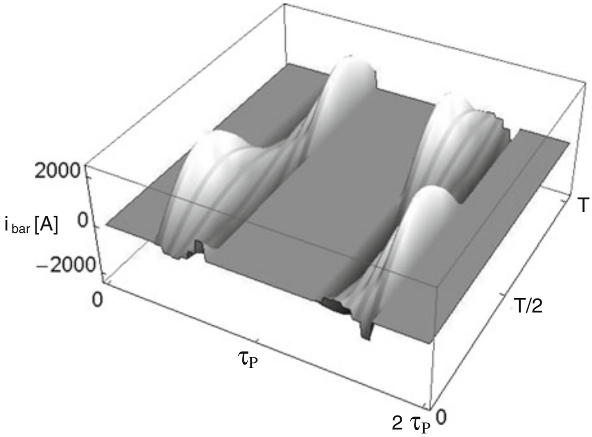

Fig. 2.99 Bar currents in a damper cage with discontinuous end rings in the interpole space during load change

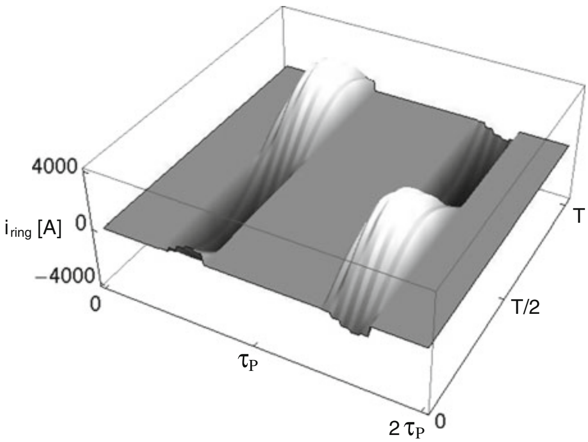

Fig. 2.100 Ring currents in a damper cage with discontinuous end rings during load change

In *discontinuous damper cage* (ring segments only on poles), the damping is not as efficient as in a continuous damper cage, since important components of ring currents are missing, Figs. 2.99 and 2.100. The missing connection between damper cage sections on salient poles results in significantly lower amplitudes of air gap MMF, as shown in Fig. 2.101. The amplitude of the positive sequence component of air gap in Fig. 2.102 equals to 14.6 %, and the amplitude of the negative sequence component to 13.2 % of the maximum MMF created by a continuous cage. The distributions of amplitudes of ring and bar segment currents of discontinuous damper cage are given in Figs. 2.102 and 2.103.

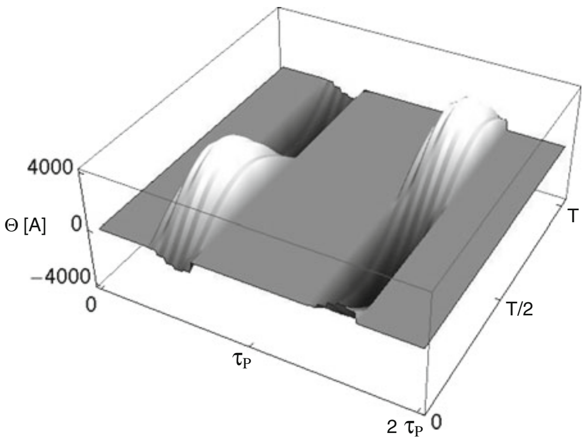

Fig. 2.101 Air gap MMF distribution created by a damper cage with discontinuous end rings during load change

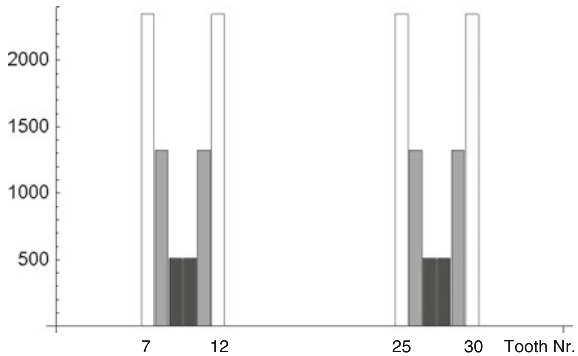

Fig. 2.102 Bar current amplitudes in a damper cage with discontinuous end rings during load change

The spectrum of air gap MMF of discontinuous cage in Fig. 2.104 shows deterioration of damper cage effects in discontinuous rings, as well as a significant increase of higher spatial harmonics of MMF created by damper cage currents.

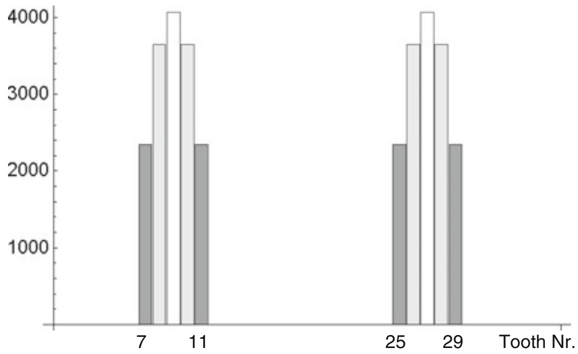

Fig. 2.103 Air gap MMF amplitudes created by currents in a damper cage with discontinuous end rings during load change. The largest MMF amplitudes are located in the center of interpole space

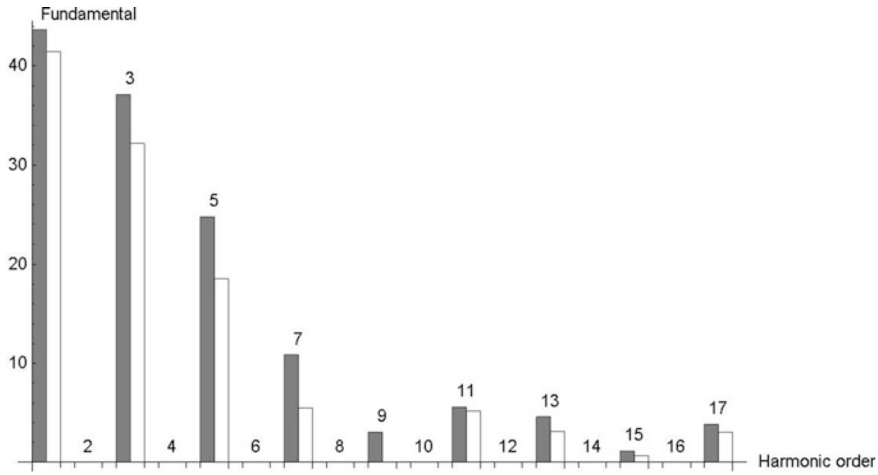

Fig. 2.104 Spectrum of the air gap MMF distribution (in % value of the largest fundamental in Fig. 2.97) created by currents in a damper cage with discontinuous end rings during load change. For each harmonic, the maximum (*gray*) and minimum (*white*) values are given

Case Study 2.8: Double-layer stator winding of a 3-phase, 281-MVA hydrogen-cooled turbogenerator 15.75 kV, 10.3 kA, two parallel circuits, cos $\varphi_r = 0.8$ is placed in 60 slots and has a pitch of 25 slots. The rotor has 14 slots per pole shifted for 9° to one another and carrying in total of 49 turns of field winding. Rated field current amounts to 4340 A and air gap is 75 mm wide. Rotor slot wedges are built of Nibrofor, a high strength copper alloy, and short-circuited on both rotor ends by means of end bells. Maximum allowed stator current unbalance is 8 %.

Negative sequence MMF caused by stator current unbalance is superimposed to the total air gap MMF. Therefore, the amount of air gap flux density created by the current unbalance of 8 % depends on the operating point of the magnetic circuit. At rated operating point the current unbalance causes a negative sequence component of the air gap flux density in the amount of 20 mT. The negative sequence component of flux density rotates at twice the synchronous speed relative to the rotor and induces in it voltages at twice the stator frequency, as shown in Fig. 2.105.

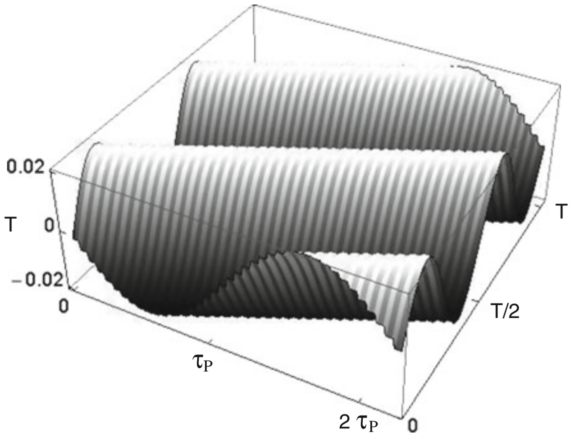

Fig. 2.105 Air gap flux density distribution at 8 % unbalanced load during one rotor revolution

The air gap flux density in Fig. 2.105 induces in damping wedges voltages which drive bar and ring currents, as shown in Figs. 2.106 and 2.107, respectively.

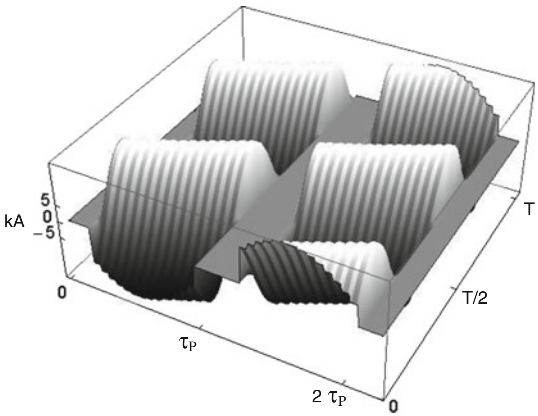

Fig. 2.106 Rotor damper bar currents at 8 % unbalanced load during one rotor revolution

The amplitudes of rotor tooth MMFs at 8 % unbalanced load are shown in Fig. 2.108. One recognizes the decreasing MMF values toward the rotor q-axis, as a consequence of the bar currents distribution in Fig. 2.109. The positive sequence component of MMF in the asymmetric distribution in Fig. 2.108 has the amount of 39.3 kA, and the negative sequence 4.7 kA. Here the positive sequence component of MMF rotates in the opposite direction to the rotor, and the negative sequence component of MMF in the direction of rotor rotation.

The spectrum of damper cage MMFs is shown in Fig. 2.110. The MMF spectrum contains only odd harmonics, since the pattern of missing bars is identical in each interpole space.

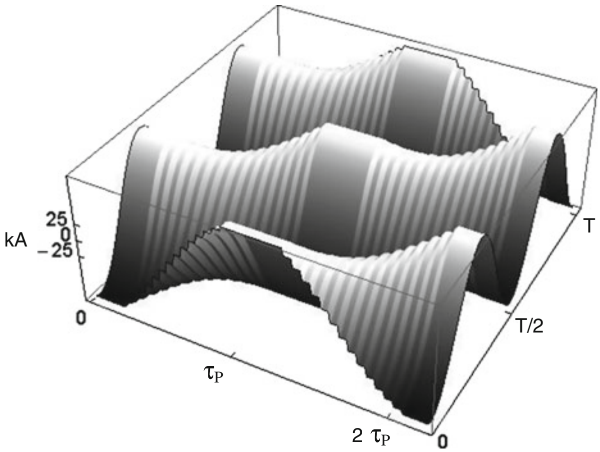

Fig. 2.107 Rotor ring currents at 8 % unbalanced load during one rotor revolution

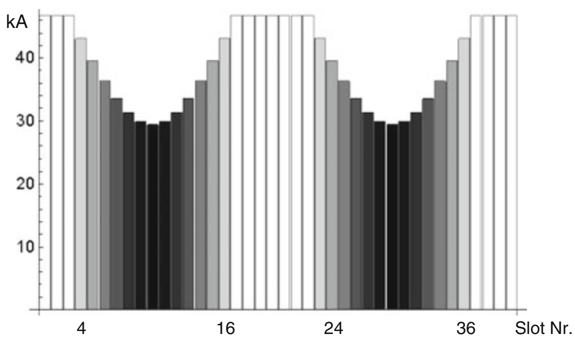

Fig. 2.108 Rotor tooth MMF amplitudes created by currents in a damper cage at 8 % unbalanced load. The largest MMF amplitudes are located in the center of poles

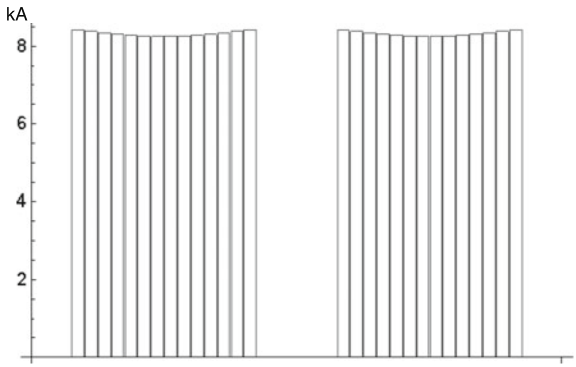

Fig. 2.109 Amplitudes of rotor bar currents corresponding to rotor tooth MMF in Fig. 2.108

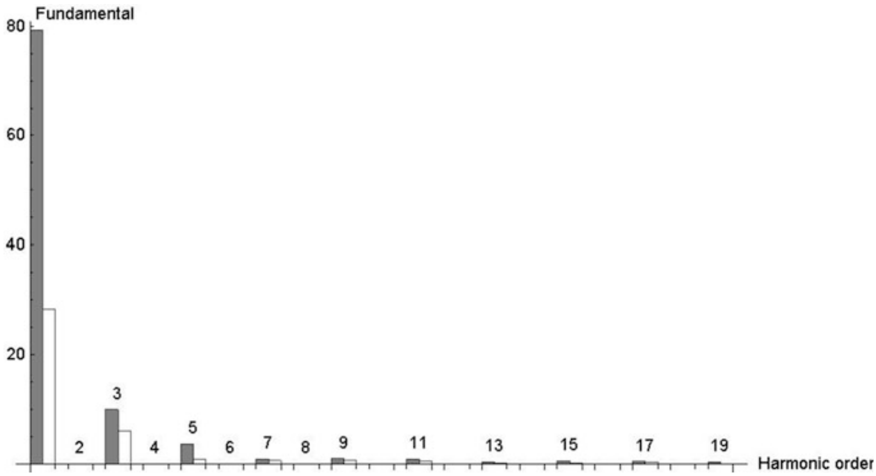

Fig. 2.110 Spectrum of the air gap MMF distribution (in % value of the largest fundamental in Fig. 2.82) created by currents in a damper cage at 8 % unbalanced load. For each harmonic, the maximum (*gray*) and minimum (*white*) values are given

2.10 Winding Failures

As illustrated in Case Study 2.6, an asymmetry of a squirrel cage winding in the form of broken bars is a source of higher harmonic components in the air gap MMF created by the squirrel cage. Very often broken bars are accompanied with pulsating torques and an increased noise level.

In case of field windings of synchronous machines, an interturn fault is a source of:

Decrease of the fundamental term of field created MMF, because short-circuited coils do not contribute to the MMF. The amount of decrease of current sheet can be quantified by means of Fig. 2.111 in which the rotor of a two-pole turbogenerator is shown. Denoting the maximum number of field coils with N_c and numbering the short-circuited coil by n, $1 \le n \le N_c$, one can write for the total effective number of turns w_{eff}

$$w_{eff} = \frac{1}{N_c w_c}\sqrt{\left[\sum_{i=1}^{n-1}\cos(i-1)\alpha_{el} + \sum_{i=n+1}^{N_c}\cos(i-1)\alpha_{el}\right]^2 + \left[\sum_{i=1}^{n-1}\sin(i-1)\alpha_{el} + \sum_{i=n+1}^{N_c}\sin(i-1)\alpha_{el}\right]^2} \quad (2.352)$$

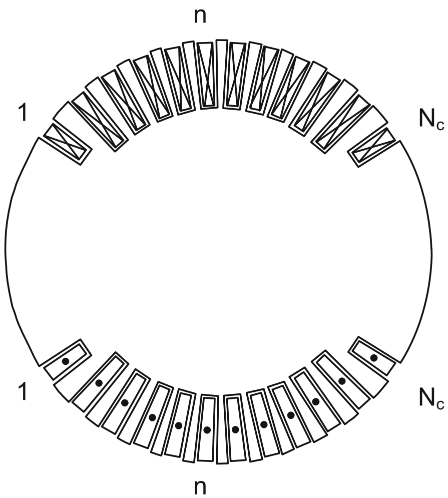

Fig. 2.111 Rotor of a two-pole turbogenerator with N_c coils. The nth coil is short-circuited

In Fig. 2.112 the winding factors of a field winding after Fig. 2.111 with 12 coils, the angle between which is 7.5° and one short-circuited coil are shown. The strongest effect on the field MMF is obtained by short-circuiting the coils in the center of the winding, i.e., slots number 6 and 7;

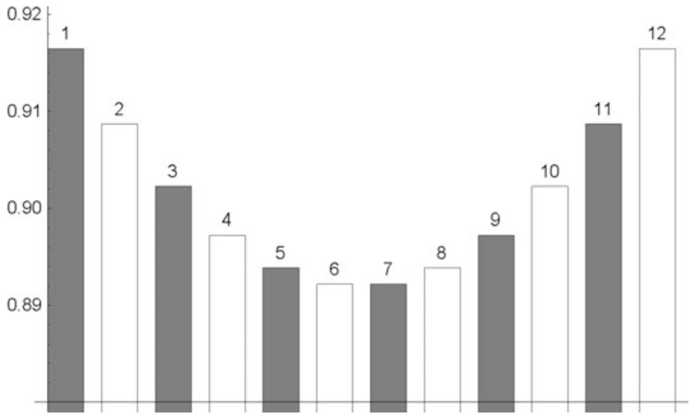

Fig. 2.112 Winding factors for a field winding with 12 coils, the angle between which is 7.5°, and one coil short-circuited

Even harmonics of MMF, which are reflected in induced voltages;

Asymmetric heating of the rotor winding, which eventually leads to rotor bowing; and

*Decrease of the field winding main and leakage inductance*s.

References

1. Ostovic V (1994) Computer-Aided Analysis of Electric Machines: a Mathematica Approach. Prentice-Hall, London
2. Richter R (1952) Lehrbuch der Wicklungen elektrischer Maschinen. Verlag G. Braun, Karlsruhe

http://www.springer.com/978-3-319-39079-6

The Art and Science of Rotating Field Machines Design:
A Practical Approach
Ostovic, V.
2017, XX, 463 p. 318 illus., Hardcover
ISBN: 978-3-319-39079-6